UNIVERSITY OF CALGARY

Pincer Ligands with Strong σ-Donors at the Central Position

by

Javier Borau-Garcia

A THESIS

SUBMITTED TO THE FACULTY OF GRADUATE STUDIES

IN PARTIAL FULFILMENT OF THE REQUIREMENTS FOR THE

DEGREE OF DOCTOR OF PHILOSOPHY

DEPARTMENT OF CHEMISTRY

CALGARY, ALBERTA

JANUARY, 2013

Abstract

Pincer ligands have been extensively investigated due to the ease by which their steric and electronic properties can be tuned. One of the most important features of pincer metal complexes is their robustness, which renders them excellent candidates for a wide variety of applications such as catalysis, medicinal chemistry, and chemical sensing. The increased robustness of pincer complexes is not associated with a loss of reactivity at the metal center, which renders them good ancillary ligands. Proper tuning of the electron donating properties of pincer ligands has allowed for some of their metal complexes to display unprecedented reactivity.

The objective of the research described herein was the synthesis and characterization of novel pincer ligand architectures, with a particular interest in ligands with strong electron donating moieties at the central position. Two PBP pincer ligand precursors with a 2-chloro-1,3,2-diazaborane central moiety were synthesized. The coordination of the ligand precursors to palladium via a B-Cl bond activation was investigated. The synthesized PBP ligands represent two of the first examples of pincer ligands with a boryl at the central donor position, and their palladium complexes are the first ever (PBP)Pd complexes. These complexes displayed good thermal stability but no catalytic activity under Heck cross-coupling reaction conditions. The synthesis of PBP and NBN pincer ligand precursors with an acyclic backbone was also explored.

PCP pincer ligand precursors with six and five membered *N*-heterocyclic carbene (NHC) moieties at the central donor position, which upon coordination would generate two five-membered metallacycles, were synthesized and characterized. Double C-H bond activation by rhodium in PCP-carbene precursors yielded the desired compounds with six membered NHC

backbones. These are among the rare examples where a double C-H bond activation leads to the formation of an NHC complex. The rhodium complexes displayed good thermal stability and promising reactivity. The analogous PCP-carbene precursor with a five membered NHC backbone could be readily deprotonated to the free carbene, allowing for the synthesis of rhodium, palladium, nickel and molybdenum complexes. These complexes have some of the shortest M-C_{NHC} bonds reported for each metal, suggesting a strong interaction between the metal center and the ligand.

Acknowledgements

First of all I would like to thank my supervisor, Prof. Roland Roesler, for giving me the opportunity to join his group and the freedom to follow my chemical curiosity while providing invaluable support and knowledge. Your passion for research motivated me to work harder every day, thanks for knowing when to push me but more importantly when to advice me. Special thanks to my committee members, Dr. Warren E. Piers, Dr. Thomas Baumgartner, Dr. Michael D. Fryzuk, and Dr. Marie Fraser for sharing their time and expertise.

During my time in the Roesler group I had the opportunity to work with some amazing people that make most days in the lab a unique experience. I would like to thank Dr. Hahn Ly for showing me the ropes on how to survive in the Roesler Lab. and on how to keep things organized and moving. Thanks to Dr. Kelly Krahulic for all the, below the belt, Mexican jokes, the great squash matches, and the afternoon americanos. Thanks to Dr. Matt Hobbs for all the, above the belt, Mexican jokes, the great discussions and conversations, for dragging me up two hikes, and for always being up for beers. Thanks to Chrissy Knapp for all those hours helping me study for my candidacy and for all the great chats. Special thanks to Michael J. Bosch, and Patrick T. Welsh for all the great times throughout their period in the Roesler group, too many to mention, even those when they seemed to be willing to kill me. I would also like to thank other Roesler group members past and present Dr. Jani Moilanen, Dr. Taryn Forster, Dr. Hongsui Sun, Dr. Surinder Randhawa Bhella, Nicole Mensik, Mark Maclean, Rashi Hiranandani, AnjanPreet Mahrok, Huy Huynh, Joshua Stessun, Felix Todea, Nick Jette, and Michael Liu for their support and friendship.

I would like to specially thank Michael J. Bosch and Patrick T. Welsh for their great contribution to the work presented in this Thesis and for making a teaching experience a learning

one as well. Thanks to Dr. Heikki M. Tuonnonen for the computational calculations for Chapter 3, and Dr. Masood Parvez for all his help and expertise with crystallography. I would also like to thank the instrumentation staff at the U of C: Dr. Michelle Forgeron, Dorothy Fox, Wade White, Qiao Wu, and Jain Jun (Johnson) Li for their invaluable help without which this project would have not been the same.

Special thanks to all my friends in Calgary: Kiyoshi, Jordan, Jansen, Doug, Derek, Amanda and Rylen, Brian, Kristen and Rich, Juan, Sam, Ashley, Kim, Stephan, Robin, Terry, Sandra, and Rachel, for all the fun times and for making this degree an enjoyable one full of adventures and new experiences. Thanks for all those late drinking nights in which we could have solved all the problems in the world.

I would like to thank my Canadian mom Terry, my Canadian dad Guy, my Canadian brothers, sisters, nieces and nephews: Deanna, Terry, Chantal and Paige; Paul, Karen, Dana, and Kristen; Darren, Alex and Ethan; Randy, Dorrie, Danielle, and Braden. You guys have given me more than I could have ever imagined thanks for all the love and support and for welcoming into your family with an open heart. I will be forever indebted with all of you and would have never been able to achieve this degree without all your love and support. I would also like to thank the Blasetti and Watson Families.

Last but certainly not least I would like to thank my dad Javier, my mom MariCarmen, my sisters Gina and Ale and all my family and friends in Mexico for all their support and unconditional love that allowed me to follow my dreams and without which I would be lost.

A mi abuelo

Un soñador que me enseño que los sueños son para vivirlos

For my grandpa

A dreamer who taught me to live out my dreams

Table of Contents

List of Tables

List of Figures

List of Schemes

List of Symbols, Abbreviations and Nomenclature

All compounds presented in this Thesis are numbered in bold according to the following guidelines:

- The first number represents the Chapter in which the compound was presented for the first time.
- For compounds previously reported in the literature, this number is followed by a letter, alphabetical in order of appearance (*e.g*. the first literature compound to appear in Chapter 2 will be **2.a**), separated from the number by a period. In the case where the 26 letters of the alphabet do not suffice for the number of presented literature compounds in a given chapter, upper case letters will be employed subsequently (e.g. the twenty-seventh literature compound to appear in Chapter 3 will be **3.A**).
- For computationally modeled species, the number is followed by a Greek letter, alphabetical in order of appearance (*e.g.* the first computationally modeled species in Chapter 3 will be 3.α).
- For novel species reported herein, the number is followed by another number, in ascending order according to the order of appearance (*e.g*. the fifth novel species to appear in Chapter 4 will be compound/complex **4.5**), separated from the first number by a period.
- For novel species reported in Chapter 3, the second number will be followed by a lower case letter which indicates the nature of the backbone in the pincer ligand:

  a = propylene **b** = naphthylene

- In order to indicate the substituents at the atom from the pendant arms of the pincer ligand, which binds or will bind to a metal center, a hyphen followed by the chemical abbreviation

of the substituents will be employed (*e.g.* the first novel species to appear in Chapter 2 with phenyl substituents at the pendant donor arm atoms will be **2.1-Ph**).

Symbol	Definition
Å	Angstrom
Ar^F	Perfluorophenyl, C_6F_5
b	Broad (NMR)
Bn	Benzyl
*n*Bu	*n*-butyl
*t*Bu	*tert*-butyl
C	Celsius
ca.	Approximately
cis	On the same side
COD	Free 1,5-cyclooctadiene
cod	η^4-coordinated 1,5-cyclooctadiene
COE	Cyclooctene
Cy	Cyclohexyl
Cp	Cyclopentadienyl
δ	Chemical shift
Δ	Difference and Heat
d	Doublet
dd	Doublet of doublets
dt	Doublet of triplets
d_x	Deuterated *x* times
DAC	Diamino carbenes
DFT	Density functional theory
DMSO	Dimethyl sulfoxide
η	Hapticity
EA	Elemental Analysis
e.g.	*exempli gratia,* for example
EI	Electron Ionization

Et	Ethyl
ESI	Electrospray ionization
hv	UV Irradiation
HHMDS	Bis(trimethylsilyl)amine
HRMS	High resolution mass spectrometry
HOMO	Highest Occupied Molecular Orbital
i.e.	*Id est,* that is
ipso	1-position of an aryl ring
IR	Infra-Red
$^{n}J_{XY}$	Hyperfine coupling constant between atoms X and Y, which are at a distance of n bonds
kcal	Kilocalorie
KHMDS	Potassium bis(trimethylsilyl)amide
LUMO	Lowest Unoccupied Molecular Orbital
μ	Bridging
m	Multiplet or mass
M	Arbitrary metal
MALDI	Matrix assisted laser desorption ionization
Me	Methyl
Mes	Mesityl
Mes*	2,4,6-tri-*tert*-butylphenyl (super mesityl)
meta (m)	3- and/or 5- position of an aryl ring
MS	Mass spectrometry
m/z	Mass/charge ratio
NBE	Norbornene
NBS	*N*-Bromosuccinimide
NHC	*N*-heterocyclic carbene
NMR	Nuclear Magnetic Resonance
ortho (*o*)	2-, and/or 6- position of an aryl ring
OTf	Trifluoromethanesulfonate
para (*p*)	4- position of an aryl ring
*i*Pr	*iso*propyl

*n*Pr	*n*-propyl
Ph	Phenyl
ppm	Parts per million
Py	Pyridine
q	Quartet
R	Arbitrary substituent
rt	Room temperature
sept.	Septet
t	Triplet
$t^1/_2$	Half life
tert	Tertiary
trans	On opposite sides
TrCl (trityl chloride)	Triphenyl methyl chloride
THF	Tetrahydrofuran
TMP	Tetramethylpiperidine
TOF	Turn over frequency or Time of flight
TON	Turn over number
v	Frequency
vs	Very strong (IR)
vs.	Versus
vt	Virtual triplet
$w^1/_2$	Width at half height
X	Arbitrary anion or any atom except H
ϕ	*phi*, dihedral angle between planes

List of Compounds

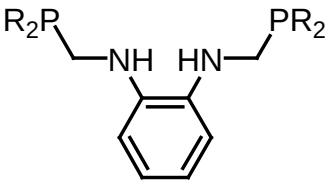

2.1-R
R = Ph, *t*Bu

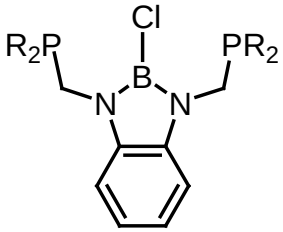

2.2-R
R = Ph, *t*Bu

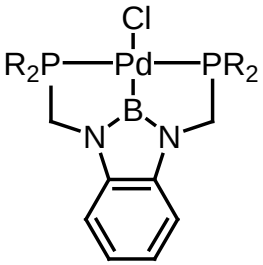

2.3-R
R = Ph, *t*Bu

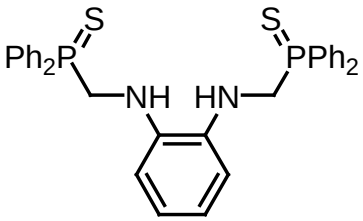

2.4

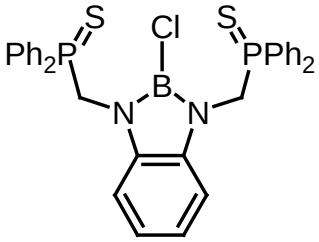

2.5

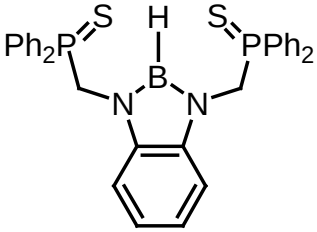

2.6

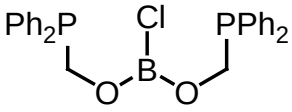

2.13-Ph

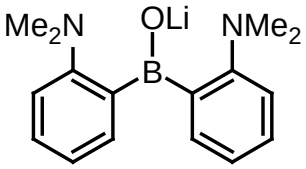

2.15-Me

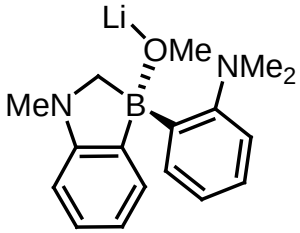

2.16-Me·LiOMe

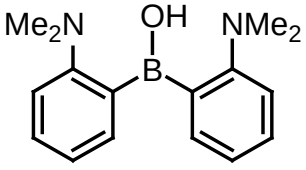

2.17-Me

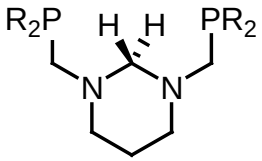

H_2(**3.1a-R**)
R = Ph, *t*Bu

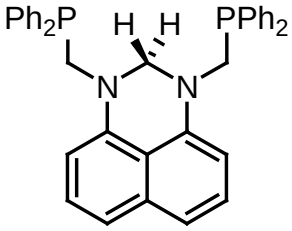

H_2(**3.1b-Ph**)

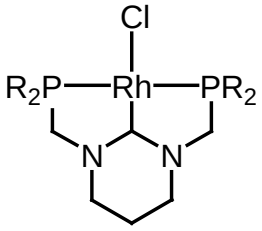

3.5a-R
R = Ph, *t*Bu

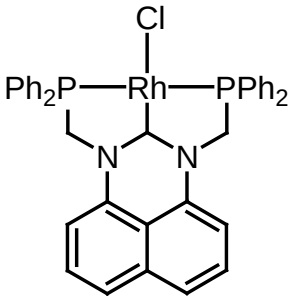

3.5b-Ph

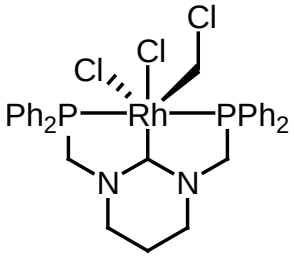

3.10a-Ph

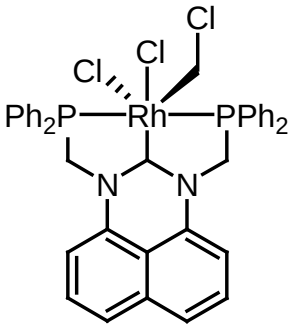

3.10b-Ph

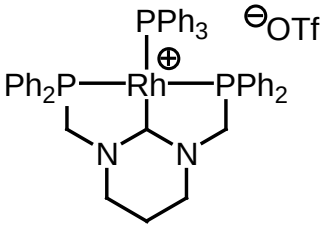

3.12a-Ph(OTf)

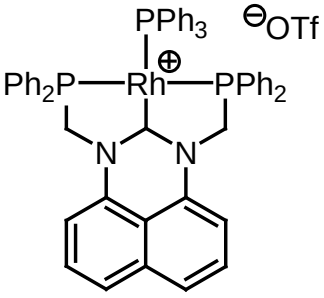

3.12b-Ph(OTf)

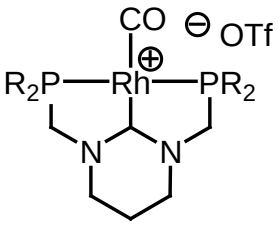

3.13a-R(OTf)
R = Ph, *t*Bu

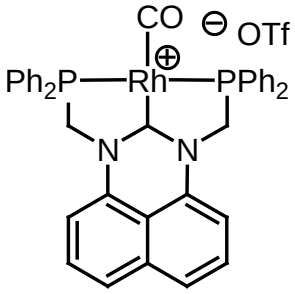

3.13b-Ph(OTf)

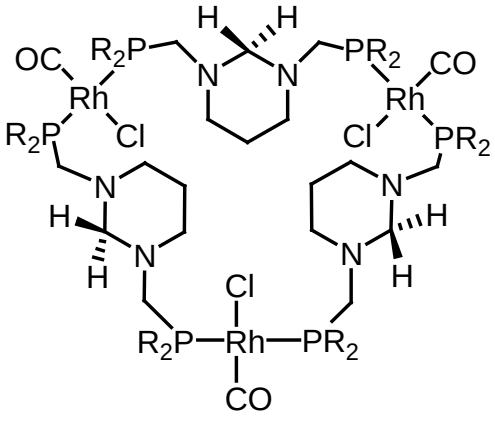

3.14a-*t*Bu
R = *t*Bu

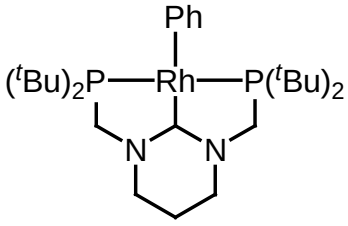

3.15a-*t*Bu

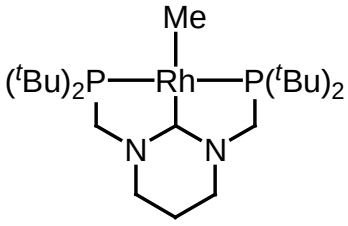

3.16a-*t*Bu

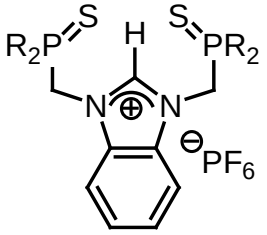

[H(**4.1-R**)](PF_6)
R = Ph, *t*Bu

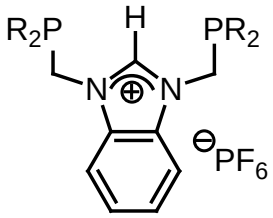

[H(**4.2-R**)](PF_6)
R = Ph, *t*Bu

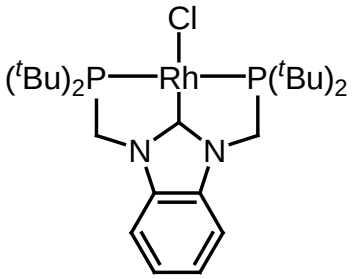

4.3-*t*Bu

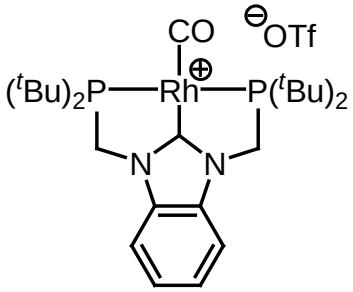

4.4-*t*Bu(OTf)

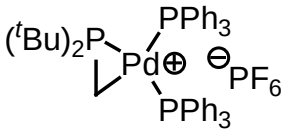

4.6-*t*Bu(PF_6)

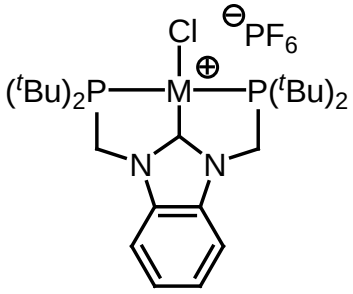

4.8-*t*Bu(PF_6) M = Pd
4.9-*t*Bu(PF_6) M = Ni

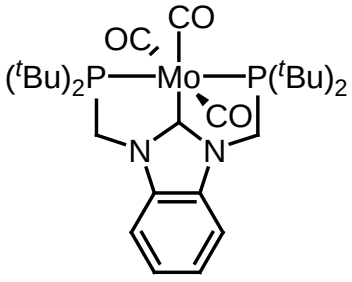

4.10-*t*Bu

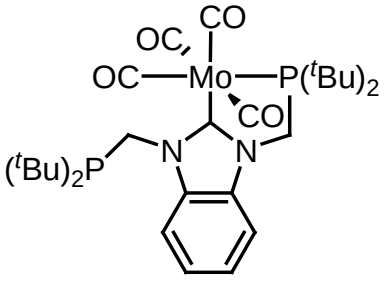

4.11-*t*Bu

Chapter One: **Introduction**

Since the early 19th century when the term "catalyst" was first employed by Jöns Jacob Berzelius, in order to explain the hastening of the combustion of certain gases in the presence of platinum observed by Sir Humphry Davy, the ability to effect chemical transformations faster, under milder conditions, and with enhanced selectivity has been one of the most important goals in chemistry. From the modest beginnings of the implementation of catalysts in industrial processes, such as the oxidation of hydrochloric acid to chlorine in the presence of cupric salts impregnated in clay bricks, to the world-changing Haber-Bosch process for the production of ammonia, and Ziegler-Natta process for ethylene polymerization, all the way to the now ubiquitous palladium cross-coupling reactions and the olefin metathesis reaction, catalysis has evolved into a shaping force of the future.

The energy and environmental crisis facing the world require the implementation of novel recycling techniques and more atom and energy efficient processes. Catalysis could hold the key to solve this crisis, and hence the design and synthesis of novel, more efficient catalysts remains a primary challenge for chemists today. Tuning the electronic and steric properties of active metal centers is one of the most reliable ways to obtain novel reactivity. In order to tune these properties of a metal center, alterations to the ligands bound to it have to be made. As such, ligand design has become one of the most important aspects of synthetic chemistry. This work focuses on the development of novel pincer ligands expected to generate robust, electron rich metal complexes.

1.1 Pincer Complexes

1.1.1 The Early Days

The chemistry of pincer ligands was pioneered in 1976 by Shaw, who reported compound H(**1.a**) and its facile metallation giving rise to complexes **1.b**, featuring the new chelating tridentate ligand **1.a** (Figure 1.1).[1] Shaw and co-workers reported the synthesis of Ni, Pd, Pt, Rh, and Ir metal complexes of ligand **1.a**, showcasing the versatility of this ligand.

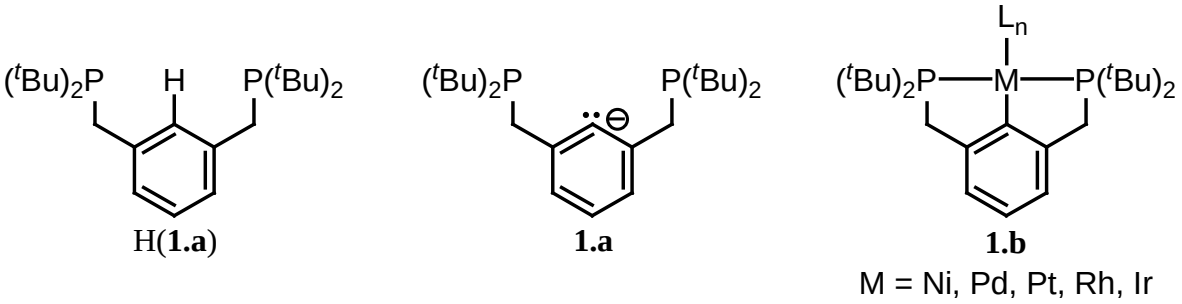

Figure 1.1 Pincer ligand precursor H(1.a), pincer ligand 1.a, and generic complex 1.b.

Two years after this seminal paper, Shaw reported the synthesis of compound H(**1.c**), an aliphatic analog of H(**1.a**), and its transition metal complexes **1.d** (Figure 1.2). This provided evidence that the metallation reactions leading to tridentate coordination could also be successfully carried out for sp^3 hybridized carbon atoms, further expanding the scope of this novel class of ligands.[2-10] Around the same time, the synthesis of ligand **1.e**, similar to **1.a** but having amine side donors instead of phosphines, and its platinum complex **1.f** (Figure 1.2) were reported.[11,12] These represent the first examples for the tuning of pincer ligands, which is one of their most relevant advantages over other ligand systems.

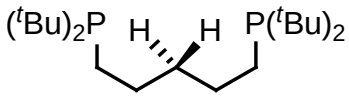

H(**1.c**)

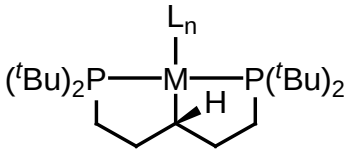

1.d

M = Pd, Pt, Rh, Ir

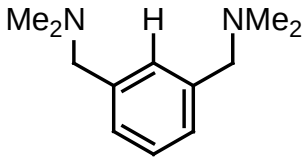

H(**1.e**)

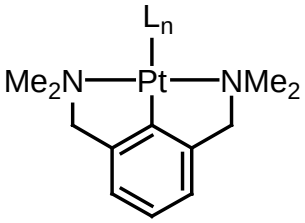

1.f

Figure 1.2 Reported pincer ligand precursors H(1.c) and H(1.e), and their metal complexes 1.d and 1.f.

By the late 1980s, the term "pincer" was coined by van Koten, as means to describe tridentate, monoanionic, meridional ligands analogous to **1.a**, with a more general representation being shown in Figure 1.3.[13] Classical "pincer" ligands are those with the general formula $[2,6\text{-}(ECH_2)_2C_6H_3]^-$, where E represents any neutral, two electron donor (*e.g.* NR_2, PR_2, AsR_2, OR, SR), and C the central, anionic aryl carbon. However, the term "pincer" quickly outgrew its classical definition and is now commonly used to describe almost all tridentate meridional ligands, and even some non-meridional ones, regardless of: i) the overall charge of the ligand, ii) the identity of the atoms with which it binds to the metal center, iii) the type of linkers between the pendant arms of the ligand and the central donor, and iv) the backbone of the ligand. The three letter code (*e.g.* PCP, NNN, SCS...) is used as a shorthand way of describing pincer ligands by highlighting the atoms that bind to the metal center, and will be employed throughout this thesis.

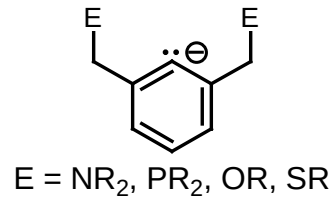

Figure 1.3 Classical pincer ligands.

The outstanding thermal stability displayed by complexes of ligands based on 2,6-disubstituted phenyls, **1.b** and **1.f**, confirmed by their high melting points and in some cases even the ability to sublime, drew interest to this novel class of ligands and their metal complexes, and by 1990 there were over 70 papers on the topic.[14] The added stability provided by the denticity of pincer ligands is explained by the chelate effect which has both thermodynamic and kinetic implications.

1.1.2 Tuning of Pincer Ligands and Pincer Complexes

The interest in pincer complexes soon switched gears and what was at first a search for novel structures soon became a property-driven field. Pincer complexes have been successfully employed for a variety of applications, including but not exclusively as catalysts in homogeneous and heterogeneous conditions,[15] as motifs for self-assembling materials,[16] as synthons for metallodendrimers,[17] as sensors[18-20] and switches,[21-24] as light harvesters and photosensitizers,[25] and in medicinal chemistry as biomarkers.[26,27] The wide variety of applications for pincer complexes is a direct reflection of one of the ligands' most appealing aspects, the number of options in which their electronic and steric properties can be tuned without compromising their ability to bind metal centers (Figure 1.4).

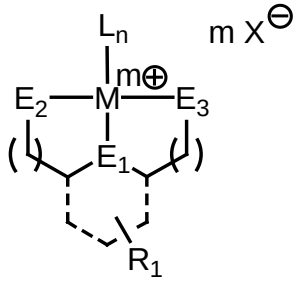

	The backbone of the pincer ligand can be altered in a variety of ways, the most common of which are: i) changing the ring size (5, 6 or 7 membered), ii) altering the ring properties (aromatic vs. non-aromatic), and iii) eliminating the ring, which leads to acyclic systems.
R_1	Substituents on the backbone can have subtle electronic effects or act as anchoring sites.
E_1	The nature of the central donor has a direct impact on the overall properties of the metal center, since in most cases the reactivity effected by the metal complexes will take place in the coordination position *trans* to E_1. Ligands with different central donors are common place in pincer chemistry.
E_2, E_3	The nature of the side arms has also become as varied, if not more, than that of the central donor. The most commonly found differences being i) soft vs. hard donors, ii) the rigidity with which they bind the metal center, iii) the steric constrains brought on by their substituents, and iv) the ligand type (i.e. neutral, charged, Lewis acidic, Lewis basic, etc.). It is important to remember that the side arms act as an umbrella which protects the E_1-M bond and as such changes on E_2 and E_3 will have a strong impact on the overall stability of the pincer complexes.
mX / L_n	The nature of the counter anions (X) and ancillary ligands (L) has a direct impact on the properties of the metal complexes, considering that the expected catalytic reactivity takes place on this face of the metal center. Labile ligands and non-coordinating counteranions have been proven to increase the reactivity of the metal centers.[14] However, gain in reactivity usually comes at a cost on the stability of the pincer complexes.
	Finally, changes in the length of the linkers have been shown to have a direct impact on the coordination pocket of the pincer ligand, and on its spatial disposition upon coordination. Furthermore, these remote positions can also be employed to convey other interesting properties to the metal environment, such as chirality, or enhanced rigidity.

Figure 1.4 Tunable aspects of pincer ligands and their effects on the metal center.

The ability to manipulate the coordination properties of pincer ligands has led to the discovery of remarkable pincer complexes with unique reactivity. Besides important advances in catalysis, discoveries in pincer chemistry have also dealt with unique stoichiometric bond activations, which are nonetheless expected to be further applicable for novel catalytic reactions.

1.1.3 The Front Line

1.1.3.1 Highlights in Catalysis

Catalysis with pincer complexes has allowed the exploration of both the enhanced properties of pincer complexes over other systems, and of altogether new catalytic reactions that can only be effected with these systems. Some recent noteworthy examples of catalytically active pincer complexes and the reactions they catalyze are:

i) The direct catalytic conversion of alcohols and amines into amides and dihydrogen (Scheme 1.1) catalyzed by [(PNN)RuH(CO)] complex **1.g** (Figure 1.5). In this case, the overall reaction is environmentally benign, has great atom efficiency and has no major by-products.[28]

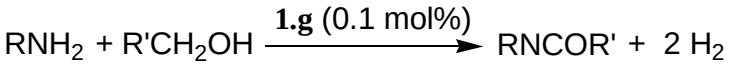

Scheme 1.1 Conversion of alcohols and amines into amides and dihydrogen.

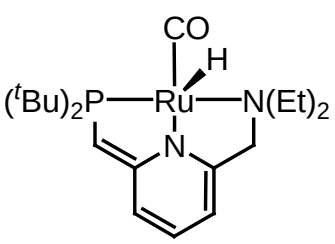

1.g

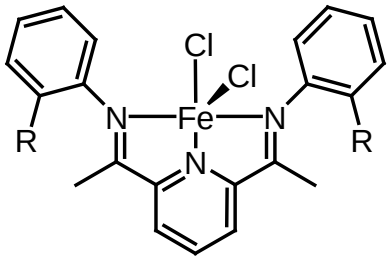

1.h: R = Me, Et, ^{i}Pr

Figure 1.5 Complexes 1.g and 1.h.

ii) The ethylene polymerization reaction catalysed by bis(imino)pyridine iron complexes **1.h** (Figure 1.5).[29] The reactivity displayed by complexes **1.h** was in part responsible for the recent rebirth of the chemistry of redox-active ligands in which the ligand involvement allowed for unique reactivity to take place at the metal center.[30]

iii) The catalytic dehydroaromatization of n-alkanes by [(PCP)Ir] complexes **1.i**, **1.j**, and **1.k** (Figure 1.6).[31] The reactivity displayed by complexes **1.i**, **1.j** and **1.k** was reported to dramatically decrease when the phosphine substituents were changed from *iso*-propyl to *tert*-butyl, in a clear example of the effect minor modifications have on the reactivity of pincer complexes.

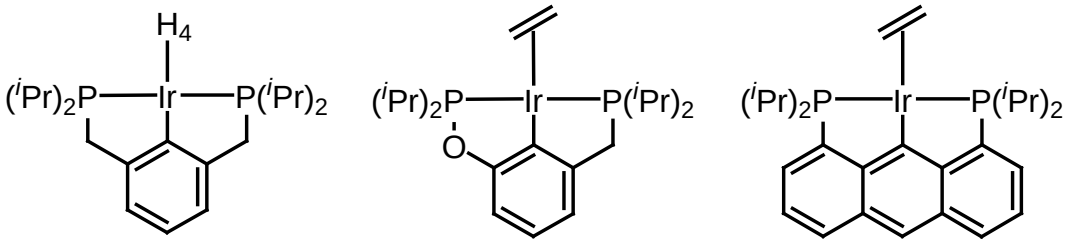

1.i **1.j** **1.k**

Figure 1.6 Complexes 1.i, 1.j and 1.k.

1.1.3.2 Highlights in Bond Activation

The most relevant advances in bond activation have been made in respect to small molecule activation. Water splitting,[32,33] activation of ammonia,[34] and nitrogen reduction[35,36] took center stage due to their relevance in the field of novel energy sources. The efficient production of hydrogen gas from water or ammonia would represent a huge step towards the viability of a hydrogen powered future. Water splitting by pincer complex **1.g** was reported in 2009 by Milstein; the mechanism proposed by the authors is outlined in Scheme 1.2.[32]

Important to note is the role played by ligand cooperativity in the observed reactivity. The first example of direct activation of an ammonia N-H bond was reported in 2005 by Hartwig (Scheme 1.3). The use of pincer complex **1.l** with a ligand featuring an acyclic backbone proved fundamental for the activation to take place. The aliphatic backbone renders the metal center more electron rich, favouring the oxidative addition to generate complex **1.m** over the coordination of ammonia, which would involve donation of electron density to an already highly electron rich metal center.[34] Besides its implication for the possible generation of hydrogen, the activation of ammonia also represented a major step towards the much sought-after catalytic synthesis of amines via hydroamination of unsaturated compounds.

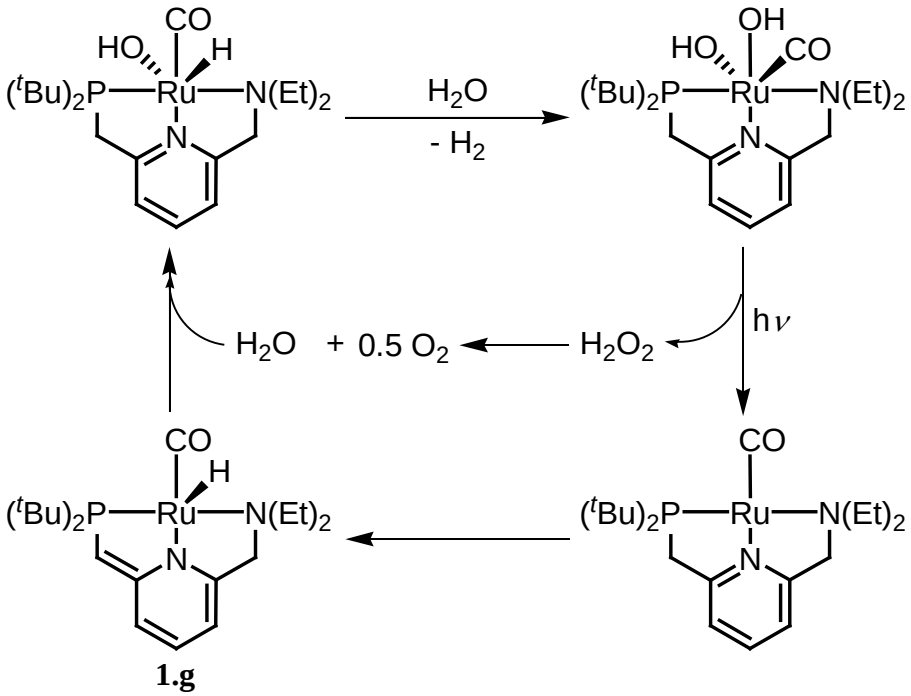

1.g

Scheme 1.2 Proposed mechanism for the formation of H_2 and O_2 from water, mediated by the pincer complex 1.g.

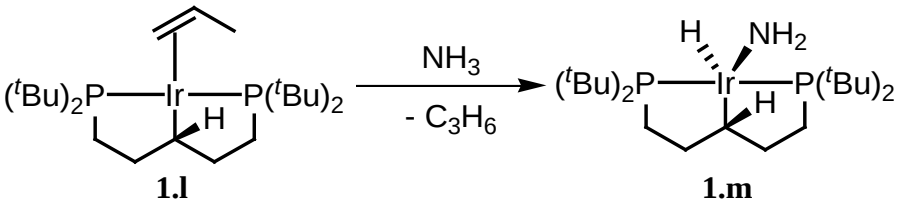

1.l **1.m**

Scheme 1.3 Activation of ammonia by pincer complex 1.l to generate the hydrido-amido complex 1.m.

The reduction of nitrogen to ammonia at room temperature and atmospheric pressure remains a long-standing goal in catalytic chemistry.[37] In 2011 Nishibayashi reported the molybdenum pincer complex **1.n**, (Figure 1.7), and its catalytic activity in the reduction of dinitrogen to ammonia.[36] Complex **1.n** is one of the two reported complexes that can effect this reaction catalytically under ambient conditions, albeit with the requirement of protons and electrons. The other example is a molybdenum complex with a triamidoamine ligand, reported in 2003 by Schrock and Yandulov.[37]

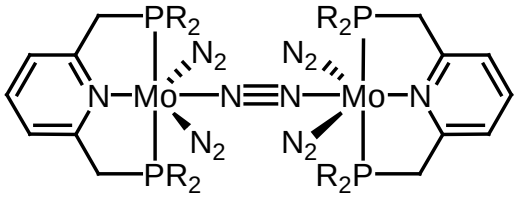

1.n: R = ^{t}Bu

Figure 1.7 Complex 1.n.

In another unique bond activation made possible by the use of a pincer complex, complex **Ir-1.b** was successful in activating aliphatic C-F bonds (Scheme 1.4), as reported in 2012 by Goldman et al..[38] Aliphatic C-F bonds are the strongest single bonds to carbon and hence the ability to effect this activation represented a milestone in transition metal chemistry.

Important to mention however, is that the C-F bond activation observed was the product of a rearrangement from an initial C-H bond activation.

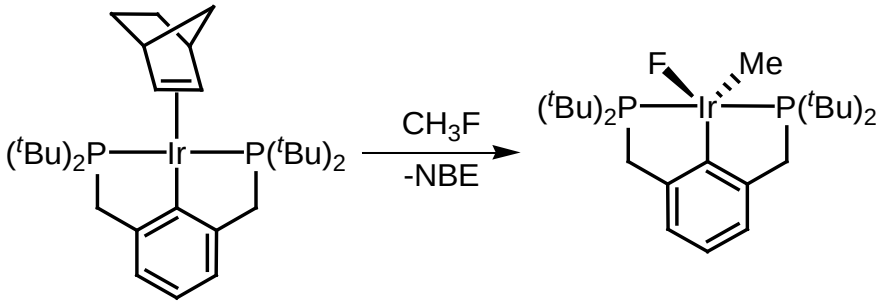

Ir-1.b

Scheme 1.4 Activation of an aliphatic C-F bond by complex Ir-1.b.

1.2 Research Objectives

The unique reactivity displayed by pincer complexes, coupled with their great thermal stability, makes the synthesis of novel pincer ligands and complexes a persistently relevant research field. The modular nature of pincer ligands gives rise to an incredibly large number of opportunities for innovation. This research project was focused mostly on the development of a series of novel pincer ligands. The approach was mostly based on ligand design, targeting the synthesis of ligands with strong electron donating properties.

The second Chapter of this thesis deals with the synthesis of pincer ligands with a boryl moiety in the central donor position, and the third and fourth Chapters with the synthesis of pincer ligands with *N*-heterocyclic carbenes (NHCs) in the central donor position.

1.3 Boryls

Boryls are divalent boron centers of the general formula BR_2^- (R = OR, NR_2, alkyl, etc.). The stability of boryls is lower in comparison to that of their heavier analogs, the alkyls, and as

such no commercially available transfer reagents of boryls, analogous to organolithium or Grignard reagents, are known. This is not surprising considering the coordinatively unsaturated nature of boryl anions and the significant difference in electronegativity between boron and carbon. However, it is these properties of boron that make M-B bonds potentially stronger than M-C bonds, since they display a higher degree of covalence, better orbital overlap, and have the potential for π-backbonding to take place.[39]

Transition metal boryl complexes are those in which a BR_2^- fragment is bonded to a metal center through a well defined two-centre two-electron bond.[40] The simplest model to describe the covalent M-B bond in metal boryls involves a trigonal planar, sp^2-hybridized boron center that σ-bonds to the metal center. The electronic demands of the boron center can be satisfied via either π-donation from the R substituents when applicable, e.g. R = N, O, or through π-backbonding from the metal center (Figure 1.8).[41]

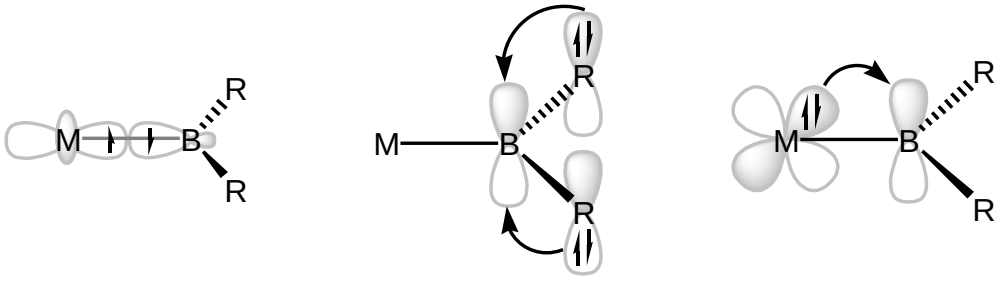

Figure 1.8 Model of σ and π bonding in metal boryls.

Metal boryl complexes have generated a lot of interest in the past few years due to the wide range of applications they have found. Boryl complexes play a key role in the metal mediated borylation of unsaturated organic substrates[42-47] and of C-H bonds.[48-55] Further, the cleavage of the M-B bond has given access to novel borylated organic species used as building

blocks in the synthesis of π-conjugated boron-based materials.[56-58] Furthermore, the strength of the M-B bond has allowed for the study of properties and reactivity of otherwise unstable boron species.[59-61] These and other applications have motivated studies of the effect the steric and electronic properties of the boryl ligand have on the reactivity of the boryl complexes.[62]

The calculated bond dissociation energies of M-B bonds have been found to be around 30 kcal mol^{-1} higher than those of analogous M-C bonds.[39,41] However, despite their strength, the reactivity of transition metal boryls has been mostly limited to that of borylation and hydroboration reactions, which involve the cleavage of the M-B bond. These reactivity patterns have prevented the use of boryls as ancillary ligands. Chapter 2 deals with the synthesis and characterization of pincer boryl ligands in order to assess if the thermodynamic and kinetic stability added by the chelate effect is enough to effectively prevent the cleavage of the M-B bond.

1.4 *N*-Heterocyclic Carbenes (NHCs)

Carbenes are neutral divalent carbon centers of the general formula $:CR_2$ (R = NR_2, OR, or alkyl). They have six valence electrons that provide them with an interesting electronic duality, being electron deficient while possessing a free pair of electrons. The two non-bonding electrons can either be paired, producing a singlet carbene, or unpaired, giving rise to a triplet carbene. These properties render carbenes highly reactive and hence, they are typically found as intermediates in organic and organometallic reactions. However, persistent singlet state carbenes can be isolated, with the most common type being *N*-heterocyclic carbenes (NHCs) due to their increased stability.[63] In NHCs, the carbene center is flanked by one or two nitrogens. The electronegativity difference between nitrogen and carbon, and the lone pair of electrons on

the nitrogen(s) promote stabilization of the carbene via inductive and mesomeric effects, respectively (Figure 1.9)[64].

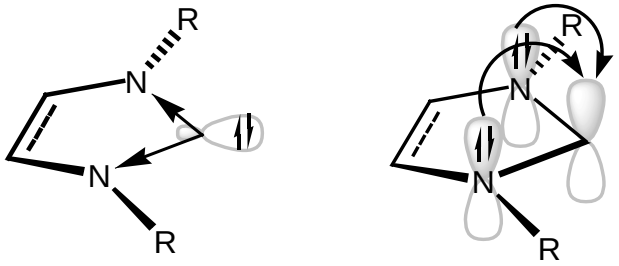

Figure 1.9 Stabilization of the singlet carbene in NHCs via inductive (left) and mesomeric (right) effects.

The first report of NHC transition metal complexes **1.o**,[65] and **1.p**[66] in 1968 by Wanzlick and Ölefe, respectively, preceded that of the isolation of a free NHC **1.q**[67] in 1991 by Arduengo by over 20 years (Figure 1.10). However, it wasn't until the isolation of complex **1.q** that the field of NHCs and their complexes started to thrive.

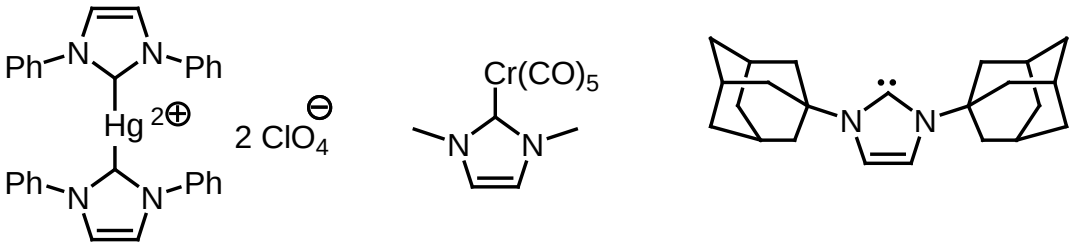

1.o **1.p** **1.q**

Figure 1.10 First reported NHC complexes 1.o and 1.p, and first isolated free NHC 1.q.

NHCs are neutral, two electron-donor ligands that bind to metal centers via a dative σ bond (Figure 1.11). NHCs have been proven to possess great electron donating properties that supersede even those of the most Lewis-basic tertiary phosphines.[68,69] Furthermore, the strength

of the M-C_{NHC} bond renders NHC complexes thermally robust. As such, NHCs have become excellent phosphine replacements as ancillary ligands in a wide number of catalytic systems.[70] Even though NHCs are mostly viewed as strong σ-donors, it is important to note that NHCs also possess a π-symmetric oriented LUMO with the right orientation to allow for π-backbonding from the metal center (Figure 1.11). The π-backbonding contribution to the strength of the M-C_{NHC} bond was at first considered negligible,[71-73] but experimental and theoretical evidence pointing towards the contribution of the π-backbonding to the strength of M-C_{NHC} bonds has since been reported.[74,75]

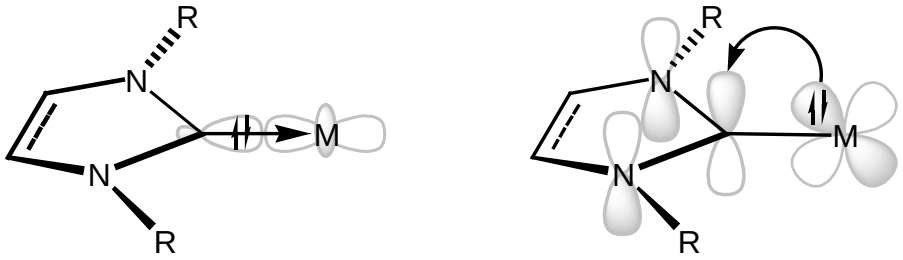

Figure 1.11 Metal-NHC bonding contributions: σ-bonding (left) and π-backbonding (right).

The incorporation of NHCs into multidentate ligand arrays as means to further increase the stability of the M-C_{NHC} bonds, and generate novel metal complexes with heightened catalytic activity has been explored. However, combining the versatility of NHCs with that of pincer ligands gives rise to a promising group of highly tunable ligands with superior coordination properties. Chapters 3 and 4 from this thesis deal with two novel NHC-based pincer systems with enhanced electron donating properties.

Chapter Two: **PBP Pincer Ligands with a Central Boryl Donor**

2.1 Introduction

Boryl ligands have been extensively studied in light of their intermediacy in borylation and hydroboration reactions, where they play a "reactive" role.[42,44,46-49,52-55] Theoretical and experimental results have shown that boryl ligands have superior σ-donating ability in comparison to other known strong σ-donors such as hydrides and silanes,[76-80] surpassing in this regard other monoanionic ligands of the *p*-block elements such as those based on C, N, and O.[81,82] Stabilizing the bond between the boryl ligand and the metal center in order to switch its role as a ligand from "reactive" to "ancillary" would allow for the exploitation of the strong electron donating properties of boryls in functionalization reactions, beyond the scope of borylations.[83,84]

The use of pincer complexes as means to stabilize highly reactive species by incorporating them in the ligand framework at the central donor position has been extensively reported over the past few decades.[14] The highly tunable nature of pincer ligands in conjunction with innovative design and original synthetic strategies have promoted the development of a large number of pincer architectures.[17] One such modification involves the exchange of conventional carbon-based frameworks[85] with other novel backbones that incorporate heteroatom functionalities, such as amido,[86-88] silyl,[89-91] and phosphido[92] units. When this project was initiated, there were no reported attempts at the synthesis of complexes with boryl-containing pincer ligands.

We therefore targeted the synthesis of a novel pincer ligand precursor with a boron donor in the central position. The synthetic target involved a di-functionalized diazaborole with pendant phosphine arms, as shown in Figure 2.1. Boryl species with amino substituents are stronger σ-donors than their oxo analogs,[93] and the trivalency of the nitrogen centers simplifies the insertion of the pendant arms. Pincer ligands with pendant phosphine arms are ubiquitous in this type of chemistry.[17]

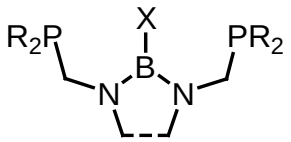

Figure 2.1 Generic proposed pincer ligand precursor with a boron donor in the central position.

2.2 Synthesis and Characterization of PBP Pincer Ligand Precursors 2.2-Ph and 2.2-*t*Bu

The synthetic route for the PBP pincer ligand precursors **2.2-Ph** and **2.2-*t*Bu** is shown in Scheme 2.1. Compound **2.1-Ph** was synthesized following a reported procedure for a related compound, *N*,*N*'-bis((diphenylphosphino)methyl)-4-methylbenzene-1,2-diamine,[94] which was synthesized from diphenylphosphine, paraformaldehyde, and 4-methylbenzene-1,2-diamine. Reaction of neat diphenylphosphine with paraformaldehyde at 125 °C for 6 h yielded a clear thick oil consisting of pure diphenylphosphinomethanol, as verified by multinuclear NMR spectroscopy. Diphenylphosphinomethanol was then reacted with half an equivalent of *o*-phenylenediamine in CH_2Cl_2 over a period of 2 days, yielding compound **2.1-Ph** (85 % isolated yield with respect to *o*-phenylenediamine).

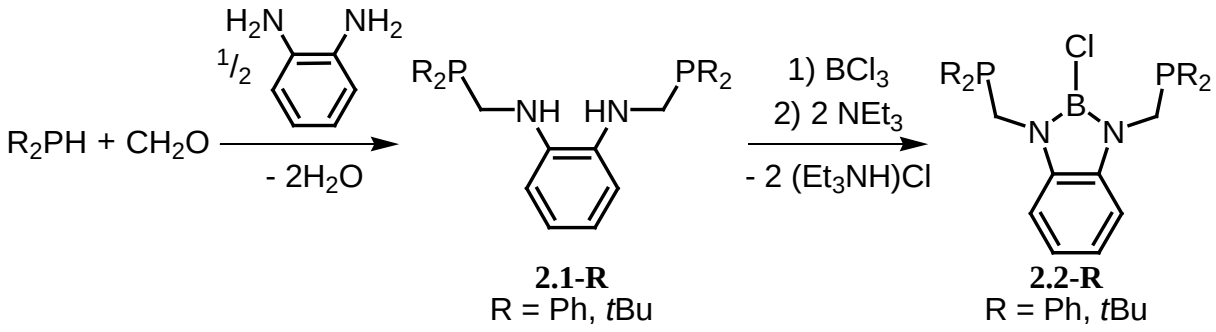

Scheme 2.1 Synthesis of PBP pincer ligand precursors 2.2-Ph and 2.2-*t*Bu.

The crystal structure of **2.1-Ph** is shown in Figure 2.2. The phosphine phenyl substituents are pointing inwards, encapsulating the N-H fragments, which seems counterintuitive considering expected steric repulsions. The asymmetric unit of the crystal only represents half of the molecular structure displayed, thus the other half was generated by symmetry. No unusual bond lengths and angles were observed.

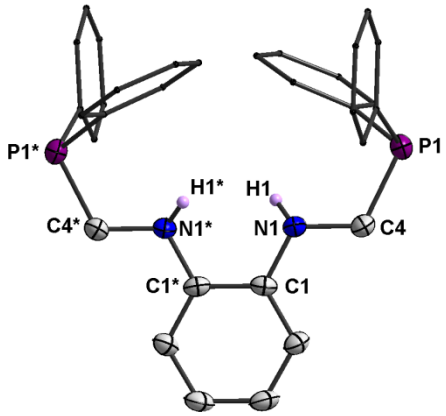

Figure 2.2 Solid-state molecular structure of 2.1-Ph with thermal ellipsoids at 50 % probability, with the exception of the phosphine substituents, which are modeled as "sticks". All hydrogen atoms except for those from the amines have been omitted for clarity.

Treatment of **2.1-Ph** with 1 equivalent of BCl_3 readily generated a Lewis acid-base adduct between the boron and one of the phosphorus pendant arms, as evidenced by the presence of a doublet in the ^{11}B NMR spectrum (d, 2.8 ppm, $^{1}J_{PB}$ = 149 Hz), and of a quartet and a singlet with a relative integration of 1:1 in the ^{31}P NMR spectrum (q, -4.8 ppm, $^{1}J_{PB}$ = 149 Hz; s, -21.5 ppm). Heating the reaction mixture for 24 h to 45 °C, followed by the addition of triethylamine and further heating for an extra 24 h afforded the desired [1,3,2]-diazaborole **2.2-Ph** (Scheme 2.1) with an isolated yield of 83 % with respect to *o*-phenylenediamine. Compound **2.2-Ph** displayed a broad resonance in the ^{11}B NMR spectrum at 25.9 ppm, indicating that there was no interaction between the Lewis-acidic boron and the Lewis-basic phosphines. Once the synthetic route for compound **2.2-Ph** was proven successful and reliable, we aimed to synthesize the PBP ligand precursor **2.2-*t*Bu**, which involved the more basic di-*tert*-butylphosphine substituents (Scheme 2.1). Pincer ligands with di-*tert*-butylphosphine substituents have been shown to generate more active metal complexes than their analogous diphenylphosphine counterparts.[14] The decision to evaluate the synthetic route using diphenylphosphine was based on the pyrophoric properties and cost (ca. 6 times more expensive) of di-*tert*-butylphosphine.[95] Compound **2.2-*t*Bu** was synthesized with an isolated yield of 52 % with respect to di-*tert*-butylphosphine. The crystal structure of compound **2.1-*t*Bu** is shown in Figure 2.3. As in the case of compound **2.1-Ph**, the asymmetric unit of the crystal of **2.1-*t*Bu** only represents half of the displayed molecular structure and the other half was generated by symmetry. Contrary to the structure of compound **2.1-Ph**, the substituents on the phosphines in compound **2.1-*t*Bu** are pointing outwards due to the increased steric demand of the *tert*-butyl substituents. The bond lengths and angles of compound **2.1-*t*Bu** are within the expected ranges. No hydrogen bonding involving the N-H hydrogen was observed.

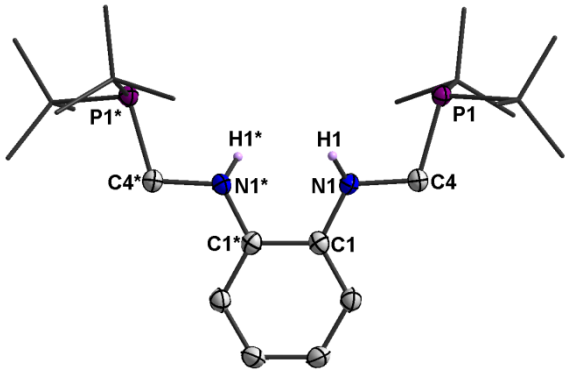

Figure 2.3 Solid-state molecular structure of 2.1-*t*Bu with thermal ellipsoids at 50 % probability, with the exception of the phosphine substituents, which are modeled as "sticks". All hydrogen atoms except for N-H have been omitted for clarity.

2.3 Synthesis and Characterization of Pd Complexes 2.3-Ph and 2.3-*t*Bu featuring PBP Pincer Ligands

Reaction of chloroborane **2.2-Ph** with $[Pd(PPh_3)_4]$ at 45 °C afforded the desired boryl transition metal complex **2.3-Ph** via oxidative addition of the B-Cl bond to the metal center (Scheme 2.2). The signal in the ^{11}B NMR spectrum shifted from 25.9 ppm to 38.9 ppm. This value is comparable to the values reported by Tanaka and coworkers for palladium complexes featuring monodentate diazaboryls ($[(dmpe)Pd(SnMe_3)(B\{N(Me)CH_2\}]$ δ = 46.9 ppm, and $[(Me_3P)_2PdCl(B\{N(Me)CH_2\}_2]$ δ = 40 ppm), supporting the formation of the Pd-B bond.[77,96] The downfield shift of the ^{31}P NMR signal from -20.3 ppm to 43.0 ppm confirmed the coordination of the phosphines to the palladium center. X-ray quality single crystals of complex **2.3-Ph** were grown from a saturated solution in CH_2Cl_2 at -35 °C. The molecular structure of **2.3-Ph** is shown in Figure 2.4. The asymmetric unit of the crystal only represents half of the molecular structure displayed and the other half was generated by symmetry.

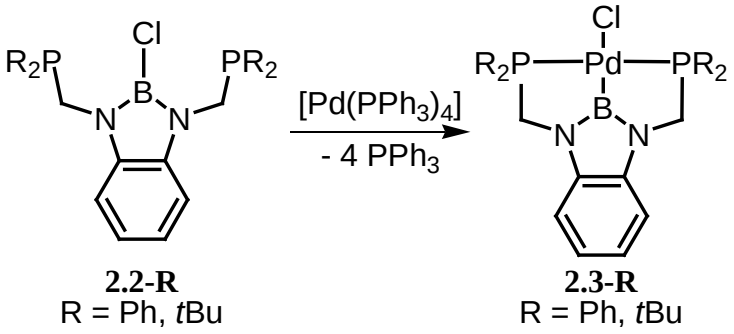

2.2-R
R = Ph, *t*Bu

2.3-R
R = Ph, *t*Bu

Scheme 2.2 Synthesis of PBP palladium complexes 2.3-Ph and 2.3-*t*Bu.

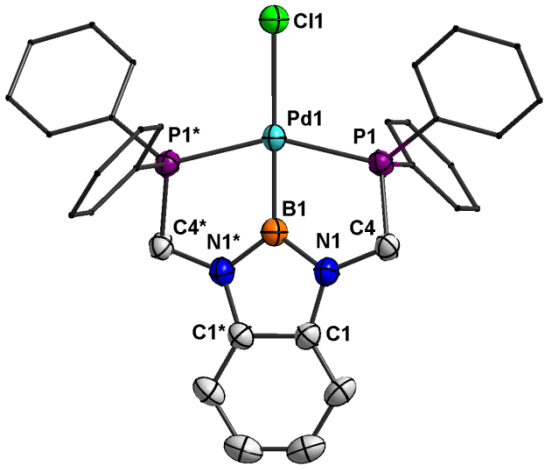

Figure 2.4 Solid-state molecular structure of 2.3-Ph with thermal ellipsoids at 50 % probability, with the exception of the phosphine substituents, which are modeled as "sticks". All hydrogen atoms have been omitted for clarity.

For the case of the PBP pincer ligand precursor with *tert*-butyl phosphine substituents, **2.2-*t*Bu**, the reaction with $[Pd(PPh_3)_4]$ had to be carried out at 100 °C in toluene in order to promote oxidative addition to the metal center. The harsher conditions required could be related to the higher steric demand of the bulky *tert*-butyl substituents. The success of the synthesis of the boryl complex **2.3-*t*Bu** was confirmed by the downfield shift of the ^{11}B NMR signal from

25.8 ppm to 38.6 ppm. The ^{31}P NMR signal also displayed the expected downfield shift from 16.1 ppm for the ligand precursor **2.2-*t*Bu** to 88.3 ppm for complex **2.3-*t*Bu**, supporting the coordination of the phosphines to the palladium. Attempts to obtain X-ray quality crystals of **2.3-*t*Bu** were unsuccessful.

Soon after obtaining the crystal structure of complex **2.3-Ph**, Nozaki and co-workers reported the synthesis of PBP pincer ligand precursor **2.a-*t*Bu**, which is closely related to **2.2-*t*Bu**, as well as the corresponding iridium complex **2.b-*t*Bu** (Scheme 2.3).[83] The premise of their research was the same: the incorporation of a boryl moiety into a pincer scaffold should help stabilize the M-B bond so that the strong electron donating ability of the boryl ligand could be exploited. The stabilization of the M-B bond was proven by the authors with the isolation of the first example of an ethylene-coordinated boryl complex.[83] The authors reported three ligand precursors based on the same pincer scaffold as that of compound **2.a-*t*Bu**, but with phenyl and cyclohexyl substituents at the phosphorus center, **2.a-Ph** and **2.a-Cy**, as well as their iridium complexes **2.b-Ph** and **2.b-Cy** (Scheme 2.3).[97] At the same time, Mirkin and co-workers reported *m*-carborane-based SeBSe and SBS pincer ligand precursors, **2.c** and **2.d**, and their palladium complexes, **2.e** and **2.f** (Scheme 2.4).[84] Later on, Hill and co-workers reported a ruthenium complex **2.g,** (Figure 2.5) with the phenyl-substituted ligand **2.a-Ph** reported by Nozaki.[97,98] More recently, Nakamura and coworkers reported a series of *m*-carborane-based NBN pincer ligand precursors, **2.h**, and their Ni, Pd and Rh complexes **2.i**, **2.j** and **2.k**, respectively (Scheme 2.4).[99] Nozaki and co-workers also reported rhodium complex **2.l**, with ligand **2.a-*t*Bu** (Figure 2.5).[100] Selected bond lengths and angles for complex **2.3-Ph**, as well as reported, related PBP pincer complexes are summarized in Table 2.1.

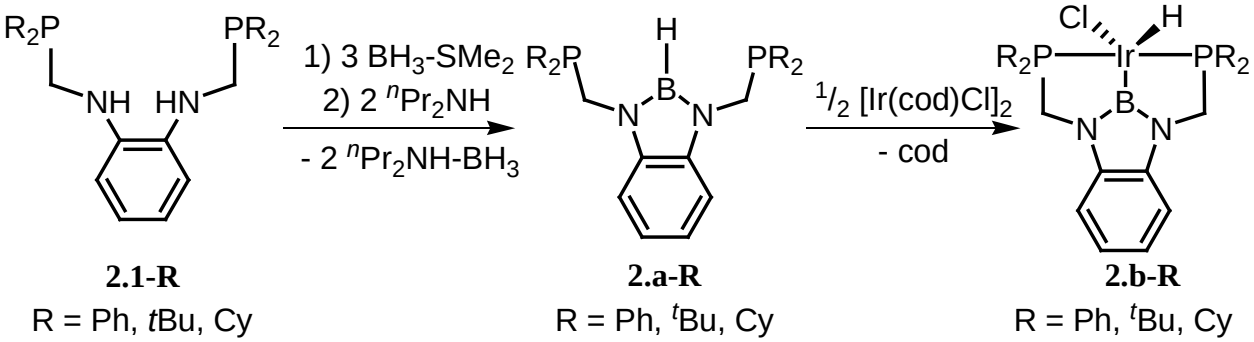

Scheme 2.3 Reported synthesis of hydroborane PBP ligand precursors 2.a-R and their [(PBP)IrHCl] complexes 2.b-R.

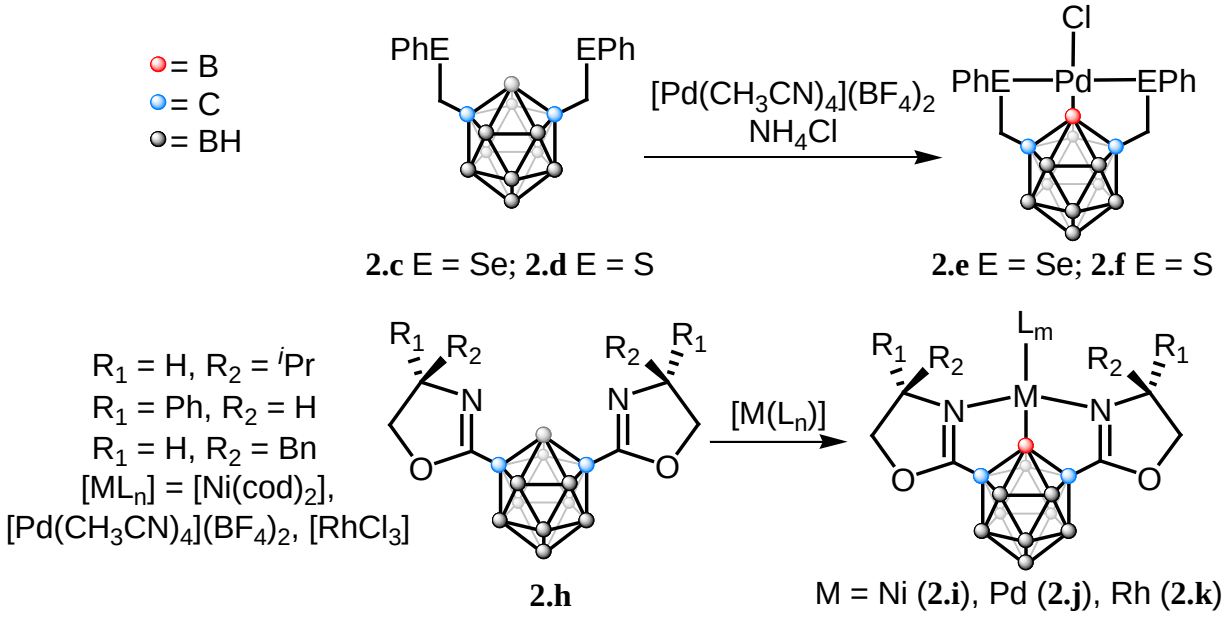

Scheme 2.4 Reported *m*-carborane based SeBSe and SBS ligand precursors 2.c and 2.d and their Pd complexes 2.e and 2.f, as well as NBN ligand precursors 2.h and their Ni (2.i), Pd, (2.j), and Rh (2.k) complexes.

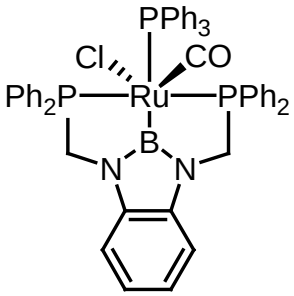

2.g

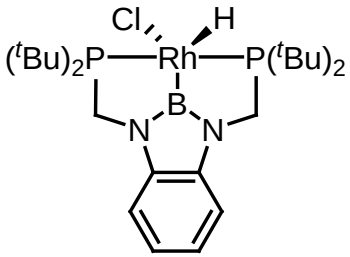

2.l

Figure 2.5 Reported complexes 2.g and 2.l.

Table 2.1 Selected bond lengths (Å) and angles (°) for PBP palladium complex 2.3-Ph, and reported PBP Ir complexes 2.b-R (R = *t*Bu, Cy), PBP Rh complex 2.l, and PBP Ru complex 2.g.

Parameter	**2.3-Ph**	**2.b-*t*Bu**	**2.b-Cy**	**2.l**	**2.g**
B-M	1.997(8)	1.971(6)	1.979(5)	1.980(7)	2.051(15)
P-M	2.321(1)	2.3273(12) 2.3357(12)	2.3103(13) 2.3109(13)	2.3417(16) 2.3431 (16)	2.369(3) 2.366(3) 2.510(4)$^{+}$
B-N	1.412(6)	1.429(7) 1.437(7)	1.435(6) 1.428(6)	1.412(9) 1.434(8)	1.459(16) 1.454(15)
M-Cl	2.468(2)	2.3963(14)	2.3836(13)	Not reported	2.496(3)
P-M-P	152.80(5)	158.12(5)	157.11(4)	158.08(6)	153.48(12) 101.5(1)$^{+}$ 104.9(1)$^{+}$
N-B-N	107.64(2)	105.8(5)	106.6(4)	107.1(6)	103.9(11)
B-M-Cl	180.00(0)*	157.67(17)	144.03(16)	Not reported	74.7(4) 175.8(2)$^{+\#}$

* The elements lay in a symmetry axis hence the positions were idealized. $^{+}$ With the PPh_3 ligand. $^{\#}$ B-M-P angle.

The metric parameters of the solid-state molecular structure of complex **2.3-Ph** are comparable with those of the other reported complexes with a PBP pincer ligand. The P-M-P bond angles for all synthesized complexes are at the narrow end of the range for metal complexes with PEP pincer ligands (E = C, N).[14,17] The Pd-B bond distance in complex **2.3-Ph** (1.997(8) Å) is statistically equivalent to those of the only other two Pd complexes with an "XBX" pincer ligand reported: **2.e** (1.982(3) Å, X = Se), and **2.f** (1.983(4) Å, X = S).[84] The Pd-Cl bond distance in complex **2.3-Ph** (2.468(2) Å) is the longest Pd-Cl bond distance reported for a four-coordinate Pd in a pincer ligand complex and the second longest for any Pd complex with a pincer ligand. The only Pd pincer complex, **2.m**, with a longer Pd-Cl bond distance (2.685(6) Å) is shown in Figure 2.6.[101] The longer Pd-Cl bond in complex **2.3-Ph** confirms the stronger *trans*-influence expected for the boryl ligand. Furthermore the Pd-Cl bond in **2.3-Ph** is longer than those measured for the only two other structurally characterized boryl pincer complexes of Pd, **2.e** (2.437(3) Å), and **2.f** (2.417(4) Å) implying that this ligand is the best electron donating boryl pincer.[84]

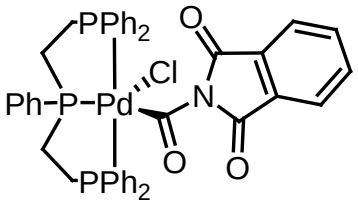

2.m

Figure 2.6 Pd pincer complex 2.m, the only reported Pd pincer complex with a Pd-Cl bond distance longer than that in complex 2.3-Ph

2.3.1 Reactivity of (PBP)Pd Complex 2.3-Ph

Palladium complexes are well known for their ability to catalyze cross-coupling reactions. In particular, some palladium pincer complexes have been proven incredibly successful in Heck cross-coupling reactions (TON 8.9 x 10^6, TOF 4 x 10^5 h^{-1}), with over 100 coupling reactions per second.[102] The ability of complex **2.3-Ph** to catalyze the cross-coupling reaction of bromobenzene and styrene was investigated (Scheme 2.5), following reaction conditions from a reported synthesis that used a related palladium pincer catalyst.[103,104]

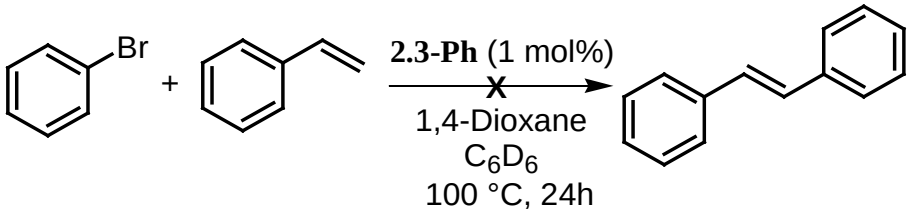

Scheme 2.5 Attempted cross-coupling reaction between bromobenzene and styrene with complex 2.3-Ph as catalyst.

The cross-coupling reaction was monitored via ^{1}H NMR spectroscopy, with naphthalene as an internal standard. Surprisingly, complex **2.3-Ph** did not catalyze the cross-coupling reaction between bromobenzene and styrene. After one day of heating at 100 °C, no appreciable conversion was observed. The presence of the catalyst in the reaction mixture even after heating was confirmed via ^{31}P NMR spectroscopy. The spectrum showed the expected signal at 42.7 ppm, which corresponds to complex **2.3-Ph**.

2.4 Synthesis and Characterization of SBS Pincer Ligand Precursor 2.5

During the design of a synthetic route for compounds **2.3** (Scheme 2.2), there was concern with the possibility of the phosphorus atoms coordinating to the boron center, generating a strong Lewis acid-base adduct and thus preventing the formation of the diazaborole ring. Even though this was later found not to be the case, the synthesis of a ligand precursor, in which the phosphines were oxidized with sulfur was investigated (Scheme 2.6). Sulfur was employed as a protecting group since it is a weaker Lewis base in comparison to phosphines (BH_3•SMe_2 is an excellent BH_3 source in several reactions),[105] and methods to reduce phosphanethiones are well described.[106-108]

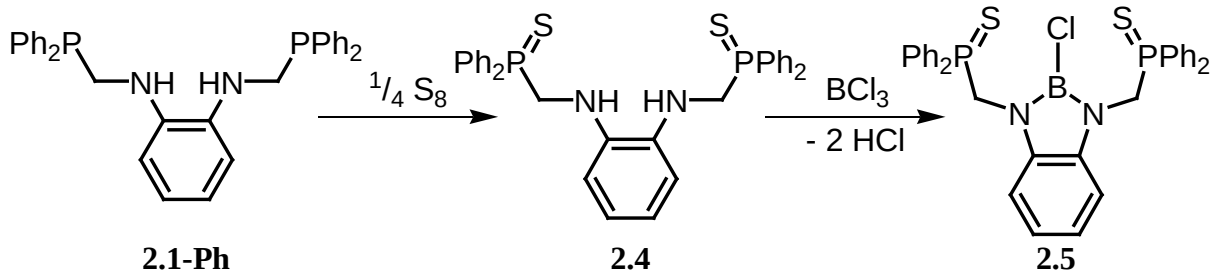

2.1-Ph **2.4** **2.5**

Scheme 2.6 Synthesis of SBS pincer ligand precursor 2.5.

The oxidation of the phosphines in compound **2.1-Ph** was carried out with elemental sulfur in CH_2Cl_2, yielding compound **2.4** as a yellow crystalline solid. The ^{31}P NMR signal for compound **2.4** is downfield shifted (δ = 41.7 ppm) in comparison to that of **2.1-Ph** (δ = -18.1 ppm), confirming the successful oxidation of the phosphorus atoms. X-ray quality crystals of compound **2.4** were obtained by slow evaporation of a saturated solution in CH_2Cl_2 at -35 °C (Figure 2.7). All bond lengths and angles of **2.4** fall within the expected ranges. The phenyl substituents on the phosphines are pointing outwards from the N-H bond, in contrast

to what was observed for the non-sulfonated compound **2.1-Ph**. The sulfur atoms point inwards and the P=S bonds align with the N-H bonds on the same half of the molecule (torsion angles: S1-P1-N1-H1 = 7.1(1)°, S2-P2-N2-H2 = 2.9(1)°). The S···H distances (S1···H1 2.82(3) Å, and S2···H2 2.85(3) Å) are below the sum of the van der Waals radii (2.89 Å) and suggest hydrogen bonding.[109]

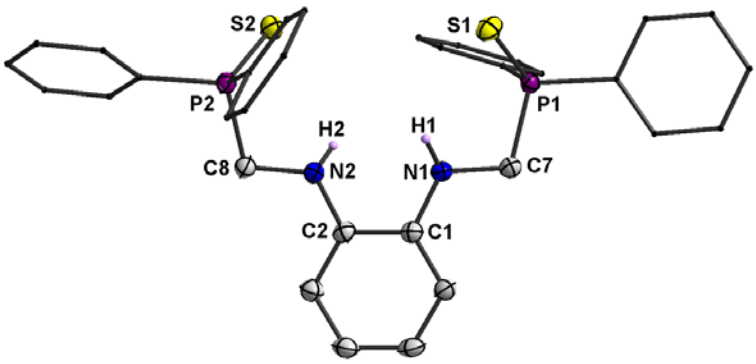

Figure 2.7 Solid-state molecular structure of 2.4 with thermal ellipsoids at 50 % probability, with the exception of the phosphine, substituents which are modeled as "sticks". All hydrogen atoms except for the N-H, and a CH_2Cl_2 solvent molecule have been omitted for clarity.

One equivalent of BCl_3 was reacted with **2.4** in order to generate the chlorodiazaborane **2.5** (Scheme 2.6). The ^{11}B NMR spectrum of a reaction sample right after addition of the BCl_3 displayed a sharp signal at δ = 10.1 ppm. The chemical shift of this NMR signal is similar to those reported for BCl_3 Lewis acid-base adducts with amines (10.0 ppm for BCl_3•NEt_3, and 10.2 ppm for BCl_3•NMe_3),[110,111] suggesting the formation of a Lewis acid-base adduct between the BCl_3 and one of the amine moieties of compound **2.4**. Coordination of the sulfur to BCl_3 should have given rise to an ^{11}B NMR chemical shift similar to that observed for the BCl_3•SMe_2 (7.1 ppm),[112] BCl_3•$S(CH)_4$ (7.5 ppm) and BCl_3•$S(CH_2)_4$ (7.9 ppm)[113] adducts. The ^{31}P NMR

spectra of the reaction mixture showed no appreciable change in the chemical shift of the phosphorus signal in relation to that of pure **2.4**, further suggesting that the boron center was not coordinating to the sulfur. The reaction mixture was heated and the progress of the reaction monitored by ^{11}B and ^{31}P NMR spectroscopy. The ^{11}B NMR spectra of compound **2.5** displayed a broad signal at 27.2 ppm, supporting the formation of the diazaborole ring. Crystals of **2.5** suitable for structural determination were obtained from a saturated solution in benzene (Figure 2.8). Selected bond lengths and angles of compound **2.5** are summarized in Table 2.2 (*vide infra*) and will be discussed in Section 2.5.

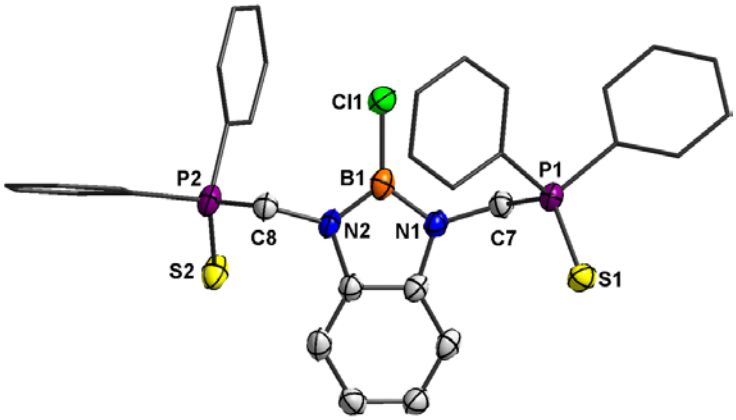

Figure 2.8 Solid-state molecular structure of 2.5, with thermal ellipsoids at 50 % probability, with the exception of the phosphine substituents, which are modeled as "sticks". All hydrogen atoms have been omitted for clarity.

2.4.1 Complexation Attempts with SBS Pincer Ligand Precursor 2.5

Even though the synthesis of PBP pincer ligand precursors **2.3-Ph** and **2.3-*t*Bu** did not require the use of a protecting group on the phosphorus (*vide supra*), compound **2.5** has the potential to be a ligand on its own and its coordination properties were investigated (Scheme 2.7).

Based on the success in the synthesis of complex **2.3-Ph**, the first attempt to synthesize a metal complex of ligand **2.5** involved the reaction with [Pd(PPh_3)$_4$]. When a solution of **2.5** in toluene was reacted with [Pd(PPh_3)$_4$], an immediate colour change from bright yellow to light orange was observed, which was believed to be due to the coordination of the sulfur atoms to the palladium center. Nevertheless, the ^{11}B and ^{31}P NMR spectra of the reaction mixture displayed no change other than the broadening of the signals corresponding to the starting materials. Heating the reaction mixture for over 6 days at 80 °C did not promote the desired reaction to occur. Instead, signs of decomposition were observed via multinuclear NMR spectroscopy. It seems that the triphenylphosphine ligands are too strong to be productively displaced by the weaker coordinating sulfurs, even if the coordination of the ligand precursor **2.5** is entropically favored.

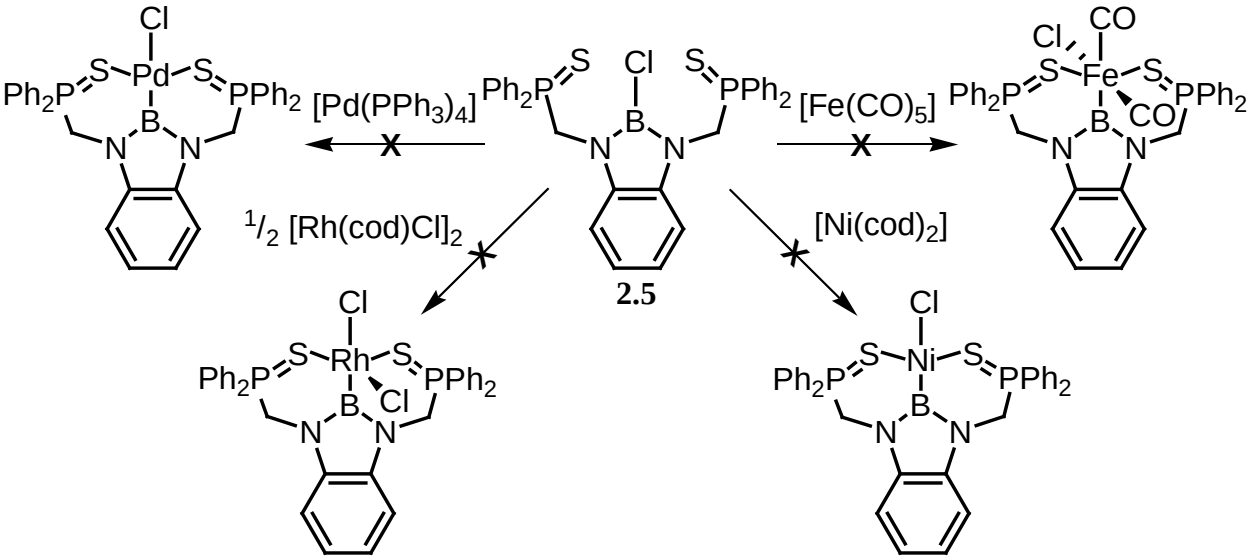

Scheme 2.7 Attempts to synthesize metal complexes with the ligand precursor 2.5.

The reaction of **2.5** with $[Rh(cod)Cl]_2$ was investigated, since the 1,5-cyclooctadiene ligand should be easier to displace than triphenylphosphine. Further, the number of reported boryl complexes of rhodium far exceeds that of palladium.[62] The addition of half an equivalent of $[Rh(cod)Cl]_2$ to a THF solution of **2.5** resulted in a change in colour from bright orange to dark brown in just 30 minutes. The signal in the ^{31}P NMR spectrum of the reaction mixture appeared at 36.5 ppm, which is upfield from that of **2.5** (δ = 39.3 ppm), suggesting sulfur coordination to the rhodium center. The ^{1}H NMR spectra of the reaction mixture revealed the signals corresponding to the free 1,5-cyclooctadiene, confirming its displacement from the rhodium complex. Nevertheless the ^{11}B NMR signal at 26.4 ppm indicated that no oxidative addition to rhodium had taken place. The reaction mixture was thus heated to 65 °C and the reaction progress monitored via multinuclear NMR spectroscopy over a period of 5 days. Unfortunately, no significant change other than minor decomposition was observed over that time. Attempts to isolate the sulfur-coordinated rhodium complex were met without success and no further experimental evidence to support the proposed nature of the complex observed by NMR spectroscopy could be obtained.

In lieu of the observed displacement of the 1,5-cyclooctadiene ligand, the reaction of the ligand precursor **2.5** with $[Ni(cod)_2]$ was also investigated (Scheme 2.7). Similar to what was observed for rhodium, the NMR spectra of the reaction mixture of **2.5** with $[Ni(cod)_2]$ confirmed the coordination of the sulfur atoms to the metal center via the upfield shift of the signal in the ^{31}P NMR spectra (δ = 37.1 ppm) and the presence of the free COD signals in the ^{1}H NMR spectra. Unfortunately, just as was the case for Pd and Rh, no changes in the ^{11}B NMR spectra were observed even after prolonged heating times.

Despite the results obtained for palladium, rhodium, and nickel, one last attempt at activating the B-Cl bond with [$Fe(CO)_5$] was carried out (Scheme 2.7). The motivation for this came from the numerous literature reports where iron was found to successfully activate B-X bonds.[62] Displacement of the carbonyl ligands from the [$Fe(CO)_5$] under UV-irradiation should further promote the oxidative addition reaction. Nevertheless no reaction, other than potential sulfur coordination, was observed between the [$Fe(CO)_5$] and the SBS ligand precursor **2.5**, even after irradiation with UV-light (λ = 254 nm) for 48 h in a mini-Rayonet photo reactor.

2.5 Synthesis and Characterization of SBS Pincer Ligand Precursor 2.6

In view of the failed attempts to oxidatively add the B-Cl bond in compound **2.5** to a transition metal center, and considering the large number of literature reports on oxidative additions of B-H bonds,[40] it was decided to reduce compound **2.5** to borane **2.6** (Scheme 2.8).

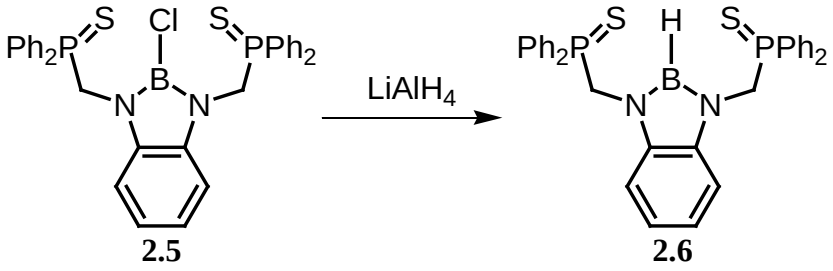

2.5 **2.6**

Scheme 2.8 Synthesis of compound 2.6 via the reduction of compound 2.5.

Compound **2.5** was reacted with 1 equivalent of $LiAlH_4$, generating the desired SBS-H ligand precursor **2.6**. The successful reduction of **2.5** into **2.6** was confirmed by the presence of a signal in the $^1H\{^{11}B\}$ NMR spectrum (δ = 4.52 ppm) corresponding to the B-H proton, which was only observable in the boron decoupled spectrum. The signal in the $^{11}B\{^1H\}$ NMR spectrum

of **2.6** (δ = 24.3 ppm) was upfield with respect to that of **2.5** (δ = 27.2 ppm). The corresponding signal in the ^{11}B NMR spectrum of **2.6** was a doublet (d, δ = 24.3, $^{1}J_{BH}$ = 140.1 Hz), further confirming that the reduction had taken place. X-ray quality crystals of compound **2.6** were obtained from slow evaporation of a saturated solution in THF at -35 °C (Figure 2.9). Select bond length and angles for **2.6** are summarized in Table 2.2.

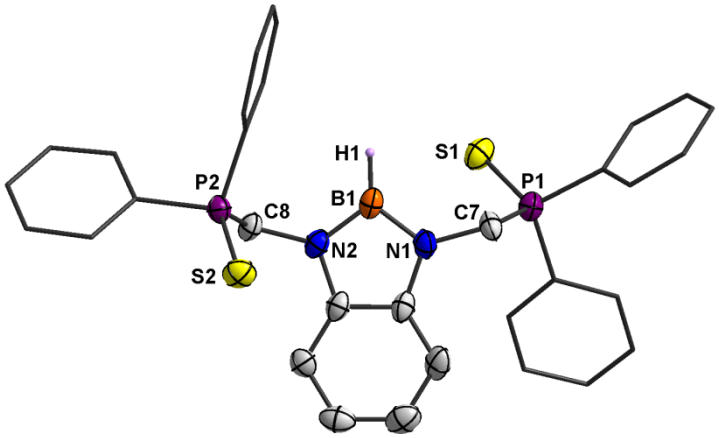

Figure 2.9 Solid-state molecular structure of 2.6 with thermal ellipsoids at 50 % probability, with the exception of the phosphine substituents, which are modeled as "sticks". All hydrogen atoms except for B-H have been omitted for clarity.

Table 2.2 Selected bond lengths (Å) and angles (°) for SBS ligand precursors 2.5 and 2.6, and the reported PBP ligand precursors 2.a-Ph,[97] and 2.a-*t*Bu.[83]

Parameter	2.5	2.6	2.a-Ph	2.a-*t*Bu
B-Cl	1.751(8)	-	-	-
B-H	-	1.07(5)	1.16(4)	1.08(2)
B-N	1.427(9), 1.416(9)	1.424(9), 1.428(9)	1.431(6), 1.428(5)	1.423(3), 1.424(3)
P-S	1.945(2), 1.949(3)	1.954(3), 1.949(3)	-	-
N-B-N	107.9(6)	106.1(7)	106.7(3)	107.7(2)

The metric parameters for compounds **2.5** and **2.6** are within the expected ranges, and are comparable to those reported by Nozaki and coworkers for the unsulfonated analogs **2.a-Ph** and **2.a-*t*Bu**.[83,97]

2.5.1 Complexation Attempts with SBS Pincer Ligand Precursor 2.6

Attempts to synthesize metal complexes of the pincer ligand precursor **2.6** were carried out as shown in Scheme 2.9. The metal reagents chosen were $[Rh(cod)Cl]_2$ and $[Fe(CO)_5]$.

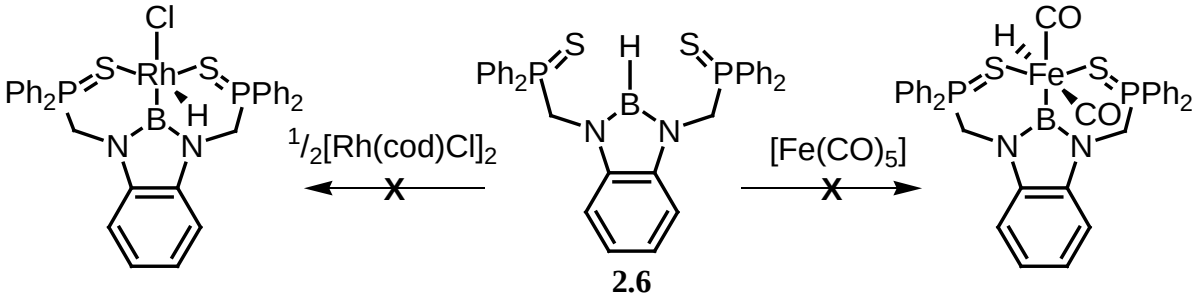

Scheme 2.9 Attempts to synthesize metal complexes with the ligand precursor 2.6.

Disappointingly, both reactions failed to produce the desired metal complexes. Similarly to what was observed for compound **2.5**, NMR spectroscopy only indicated potential coordination of the sulfur atoms to the metal center, without activation of the B-H bond. Attempts to isolate the metal complexes with the sulfur bound ligand were met without success.

The failure to synthesize metal complexes with the SBS ligand precursors **2.5** and **2.6**, the lack of catalytic activity observed for the palladium complex **2.3-Ph**, and the reports by Nozaki of the Ir and Rh complexes **2.b** and **2.l**,[83,100] prompted us to investigate new boryl pincer ligand architectures.

2.6 Towards Acyclic Boryl Pincer Ligand Precursors

In principle, pincer ligands based on acyclic backbones should coordinate to metal centers more effectively than their cyclic analogs, owing to their reduced geometric constraints.[3] An implication of this would be better orbital overlap, and thus better electronic communication between the ligand and the metal center. Metal complexes of pincer ligands with acyclic backbones have been found to possess enhanced or unique reactivity in comparison to complexes with analogous cyclic backbones.[34,114-117] With this in mind, we set out to synthesize an acyclic pincer ligand with a central boryl donor.

2.6.1 Synthetic Attempts

2.6.1.1 Acyclic PBP Pincer Ligand Precursors with Phosphine Amine Pendant Arms

Based on the knowledge obtained during the synthesis of the cyclic boryl ligand precursors **2.2-Ph** and **2.2-*t*Bu**, a synthetic route that involved the functionalization of a primary amine with a phosphinomethanol, followed by reaction with half an equivalent of BCl_3 seemed appropriate (Scheme 2.10).

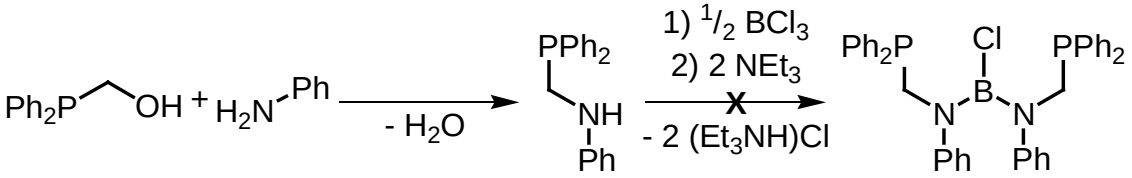

2.7 **2.8-Ph**

Scheme 2.10 Proposed synthesis of acyclic PBP pincer ligand precursor 2.8-Ph.

A paper by Le Floch reporting the synthesis of the phosphine-amine moiety **2.7** was published after the first attempts at its synthesis were carried out.[118] The authors reported the

required experimental conditions to obtain the mono-functionalized amine **2.7**, which were welcomed as all preliminary attempts at this demanding synthesis yielded mixtures of non-, mono- and di-functionalized amines in varying amounts. Phosphine-amine **2.7** was hence synthesized and its purity was assessed by multinuclear NMR spectroscopy prior to use.[118] The reaction of **2.7** with BCl_3 in the presence of triethylamine and under heating at 50 °C failed to generate the desired compound **2.8-Ph**, in contrast to what had been observed for the synthesis of the cyclic analogs **2.2-Ph** and **2.2-*t*Bu** (*vide supra*). Other synthetic attempts to obtain the desired acyclic boryl pincer ligand precursor from the phosphine-amine **2.7** were carried out and are summarized in Scheme 2.11. A variety of reaction conditions were investigated, namely the use of different solvents (THF, benzene, and dichloromethane, the latter with the exception of the deprotonation reaction), the mixing of the reagents at different reaction temperatures (-78 °C, -30 °C, and room temperature). Furthermore, the reaction mixtures were analyzed via multinuclear NMR spectroscopy both prior and during heating at the solvent's boiling point temperature for a period of 48 h. Unfortunately, all attempts to synthesize the acyclic boryl ligand precursor **2.8-Ph** or its borate analog **2.9-Ph** from the phosphine-amine precursor **2.7** were not successful.

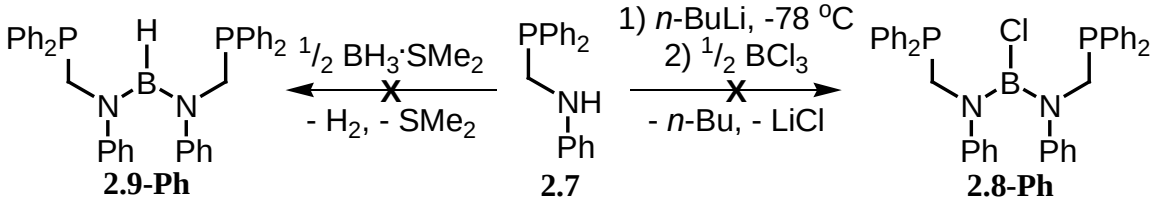

Scheme 2.11 Attempts to synthesize an acyclic PBP pincer ligand precursor from phosphine-amine 2.7.

The next attempt to obtain the desired acyclic pincer ligand precursor with a central boryl donor used 2-diphenylphosphine-1*H*-pyrrole. The proposed synthesis for compound **2.11-Ph** is presented in Scheme 2.12. 2-Diphenylphosphine-1*H*-pyrrole (**2.10**) was synthesized according to a literature procedure, and its purity was confirmed by multinuclear NMR spectroscopy prior to use.[119] The first attempt to synthesize compound **2.11-Ph** involved the reaction of 2 equivalents of **2.10** with half an equivalent of BCl_3. The ^{31}P and ^{11}B NMR spectra of the reaction mixture obtained right after addition of half an equivalent of BCl_3 displayed similar results as those observed during the synthesis of compounds **2.2-Ph** and **2.2-*t*Bu**, namely the presence of the signals arising from the formation of a Lewis acid-base adduct between the phosphorus atom and the boron center. The reaction mixture was stirred at room temperature for 48 h and the reaction progress was monitored every 12 h, after which it was concluded that the reaction was not proceeding at room temperature. The reaction mixture was then heated to 45 °C for 2 h and analyzed via multinuclear NMR spectroscopy. Unfortunately, this indicated that an intractable mixture of products was obtained. Furthermore, no difference was observed when the reaction was carried out in the presence of triethylamine as a base. Other attempts to synthesize compound **2.11-Ph** and its borate analog **2.12-Ph** were carried out (Scheme 2.13). The same reaction conditions as those employed in the attempts to synthesize compounds **2.8-Ph** and **2.9-Ph** (*vide supra*) were also employed in the attempted synthesis of compounds **2.11-Ph** and **2.12-Ph**. Unfortunately, similar to what was observed for the synthesis of **2.8-Ph** and **2.9-Ph**, all attempts to synthesize compounds **2.11-Ph** and **2.12-Ph** failed.

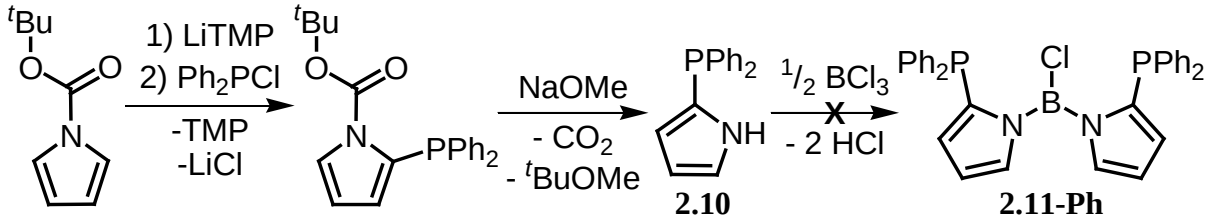

Scheme 2.12 Proposed synthesis for PBP pincer ligand precursor 2.11-Ph.

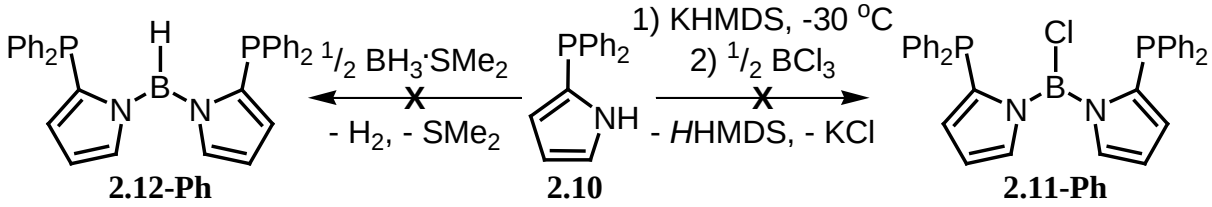

Scheme 2.13 Attempts to synthesize an acyclic PBP pincer ligand precursor from 2-phosphine-1*H*-pyrrole, 2.10.

2.6.1.2 Acyclic PBP Pincer Ligand Precursors with Phosphinomethoxy Pendant Arms, **2.13-Ph**

The least synthetically intensive of the attempts to generate an acyclic PBP pincer ligand precursor involved the reaction of one equivalent of diphenylphosphinomethanol with BCl_3 (Scheme 2.14). The reaction was carried out in the presence of triethylamine as a base, and was heated at 80 °C overnight to ensure completion. The ^{11}B NMR spectra of **2.13-Ph** showed a broad signal at 18.3 ppm which was slightly upfield shifted from that observed for other borochloridates (24.3 ppm for $(MeO)_2BCl$,[110] 23.3 ppm for $(EtO)_2BCl$,[120] and 22.0 ppm for $(PhO)_2BCl$[121]). The $^{31}P\{^1H\}$ NMR spectrum of **2.13-Ph** shows a signal at -11.2 ppm, which is upfield shifted with respect to that of diphenylphoshphinomethanol (-9.9 ppm). The small difference in the ^{31}P NMR chemical shift between the signal of the product and the starting material might indicate that no reaction had taken place, but a similarly small change

was also observed between the signals on the ^{31}P NMR spectra of the non-borylated compounds **2.1-Ph** and **2.1-*t*Bu**, and the borylated compounds **2.2-Ph** and **2.2-*t*Bu** (*vide supra*). In the ^{1}H NMR spectra, the disappearance of the signal corresponding to the -OH proton of the diphenylphosphinomethanol and the broadening and slight down field shift (4.43 ppm to 4.38 ppm) of the signal corresponding to the CH_2 linkers between the phosphorus and the oxygen atoms further support the successful synthesis of compound **2.13-Ph**.

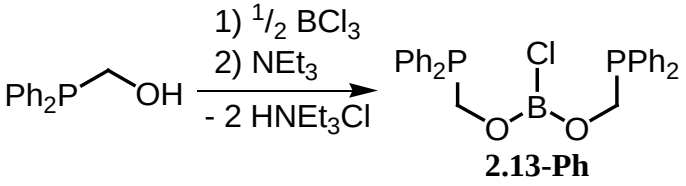

2.13-Ph

Scheme 2.14 Synthesis of acyclic PBP pincer ligand precursor 2.13-Ph.

Compound **2.13-Ph** was isolated as a thick colorless solvent-containing oil, due to its high solubility in most common organic solvents. Although ligand precursor **2.13-Ph** could not be isolated in pure state, studies of its coordination properties (Scheme 2.15) were carried out in hopes that its metal complexes would be easier to purify. Unfortunately though, the reactions of compound **2.13-Ph** with $[Pd(PPh_3)_4]$, $[Pd(Cp)(C_3H_5)]$, and $[Rh(cod)Cl]_2$ yielded intractable mixtures. It appears that the acyclic B-O bond in **2.13-Ph** is too reactive.

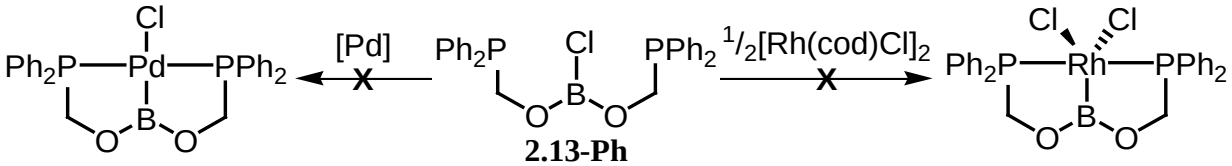

2.13-Ph

[Pd] = $[Pd(PPh_3)_4]$, $[Pd(Cp)(C_3H_5)]$

Scheme 2.15 Attempts to synthesize metal complexes of the acyclic PBP ligand precursor 2.13-Ph.

2.6.1.3 Acyclic NBN Pincer Ligand Precursor with Aniline Pendant Arms, **2.17-Me**

The last attempt to synthesize a boryl pincer ligand with an acyclic backbone that will be discussed here (Scheme 2.16) involved the use of *N*,*N'*-dimethylaniline as the pincer scaffold pendant arms. The proposed synthetic pathway was inspired by the work done by Roesler, et al. on the synthesis of ansa-aminoborane (2-[bis(pentafluorophenyl)boryl]-*N*,*N'*-diphenylaniline).[122] The synthesis of compound **2.14-Me** involved the reaction of 2-lithio-*N*,*N'*-dimethylaniline with half an equivalent of trimethoxyborane in toluene/hexanes (4:1) at -78 °C, followed by warming the reaction to room temperature overnight. Filtration of the precipitated lithium methoxide, and removal of volatiles under vacuum yielded a yellow oil (95 % crude yield).

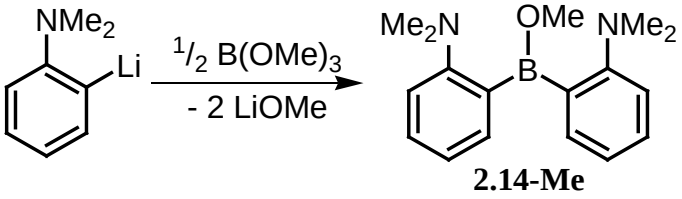

2.14-Me

Scheme 2.16 Proposed route for the synthesis of compound 2.14-Me.

The ^{1}H NMR spectra of the isolated oil was complex and appeared to be due to a mixture of products. However, the ^{11}B NMR spectra only featured two singlet signals, a broad one at 5.1 ppm and a sharp one at 3.3 ppm. The contrast between the simplicity of the ^{11}B NMR spectra and the complexity of the ^{1}H NMR spectra indicated that side reactions could have been taking place, rendering the obtained compound less symmetric than the expected product **2.14-Me**, thus complicating the ^{1}H NMR spectra but not the ^{11}B NMR one.

In order to separate the components of the reaction mixture, crystallization attempts in different solvent systems were performed. Two of these recrystallization attempts, one involving the slow evaporation of a concentrated solution in hexanes at -30 °C, and the other the slow evaporation of a concentrated solution in benzene at room temperature yielded X-ray quality crystals of two of the compounds present in the reaction mixture (**2.15-Me** and **2.16-Me**·LiOMe, Figure 2.10). The structures for compounds **2.15-Me** and **2.16-Me**·LiOMe are presented in Figure 2.11 and Figure 2.12, respectively, and selected bond lengths and angles summarized in Table 2.3. Unfortunately, only small amounts of the crystals of each compound could be obtained and hence they could not be fully characterized.

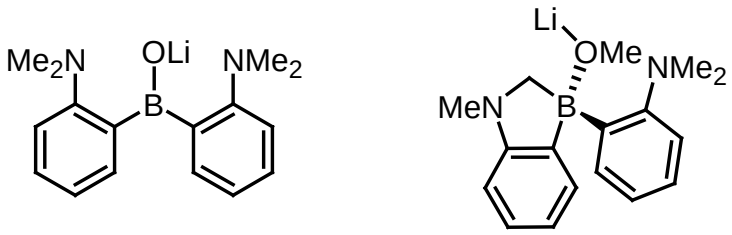

2.15-Me **2.16-Me**·LiOMe

Figure 2.10 Compounds 2.15-Me and 2.16-Me·LiOMe obtained during the attempted synthesis of compound 2.14-Me

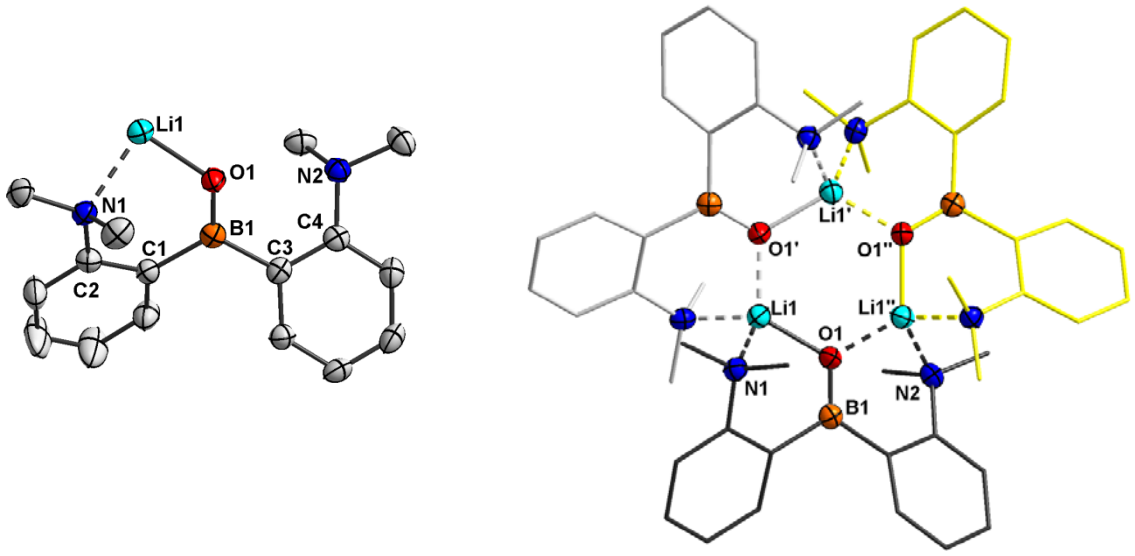

Figure 2.11 Left: Monomeric fragment of the solid-state molecular structure of 2.15-Me with thermal ellipsoids at 50 % probability; right: trimeric structure adopted by compound 2.15-Me in the solid-state with heteroatoms represented with thermal ellipsoids at 50 % probability and the organic framework modeled as "sticks". All hydrogen atoms have been omitted for clarity.

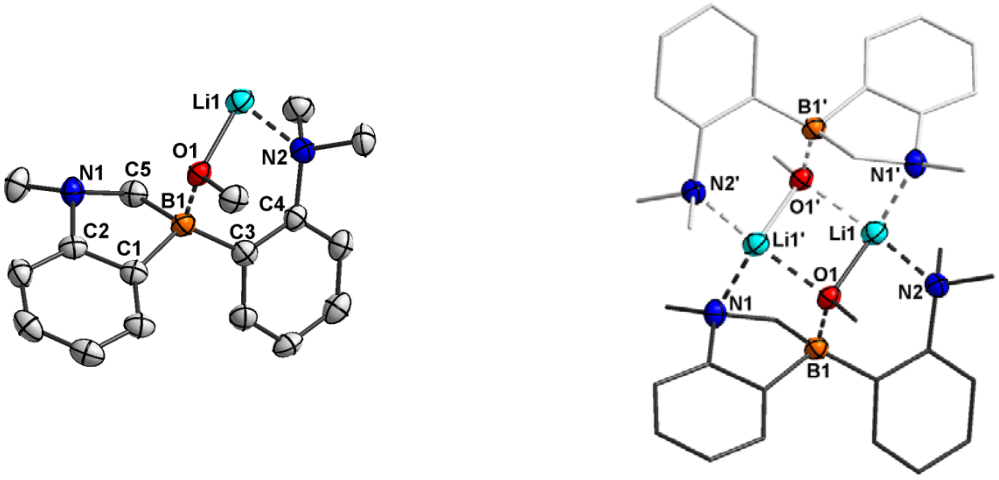

Figure 2.12 Left: Monomeric fragment of the solid-state molecular structure of 2.16-Me·LiOMe with thermal ellipsoids at 50 % probability; right: dimeric structure adopted by compound 2.16-Me·LiOMe in the solid-state with heteroatoms represented with thermal ellipsoids at 50 % probability and the organic framework modeled as "sticks". All hydrogen atoms have been omitted for clarity.

Table 2.3 Selected bond lengths (Å) and angles (°) for compounds 2.15-Me and 2.16-Me·LiOMe.

Parameter	**2.15-Me**	**2.16-Me**·LiOMe
B1-C1	1.631(4)	1.619(5)
B1-C3	1.609(3)	1.629(5)
B1-C5	-	1.620(7)
B1-O1	1.302(4)	1.549(6)
O1-Li1	1.848(5)	1.915(6)
Li1-O1'	1.851(8)	2.041(7)
N1-Li1	2.222(7)	2.200(9)[a]
N2-Li1	2.212(6)[b]	2.076(7)

Parameter	**2.15-Me**	**2.16-Me**·LiOMe
C1-B1-C3	117.7(2)	119.6(3)
C1-B1-O1	120.5(3)	105.7(3)
C3-B1-O1	121.8(2)	114.4(3)
C1-B1-C5	-	97.1(3)
C3-B1-C5	-	110.5(3)
C5-B1-O3	-	107.6(3)
O1-B1-C2-N1	25.8(2)	82.6(3)
O1-B1-C4-N2	18.8(2)	30.3(3)

[a] N1'-Li1. [b] N2-Li".

Compounds **2.15-Me** and **2.16-Me** appear to be the result of side reactions of the desired compound **2.14-Me**. Specifically, compound **2.15-Me** is the lithium borinate of the borinic acid that would form if the methoxy group on compound **2.14-Me** was to be substituted with a hydroxyl group, and compound **2.16-Me** is the result of an intramolecular reaction between a C-H bond from one of the methyl substituents of the dimethylamino groups and the boron center. The activation product **2.16-Me** co-crystallizes with a lithium methoxide molecule as a Lewis acid-base adduct **2.16-Me**·LiOMe, having a tetra-coordinate boron that has a distorted tetrahedral geometry. On the other hand, the boron in compound **2.15-Me** is tri-coordinate and has a trigonal planar geometry with the sum of the three angles around it adding up to exactly 360°. Compound **2.15-Me** forms trimers in the solid-state, held together by interactions of the lithium with both the oxygen and nitrogen atoms. The core of the trimer is a six-membered Li_3O_3 ring and the boron atoms from the three **2.15-Me** moieties in the trimer lie only 0.068(2)

Å outside of the plane generated by the hexagonal core. Compound **2.16-Me**·LiOMe crystallizes as a dimer, which is also held together by similar interactions of lithium with nitrogen and oxygen atoms. The dimer has a four-membered Li_2O_2 core, however, the boron centers do not lie on the plane generated by the central square, but are 1.415(6) Å away from it. All the lithium atoms in the **2.15-Me** trimer and the **2.16-Me**·LiOMe dimer have distorted tetrahedral geometries.

Based on the nature of compounds **2.15-Me** and **2.16-Me**·LiOMe, it was proposed that the product of their hydrolysis should be the borinic acid **2.17-Me** (Scheme 2.17). Similar hydrolysis of diaryl borinates has been previously reported.[123]

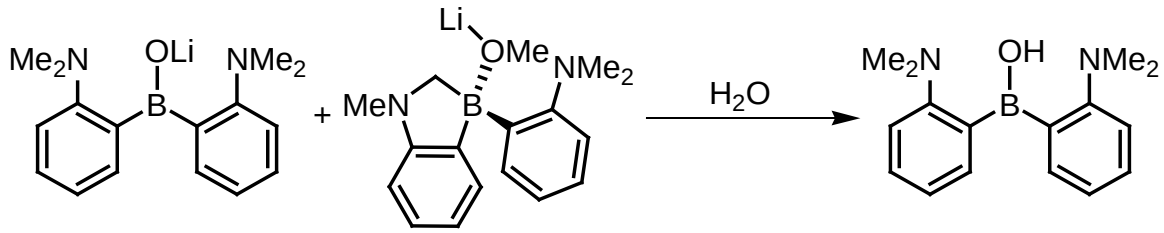

2.15-Me **2.16-Me**·LiOMe **2.17-Me**

Scheme 2.17 Synthesis of 2.17-Me via the hydrolysis of compounds 2.15-Me and 2.16-Me.

The ^{1}H NMR spectra of what is believed to be the expected borinic acid **2.17-Me** obtained in the hydrolysis reaction displayed a singlet at 2.73 ppm, integrating for 12H (corresponding to the methyl protons from the dimethylamino groups), and four multiplets in the aromatic region at 7.23, 7.32, 7.41, and 7.62 ppm, respectively, each one integrating for 2H (corresponding to the protons on the disubstituted phenyl rings). The ^{11}B NMR spectrum of **2.17-Me** displayed only one signal, a broad singlet at 3.9 ppm. Unfortunately due to time constraints, we were unable to investigate the synthesis of the desired NBN pincer ligand

precursor or to fully characterize compound **2.17-Me**, and hence its structure remains unconfirmed at this point.

2.7 Conclusions and Outlook

Along with the groups of Nozaki and Mirkin, we were successful in the synthesis of two of the first known examples of pincer ligands with a central boryl donor (EBE) and their transition metal complexes, which was until recently a missing member of the family of pincer complexes with heteroatom functionalities. Ligand precursors **2.2-Ph** and **2.2-*t*Bu** were reacted with [Pd(PPh_3)$_4$] and [Pd(η^3-C_3H_5)Cp] respectively, in order to generate complexes **2.3-Ph** and **2.3-*t*Bu**, which are the first examples of Pd complexes with a PBP pincer ligand. The observed Pd-Cl bond distance in complex **2.3-Ph** represents the longest Pd-Cl bond observed in a square planar pincer complex, confirming the strong *trans*-influence of the boryl ligand, and suggesting a highly electron rich Pd center. The stability displayed by complex **2.3-Ph** in the presence of styrene under Heck cross-coupling reaction conditions confirmed that the inclusion of the boryl moiety in the central donor position of the pincer scaffold stabilized the reactive M-B bond. However, the lack of reactivity displayed by complex **2.3-Ph** towards a commonplace Heck cross-coupling reaction is puzzling and future work focused on clarifying this observation is required. Furthermore, focus on finding reactions that can take advantage of the high electron density at Pd and, in particular, attempts to remove the counteranion from the coordination sphere in order to generate the more reactive tricoordinate species should be a priority.

Besides the PBP pincer ligands **2.2-Ph** and **2.2-*t*Bu**, the SBS pincer ligand precursors **2.5** and **2.6** were also successfully synthesized. However, attempts to coordinate them to suitable

metal centers were unsuccessful, and activation of the B-Cl bond in compound **2.5** or the B-H bond in compound **2.6** was not observed. Coordination of the sulfur atoms in **2.5** and **2.6** to the metal centers employed could be inferred from the shifts observed for the signals in the ^{31}P NMR spectra. Unfortunately, the sulfur bound metal complexes could not be isolated. Future work regarding ligand precursors **2.5** and **2.6** should involve attempts to isolate these sulfur bound complexes and investigate the viability of promoting the activation of the B-Cl or B-H bond in these metal complexes. Furthermore, attempts to coordinate the ligands with larger metals such as molybdenum and tungsten should also be considered, since these are expected to better accommodate the 6-membered phosphorus and sulfur containing metallacycles. The larger metal centers should force the pincer ligand to increase its bite angle and allow for a closer approach of the metal center to the B-Cl or B-H bond, promoting the oxidative addition reaction.

The synthesis of an acyclic pincer ligand precursor **2.13-Ph** was achieved. Preliminary studies on the coordinating properties of compound **2.13-Ph** were unsuccessful, but more thorough evaluations need to take place. In particular, more attempts at the isolation of the pure ligand precursor should be made, and more studies on its coordination properties towards other metal centers besides rhodium should also be carried out.

Finally, promising results towards the synthesis of a second acyclic pincer ligand precursor, **2.17-Me**, were obtained. The scale-up synthesis of compound **2.17-Me**, as well as the synthesis of similar precursors with bulkier substituents on nitrogen should be a priority. The bulkier substituents at nitrogen should help avoid the formation of activated products such as **2.16-Me**·LiOMe. Promising results towards the synthesis of a 2,2,6,6-tetramethylpyperidine (TMP) substituted compound **2.18-TMP**, analogous to **2.17-Me**, have been recently obtained in

the Roesler Lab (Scheme 2.18). Attempts to exchange the hydroxyl group in compound **2.17-Me** and the methoxy group in compound **2.18-TMP** with either chlorine or hydride are under way. Once the chloride and/or hydride are obtained, attempts to coordinate these compounds to suitable metal centers should be carried out.

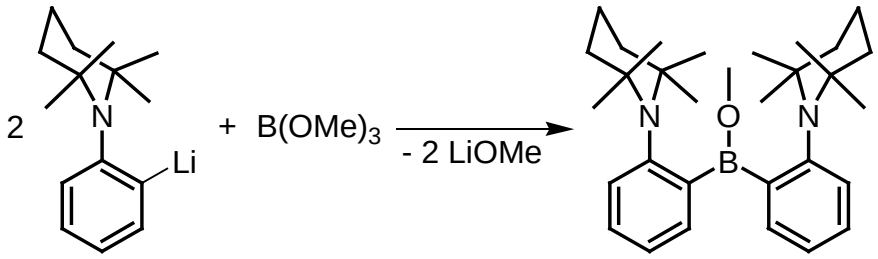

2.18-TMP

Scheme 2.18 Proposed synthesis of compound 2.18-TMP

Chapter Three: **PCP Pincer Ligands with a Central 6-Membered *N*-Heterocyclic Carbene Donor**

3.1 Introduction

N-heterocyclic carbenes (NHCs) have been extensively investigated in light of their outstanding ligand properties, which have rendered them critical components in several catalytic systems.[124] Most NHCs are excellent σ-donors and weak π-acceptors, giving rise to strong M-C bonds.[125] Furthermore, these properties can be successfully altered via synthetic modifications, allowing for the fine tuning of the σ-donor/π-acceptor abilities of NHCs.[126,127]

Despite the strength of the M-C bond in NHC metal complexes, side reactions leading to the cleavage of the M-C bond or functionalization of the carbene carbon, such as migratory insertion,[128-130] reductive elimination,[131] and C-H bond activation[132] have been reported. These side reactions are considered likely candidates for catalyst deactivation pathways that ultimately limit the scope of NHCs in catalysis.[70,133]

Incorporating NHCs into multidentate ligand systems has been shown to generate stable metal complexes.[134-136] The synthesis of pincer ligands with NHC moieties has proven particularly effective, and NHCs have been integrated to pincer scaffolds as donors either at the pendant arms or at the central position (Figure 3.1). Transition metal complexes of such NHC pincer ligands display higher thermal stability without sacrificing catalytic activity.[14,17,106,137]

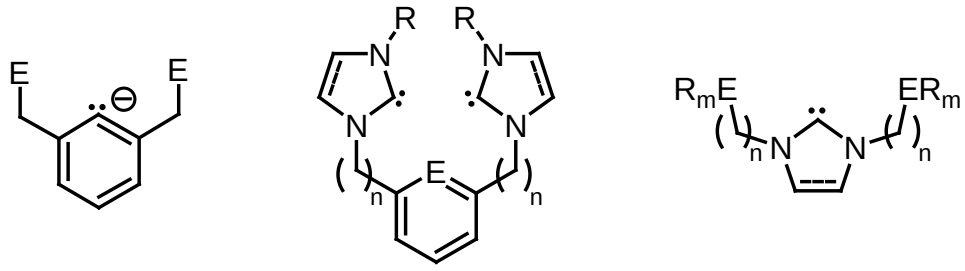

Figure 3.1 Left: classic pincer ligand scaffold; center: pincer ligands with pendant NHC donors; right: pincer ligands with central NHC donor.

The systems having the NHC moieties located at the central donor position of the pincer scaffold (Figure 3.1, right) are expected to be the most effective at stabilizing the M-C bond.[137] A literature search of pincer ligands with a diamino carbene (DAC) in the central donor position returned the series shown in Figure 3.2. Even though the inclusion of the NHC into a pincer ligand scaffold has been shown to stabilize the M-C bond, there are some examples where the pincer metal complexes undergo side reactions under experimental conditions that are common place for catalytic regimes.[138,139] Out of the 34 ligands reported, only **3.a**, **3.e**, **3.h**, **3.i**, **3.z**, **3.D**, and **3.F** generate five membered metallacycles upon coordination. This is a significant distinction with respect to the classical pincer ligands, which commonly generate five membered metallacycles (Figure 3.1, left). Six membered and larger metallacycles give rise to an undesired ring strain that distorts the coordination geometry around the metal center. This strain could render the interaction between the ligand and the metal center weaker, thus reducing the stability of these complexes. None of the carbene-based pincer ligands that generate five membered metallacycles have phosphine donors at the pendant arms, a striking fact considering the prevalence of phosphine donors in pincer chemistry.

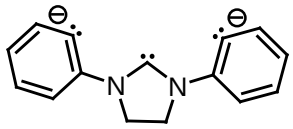

3.a

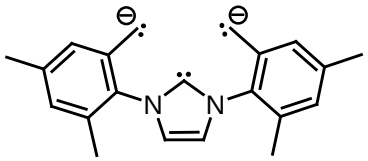

3.b

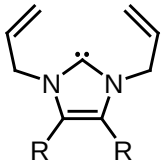

3.c
R = H, Me, Cl

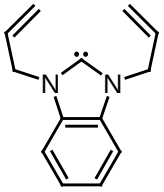

3.d

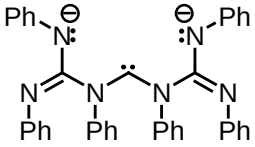

3.e

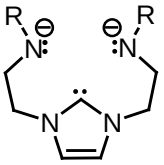

3.f
R = *p*Tol, Mes

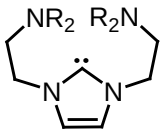

3.g
R = ^{i}Pr

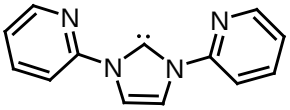

3.h

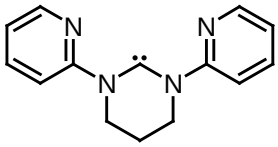

3.i

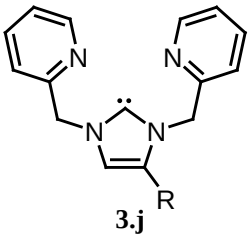

3.j
R = H, I

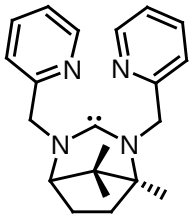

3.k

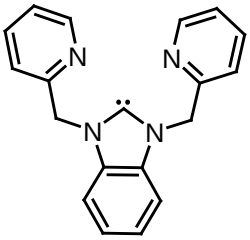

3.l

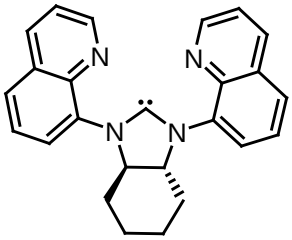

3.m

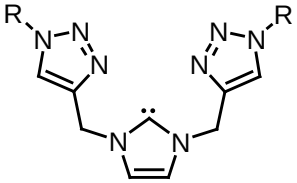

3.n
R = $C_{18}H_{40}$

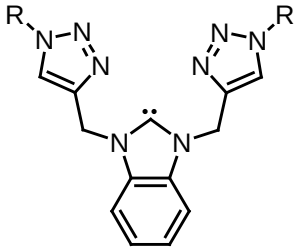

3.o
R = Bz

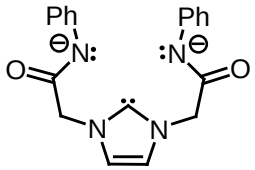

3.p

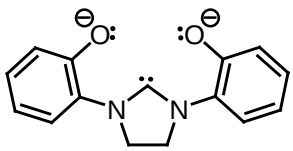

3.q

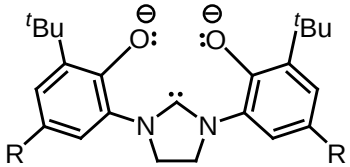

3.r
R = H, ^{t}Bu

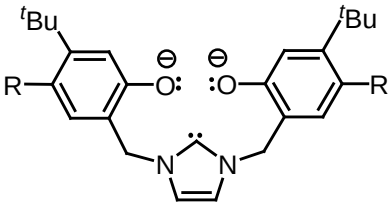

3.s
R = Me, ^{t}Bu

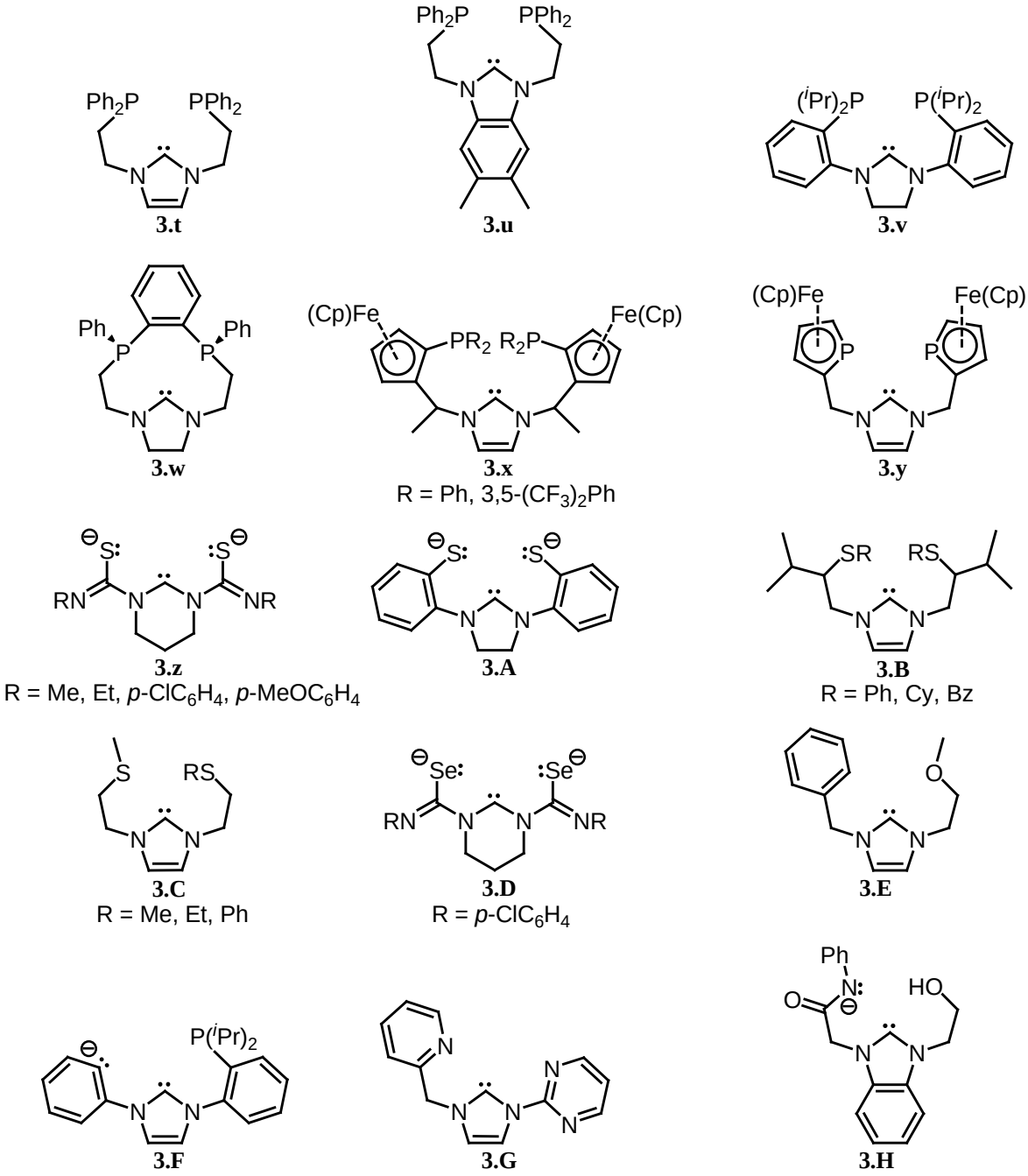

Figure 3.2 Reported pincer ligands with a diamino carbene (DAC) at the central donor position 3.a,[140] 3.b,[141] 3.c,[142] 3.d,[143] 3.e,[144] 3.f,[145,146] 3.g,[147] 3.h,[148] 3.i,[149] 3.j,[150,151] 3.k,[152,153] 3.l,[154,155] 3.m,[156] 3.n,[157] 3.o,[150] 3.p,[158] 3.q,[159] 3.r,[160] 3.s,[161-163] 3.t,[137,164,165] 3.u,[166] 3.v,[106,138,139] 3.w,[167-170] 3.x,[171,172] 3.y,[173] 3.z,[174-178] 3.A,[179] 3.B,[180] 3.C,[181] 3.D,[182] 3.E,[183] 3.F,[139] 3.G,[150] 3.H.[184]

With this in mind, the synthesis of a pincer ligand having phosphine donors at the pendant arms and with an NHC at the central position was targeted (Figure 3.3), which upon coordination would generate five membered metallacycles.

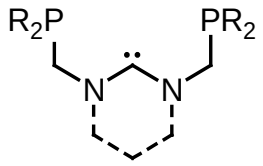

Figure 3.3 Targeted generic pincer ligand precursor with an NHC donor in the central position.

The targeted ligand precursor incorporated a six-membered carbene instead of the more commonly employed five-membered analog. Only four examples of pincer complexes with six membered NHC carbene backbones have been reported (**3.i**, **3.k**, **3.z** and **3.D**, Figure 3.2), despite the ubiquity of pincer ligands with six membered ring backbones. The six-membered ring at the backbone of the pincer ligand gives rise to a relatively wide N-C-N bond angle, pushing the pendant arms of the ligand forward and thus providing a better metal binding pocket. Furthermore, six membered carbenes have been shown to be better σ-donors than their five membered analogs.[185]

3.2 Synthesis and Characterization of PCP Pincer Ligand Precursors H_2(3.1a-Ph) and H_2(3.1b-Ph)

The first step in the proposed synthesis of ligands **3.1a-Ph** and **3.1b-Ph** involved the *N*,*N'*-difunctionalization of 1,3-diaminopropane and 1,8-diaminonaphthalene with two equivalents of diphenylphosphinomethanol (Scheme 3.1), to ultimately yield compounds **3.2a-Ph** and **3.2b-Ph**, respectively. However, the reaction could not be stopped at the stage of

the *N*,*N'*-dialkylation, as had been done in the synthesis of compounds **2.1-Ph** and **2.1-*t*Bu** (Chapter 2).[83,97] Instead, the reaction proceeded to the ring closed products **3.3a-Ph** and **3.3b-Ph**, with concomitant elimination of one equivalent of diphenylphosphine (Scheme 3.1).

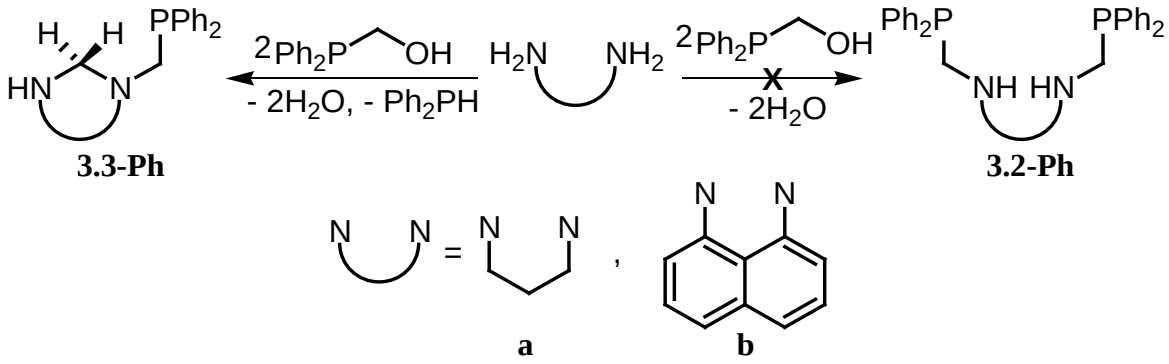

Scheme 3.1 Attempted synthesis of *N*,*N'*-disubstituted diamines 3.2a-Ph and 3.2b-Ph, where the reactions yielded the ring closed compounds 3.3a-Ph and 3.3b-Ph.

When three equivalents of diphenylphosphinomethanol were employed, the disubstituted ring closed products H_2(**3.1a-Ph**) and H_2(**3.1b-Ph**) were obtained. A more efficient synthesis of these compounds starting from the ring-closed hexahydropyrimidine and *2,3*-dihydro-*1H*-perimidine starting materials was employed (Scheme 3.2).

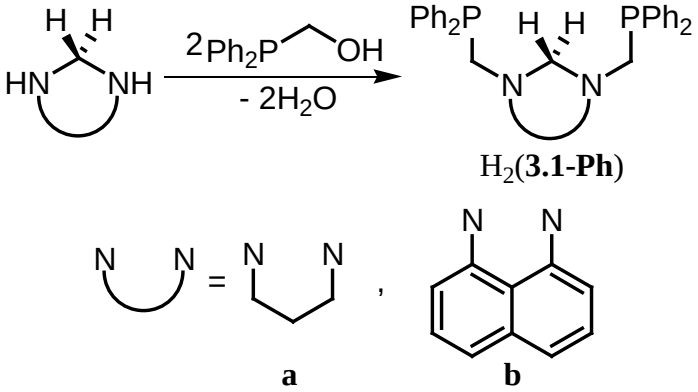

Scheme 3.2 Synthesis of PCP pincer ligand precursors H_2(3.1a-Ph) and H_2(3.1b-Ph).

The ^{1}H NMR spectrum of compound H_2(**3.1a-Ph**) displayed the expected signals for the methylene linkers between the phosphines and the amines at δ = 3.26 ppm (d, $^{2}J_{PH}$ = 4.5 Hz), as well as the methylene moiety between the two amines at δ = 3.67 ppm (s). The ^{1}H NMR spectrum of compound H_2(**3.1b-Ph**) displayed the signals corresponding to both type of methylene linkers (δ = 4.00 ppm, d, $^{2}J_{PH}$ = 4.6 Hz, and δ = 4.18 ppm, s) as well. The ^{31}P NMR spectra of each compound had only one signal, as expected, at δ = -25.9 ppm for $H_{2(}$**3.1a-Ph**), and δ = -25.5 ppm for H_2(**3.1b-Ph**). X-ray quality crystals of compound H_2(**3.1b-Ph**) were obtained via slow evaporation of a concentrated solution in CH_2Cl_2 at -35 °C (Figure 3.4). The metric parameters of the solid-state molecular structure of compound H_2(**3.1b-Ph**) are within the expected ranges.

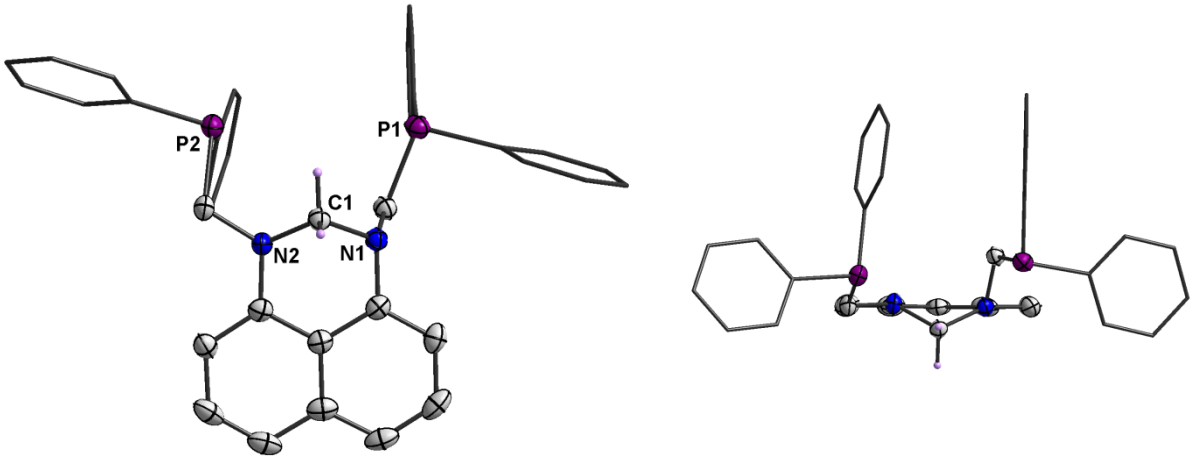

Figure 3.4 Orthogonal views of the solid-state molecular structure of compound H_2(3.1b-Ph) with thermal ellipsoids at 50 % probability, with the exception of the phosphine substituents, which are modeled as "sticks". All hydrogen atoms, except the NCH_2N protons, have been omitted for clarity.

One of the most common routes for the synthesis of NHC metal complexes involves the deprotonation of a formamidinium precursor in order to generate transient, and sometimes stable free carbenes, which can then be trapped via coordination to a suitable metal center.[124,125] Attempts to generate the amidinium cations of compounds H_2(**3.1a-Ph**) and H_2(**3.1b-Ph**) via halogenation with NBS and hydride abstraction with trityl chloride (TrCl) were carried out. Unfortunately neither reaction yielded the desired amidinium cations due to competitive reactions at either the methylene linkers of the pendant arms, or the phosphines. Reactions with NBS yielded complex mixtures, in which bromination of the phosphines was observed. On the other hand, the reaction with trityl chloride proceeded cleanly at the methylene linkers, yielding the less symmetrical compounds [H(**3.4a-Ph**)][Cl] and [H(**3.4b-Ph**)][Cl], respectively (Scheme 3.3), as evidenced by multinuclear NMR spectroscopy. Attempts to isolate compounds [H(**3.4a-Ph**)][Cl] and [H(**3.4b-Ph**)][Cl] were not carried out.

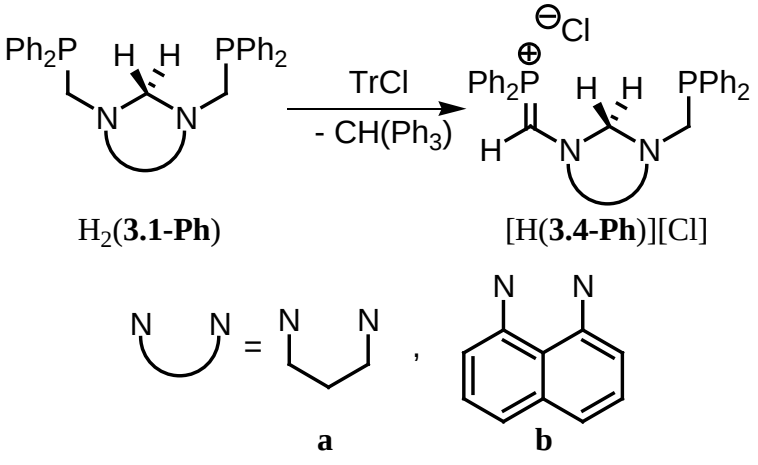

Scheme 3.3 Synthesis of compounds [H(3.4a-Ph)][Cl] and [H(3.4b-Ph)][Cl].

Following the lack of success in synthesizing the amidinium carbene precursors, attempts to coordinate the ligand precursors H_2(**3.1a-Ph**) and H_2(**3.1b-Ph**) via a double C-H bond activation were carried out.

3.3 Synthesis and Characterization of (PCP)Rh Complexes 3.5a-Ph and 3.5b-Ph

The synthesis of transition metal complexes of Fischer carbenes via a double C-H bond activation had been observed.[186] An early example of this was reported by Shaw and coworkers for the synthesis of the endocyclic carbene-alkylidene iridium pincer complex **3.I** (Scheme 3.4) via reversible elimination of hydrogen from the pincer complex **Ir-1.d**.[3] Attempts to synthesize the desired metal complexes of ligands **3.1a-Ph** and **3.1b-Ph** via a double C-H bond activation were carried out.

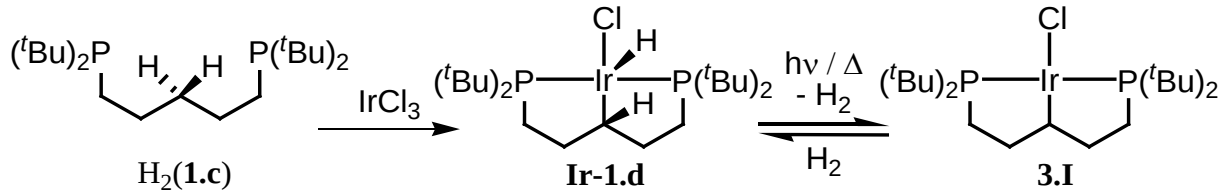

H_2(**1.c**) **Ir-1.d** **3.I**

Scheme 3.4 Reported synthesis of alkylidene [(PCP)IrCl] complex 3.I via a double C-H bond activation.

Reaction of either ligand precursor H_2(**3.1a-Ph**) or H_2(**3.1b-Ph**) with a stoichiometric amount of $[Rh(cod)Cl]_2$ in THF at 55 °C resulted in the clean formation of the desired complexes **3.5a-Ph** and **3.5b-Ph**, respectively (Scheme 3.5). The complexes precipitated out from THF solutions as X-ray quality single crystals. The solubility of the complexes in THF and hydrocarbons was poor. Their solubility was better in halogenated solvents and

dimethylsulfoxide, but their reactivity towards these solvents made their spectroscopic characterization challenging.

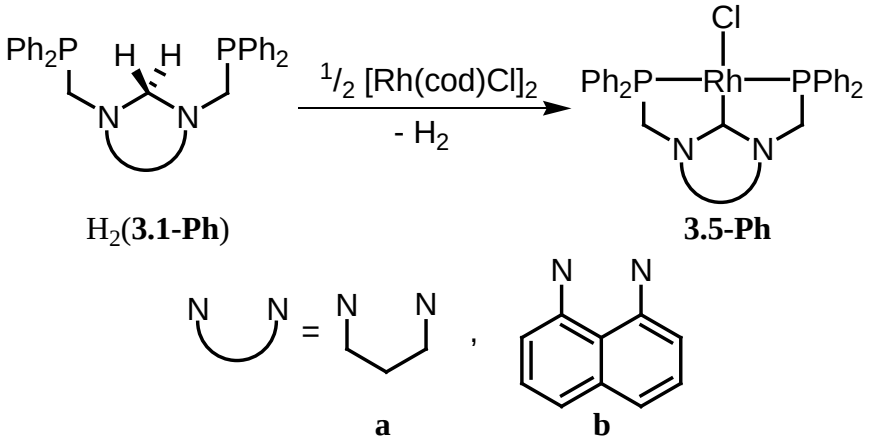

Scheme 3.5 Synthesis of [(PCP)RhCl] complexes 3.5a-Ph and 3.5b-Ph via a double C-H bond activation.

The ^{31}P NMR spectrum of complex **3.5b-Ph** displayed a signal at 24.3 ppm ($^{1}J_{RhP}$ = 152.3 Hz), which is downfield shifted with respect to that of the ligand precursor, H_2(**3.1b-Ph**) (δ = -25.5 ppm) confirming coordination of the phosphines to the Rh metal center. The ^{13}C{^{1}H} NMR spectrum featured a low-field doublet of triplet resonance at 207.0 ppm ($^{1}J_{RhC}$ = 62.0 Hz and $^{2}J_{PC}$ = 9.0 Hz) supporting the formation of the carbene complex. The previously reported NHC-based PCP pincer complexes of rhodium failed to provide a signal for this carbon.[139,165] The formation of complex **3.5a-Ph** was also confirmed by the downfield shift of the phosphorus resonance from -25.9 ppm to 25.8 ppm ($^{1}J_{RhP}$ = 153.9 Hz). However, the signal in the ^{13}C{^{1}H} NMR spectrum corresponding to the carbene center of complex **3.5a-Ph** (δ = 204.6 ppm) was not as nicely resolved as that for complex **3.5b-Ph**.

The structures of complexes **3.5a-Ph** and **3.5b-Ph** were unambiguously determined via X-ray crystallography (Figure 3.5). Selected bond lengths and angles are summarized in Table 3.1.

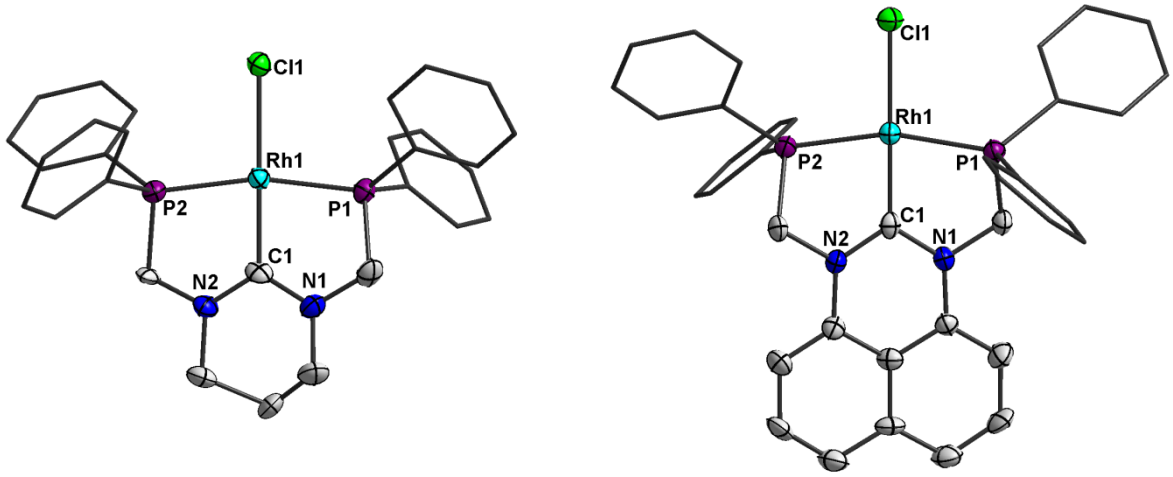

Figure 3.5 Solid-state molecular structures of 3.5a-Ph (left), and 3.5b-Ph (right) with thermal ellipsoids at 50 % probability, with the exception of the phosphine substituents, which are modeled as "sticks". All hydrogen atoms and a THF solvent molecule present in the structure of 3.5a-Ph have been omitted for clarity.

Table 3.1 Selected bond lengths (Å) and angles (°) for [(PCP)RhCl] complexes 3.5a-Ph and 3.5b-Ph.

Parameter	**3.5a-Ph**	**3.5b-Ph***	Parameter	**3.5a-Ph**	**3.5b-Ph***
C1-Rh1	1.99(1)	1.958(5)	C1-N2	1.353(2)	1.377(5)
Cl1-Rh1	2.417(3)	2.426(1)	C1-Rh1-Cl1	179.3(3)	180.0
P1-Rh1	2.242(3)	2.251(1)	P1-Rh1-P2	166.1(1)	163.97(4)
P2-Rh1	2.242(3)	2.251(1)	N1-C1-N2	116.4(5)	115.0(2)
C1-N1	1.371(2)	1.377(5)			

* The asymmetric unit for complex **3.5b-Ph** represents half of the molecule.

The structures of **3.5a-Ph** and **3.5b-Ph** are similar to those of the only other two structurally characterized rhodium complexes with NHC-based pincer ligands that generate five membered metallacycles upon coordination (**3.J**[182] and **3.K**,[139] Figure 3.6), as well as to those of analogous complexes with pyridine-based PNP pincer ligands.[187-189]

The Rh1-C1 bond distances in complexes **3.5a-Ph** (1.958(5) Å) and **3.5b-Ph** (1.99(1) Å) are slightly longer than the Rh-C_{NHC} bond observed in the analogous complex **3.J** (1.929(1) Å),[182] but comparable to the values measured in complexes **3.K-Me** (1.966(3) Å) and **3.K-H** (1.976(2) Å).[139] The P-Rh-P bond angles (163.97(4)° in **3.5a-Ph** and 166.1(1)° in **3.5b-Ph**) are in the range observed for classical pincer complexes (158° - 170°).[14,17,83]

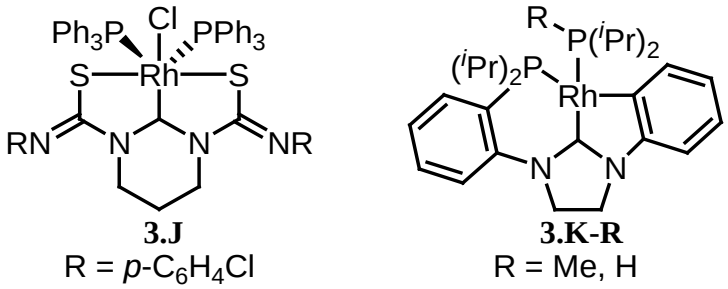

3.J
R = *p*-C_6H_4Cl

3.K-R
R = Me, H

Figure 3.6 Reported NHC-based pincer complexes of Rh that contain 5 membered metallacycles 3.J,[182] and 3.K-R.[139]

The formation of complexes **3.5a-Ph** and **3.5b-Ph** (Scheme 3.6) most likely involves the coordination of the phosphines, followed by a C-H bond activation giving rise to the Rh(III) alkyl species **3.6a-Ph** and **3.6b-Ph,** respectively. After the first C-H bond activation, two isomers of **3.6a-Ph** and **3.6b-Ph** can be formed: The *cis* isomers have the rhodium hydride and the alkyl hydrogen pointing in the same direction, and the *trans* isomers in which they point in opposite directions. The ***cis*-3.6** isomers of complexes **3.6a-Ph** and **3.6b-Ph** could undergo H_2

elimination either directly in a concerted fashion, or stepwise via hydride migration, generating the Rh(III) *cis*-dihydrides ***cis*-3.7**, followed by reductive elimination of H_2. The ***trans*-3.6** isomers do not have the proper orientation for a viable concerted mechanism, and subsequent hydride migration gives rise to Rh(III) *trans*-dihydrides ***trans*-3.7**, in which the proper disposition for reductive elimination of H_2 is not present. A similar double C-H bond activation has been observed for pendant N-methyl and N-methylene groups in iridium complexes where the corresponding Ir(III) carbene dihydrides were isolated and proved to be stable towards dihydrogen elimination.[190]

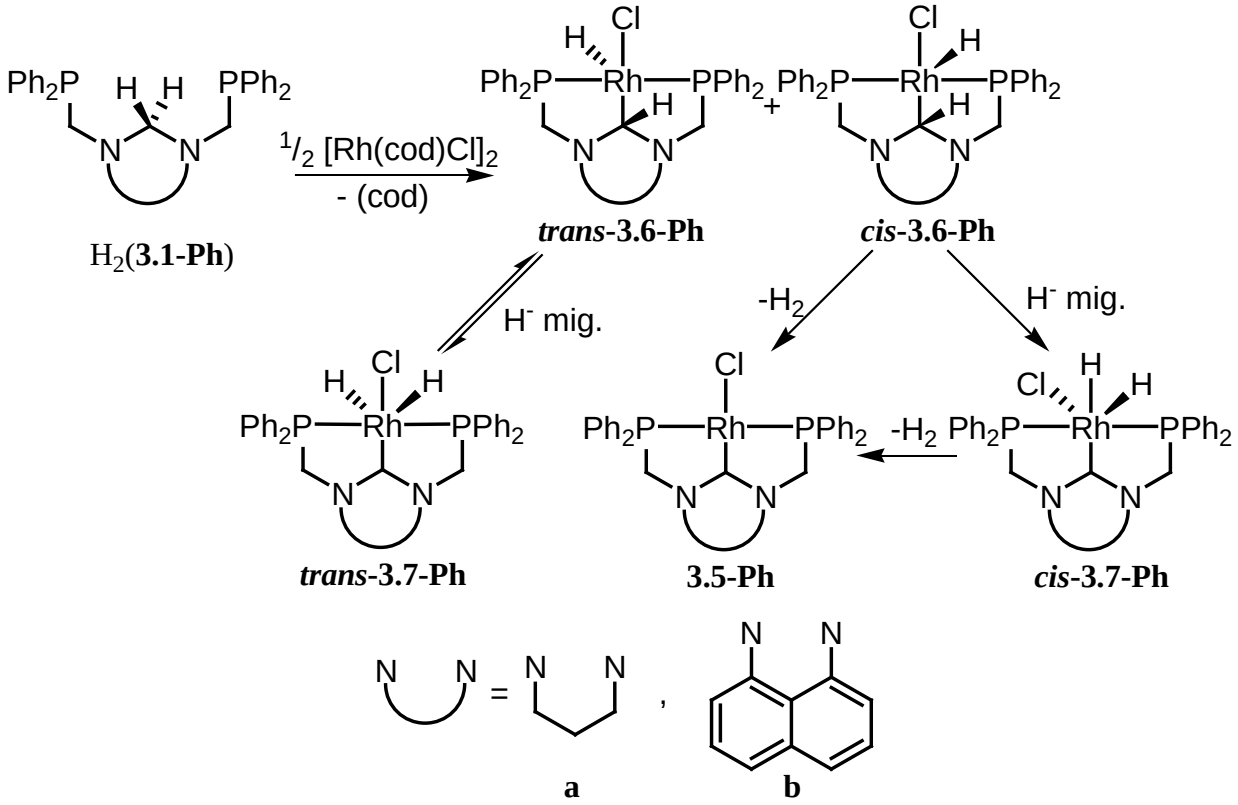

Scheme 3.6 Possible pathways for the observed double C-H activation with H_2 elimination for the synthesis of complexes 3.5a-Ph and 3.5b-Ph.

The hydrogen elimination step leading to the formation of compounds **3.5a-Ph** and **3.5b-Ph** is, for all intents and purposes, irreversible in contrast to what was observed by Shaw for complex **3.I** (Scheme 3.4, *vide supra*) and by Piers for complex **3.L** (Scheme 3.7).[191] Attempts to generate the Rh(III) hydride species **3.7-aPh**, and **3.7b-Ph** by subjecting solutions of complexes **3.5a-Ph** and **3.5b-Ph**, respectively, to four atmospheres of H_2 were unsuccessful. The ^{1}H and ^{31}P NMR spectra of the reaction mixtures showed no signs for the formation of complexes **3.7**. Such absence of reactivity towards H_2 is in agreement with the higher stability of the NHC core of these complexes in comparison to that of the alkylidene analogs.[3,191]

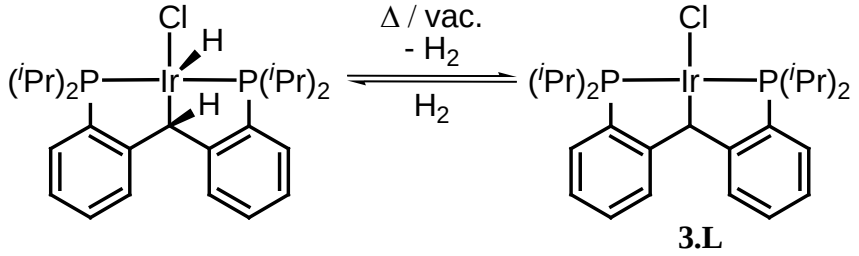

Scheme 3.7 Reversible H_2 addition reported for [PCPIrCl] complex 3.L.[191]

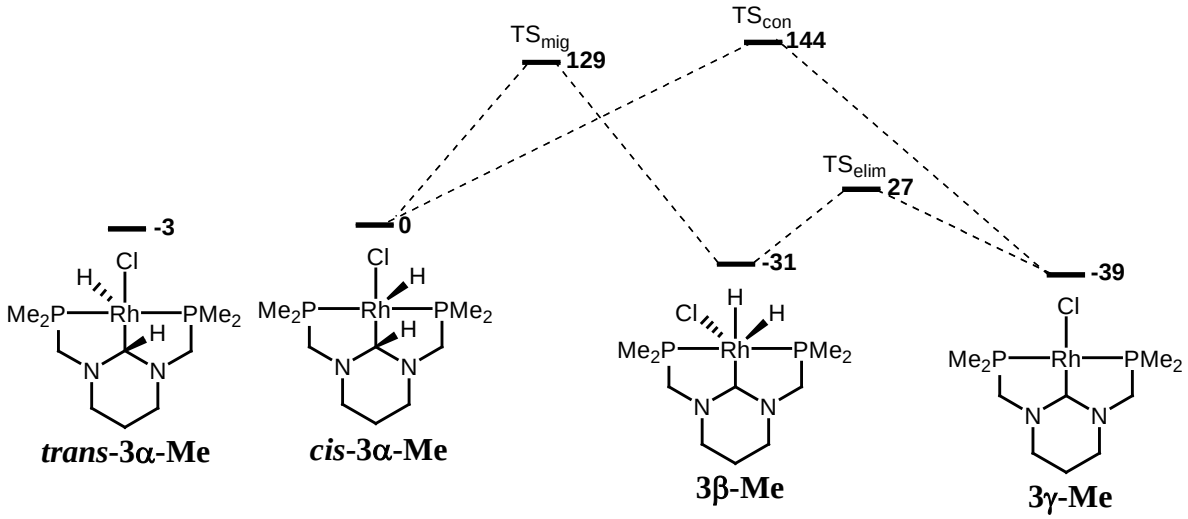

Scheme 3.8 Computed energetics (kJ·mol^{-1}) of the proposed mechanisms for the formation of the *P,P,P',P'*-Me_4 analog 3γ-Me of complexes 3.5a-Ph and 3.5b-Ph.

In order to better understand the possible mechanism involved in the double C-H bond activation that leads to the formation of complexes **3.5a-Ph** and **3.5b-Ph**, computational analysis on the model system **3γ-Me**, with methyl substituents at phosphorus (Scheme 3.8), were conducted by Dr. Heikki M. Tuonnonen. The free energies calculated for the *cis* and *trans* isomers of complex ***3α*-Me** revealed only a minor energy difference (3 $kJmol^{-1}$) favoring the *trans* isomer. Transition states leading to the elimination of H_2 from the *trans* isomer could not be identified computationally (Scheme 3.6). However, transition states for the two possible mechanisms for H_2 evolution from ***cis*-3α-Me**, the concerted mechanism (TS_{con}), and the hydride migration (TS_{mig}) followed by reductive elimination mechanism (TS_{elim}) (Scheme 3.8), could be calculated. The activation energy for the concerted mechanism (TS_{con} = 144 $kJmol^{-1}$) is in the same ballpark as the activation energy for hydride migration (TS_{mig} = 129 $kJmol^{-1}$). The activation energy for H_2 reductive elimination from the Rh(III) dihydride complex **3β-Me** is 58 $kJmol^{-1}$. The final product, complex **3γ-Me**, is -39 $kJmol^{-1}$ lower in energy than complex ***cis*-3α-Me**. The more energetically favourable mechanism is the stepwise hydride migration - reductive elimination, but only by a few $kJmol^{-1}$.

The transient alkyl Rh(III) intermediates **3.6a-Ph** and **3.6b-Ph** could be observed in the ^{1}H and ^{31}P NMR spectra of the reaction mixtures. Presented in Figure 3.7 are the NMR spectra recorded during the formation of complex **3.5b-Ph**. The ^{1}H NMR spectra of the reaction mixture for the synthesis of complex **3.5b-Ph** displayed an upfield resonance at δ = -17.7 ppm, with the expected doublet of doublets of triplets coupling pattern for intermediate **3.6b-Ph** ($^{1}J_{RhH}$ = 22.4 Hz, $^{2}J_{PH}$ = 6.2 Hz, $^{2}J_{HH}$ = 6.2 Hz). The ^{1}H NMR spectra of the reaction mixture for the synthesis of complex **3.5a-Ph** displayed two upfield signals both with the expected coupling patterns (δ = -17.7 ppm, $^{1}J_{RhH}$ = 24.3 Hz, $^{2}J_{PH}$ = 6.9 Hz, $^{2}J_{HH}$ = 6.9 Hz; and δ = -18.6 ppm,

$^{1}J_{RhH}$ = 17.4 Hz, $^{2}J_{PH}$ = 5.8 Hz, $^{2}J_{HH}$ = 5.8 Hz) which disappeared at different rates over time and were tentatively assigned to the two isomers ***cis*-3.6a-Ph** and ***trans*-3.6a-Ph** (Scheme 3.6). As mentioned, the *trans* isomers do not have the proper orientation for hydrogen elimination to occur. The only four structurally characterized Rh-PCP pincer complexes with a (CH)-Rh-H moiety, analogous to those in **3.6a-Ph** and **3.6b-Ph**, have a *trans* configuration.[4,192] Considering that the synthesis of complexes **3.5a-Ph** and **3.5b-Ph** is quantitative, we postulate that an equilibrium is taking place between the *cis* and *trans* isomers, which allows the formation of the Rh(III) dihydride species ***cis*-3.7a-Ph** and ***cis*-3.7b-Ph**, respectively (Scheme 3.6). The lack of a signal in the NMR spectra corresponding to the Rh(III) dihydride species **3.7a-Ph** and **3.7b-Ph** is in line with the relatively small activation energy barrier calculated for the elimination of H_2 from the modeled complex **3β-Me** to generate **3γ-Me** (Scheme 3.8).

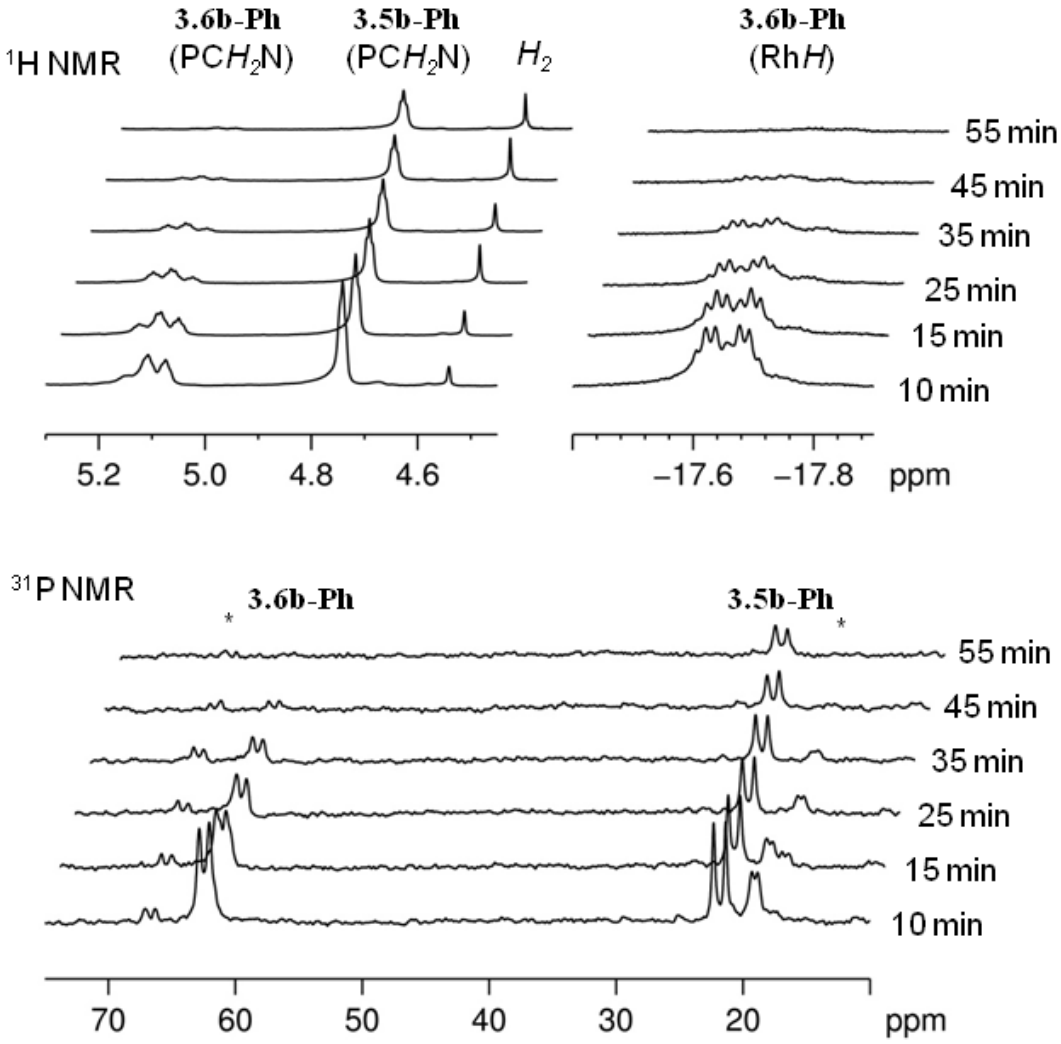

Figure 3.7 ^{1}H (above) ^{31}P (below) NMR spectra that support the transient formation of 3.6b-Ph during the synthesis of 3.5b-Ph from H_2(3.1b-Ph) and $^{1}/_{2}$[Rh(cod)Cl]$_2$ in THF at 25 °C. The signals corresponding to complex 3.5b-Ph decrease with time as the complex crystallizes out of solution and * denotes unidentified species.

The two proposed mechanisms (Scheme 3.6), i) the concerted H_2 elimination and ii) the stepwise elimination of hydrogen via hydride migration and then reductive elimination, are not the only two possible mechanisms. Another available path for the synthesis of complexes **3.5a-Ph** and **3.5b-Ph** could involve the hydrogenation of cyclooctadiene (COD) present in the

reaction mixture. Rhodium catalyzed hydrogenation of COD is well documented, and as such the plausible hydrogenation of COD by the proposed transient Rh hydride species represents a viable mechanism for the synthesis of complexes **3.5a-Ph** and **3.5b-Ph**.[193] A mechanism involving the π-coordination of COD to either isomer of both **3.6a-Ph** and **3.6b-Ph**, followed by olefin insertion to yield the Rh(III) dialkyl species **3.8a-Ph** or **3.8b-Ph**, repectively (Scheme 3.9), needs to be considered. Similar to what was proposed for the hydrogen elimination, the *cis* isomers of the dialkyl Rh(III) species ***cis*-3.8-aPh**, and ***cis*-3.8b-Ph** can eliminate COE via two different paths: a concerted mechanism, or a stepwise hydride migration leading to the alkyl-hydride Rh(III) species ***cis*-3.9-aPh** and ***cis*-3.9b-Ph**, followed by reductive elimination of COE. On the other hand, for the same reasons as those provided during the explanation of the hydrogen elimination mechanisms, the trans isomers ***trans*-3.8a-Ph** and ***trans*-3.8b-Ph**, cannot lead to the elimination of COE with formation of the final rhodium complexes and hence, the paths involving these isomers will not be discussed.

Evidence supporting the H_2 elimination pathway over the hydrogenation of COD came from the observation of gas evolution as the reaction progressed. This was further supported by the presence of a small sharp signal at 4.56 ppm in the ^{1}H NMR spectra of the reaction mixtures (Figure 3.7), which compares favourably with the reported ^{1}H NMR signal for H_2 gas in THF at room temperature (δ = 4.55 ppm).[194] However, these observations do not provide evidence on whether the hydrogenation of COD to COE took place during the synthesis of complexes **3.5a-Ph** and **3.5b-Ph**. In order to find which pathway was involved, the reaction mixtures were analyzed via ^{1}H NMR spectroscopy and GC-MS as the reactions progressed. The ^{1}H NMR spectra of the reaction mixtures displayed the corresponding signals for the free COD ligand, but no signals corresponding to COE could be observed. The GC-MS chromatograms of the

mixtures confirmed the NMR spectroscopy data. The chromatograms only displayed one major signal corresponding to COD, and no signal corresponding to COE could be observed. This confirmed the initial postulate, according to which the synthesis of complexes **3.5a-Ph** and **3.5b-Ph** proceeded via H_2 elimination.

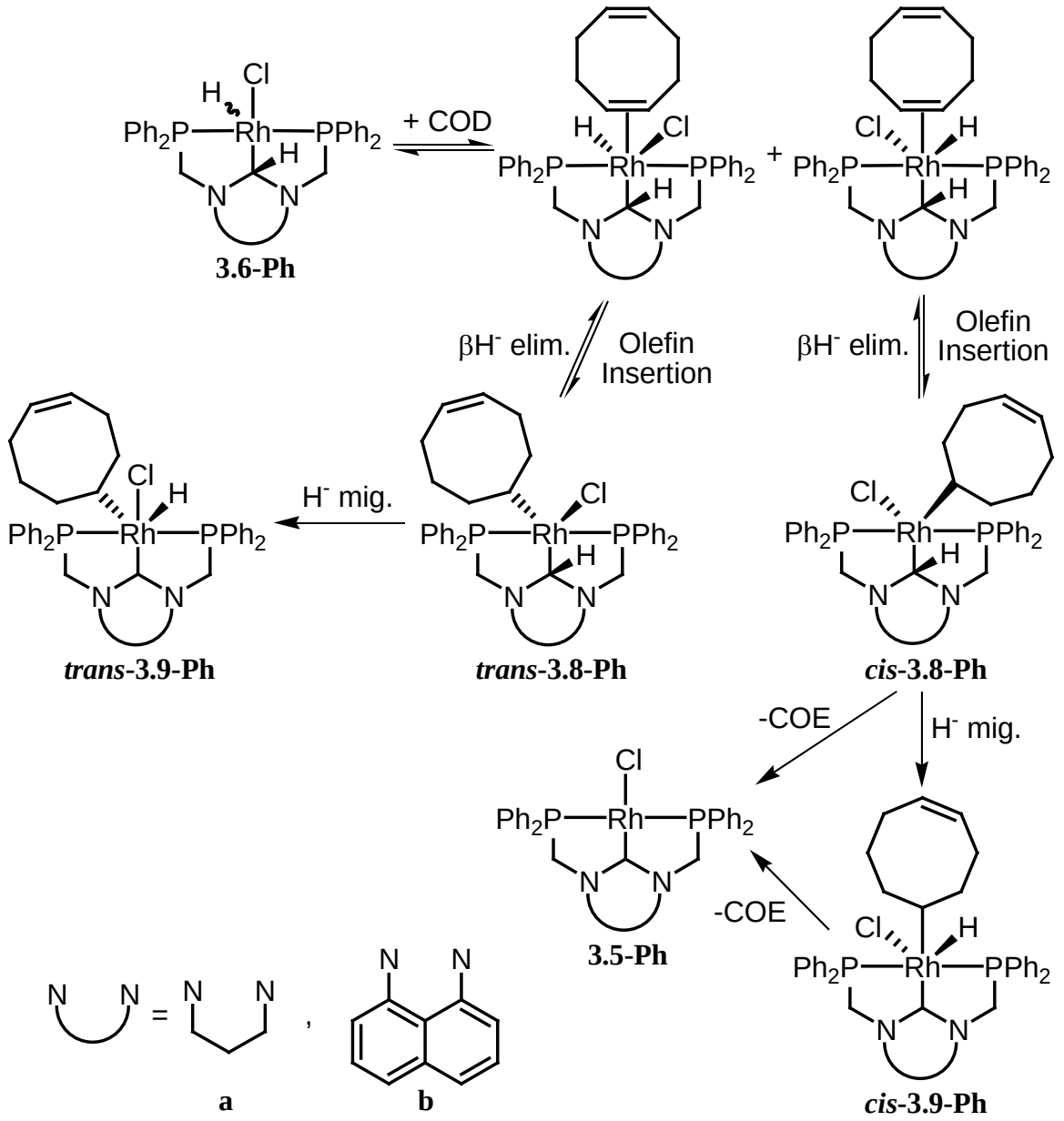

Scheme 3.9 Proposed mechanism for the formation of complexes 3.5a-Ph and 3.5b-Ph via the hydrogenation of COD.

3.4 Synthesis and Characterization of (PCP)Rh Complexes 3.10a-Ph and 3.10b-Ph

The low solubility of complexes **3.5a-Ph** and **3.5b-Ph** in THF and common hydrocarbon solvents prompted the evaluation of their solubility in halogenated solvents, for the purpose of full spectroscopic characterization. Complexes **3.5a-Ph** and **3.5b-Ph** both displayed excellent solubility in dichloromethane-d_2. However, these solutions were not stable and both complexes quickly reacted with the halogenated solvent via oxidative addition of a C-Cl bond, generating complexes **3.10a-Ph** and **3.10b-Ph**, respectively (Scheme 3.10). The $t_{1/2}$ for the reaction of dichloromethane-d_2 with complexes **3.5a-Ph** and **3.5b-Ph** at room temperature are 5 and 30 min, respectively. Such reactivity towards dichloromethane has been previously reported for another rhodium complex with a carbene-based PCP ligand, complex **3.M** (Scheme 3.11).[165] Lee reported this complex as a transient species that could not be isolated. If synthesized in the presence of dichloromethane, **3.M** readily reacted to produce complex **3.N**.

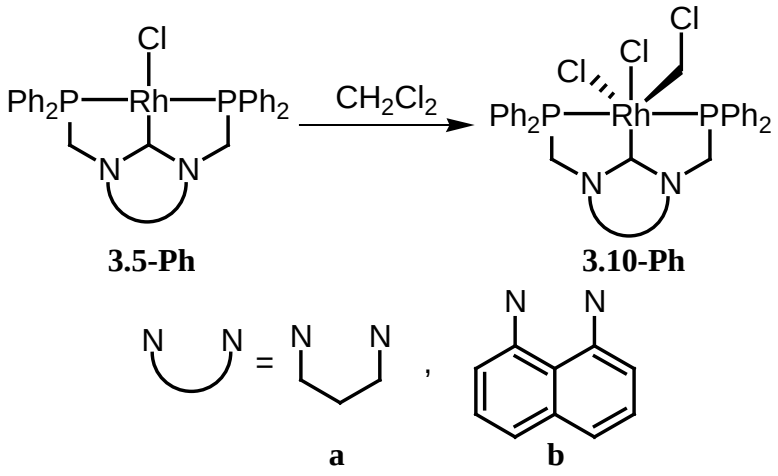

Scheme 3.10 Reaction of 3.5a-Ph and 3.5b-Ph with dichloromethane to yield Rh(III) complexes 3.10a-Ph and 3.10b-Ph.

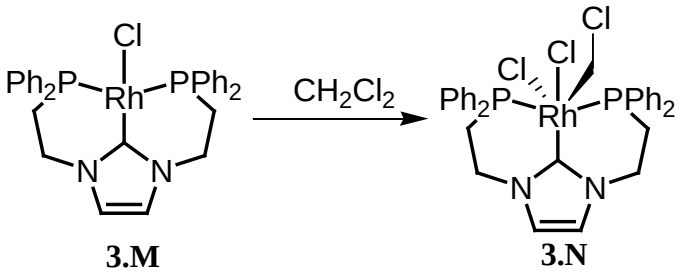

3.M **3.N**

Scheme 3.11 Reported reactivity of complex 3.M with dichloromethane to generate complex 3.N.

The reactivity of complex **3.5b-Ph** with dichloromethane-d_2 was followed via ^{1}H NMR spectroscopy. The spectra showed the transformation of the resonance corresponding to the methylene linkers of the ligand from a virtual triplet (δ = 4.67 ppm, J_{PH} = 2.4Hz) to a pair of doublets of virtual triplets (δ = 5.27 ppm, $^2J_{HH}$ =14.8 Hz, J_{PH} = 2.5 Hz) (δ = 5.58 ppm, $^2J_{HH}$ = 14.8 Hz, J_{PH} = 2.5 Hz). The increase in the number of signals in the NMR spectrum is a direct consequence of the lower symmetry of complex **3.10b-Ph** with respect to complex **3.5b-Ph**, which renders the protons on the methylene linkers inequivalent. The ^{1}H NMR spectrum of complex **3.10a-Ph** also showed a similar set of signals (δ = 4.74 ppm, $^2J_{HH}$ = 13.4 Hz, J_{PH} = 3.0 Hz) (δ = 4.80 ppm dpt, $^2J_{HH}$ = 13.4 Hz, J_{PH} = 3.0 Hz). The resonances in the ^{31}P NMR spectra of complexes **3.10a-Ph** and **3.10b-Ph**, at 28.4 ppm ($^1J_{RhP}$ = 108.6) and 25.2 ppm ($^1J_{RhP}$ = 105.3), respectively, are slightly downfield shifted with respect to those of the parent complexes **3.5a-Ph** and **3.5b-Ph**, at 25.8 ppm ($^1J_{RhP}$ = 153.9 Hz) and 24.3 ppm ($^1J_{RhP}$ = 152.3 Hz). Also of note is the decrease in the $^1J_{RhP}$ coupling constants by about 33 % when going from complexes **3.5a-Ph** and **3.5b-Ph** to complexes **3.10a-Ph** and **3.10b-Ph**. The ^{13}C{^{1}H} NMR spectra of complexes **3.10a-Ph** and **3.10b-Ph** displayed the characteristic downfield resonance with a doublet of triplets coupling pattern, which corresponds to the carbene centers at 201.2 ppm ($^1J_{RhC}$ = 45.3 Hz, $^2J_{PC}$ = 5.2 Hz) and 203.9 ppm ($^1J_{CRh}$ = 49.1 Hz,

$^2J_{PC}$ = 5.2 Hz), respectively. The signals corresponding to the carbon from the Rh*C*D_2Cl could not be observed in either spectra. Complexes **3.10a-Ph** and **3.10b-Ph** precipitated from the dichloromethane-d_2 solution over time, further showcasing the low solubility of the rhodium complexes of these ligands.

X-ray quality single crystals of complex **3.10b-Ph** were obtained by slow diffusion of diethyl ether into a concentrated solution of the complex in dichloromethane-d_2 (Figure 3.8). The crystals showed disorder throughout the lattice due to exchange in the position of the Cl2 and the C2-Cl3 moiety. The positions for all the disordered atoms could be modeled but due to the higher atomic number of chlorine over carbon, the refinement of C2 and C2' had to be kept isotropic making all bond lengths and angles pertaining C2 and C2' unreliable.

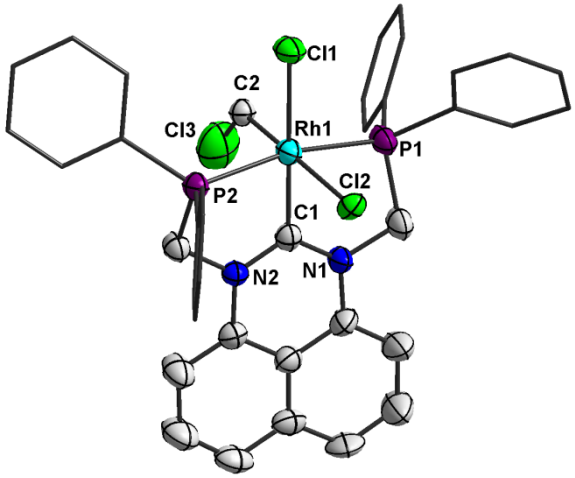

Figure 3.8 Solid-state molecular structure of complex 3.10b-Ph with thermal ellipsoids at 50 % probability, with the exception of the phosphine substituents, which are modeled as "sticks". All hydrogen atoms and a dichloromethane solvent molecule have been removed for clarity. Selected bond lengths (Å) and angles (°): Rh1-C1 2.007(10), Rh1-P1 2.288(2), Rh1-P2 2.287(2), Rh1-Cl1 2.429(3), Rh1-Cl2 2.538(7), C1-N1 1.340(9), C1-N2 1.369(8), C1-Rh1-Cl1 178.7(3), P1-Rh1-P2 167.13(8), N1-C1-N2 118.6(7). Dihedral angle between the main planes defined by N1-C1-N2-Rh1 and C1-Rh1-P1-P2 ϕ = 11.9°.

The Rh1-C1 bond length in complex **3.10b-Ph** (2.007(10)Å) is statistically equivalent to that reported for complex **3.N** (2.008(9)Å).[165] The P-Rh-P angle in complex **3.10b-Ph** (167.13(8)°) is smaller than that in complex **3.N** (175.00(9)°), and falls in the range observed for classical PCP pincer ligands (158°-170°).

3.5 Synthesis and Characterization of Cationic (PCP)Rh Complexes [3.12a-Ph][OTf] and [3.12b-Ph][OTf]

The synthesis of cationic Rh(I) complexes was done in an attempt to generate more soluble complexes. The reactions of a THF suspension of either complex **3.5a-Ph** or **3.5b-Ph** with a stoichiometric amount of silver triflate were carried out as a means to generate complexes [**3.11a-Ph**][OTf] and [**3.11b-Ph**][OTf], respectively (Scheme 3.12). The ^{1}H and ^{31}P NMR spectra of the reaction mixtures revealed that intractable mixture of products were obtained. These pointed towards the low stability of complexes [**3.11a-Ph**][OTf] and [**3.11b-Ph**][OTf].

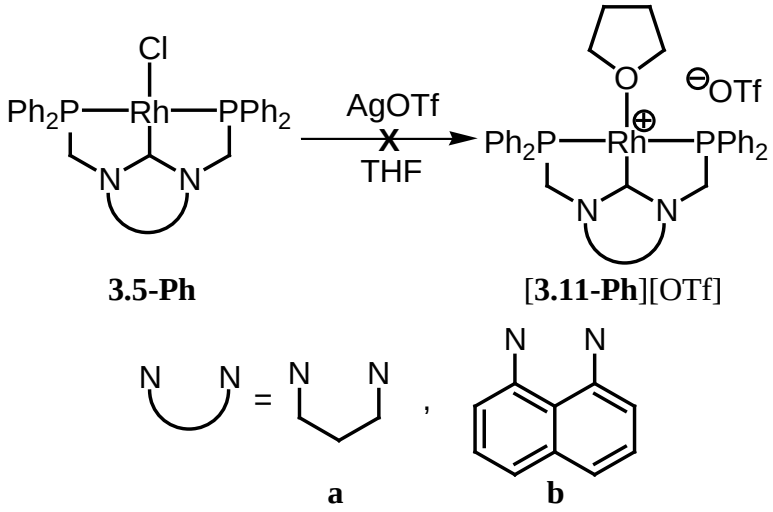

Scheme 3.12 Proposed synthesis of complexes [3.11a-Ph][OTf] and [3.11b-Ph][OTf].

In order to increase the stability of the in-situ generated cationic complexes, a better neutral ligand (PPh_3) was added to the reactions, leading to the successful synthesis of complexes [**3.12a-Ph**][OTf] and [**3.12b-Ph**][OTf] (Scheme 3.13).

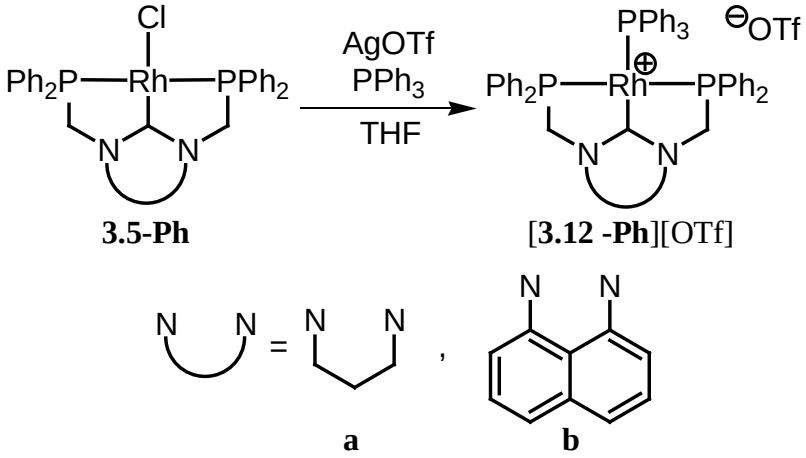

Scheme 3.13 Synthesis of cationic [(PCP)Rh(PPh_3)][OTf] complexes [3.12a-Ph][OTf] and [3.12b-Ph][OTf].

Unfortunately, complexes [**3.12a-Ph**][OTf] and [**3.12b-Ph**][OTf] precipitate from THF solution and would not redissolve. However, both complexes were dissolved in the less reactive halogenated solvent, bromobenzene-d_5, allowing for spectroscopic characterization. The $^{31}P\{^1H\}$ NMR spectra of complexes [**3.12a-Ph**][OTf] and [**3.12b-Ph**][OTf] expectedly displayed two signals, each with the corresponding coupling patterns: a doublet of triplets for the signal of the triphenylphosphine and a doublet of doublets for the signal of the PCP phosphines (δ = 35.5 ppm ($^1J_{RhP}$ = 122.0 Hz, $^2J_{PP}$ = 34.4 Hz) and δ = 40.7 ppm ($^1J_{RhP}$ = 148.6 Hz, $^2J_{PP}$ = 34.4 Hz) for [**3.12a-Ph**][OTf], and δ = 32.6 ppm ($^1J_{RhP}$ = 119.5 Hz, $^2J_{PP}$= 34.9 Hz) and δ = 38.1 ppm ($^1J_{RhP}$ = 144.9 Hz, $^2J_{PP}$ = 34.9 Hz) for [**3.12b-Ph**][OTf]). Complex [**3.12b-Ph**][OTf] was stable enough in bromonbenzene-d_5 to allow for recrystallization

(Figure 3.9). The more reactive complex [**3.12a-Ph**][OTf] however, would react with the bromobenzene-d_5 with a $t_{1/2}$ = 36 h and could not be recrystallized.

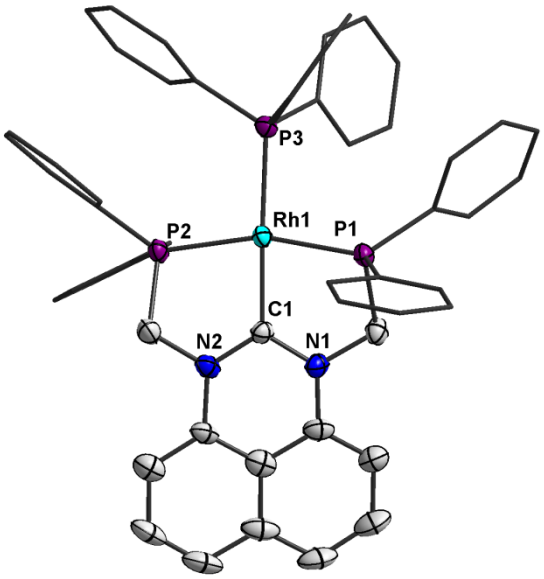

Figure 3.9 Solid-state structure of the cation in complex [3.12b-Ph][OTf] with thermal ellipsoids at 50 % probability with the exception of the phosphine substituents, which have been modeled as "sticks". The hydrogen atoms, OTf counteranion and a bromobenzene-d_5 solvent molecule have been removed for clarity. Selected bond lengths (Å) and bond angles (°) C1-Rh1 2.025(4), Rh1-P1 2.263(2), Rh1-P2 2.248(2), Rh1-P3 2.326(1), C1-N1 1.373(8), C1-N2 (1.359(7), C1-Rh1-P3 173.8(1), P1-Rh1-P2 161.5(6), N1-C1-N2 116.5(5).

The Rh1-C1 bond distance of complex [**3.12b-Ph**][OTf] (2.025(4)Å) is comparable to those measured in complexes **3.10b-Ph** and **3.N** (2.007(10)Å, 2.008(9)Å), but are longer than that observed for complex **3.5b-Ph** (1.958(5)Å). The P1-Rh1-P2 bond angle of complex [**3.12b-Ph**][OTf] (161.5(6)°) is smaller than those observed for complexes **3.5b-Ph** and **3.10b-Ph** (163.97(4)°, 167.13(8)° respectively), in accordance with the need of the phosphine side arms to bend back in order to accommodate the more sterically demanding triphenylphosphine ligand in the complex.

3.5.1 *Hydrosilylation of Acetophenone with Diphenylsilane Catalyzed by Complex [3.12b-Ph][OTf]*

Rhodium complexes, such as [**3.12a-Ph**][OTf] and [**3.12b-Ph**][OTf], have been successfully employed as catalysts for the hydrosilylation of ketones.[195-198] Consequently, attempts to hydrosilylate acetophenone with diphenylsilane in the presence of a catalytic amount of complex [**3.12a-Ph**][OTf] or [**3.12b-Ph**][OTf] were carried out (Scheme 3.14).

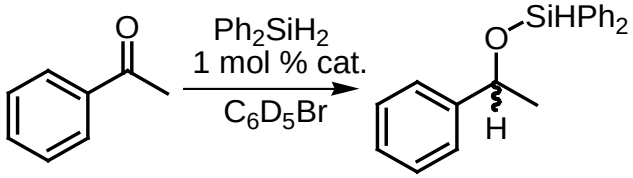

cat. = [**3.12a-Ph**][OTf] or [**3.12b-Ph**][OTf]

Scheme 3.14 Hydrosilylation of acetophenone with diphenylsilane.

The hydrosilylation reactions were carried out in bromobenzene-d_5 and monitored via ^{1}H NMR spectroscopy. The reaction catalyzed by complex [**3.12a-Ph**][OTf] displayed only approximately 5 % conversion of the starting materials to the product. The low conversion displayed by catalyst [**3.12a-Ph**][OTf] was linked to the previously observed competitive activation of bromobenzene-d_5 by the complex. Conversely, the reaction catalyzed by complex [**3.12b-Ph**][OTf] showed the steady formation of the desired hydrosilylation product. The evidence for the success of the reaction was the presence of the signal corresponding to the methyl group of the hydrosilylated product (δ = 1.40 ppm) in the ^{1}H NMR spectrum, which increased in intensity as the reaction progressed. Further, the decrease in the intensity of the signal corresponding to the methyl group from the acetophenone starting material (δ = 2.23 ppm) was also observed in the spectrum. The turnover frequency (TOF) of the reaction catalyzed by

complex [**3.12b-Ph**][OTf] was determined to be 9.1 h^{-1}. Such a TOF is significantly smaller than that displayed by other cationic Rh(I)-C_{NHC} catalysts, such as complex **3.O** (Figure 3.10), which has a reported TOF = 1128 h^{-1} for the same reaction.[195] The small TOF displayed by complex [**3.12b-Ph**][OTf] was also attributed to the competitive activation of bromobenzene-d_5 leading to catalyst deactivation.

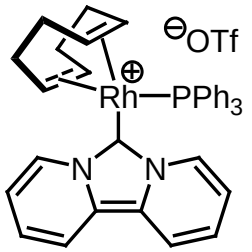

3.O

Figure 3.10 Reported NHC Rh complex 3.O.

3.6 Synthesis and Characterization of PCP Pincer Ligand Precursor H_2(3.1a-*t*Bu) and its (PCP)Rh Complex 3.5a-*t*Bu

Considering the difficulties in dissolving complexes **3.5a-Ph** and **3.5b-Ph** encountered, the focus of the project shifted towards the synthesis of a more soluble analog of ligand H_2(**3.1a-Ph**), with *tert*-butyl substituents on the phosphorus centers instead of phenyls. The synthesis of the *tert*-butyl substituted ligand precursor H_2(**3.1a-*t*Bu**) was carried out following a similar synthetic route as that employed for the synthesis of H_2(**3.1a-Ph**) (Scheme 3.15). Due to the higher reactivity displayed by the Rh complexes of the aliphatic backbone ligand **3.1a-Ph** over those of the aromatic backbone ligand **3.1b-Ph**, only the synthesis of the *tert*-butyl substituted ligand precursor based on the aliphatic carbene backbone was investigated. Furthermore, the aliphatic backbone should provide overall better solubility properties than the rigid aromatic one.

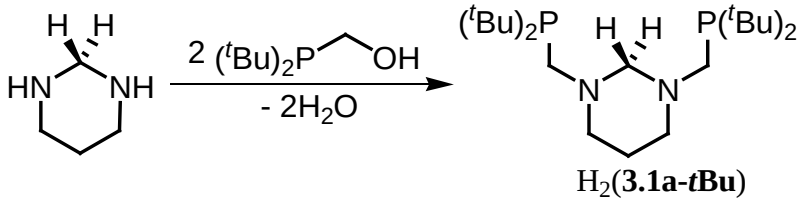

H_2(**3.1a-*t*Bu**)

Scheme 3.15 Synthesis of PCP pincer ligand precursor H_2(3.1a-*t*Bu).

For the synthesis of H_2(**3.1a-*t*Bu**), two equivalents of di-*tert*-butylphosphinomethanol were reacted with one equivalent of tetrahydropyrimidine in dichloromethane. The reaction mixture was stirred for 48h, dried with calcium hydride, and filtered. The filtrate was dried under vacuum yielding compound H_2(**3.1a-*t*Bu**) as a thick colorless oil. The ^{1}H NMR spectrum of the compound displayed the expected doublet signal for the methylene linkers from the side arms at 2.67 ppm, with $^1J_{PH}$ = 3.0 Hz. The ^{31}P NMR spectrum had only one signal, as expected (δ = 11.6 ppm).

The ligand precursor H_2(**3.1a-*t*Bu**) was reacted with half an equivalent of $[Rh(cod)Cl]_2$ in THF, and heated to 60 °C to readily generate complex **3.5a-*t*Bu** (Scheme 3.16). Similar to what was observed for the synthesis of complexes **3.5a-Ph** and **3.5b-Ph**, the reaction mixture evolved a gas over time, albeit more slowly. In a similar fashion to what was done for the synthesis of complexes **3.5a-Ph** and **3.5b-Ph**, the progress of the reaction during the synthesis of complex **3.5a-*t*Bu** was monitored via multinuclear NMR spectroscopy. Surprisingly, the synthesis of complex **3.5a-*t*Bu** required 72h of heating in order to reach completion, in comparison to the 2 - 3h required for the synthesis of complexes **3.5a-Ph** and **3.5b-Ph**. The reaction times could be shortened to 48h by heating the reaction to 80 °C in benzene instead of to 60 °C in THF. The ^{1}H NMR spectrum of the monitored reaction displayed the presence of a

small sharp signal at 4.47 ppm, which matched the reported chemical shift for H_2 gas in benzene.[194] The ^{1}H NMR spectra also displayed a high-field doublet of triplets resonance at 6.26 ppm ($^1J_{RhH}$ = 18.3 Hz, $^2J_{PH}$ = 13.0 Hz) corresponding to a rhodium hydride. Such a resonance was not unexpected, considering that the reaction for the synthesis of both complexes **3.5a-Ph** and **3.5b-Ph** had displayed similar high-field resonances, which were attributed to Rh(III) alkyl-hydride intermediates **3.6a-Ph** and **3.6b-Ph**, respectively (Scheme 3.6, *vide supra*). However, the resonance observed in the reaction mixture for the synthesis of complex **3.5a-*t*Bu** was unique with respect to those observed for the reactions of complexes **3.5a-Ph** and **3.5b-Ph**, in that it only featured coupling to two different types of nuclei instead of three.

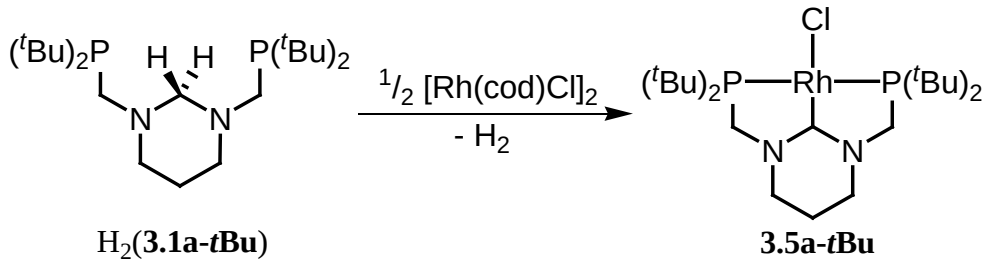

H_2(**3.1a-*t*Bu**) **3.5a-*t*Bu**

Scheme 3.16 Synthesis of complex 3.5a-*t*Bu.

The increased reaction time for the synthesis of complex **3.5a-*t*Bu** along with the observed lack of coupling pattern for the upfield signal of an intermediate associated to its synthesis may suggest that another mechanism than that proposed for the formation of complexes **3.5a-Ph** and **3.5b-Ph** is at play. The involvement of the COD present in the reaction mixture was the most plausible explanation. To probe this theory, the progress of the reaction was monitored via GC-MS. The obtained chromatograms displayed two main signals, one corresponding to COD (60 %), and the other one to COE (30 %), even after completion of the reaction had been confirmed by multinuclear NMR spectroscopy.

The presence of COE suggests that a different mechanism than that proposed for the formation of **3.5a-Ph** and **3.5b-Ph** is responsible for the formation of a proportion of complex **3.5b-*t*Bu**. However, the evolution of a gas during the synthesis, the ^{1}H NMR signal corresponding to the resonance of H_2, and the fact that not all COD was hydrogenated after completion of the reaction, indicate that elimination of hydrogen is also taking place during the synthesis of **3.5b-*t*Bu**. Hence, a competitive mechanism is proposed, in which both the elimination of H_2 and the hydrogenation of COD take place (Scheme 3.17).

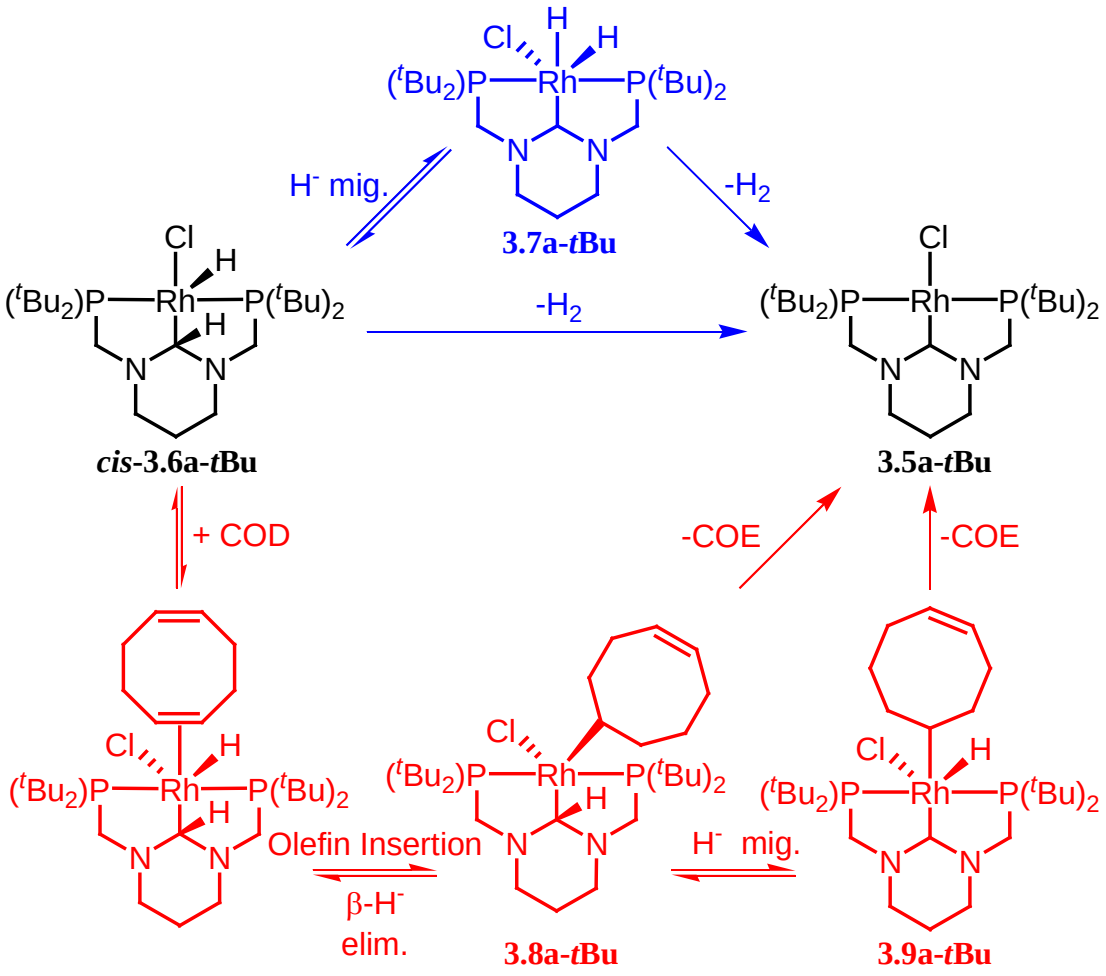

Scheme 3.17 Proposed mechanisms for the double C-H bond activation leading to the synthesis of complex 3.5a-*t*Bu

For the same mechanistic reasons that were provided for the synthesis of complexes **3.5a-Ph** and **3.5b-Ph**, the *trans* isomers of the reaction intermediates are not expected to lead to product formation and hence have been omitted from the schematic. In Scheme 3.17, the blue path represents the elimination of H_2, which can occur via either a concerted mechanism, or a stepwise hydride migration - reductive elimination mechanism, and the red path represents the mechanism involving the hydrogenation of COD. The first step for the latter would be the π-coordination of the olefin, followed by olefin insertion. From here, intermediate **3.8a-*t*Bu** can either eliminate COE in a concerted mechanism or in a stepwise fashion as well. Based on these two working mechanisms, the upfield doublet of triplets resonance in the ^{1}H NMR spectra recorded during the synthesis of complex **3.5a-*t*Bu** could be assigned to one of three intermediates: ***trans*-3.7a-*t*Bu**, ***cis*-3.9a-*t*Bu**, or ***trans*-3.9a-*t*Bu**. However, attempts to determine the identity of the intermediate responsible for this resonance were not carried out.

The ^{1}H NMR spectra of complex **3.5a-*t*Bu** displayed all the expected signals. Both, the signal corresponding to the phosphine *tert*-butyl substituents at 1.39 ppm ($^1J_{PH}$ = 6.3 Hz) and the signal corresponding to the methylene linkers on the side arms at 3.49 ppm, appeared as virtual triplets thus confirming the symmetric nature of the complex. The ^{31}P{^{1}H} NMR spectrum of complex **3.5a-*t*Bu** displayed the characteristic doublet resonance at 62.0 ppm ($^1J_{RhP}$ = 157.3 Hz), which is downfield with comparison to those of complexes **3.5a-Ph** (δ = 25.8 ppm) and **3.5b-Ph** (δ = 24.3 ppm). The observed difference in chemical shifts is in accordance with going from the phenyl substituted phosphines to the more basic *tert*-butyl substituted ones. More importantly, the ^{13}C{^{1}H} NMR spectrum of complex **3.5a-*t*Bu** displayed the downfield resonance for the carbene carbon (δ = 208.9 ppm, $^1J_{RhC}$ = 58.6 Hz, $^2J_{PC}$ = 8.2 Hz) with the expected doublet of triplets coupling pattern.

Similar to what was observed for complexes **3.5a-Ph** and **3.5b-Ph**, complex **3.5a-*t*Bu** crystallized out of THF as the reaction progressed, but different from **3.5a-Ph** and **3.5b-Ph**, complex **3.5a-*t*Bu** could be as easily redissolved in THF by simply heating the solution to the boiling point. The structure of complex **3.5a-*t*Bu** was determined via X-ray crystallography (Figure 3.11). All relevant metric parameters from complex **3.5a-*t*Bu** compare favourably with those of complexes **3.5a-Ph** and **3.5b-Ph**.

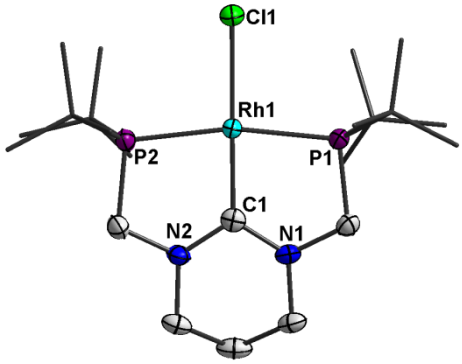

Figure 3.11 Solid-state molecular structure of complex 3.5a-*t*Bu with thermal ellipsoids at 50 % probability, with the exception of the phosphine substituents, which are modeled as "sticks". All hydrogen atoms have been omitted for clarity. Selected bond lengths (Å) and bond angles(°): Rh1-C1 1.958(3), Rh1-Cl1 2.4374(9), Rh1-P1 2.2649(9), Rh1-P2 2.2640(9), C1-N1 1.368(4), C1-N2 1.378(5), C1-Rh1-Cl1 177.22(9), P1-Rh1-P2 165.66(4), N1-C1-N2 115.5(3). Dihedral angle between the main planes defined by N1-C1-Rh1-N2 and P1-Rh1-P2-C1 ϕ = 6.3.

3.7 Synthesis and Characterization of (PCP)Rh Carbonyl Complexes [3.13a-Ph][OTf], [3.13a-*t*Bu][X] (X = Cl, OTf), and [3.13b-Ph][OTf]

The ability of carbonyl ligands to π-backbond, along with their characteristic IR absorption frequencies, give rise to an excellent handle for the assessment of the electron donating properties of other ligands bound to the carbonyl complexes.[68,199] The syntheses of carbonyl complexes **[3.13a-Ph**][Cl], [**3.13a-*t*Bu**][Cl], and [**3.13b-Ph**][Cl] were attempted as means to assess the electron-donating properties of ligands **3.1a-Ph**, **3.1a-*t*Bu**, and **3.1b-Ph**, respectively. The reactions of half an equivalent of $[Rh(CO)_2Cl]_2$ with ligand precursors H_2(**3.1a-Ph**), H_2(**3.1a-*t*Bu**), and H_2(**3.1b-Ph**) were carried out (Scheme 3.18).

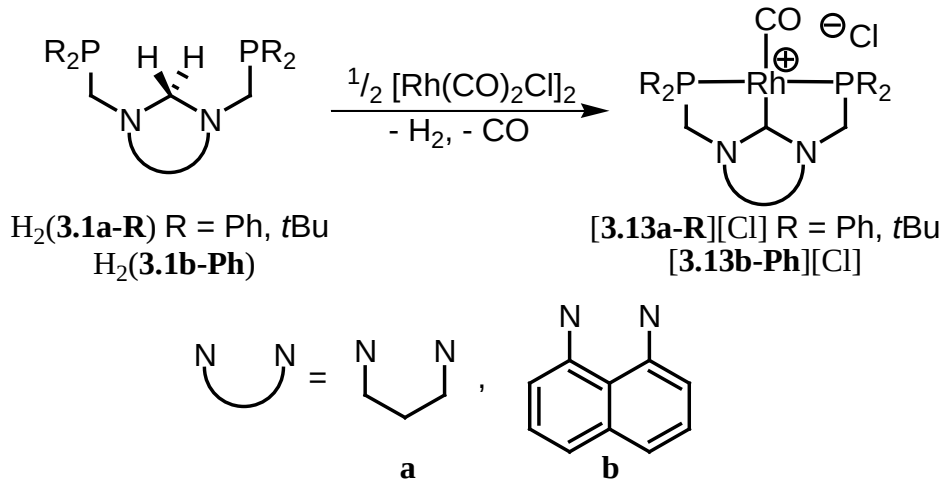

Scheme 3.18 Synthesis of Rh-carbonyl complexes [3.13a-Ph][Cl], [3.13a-*t*Bu][Cl] and [3.13b-Ph][Cl].

The reaction of ligand precursors H_2(**3.1a-Ph**) and H_2(**3.1b-Ph**) with $[Rh(CO)_2Cl]_2$ did not prove to be a reliable method to synthesize the carbonyl complexes [**3.13a-Ph**][Cl] and [**3.13b-Ph**][Cl], respectively, while the reaction of ligand precursor H_2(**3.1a-*t*Bu**) with $[Rh(CO)_2Cl]$ in benzene at 80 °C generated X-ray quality crystals of an unexpected trimer, complex **3.14a-*t*Bu** (Figure 3.12). The solid-state molecular structure (Figure 3.13) revealed that the trimer is composed of Rh(CO)Cl moieties bridged by H_2(**3.1a-*t*Bu**) ligands. Each H_2(**3.1a-*t*Bu**) fragment is bonded to two rhodium centers via its phosphines in a μ_2 fashion. The packing arrangement of the crystal structure revealed that two molecules of **3.14a-*t*Bu** form a pocket in which a benzene molecule is encapsulated (Figure 3.14).

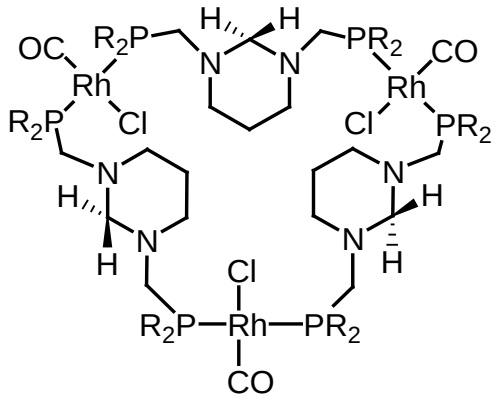

R = ^{t}Bu, **3.14a-*t*Bu**

Figure 3.12 Trimer complex 3.14a-*t*Bu.

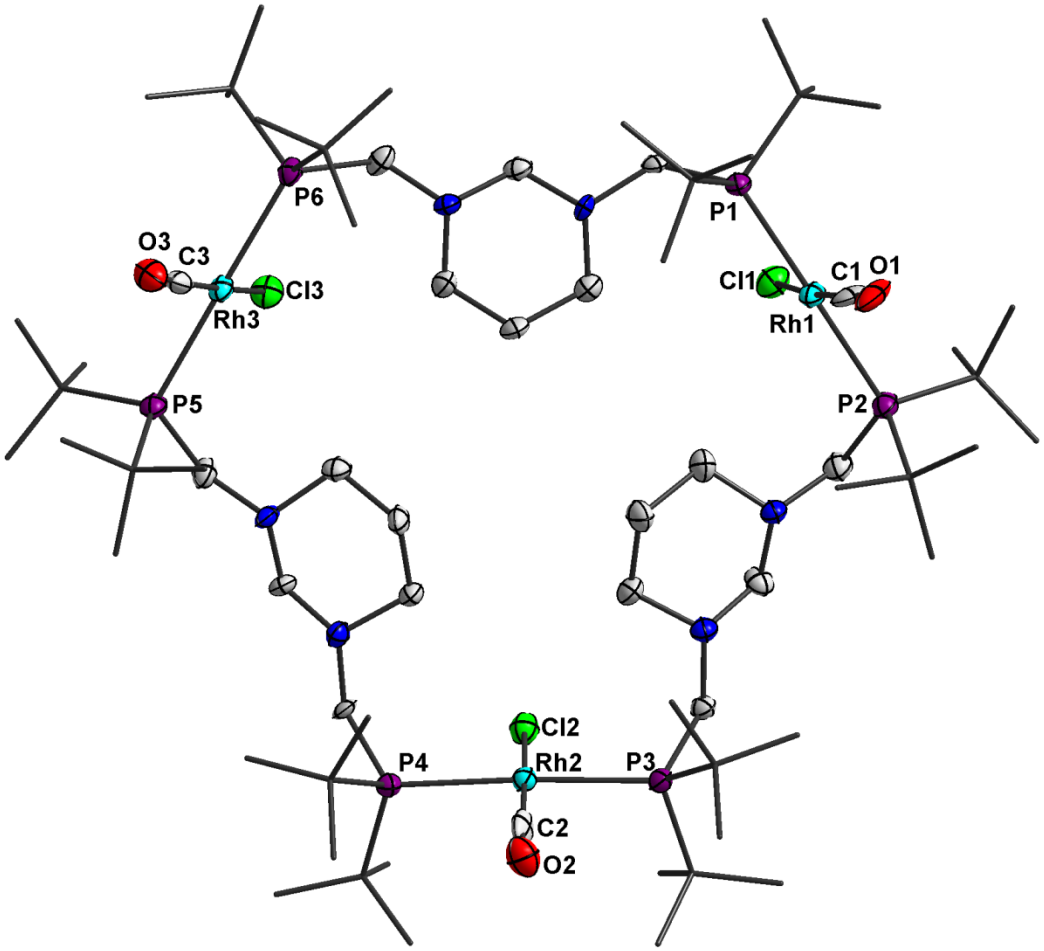

Figure 3.13 Solid-state molecular structure of complex 3.14a-*t*Bu with thermal ellipsoids at the 50 % probability, with the exception of the phosphine substituents, which have been modeled as "sticks". All hydrogen atoms and benzene solvent molecules have been removed for clarity. Selected bond lengths (Å) and bond angles (°): Rh1-C1 1.795(8), Rh2-C2, 1.788(9), Rh3-C3 1.800(9), C1-O1 1.061(10), C2-O2 1.105(16), C3-O3 1.118(9), Rh1-P1 2.372(3), Rh1-P2 2.384(3), Rh2-P3 2.361(2), Rh2-P4 2.363(2), Rh3-P5 2.380(3), Rh3-P6 2.382(3), Rh1-Cl1 2.392(3), Rh2-Cl2 2.411(5), Rh3-Cl3 2.384(2), C1-Rh1-Cl1 173.9(4), P1-Rh1-P2 178.21(9), C2-Rh2-Cl2 173.4(5), P3-Rh2-P4 174.94(9), C3-Rh3-Cl3 175.0(3), P5-Rh3-P6 178.80(8).

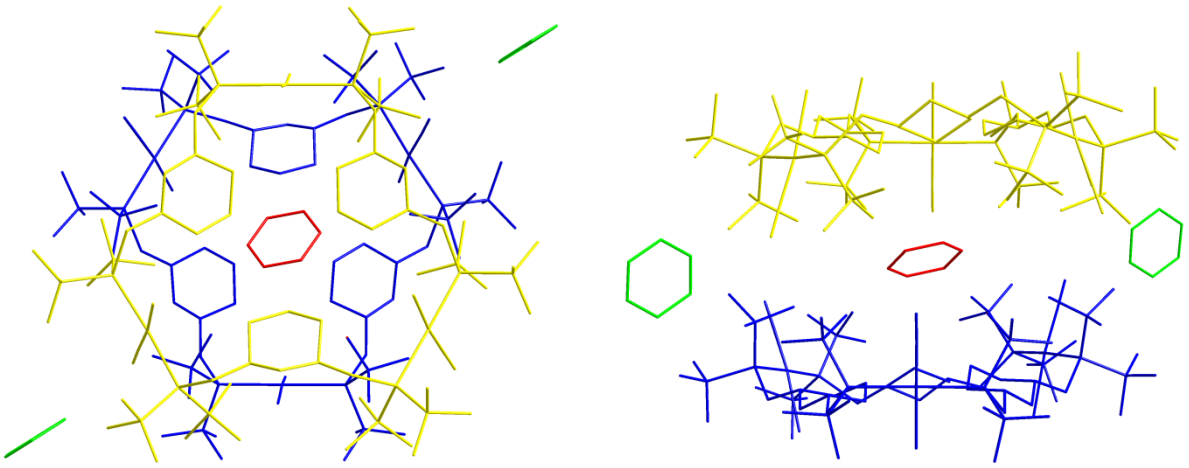

Figure 3.14 Left: top view, and right: side view of crystal packing of two molecules of complex 3.14a-*t*Bu (blue and yellow) displaying the pocket generated in which a benzene molecule is encapsulated (red) and two other benzene molecules are positioned on the periphery (green).

When the reaction between compound H_2(**3.1a-*t*Bu**) and $[Rh(CO)_2Cl]_2$ was carried out in THF instead of benzene, the desired complex [**3.13a-*t*Bu**][Cl] could be synthesized in good yield (90 %). The ^{1}H NMR spectrum of the reaction mixture displayed a signal at 9.6 ppm, which was assigned to formaldehyde proposed to be generated via the hydrogenation of CO in the reaction.

The ^{1}H NMR spectrum of complex [**3.13a-*t*Bu**][Cl] displayed the signal for the *tert*-butyl phosphine substituents, a virtual triplet at 1.31 ppm ($^1J_{PH}$ = 7.2 Hz) and the signal for the methylene pendant arm linkers, a broad virtual triplet at 4.22 ppm. The coupling pattern displayed by these two signals suggests that the complex [**3.13a-*t*Bu**][Cl] is a square planar symmetrical complex, which is in contrast with what was reported for the Rh-carbonyl complex **3.P** (Figure 3.15).[165] Complex **3.P** is the only other reported Rh-carbonyl complex with an NHC-based PCP pincer ligand. The ^{31}P NMR spectrum of complex [**3.13a-*t*Bu**][Cl] displayed

the expected doublet resonance (δ = 82.8 ppm, $^{1}J_{RhP}$ = 129.8 Hz), which is downfield shifted with respect to that observed for complex **3.5a-*t*Bu** (δ = 62.0 ppm). The $^{13}C\{^{1}H\}$ NMR spectrum of complex [**3.13a-*t*Bu**][Cl] displayed two downfield shift signals with the characteristic doublet of triplets coupling pattern, one corresponding to the carbonyl ligand (δ = 199.6 ppm, $^{1}J_{RhC}$ = 58.6 Hz, $^{2}J_{PC}$ = 11.8 Hz) and one corresponding to the carbene center (δ = 203.5 ppm, $^{1}J_{RhC}$ = 42.1 Hz, $^{2}J_{PC}$ = 8.3 Hz).

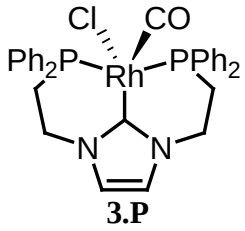

3.P

Figure 3.15 Reported Rh-carbonyl complex 3.P.

The difference in the signals observed in the NMR spectra of complex [**3.13a-*t*Bu**][Cl] in comparison to those of the NMR spectra of complex **3.5a-*t*Bu** confirmed that a new species was synthesized. The ^{1}H NMR spectrum of complex [**3.13a-*t*Bu**][Cl] suggested that the complex was symmetric hence, a square planar cationic complex [**3.13a-*t*Bu]**$^{+}$ with the chloride anion not coordinated was proposed. In order to confirm the proposed structure, an anion exchange reaction was carried out (Scheme 3.19). A THF solution of complex [**3.13a-*t*Bu**][Cl] was reacted with a stoichiometric amount of silver triflate. The reaction mixture was stirred, filtered, and the volatiles from the filtrate removed under vacuum, yielding complex [**3.13a-*t*Bu**][OTf]. The ^{1}H and ^{31}P NMR spectra of complex [**3.13a-*t*Bu**][OTf] were identical to those of complex [**3.13a-*t*Bu**][Cl], and the $^{13}C\{^{1}H\}$ NMR spectrum only differed by the presence of a signal

corresponding to the carbon of the OTf^- counter anion, confirming the proposed structure for complex [**3.13a-*t*Bu**][Cl].

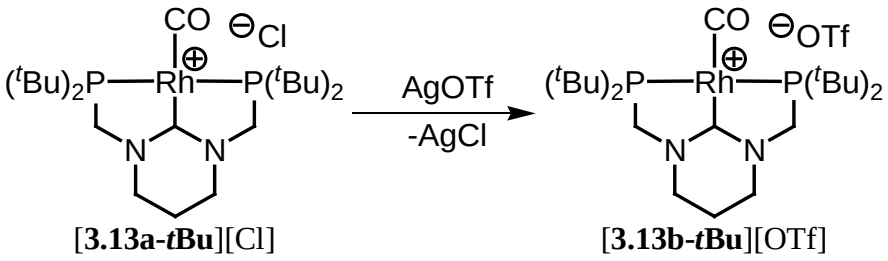

[**3.13a-*t*Bu**][Cl] [**3.13b-*t*Bu**][OTf]

Scheme 3.19 Anion exchange reaction between [3.13a-*t*Bu][Cl] and AgOTf to generate [3.13a-tBu][OTf].

In order to synthesize the desired Rh-carbonyl complexes [**3.13a-Ph**][X] and [**3.13b-Ph**][X] an alternative route had to be employed (Scheme 3.20). $CO_{(g)}$ was bubbled through THF solutions of complexes **3.5a-Ph** and **3.5b-Ph** for a period of 15min, then one equivalent of silver triflate dissolved in THF was slowly added to each reaction. The reaction mixtures were stirred under a stream of $CO_{(g)}$ for an additional 30 min and then filtered. All the volatiles from the filtrate were removed under vacuum, yielding the desired rhodium carbonyl complexes [**3.13a-Ph**][OTf] and [**3.13b-Ph**][OTf].

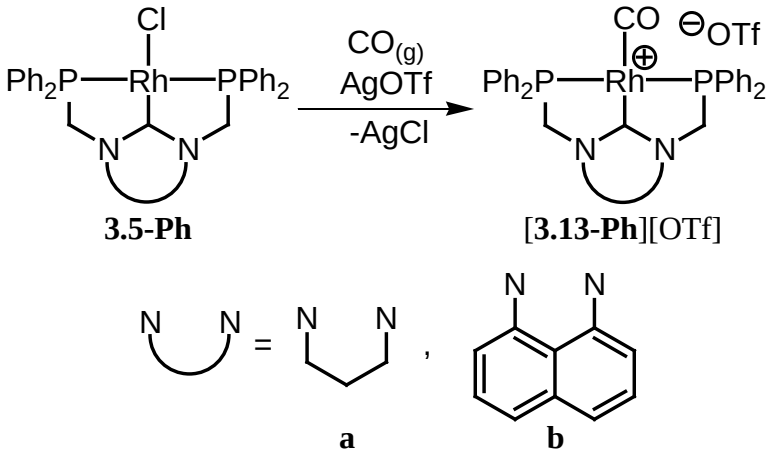

Scheme 3.20 Synthesis of Rh-carbonyl complexes [3.13a-Ph][OTf] and [3.13b-Ph][OTf].

The ^{1}H NMR spectra of complexes [**3.13a-Ph**][OTf] and [**3.13b-Ph**][OTf] displayed the expected resonances with a virtual triplet coupling pattern for the methylene linkers on the side arms at 4.85 ppm ($^{2}J_{PH}$ = 2.4 Hz) and 5.25 ppm ($^{2}J_{PH}$ = 2.6 Hz), respectively. The ^{31}P NMR spectra of the complexes displayed the doublet resonances at 43.2 ppm ($^{1}J_{RhP}$ = 135.6 Hz) for [**3.13a-Ph**][OTf] and 38.8 ppm ($^{1}J_{RhP}$ = 131.2 Hz) for [**3.13b-Ph**][OTf]. The ^{13}C{^{1}H} NMR spectra of the complexes displayed two down field signals for the corresponding carbonyl ligands and the carbene centers at 197.1 ppm and 205.4 ppm ($^{1}J_{RhC}$ = 42.02 Hz, $^{2}J_{PC}$ = 9.6 Hz) for complex [**3.13a-Ph**][OTf], and 195.2 ppm and 208.5 ppm ($^{1}J_{RhC}$ = 48.0 Hz, $^{2}J_{PC}$ = 10.0 Hz) for complex [**3.13b-Ph**][OTf]. In both cases only the signal corresponding to the carbene center was fully resolved into the doublet of triplets, unlike what was observed for complex [**3.13a-*t*Bu**][OTf], where both signals were fully resolved.

X-ray quality crystals of complexes [**3.13a-Ph**][OTf] and [**3.13a-*t*Bu**][OTf] were obtained through slow evaporation of concentrated solutions of the complexes in THF at room temperature, allowing for the unambiguous characterization of both complexes (Figure 3.16). All attempts to crystallize complex [**3.13b-Ph**][OTf] failed. Selected bond lengths and angles for

complexes [**3.13a-Ph**][OTf] and [**3.13a-*t*Bu**][OTf] are summarized in Table 3.2. The synthesis of the Rh-carbonyl complex [**4.4-*t*Bu**][OTf] (Figure 3.17) was also investigated, and will be fully presented in Chapter 4. However, the solid-state molecular structure of complex [**4.4-*t*Bu**][OTf] (Figure 3.17), and its relevant metric parameters are presented in Table 3.2, due to their significance to the discussion.

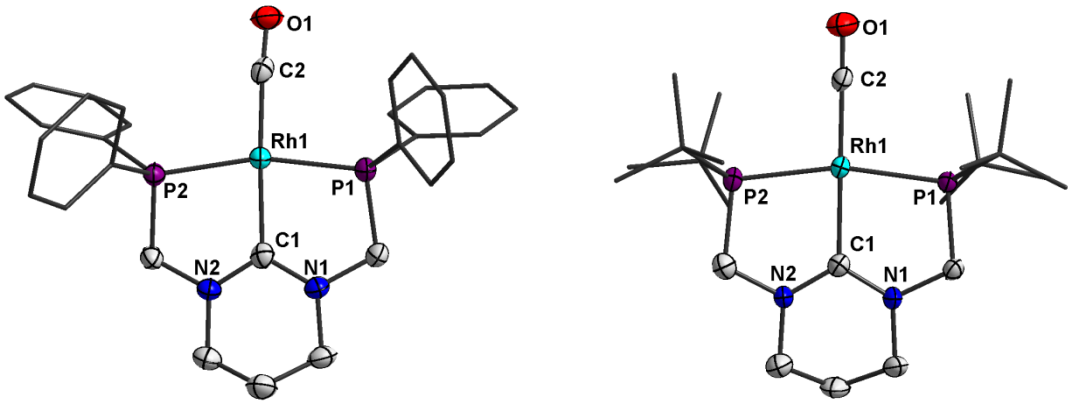

Figure 3.16 Solid-state structure of the cations of complexes [3.13a-Ph][OTf] (left) and [3.13a-*t*Bu][OTf] (right) with thermal ellipsoids at 50 % probability, except for the phosphine substituents, which have been modeled as "sticks". All hydrogen atoms and the OTf counter anions have been omitted for clarity.

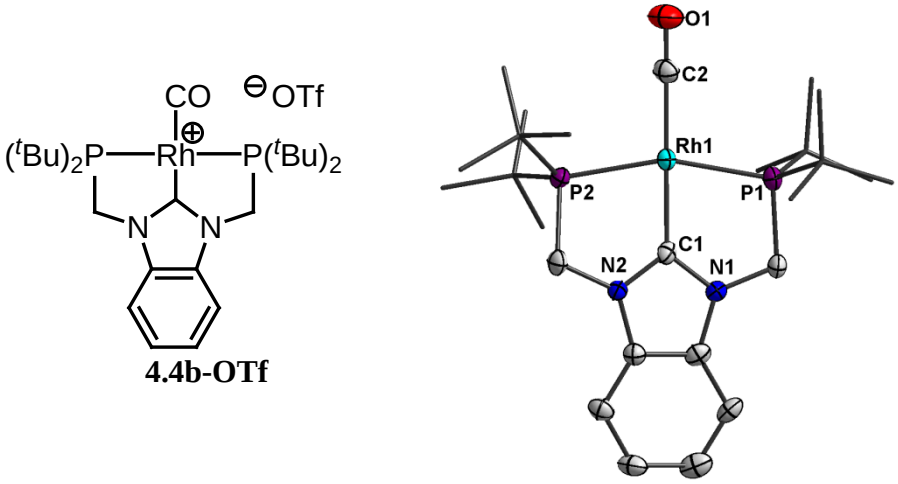

Figure 3.17 Rh-carbonyl complex [4.4-*t*Bu][OTf] and solid-state structure of its cation with thermal ellipsoids at the 50 % probability, with the exception of the phosphine substituents, which are modeled as "sticks". All hydrogen atoms and the triflate counter anion have been removed for clarity.

Table 3.2 Selected bond lengths (Å) and angles (°) for cations [3.13a-Ph]$^+$, [3.13a-*t*Bu]$^+$, and 4.4-*t*Bu$^+$.

Parameter	**[3.13a-Ph]$^+$**	**[3.13a-*t*Bu]$^+$**	**4.4-*t*Bu$^+$**
Rh1-C1	2.065(3)	2.081(5)	1.978(7)
Rh1-P1	2.247(1)	2.285(1)	2.302(2)
Rh1-P2	2.269(1)	2.284(1)	2.300(2)
Rh1-C2	1.865(4)	1.858(7)	1.869(9)
C2-O1	1.141(5)	1.148(8)	1.150(9)
C1-N1	1.340(5)	1.340(7)	1.343(9)
C1-N2	1.341(5)	1.347(7)	1.349(8)
C1-Rh1-C2	174.9(2)	177.2(2)	175.9(3)
P1-Rh1-P2	163.83(3)	164.63(5)	160.41(7)
N1-C1-N2	117.6(3)	117.9(6)	106.8(5)
ϕ	7.6	4.9	7.4

(ϕ) = dihedral angle between the main planes defined by N1-C1-N2-Rh1 and C1-Rh1-P1-P2.

The reported complexes **3.Q**,[1,200] **3.R**,[201] **3.S**,[202] **3.T**,[188] **3.U**,[203,204] and **3.V**[204] (Figure 3.18) are analogous square planar Rh-carbonyl pincer complexes that have been structurally characterized.

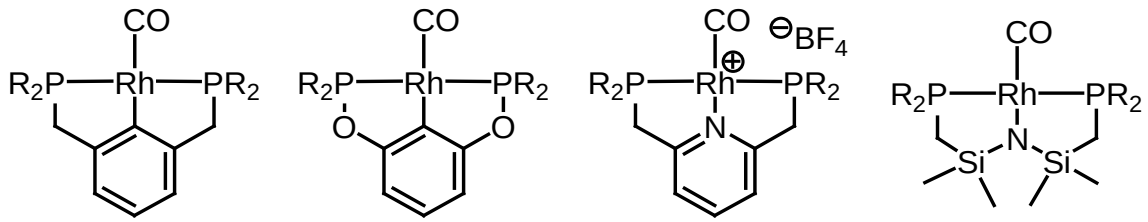

3.Q: R = ^{t}Bu
3.R: R = Pyrrole

3.S: R = ^{t}Bu

3.T: R = ^{t}Bu

3.U: R = Ph
3.V: R = ^{i}Pr

Figure 3.18 Rh-carbonyl pincer complexes 3.Q, 3.R, 3.S, 3.T, 3.U, and 3V.

The Rh-C bonds between the metals and the NHCs in complexes [**3.13a-Ph**][OTf] (2.065(3)Å) and [**3.13a-*t*Bu**][OTf] (2.081(5)Å) (Figure 3.16), are longer than those observed for the other Rh complexes reported in this Chapter: **3.5a-Ph** (1.99(1)Å), **3.5a-*t*Bu** (1.958(3)), **3.5b-Ph** (1.958(5)Å), **3.10b-Ph** (2.007(1) Å), and [**3.12b-Ph**][OTf] (2.025(4) Å). This is in accordance with the stronger *trans*-influence of the carbonyl ligand over chloride and triphenylphosphine. Furthermore the Rh-C bond distances in complexes [**3.13a-Ph**][OTf] and [**3.13a-*t*Bu**][OTf] are similar to those reported for complexes **3.Q** (2.084(9)Å), **3.R** (2.094(2)Å), and **3.S** (2.043(3)Å) (Figure 3.18). On the other hand, the Rh-C_{NHC} bond in complex [**4.4-*t*Bu**][OTf] (1.978(7) Å) (Figure 3.17) is shorter than all the other ones reported. This is counterintuitive considering that six-membered NHCs are expected to be stronger σ-donors than their five membered analogs.[205]

The Rh-C bond distances to the carbonyl carbon of complexes [**3.13a-Ph**][OTf] (1.865(4)Å), [**3.13a-*t*Bu**][OTf] (1.858(7)Å) (Figure 3.16), and [**4.4-*t*Bu**][OTf] (1.869(9)Å) (Figure 3.17) are in the range of those observed for [(PCP)Rh(CO)] complexes **3.Q** (1.848(16)Å), **3.R** (1.887(3)Å), and **3.S** (1.884(3)Å), and longer than those of [(PNP)Rh(CO)] complexes **3.T** (1.818(5)Å), **3.U** (1.811(3)Å), and **3.V** (1.802(3)Å) (Figure 3.18). This points towards a stronger *trans*-influence of NHCs and phenylene ligands over amide and pyridine ones. The carbonyl C≡O bond distances of complexes [**3.13a-Ph**][OTf] (1.141(5)Å), [**3.13a-*t*Bu**][OTf] (1.148(8)Å), and [**4.4-*t*Bu**][OTf] (1.150(9)Å) are similar to those of complexes **3.R** (1.147(3)Å), **3.T** (1.144(6)Å), and **3.U** (1.152(3)Å), but shorter than that for complex **3.V** (1.171(3)Å), and longer than those of complexes **3.Q** (1.128(16)Å), and **3.S** (1.133(4)Å). The difference in the C≡O bond lengths should be, to some extent, representative of the bond order of the CO ligand and hence, dependent on the σ-donating properties of the ligand *trans* to the carbonyl. However, the variation of the bond lengths is limited to a small range (0.05 Å) and hence the sensitivity of the measurement is not considered a reliable source for comparison of subtle electronic changes. Instead, the IR stretching frequency of the CO ligand is considered a more accurate comparison point, since the range in which the absorption band appears spans over 200 wave numbers.[205] Table 3.3 summarizes the IR absorption bands for the CO stretch vibration of the carbonyl-Rh complexes [**3.13a-Ph**][OTf], [**3.13a-*t*Bu**][OTf], [**3.13b-Ph**][OTf], [**4.4-*t*Bu**][OTf], **3.P**,[165] **3.Q**,[1,200] **3.R**,[201] **3.S**,[202] **3.T**,[188] **3.U**,[203,204] **3.V**.[204]

Table 3.3 IR absorption bands (cm^{-1}) for the CO stretch vibration of presented Rh-carbonyl complexes.

Complex	IR *v* (cm^{-1})	Complex	IR *v* (cm^{-1})

[**3.13a-Ph**][OTf]	1980	**3.R**	1969
[**3.13a-*t*Bu**][OTf]	1962	**3.S**	1945
[**3.13b-Ph**][OTf]	2010	**3.T**	1982
[**4.4-*t*Bu**][OTf]	1974	**3.U**	1950
3.P	1933	**3.V**	1932
3.Q	1925		

Lower IR absorption frequencies can be related to a weaker C≡O bond. The IR absorption frequency of a coordinated carbonyl ligand is related to the electronic character of the bonded metal center. Electron-rich metal centers can more readily donate electron density into the σ-antibonding orbital of the carbonyl ligand via π-backbonding, hence weakening the C≡O interaction. In a similar fashion, the electronic character of the metal center is dependent on the ligands bound to it. Overall, a relationship between the IR absorption frequency of the carbonyl and the electron donating properties of the ligands bound to the metal center can be made.[68,206] Ligands *trans* to the carbonyl ligand have been shown to have a prominent effect over the IR absorption frequency, however, ligands *cis* to the carbonyl have also been shown to have an effect on it.[207]

Taking this into consideration, it would appear that out of all the NHC based pincer complexes reported, **3.P** (1933 cm^{-1}) has the most electron rich metal center. Nevertheless, it is important to point out that complex **3.P** is a penta-coordinate complex [(PCP)Rh(CO)Cl] and hence a direct comparison with the square-planar, cationic complexes [**3.13a-Ph**][OTf], [**3.13a-*t*Bu**][OTf], [**3.13b-Ph**][OTf], and [**4.4-*t*Bu**][OTf] cannot be made.

Across the series of complexes [**3.13a-Ph**][OTf], [**3.13a-*t*Bu**][OTf], [**3.13b-Ph**][OTf], and [**4.4-*t*Bu**][OTf], [**3.13a-*t*Bu**][OTf] (Figure 3.16), which is based on a six membered NHC

with the more basic *tert*-butylphosphines in the side arms, is in fact the one with the lowest absorption frequency (1962 cm^{-1}). Complex [**3.13a-*t*Bu**][OTf] is followed by complex [**4.4-*t*Bu**][OTf] (Figure 3.17) (1974 cm^{-1}), and then complex [**3.13a-Ph**][OTf] (Figure 3.16) (1980 cm^{-1}). The order in which these two complexes follow showcases the effect *cis*-ligands have on the CO stretching frequency. Six membered carbenes have been shown to be stronger σ-donors than their five member congeners (e.g. comparing complex [**3.13a-*t*Bu**][OTf] with complex [**4.4-*t*Bu**][OTf]). Nevertheless, the difference in IR absorption frequency between complexes [**4.4-*t*Bu**][OTf] and [**3.13a-Ph**][OTf], due to the size of the NHC backbone ring, is compensated by the effect of the more basic *tert*-butyl substituted phosphines in complex [**4.4-*t*Bu**][OTf]. Complex [**3.13b-Ph**][OTf] (Scheme 3.20) (2010 cm^{-1}) displays the highest absorption frequency of the series. This was attributed to the stronger π-accepting properties of the perimidin-2-ylidines, which compete for the electron density at the metal center.

The carbonyl stretching frequencies observed for the complexes **3.Q**, **3.R**, **3.S**, **3.U**, and **3.V** (Figure 3.18) (1925 cm^{-1}, 1969 cm^{-1}, 1945cm^{-1}, 1932 cm^{-1} and 1950 cm^{-1}) respectively, are lower than those observed for the NHC-based complexes, pointing to the more electron-rich nature of the rhodium metal center in these complexes over those in complexes [**3.13a-Ph**][OTf], [**3.13a-*t*Bu**][OTf], [**3.13b-Ph**][OTf], [**4.4-*t*Bu**][OTf]. On the other hand complex **3.T** displays a higher (1982 cm^{-1}) IR absorption frequency than complexes [**3.13a-Ph**][OTf], [**3.13a-*t*Bu**][OTf], and [**4.4-*t*Bu**][OTf], pointing towards the more electron-rich nature of the rhodium center in the latter complexes over that in **3.T**.

3.8 Synthesis and Characterization of Aryl and Alkyl (PCP)Rh Complexes 3.15a-*t*Bu and 3.16a-*t*Bu

Considering that the complexes of ligand **3.1a-*t*Bu** displayed good solubility in THF and toluene, and that, out of the complexes reported herein, the carbonyl rhodium complex [**3.13a-*t*Bu**][OTf] was deemed the one with the most electron rich metal center, the research focus of this project shifted towards the development of reactive rhodium complexes with ligand **3.1a-*t*Bu**. The synthesis of organorhodium(I) species was attempted, since analogous organorhodium(I) complexes, **3.W**,[187,189,208,209] **3.X**,[210] and **3.Y**[211] (Figure 3.19) with neutral PNP pincer ligands have been shown to be quite reactive.[187,189,208-212] The reaction of complex **3.5a-*t*Bu** with stoichiometric amounts of phenyl-lithium was shown to produce the desired [(PCP)Rh-phenyl] complex **3.15a-*t*Bu** (Scheme 3.21).

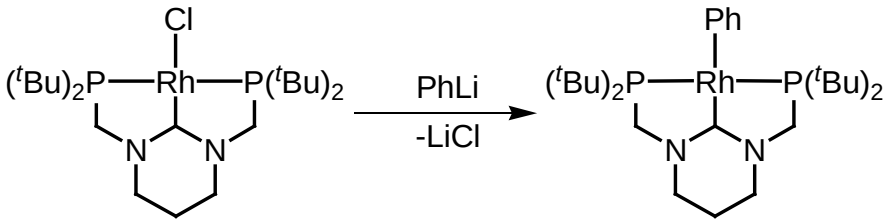

3.5a-*t*Bu **3.15a-*t*Bu**

Scheme 3.21 Synthesis of rhodium-phenyl complex 3.15a-*t*Bu.

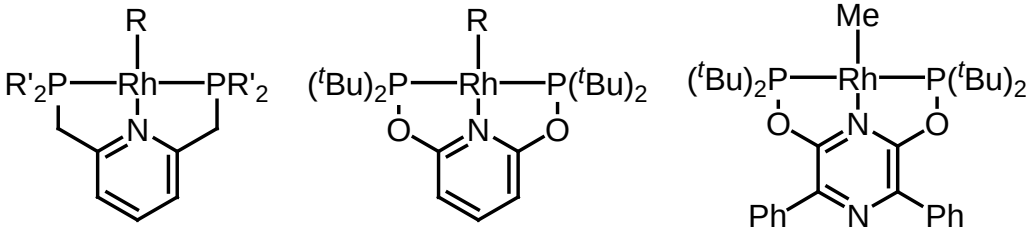

3.W
R = Me, Ph
R' = *t*Bu, Ph

3.X
R = Me, Ph

3.Y

Figure 3.19 Reported organorhodium(I) complexes with a neutral PNP pincer ligand.

The successful synthesis of complex **3.15a-*t*Bu** was confirmed via multinuclear NMR spectroscopy. The ^{1}H NMR spectrum of complex **3.15a-*t*Bu** had the expected resonances for the pincer ligand, but more importantly it also displayed the signals for the protons from the phenyl ring at 7.03 ppm (virtual triplet, J_{HH} = 7.2 Hz), 7.32 ppm (virtual triplet, J_{HH} = 7.4 Hz), and 8.14 ppm (broad doublet, J_{HH} = 7.3 Hz). The ^{31}P NMR spectrum of complex **3.15a-*t*Bu** displayed the usual doublet resonance, δ = 65.1 ppm ($^{1}J_{RhP}$ = 167.9 Hz), which is slightly downfield from that of complex **3.5a-*t*Bu**, δ = 62.0 ppm ($^{1}J_{RhP}$ = 157.3 Hz). More importantly the ^{13}C{^{1}H} NMR spectrum of complex **3.15a-*t*Bu** featured the characteristic signal for the carbene carbon with the usual doublet of triplets coupling pattern, δ = 178.9 ppm ($^{1}J_{RhC}$ = 27.3 Hz, $^{2}J_{PC}$ = 13.9 Hz), this is significantly upfield shifted in comparison to the signal for complex **3.5a-*t*Bu**, δ = 208.9 ppm ($^{1}J_{RhC}$ = 58.6 Hz, $^{2}J_{PC}$ = 8.2 Hz). The ^{13}C{^{1}H} NMR spectrum of complex **3.15a-*t*Bu** also had all the signals for the phenyl ligand: δ = 119.4 ppm, 125.1 ppm ($^{3}J_{RhC}$ = 1.1 Hz), 128.9 ppm, and 143.7 ppm ($^{3}J_{PC}$ = 1.86 Hz).

X-ray quality crystals of complex **3.15a-*t*Bu** were obtained via slow evaporation of a concentrated solution in THF at room temperature. The solid-state molecular structure of the complex, as well as selected bond lengths and angles are presented in Figure 3.20. Complex **3.15a-*t*Bu** is the first crystallographically characterized Rh-phenyl complex with a neutral pincer ligand. The Rh1-C1 bond distance in complex **3.15a-*t*Bu** (2.022(5) Å) is longer than that in Rh-Cl complex **3.5a-*t*Bu** (1.958(3) Å), in agreement to what is expected for the stronger *trans*-influence of the $C_6H_5^-$ over the Cl^- ligand.[213] However, the Rh1-C1 bond in complex **3.15a-*t*Bu** is shorter than that in Rh-CO complex [**3.13a-*t*Bu**][OTf] (2.081(5)), in dissagrement to the *trans*-influence series. The reason for the observed elongation of the Rh1-C1

bond is assumed to be linked to be the ability of the carbonyl ligand to compete with the carbene center for the available electron density at the metal center through π-backbonding. The phenyl ligand in complex [**3.13a-*t*Bu**][OTf] is perpendicular with respect to the plane of the metal ϕ2 = 83.9°), hence minimizing the steric repulsion between the bulky *tert*-butyl substituents and the phenyl ring.

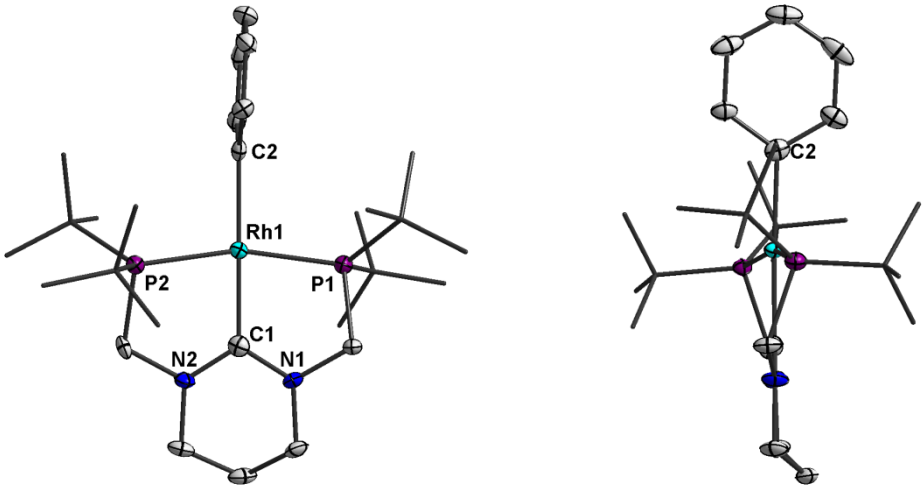

Figure 3.20 Solid-state molecular structure of complex 3.15a-*t*Bu with thermal ellipsoids at the 50 % probability, with the exception of the phosphine substituents, which have been modelled as sticks. All hydrogen atoms have been removed for clarity. Selected bond lengths (Å) and bond angles (°): Rh1-C1 2.022(5), C2-Rh1 2.120(5), Rh1-P1 2.251(2), Rh1-P2 2.249(2), C1-N1 1.356(8), C1-N2 1.359(7), C1-Rh1-C2 177.9(8), P1-Rh1-P2 163.05(6), N1-C1-N2 115.8(5). Dihedral angle between the main planes defined by, C1-P2-Rh1-P1 and the six carbon atoms from the phenyl ring ϕ2 = 83.9.

The reactivity of complex **3.15a-*t*Bu** towards molecules with acidic protons (i.e. methanol, phenol, ammonia, hydrazine, and water) was investigated (Scheme 3.22). It was soon found that, unless purified by crystallization, all isolated samples of **3.15a-*t*Bu** contained residual amounts of LiCl, which readily interfered with the reactivity studies. The presence of LiCl in the reaction mixtures lead to formation of the parent Rh-Cl complex

3.5a-*t*Bu regardless of the reaction being studied (Scheme 3.22). A reaction between the Rh-phenyl complex **3.15a-*t*Bu** and the molecules with an acidic proton took place for all the studied cases, as was shown by the elimination of benzene, confirmed via ^{1}H NMR spectroscopy of the reaction mixtures. However, all attempts to obtain the reaction products out of the reaction mixtures led to the isolation of complex **3.5a-*t*Bu**. We postulate that the lattice energy of complex **3.5a-*t*Bu** is driving these reactions.

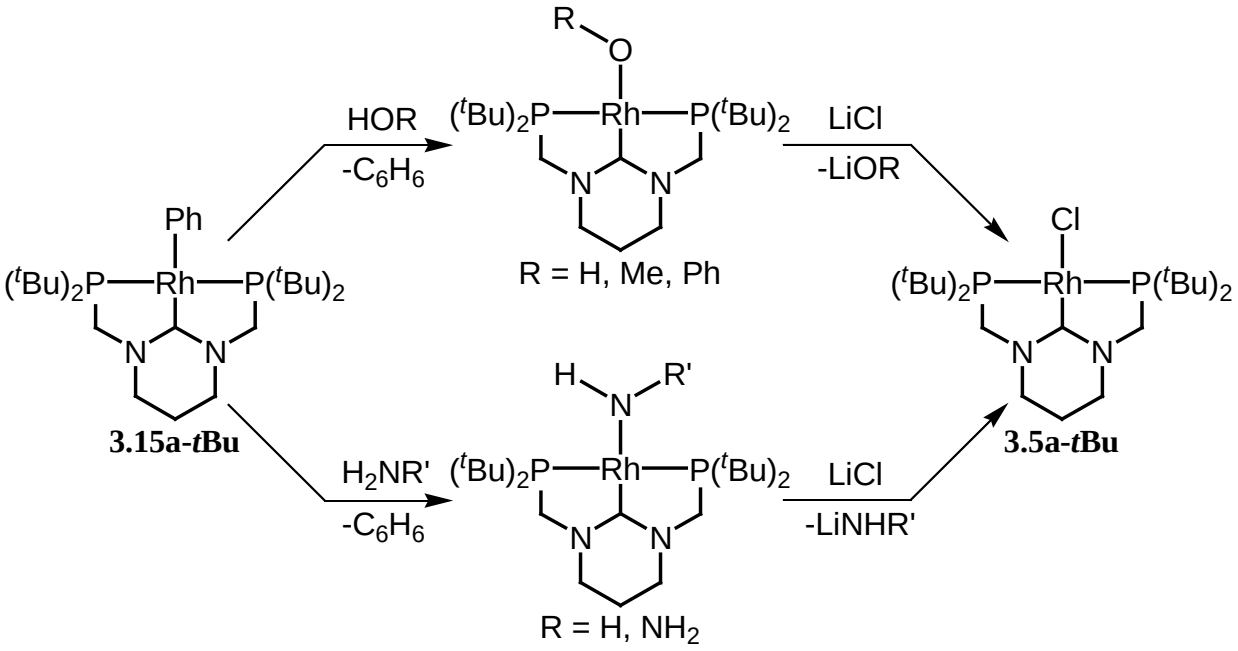

Scheme 3.22 Reactivity studies carried out for complex 3.15a-*t*Bu.

As mentioned earlier, crystallization of complex **3.15a-*t*Bu** was proven successful in the isolation of LiCl free complex. However, this method only allowed for the isolation of 15 to 30 mg of the complex at a time, in time intervals of 10 to 15 days for the crystals to grow, hence this method prove to be extremely time consuming and impractical.

The ether solution of phenyl-lithium used for the synthesis of complex **3.15a-*t*Bu** was assumed to be the source of LiCl in solution. Different from phenyl lithium, methyl lithium can

be readily isolated out of ethereal solutions into a solid and hence, the decision to synthesize methyl complex **3.16a-*t*Bu** instead of the phenyl complex **3.15a-*t*Bu** was made. The use of a solvent-free lithium salt ensured the absence of any ether in the reaction mixture, which should allow the LiCl to fully precipitate. Rhodium-methyl complex **3.16a-*t*Bu** could be readily synthesized by reacting complex **3.5a-*t*Bu** with one equivalent of methyl lithium in toluene for 30 min (Scheme 3.23). Filtration of the resulting suspension followed by removal of the volatiles from the filtrate yielded complex **3.16a-*t*Bu** as a yellow powder. Complex **3.16a-*t*Bu** is closely related to the methyl complex **3.Z**, (Figure 3.21), reported by Fryzuk and coworkers, [139] as well as to the methyl complexes **3.W**, **3.X** and **3.Y** (Figure 3.19).

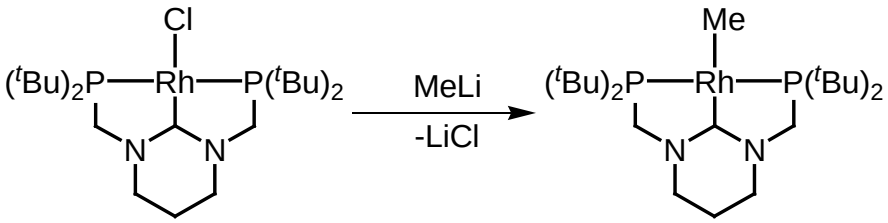

3.5a-*t*Bu **3.16a-*t*Bu**

Scheme 3.23 Synthesis of rhodium-methyl complex 3.16a-*t*Bu.

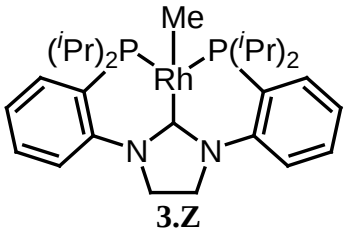

3.Z

Figure 3.21 Reported [(PCP)RhMe] complex 3.Z

The ^{1}H NMR spectrum of complex **3.16a-*t*Bu** displayed the expected signals for the pincer ligand, but more importantly, it displayed the upfield resonance for the methyl protons as the expected doublet of triplets at 0.29 ppm ($^2J_{RhH}$ = 1.64 Hz, $^3J_{PH}$ = 5.5 Hz). The ^{31}P NMR

spectrum showed the expected doublet resonance at 68 ppm ($^1J_{RhP}$ = 167.3 Hz), which is downfield with respect to that of complex **3.15a-*t*Bu** (δ = 65.1 ppm). The $^1H\{^{13}C\}$ NMR spectrum of complex **3.16a-*t*Bu** showed both the upfield signal for the methyl carbon at -15.5 ppm ($^1J_{RhC}$ = 20.0 Hz, $^2J_{PC}$ = 12.5 Hz), and the downfield signal for the carbene carbon, at 217.7 ppm ($^1J_{RhC}$ = 40.3 Hz, $^2J_{PC}$ = 8.5 Hz). Both signals had similar doublet of triplets coupling patterns. The signal corresponding to the methyl carbon was similar to that reported for complex **3.Z**, at −10.3 ppm ($^1J_{RhC}$ = 19 Hz, $^2J_{PC}$ = 13 Hz).[139]

X-ray quality crystals of complex **3.16a-*t*Bu** were obtained by slow evaporation of a concentrated toluene solution at room temperature. The solid-state molecular structure and selected bond lengths and angles are presented in Figure 3.22.

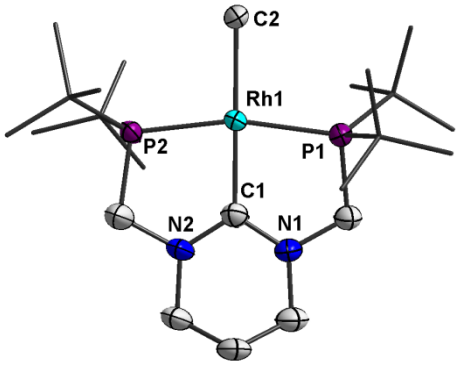

Figure 3.22 Solid-state molecular structure of complex 3.16a-*t*Bu with thermal ellipsoids at the 50 % probability, with the exception of the phosphine substituents, which have been modelled as "sticks". All hydrogen atoms have been removed for clarity. Selected bond lengths (Å), and bond angles (°): Rh1-C1 2.004(8), Rh1-C2 2.189(8), P1-Rh1 2.2413(11), P2-Rh1 2.2316(11), C1-N1 1.356(6), C1-N2 1.360(8), C1-Rh1-C2 178.2(3), P1-Rh1-P2 165.5(5), C1-N1-C2 114.7(4). Dihedral angle between the main planes generated by N2-C1-N1-Rh1 and P2-Rh1-P1-C1: ϕ = 6.4.

The Rh1-C1 bond distance in complex **3.16a-*t*Bu** (2.004(8)Å) fits well in the series of the other structurally characterized neutral complexes with ligand **3.1a-*t*Bu**: **3.5a-*t*Bu** (1.958(3) Å), and **3.15a-*t*Bu** (2.022(5) Å), with regards to the *trans*-influence strength of the ligands *trans* to the carbene $C_6H_5^- > CH_3^- > Cl^-$.[213] The Rh-Me bond distance in complex **3.16a-*t*Bu** (2.189(8) Å) is longer than those reported for complexes **3.W-*t*Bu** (2.102(6) Å),[187] and **3.Y** (2.160(2) Å).[211] The P1-Rh1-P2 angle in complex **3.16a-*t*Bu** (165.5(5)°) is in the expected range for classical pincer complexes 155-170°.

The thermal decomposition of complex **3.Z** via a P-C bond activation leading to the formation of complex **3.K-Me** (Figure 3.6) was reported by Fryzuk and coworkers.[139] The thermal stability of the analogous organorhodium complexes, **3.15a-*t*Bu** and **3.16a-*t*Bu**, was tested by heating toluene solutions of the complexes to 110 °C. The samples were monitored via multinuclear NMR spectroscopy and no signs of decomposition were observed even after 72 h of continued heating. The added thermal stability of complexes **3.15a-*t*Bu** and **3.16a-*t*Bu** could be explained by the better coordination geometry provided by the five membered metallacycles generated by ligand **3.1a-*t*Bu**.

Unfortunately, all efforts to eliminate the LiCl by-product were proven unsuccessful, and reactivity studies carried out with complex **3.16a-*t*Bu** had a similar fate as those for complex **3.15a-*t*Bu**. The need for a different transmetallation reagent other than organolithium compounds was clear. Accordingly, the reaction of complex **3.5a-*t*Bu** with diphenylzinc was attempted (Scheme 3.24). However, the reaction did not progress as expected, and no reactivity was observed.

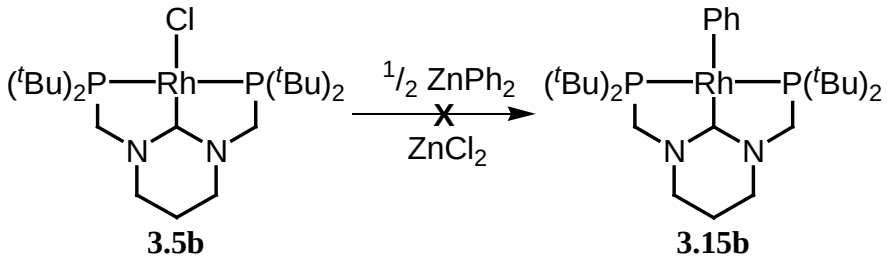

3.5b **3.15b**

Scheme 3.24 Attempted synthesis of complexes 3.15a-*t*Bu with diphenylzinc.

3.9 Conclusions and Outlook

The synthesis of the first NHC-based PCP pincer ligands **3.1a-Ph**, **3.1a-*t*Bu**, and **3.1b-Ph**, which upon coordination generate two five membered metallacycles was achieved. The coordination geometry provided by these ligands in their rhodium complexes **3.5a-Ph**, **3,5a-*t*Bu** and **3.5b-Ph** is similar to that found for the classical phenylide and pyridine-based analogs. The favourable coordination environment generated by the methylene linkers gives rise to shortened Rh-C_{NHC} bond distances, indicating strong bonding between the carbene and the rhodium center and rendering the latter more electron rich. Ligand **3.1a-*t*Bu** was shown to be the strongest σ-donating NHC pincer ligand reported to date, as confirmed by the IR absorption frequency of the CO in the carbonyl complex [**3.13a-*t*Bu**][OTf].

The synthesis of the rhodium complexes of these ligands proceeds via a double C-H bond activation followed by the elimination of hydrogen, and for the case of complex **3.5a-*t*Bu** the competitive hydrogenation of COD. The synthesis of NHC complexes via such activation is unprecedented and hence, this methodology provides access to hitherto unknown NHC-based pincer ligands. However, attempts to coordinate ligand **3.1a-*t*Bu** to metal centers other than

rhodium have been unsuccessful. Investigation into the reaction conditions required by other metals centers for the double C-H bond activation to take place remains a priority of this project.

The rhodium complexes **3.5a-Ph**, **3.5a-*t*Bu**, and **3.5b-Ph** are air and water stable complexes that can be stored for over one year without apparent decomposition. Furthermore, complex **3.5a-*t*Bu** also displayed great thermal stability and could be heated in solution to 110 °C for extended periods of time without signs of decomposition. The low solubility of complexes **3.5a-Ph** and **3.5b-Ph**, and their cationic complexes [**3.12a-Ph**][OTf] and [**3.12b-Ph**][OTf] was a major limiting factor for the proper evaluation of the reactivity properties of the complexes. The ability of complexes [**3.12a-Ph**][OTf] and [**3.12b-Ph**][OTf] to catalyze the hydrosilylation of acetophenone with diphenylsilane was evaluated. Complex [**3.12a-Ph**][OTf] displayed moderate activity with TOF ~ 10 h^{-1} while complex [**3.12b-Ph**][OTf] displayed only limited activity due to competitive activation of the reaction solvent.

The better solubility of complex **3.5a-*t*Bu** allowed for more reactivity studies to be investigated with this complex. The transmetallation of complex **3.5a-*t*Bu** with organolithium reagents allowed for the synthesis of organorhodium complexes **3.15a-*t*Bu** and **3.16a-*t*Bu**. Unfortunately the presence of LiCl by-product could not be avoided and all reactivity studies involving complexes **3.15a-*t*Bu** and **3.16a-*t*Bu** led to the isolation of the stable complex **3.5a-*t*Bu**. Nevertheless, the formation of benzene or methane from the reaction of molecules with acidic protons with complexes **3.15a-*t*Bu** and **3.16a-*t*Bu**, respectively, does suggest that the desired activation reactivity is taking place. The synthesis of complex **3.15a-*t*Bu** with diphenylzinc as the transmetallation reagent was attempted but unsuccessful. Efforts should be focused on the synthesis of pure organorhodium complexes **3.15a-*t*Bu** and **3.16a-*t*Bu** without the

use of organolithium reagents. Further, the reactivity of these complexes towards activation of water, ammonia, and alcohols should be evaluated.

Finally, the reduction of complex **3.5a-*t*Bu** in order to generate a Rh(0) complex represents an interesting avenue worth exploring. Rh(0) complexes are rare with only a few examples of monomeric complexes reported to date.[214,215] The soft donors along with the possibility for π-backbonding to take place make ligand **3.1a-*t*Bu** an excellent candidate for the stabilization of low oxidation state metal centers.

Chapter Four: **PCP Pincer Ligands with a Central 5-Membered *N*-Heterocyclic Carbene Donor**

4.1 Introduction

The robustness displayed by the rhodium pincer complexes described in Chapter 3 was quite promising. The formation of two five-membered metallacycles upon coordination appeared to have a direct impact on the stability displayed by the complexes. However, the synthetic inaccessibility of the amidinium cations of ligand precursors H_2(**3.1a-Ph**), H_2(**3.1a-*t*Bu**), and H_2(**3.1b-Ph**) limited the scope of the developed systems. In particular, the double C-H bond activation required to synthesize the metal complexes **3.5a-Ph**, **3.5a-*t*Bu**, and **3.5b-Ph** is not common for the synthesis of NHC metal complexes,[216] and attempts to synthesize complexes with other metal centers other than Rh (*i.e.* Ir, Pd, Pt) were met without success.

The synthesis of a ligand precursor that generates five membered metallacycles upon coordination, and which could provide a wider scope in regards to the ease of complexation to a variety of metals was envisioned. Combining aspects used for the synthesis of the boryl-pincer ligands from Chapter 2 and the experience gained with the pincer NHC ligands described in Chapter 3, a generic target was proposed (Figure 4.1). The ligand precursors with a central amidinium moiety should allow for metallation with a variety of metal centers.[70]

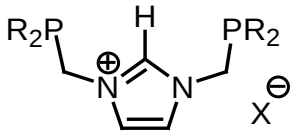

Figure 4.1 Proposed generic pincer ligand precursor with an NHC donor the central position.

The synthetic target is closely related to the boryl pincer ligand precursors reported in Chapter 2 but with a carbene in place of the boryl center. The difunctionalization of 1,2-diamines via reaction with disubstituted phosphinomethanols Ph_2PCH_2OH and $(^tBu)_2PCH_2OH$ had already been proven effective (Scheme 4.1).[94] This is a clear advantage over the use of the 1,3-diamines, where an undesired ring closing reaction was observed under the conditions required for difunctionalization. The reported synthesis of imidazolium salts from 1,2-disubstituted amines is ubiquitous for NHCs.[217,218]

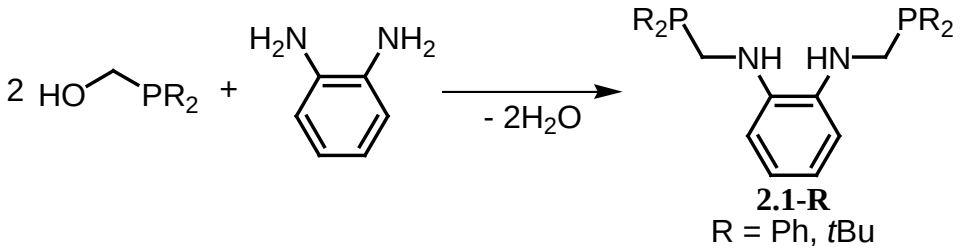

Scheme 4.1 Difunctionalization of *o*-Phenylenediamine.

4.2 Synthesis and Characterization of PCP Pincer Ligand Precursors [H(4.2-R)][PF_6] (R = Ph, *t*Bu)

The synthesis of the desired pincer ligand precursor with an imidazolium salt at the central donor position, [H(**4.2-Ph)**][PF_6], was based on the previously synthesized compound **2.4-Ph** (Scheme 4.2). In a similar fashion to what Fryzuk and coworkers reported for the

synthesis of compound [**H(3.v)**][PF_6] (Figure 4.2),[106] a sulfurated starting material was used. The reason for this was that the subsequent ring closing reactions with an orthoester leaded to the oxidation of the phosphines to the phosphine oxides, which are usually harder to reduce than analogous phosphanethiones. Hence, sulfur acts as a protecting group preventing the formation of phosphine oxides.

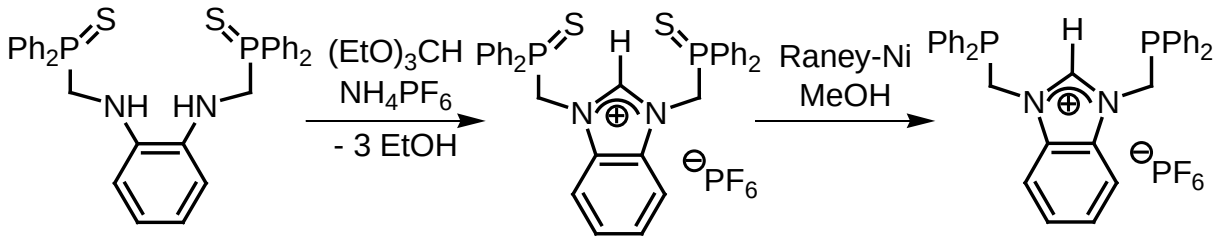

2.4-Ph [H(**4.1-Ph**)][PF_6] [H(**4.2-Ph**)][PF_6]

Scheme 4.2 Synthesis of pincer ligand precursor [H(4.2-Ph)][PF_6].

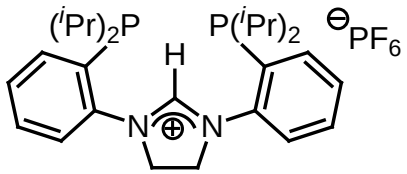

[H(**3.v**)][PF_6]

Figure 4.2 Reported pincer ligand precursor [H(3.v)][PF_6].[106]

Compound **2.4** was suspended in an excess of either trimethylorthoformate or triethylorthoformate, with the orthoester serving as both a reagent and the solvent for the reaction. One equivalent of NH_4PF_6 was then added. The ammonium salt served as a proton source for the elimination of the final equivalent of alcohol in the ring closing step and provided the counteranion in the formation of the imidazolium salt [H(**4.1-Ph**)][PF_6]. The reaction mixture was maintained at a temperature 10 °C below the boiling point of the orthoester (101 °C

for $(MeO)_3CH$ and 146 °C for $(EtO)_3CH$) for 4 h and the alcohol by-product was distilled as the reaction progressed. The intermediate compound, [H(**4.1-Ph**)][PF_6], fully precipitated upon the addition of pentane, and was isolated as an off-white crystalline solid.

The successful synthesis of compound [H(**4.1-Ph**)][PF_6] was confirmed by the presence of the characteristic downfield imidazolium proton signal in the ^{1}H NMR spectrum at 9.69 ppm, along with the disappearance of the signals corresponding to the amine protons from the starting material **2.4** at 4.25 ppm. The ^{31}P NMR spectrum of compound [H(**4.1-Ph**)][PF_6] displays the signal corresponding to the phosphines on the imidazolium ring (δ = 40.9 ppm), which is slightly shifted upfield from that of the phosphines in compound **2.4** (δ = 41.7 ppm). The spectrum also confirms the presence of the hexafluorophosphate counter anion, with a signal at -143.1 ppm (septet, $^1J_{PF}$ = 711 Hz), and the expected relative integration of 1:2 with respect to the imidazolium bound phosphines signal. The presence of the PF_6^- counteranion was further confirmed by the doublet signal in the ^{19}F NMR spectrum at δ = -72.2 ppm, with a matching coupling constant. The success of the ring closing reaction was also supported by the $^{13}C\{^1H\}$ NMR spectrum of compound [H(**4.1-Ph**)][PF_6], which showed a signal at 142.8 ppm, corresponding to the NC(H)N carbon.

The desulfurization of [H(**4.1-Ph**)][PF_6] was carried out via a slightly modified reported procedure.[219] Activated Raney-Ni catalyst, roughly 10-fold excess in weight, was dried and mixed with [H(**4.1-Ph**)][PF_6] and the solids were suspended in deoxygenated methanol. The reaction mixture was degassed and stirred at room temperature, monitoring the progress of the reaction via ^{31}P NMR spectroscopy. No signal for the starting material could be observed after 5 days. The solution was filtered and compound [H(**4.2-Ph**)][PF_6] was extracted from the precipitate with dichloromethane. All the extracted fractions were combined and the volatiles

were removed under vacuum yielding compound [H(**4.2-Ph**)][PF_6] as an off-white crystalline solid (yield 10-15 %).

The successful synthesis of compound [H(**4.2-Ph**)][PF_6] was confirmed by the upfield shift of the ^{31}P NMR signal corresponding to the imidazolium bound phosphines from 40.9 ppm ([H(**4.1-Ph**)][PF_6]) to -13.7 ppm ([H(**4.2-Ph)**][PF_6]). X-ray quality crystals of [H(**4.2-Ph**)][PF_6] were obtained by slow evaporation from a concentrated solution in dichloromethane at -35 °C. The solid-state structure of the cation in [H(**4.2-Ph**)][PF_6] is shown in Figure 4.3, and the selected bond lengths and angles are summarized in Table 4.1. The measured metric parameters are within the expected ranges and will be discussed later on.

The low yield of [H(**4.2-Ph**)][PF_6] was attributed mostly to the low solubility of the starting material [H(**4.1-Ph**)][PF_6] in methanol, which limited the success of the desulfurization reaction. Several attempts to improve the yield of the reaction were carried out without success, and in all cases only small quantities of the desired ligand precursor could be isolated (25 - 50 mg). Attempts to further evaluate the coordination properties of the isolated ligand precursor [H(**4.2-Ph**)][PF_6] were held back and the focus shifted towards the synthesis of the analogous compound [H(**4.2-*t*Bu**)][PF_6] (Scheme 4.3). The *tert*-butyl substituents in [H(**4.2-*t*Bu**)][PF_6] were expected to increase the solubility of the resultant compound in common organic solvents.

In order to synthesize compound [H(**4.2-*t*Bu**)][PF_6], the sulfurated precursor **2.4-*t*Bu**, which had not been investigated during the synthesis of the boryl pincer ligands from Chapter 2, had to be synthesized. Compound **2.4-*t*Bu** was easily obtained by reacting compound **2.1-*t*Bu** with a stoichiometric amount of elemental sulfur in dichloromethane. Removal of the volatiles under vacuum yielded compound **2.4-*t*Bu** as a yellow crystalline powder with an isolated yield

of 98 %. The successful oxidation of the phosphines was confirmed by the presence of a ^{31}P NMR signal at 79.6 ppm, upfield shifted in comparison with that of **2.1-*t*Bu** (δ = 30.1 ppm). Compound **2.4-*t*Bu** was employed in the ring closing reaction in order to obtain the imidazolium salt [H(**4.1-*t*Bu**)][PF_6], following the same procedure as the one described for the synthesis of the analogous compound [H(**4.1-Ph**)][PF_6] (*vide supra*). Just as with [H(**4.1-Ph**)][PF_6], the successful synthesis of the imidazolium salt [H(**4.1-*t*Bu**)][PF_6] was confirmed by the presence of a downfield signal in the ^{1}H NMR spectrum (δ = 10.07 ppm) along with the signals corresponding to the hexafluorophosphate counter anion in the ^{31}P NMR spectrum (δ = -143.5) and the ^{19}F NMR spectrum (δ = -72.3 ppm). The signal for the NCN carbon in the ^{13}C{^{1}H} NMR spectrum was observed at δ = 143.1 ppm.

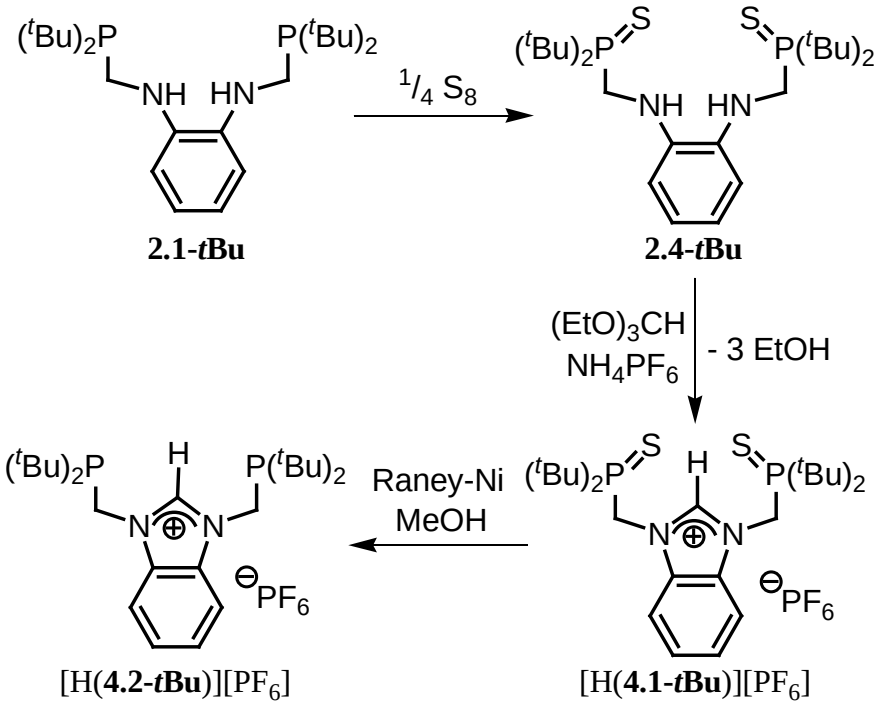

Scheme 4.3 Synthesis of pincer ligand precursor [H(4.2-*t*Bu)][PF_6].

The desulfurization of compound [H(**4.1-*t*Bu**)][PF_6] was carried out in a similar fashion to that described for compound [H(**4.1-Ph**)][PF_6]. However, due to the higher solubility of compound [H(**4.1-*t*Bu**)][PF_6] in common organic solvents, complete reduction was achieved after a reaction time of 36h. Compound [H(**4.2-*t*Bu**)][PF_6] was isolated in 65 % yield with respect to [H(**4.1-*t*Bu**)][PF_6]. The only minor caveat to this reaction was that any attempts to scale it up over the 1 gram scale resulted in incomplete desulfurization, and isolation of an inseparable mixture of sulfurated/desulfurated compounds. Furthermore, attempts to further desulfurize the resulting mixture with fresh Raney-Ni were also unsuccessful. X-ray quality crystals of compound [H(**4.2-*t*Bu**)][PF_6] were obtained by slow evaporation of a solution in dichloromethane at -35 °C. The solid-state structure of the cation in [H(**4.2-*t*Bu**)][PF_6] is presented in Figure 4.4, and selected bond lengths and angles summarized in Table 4.1.

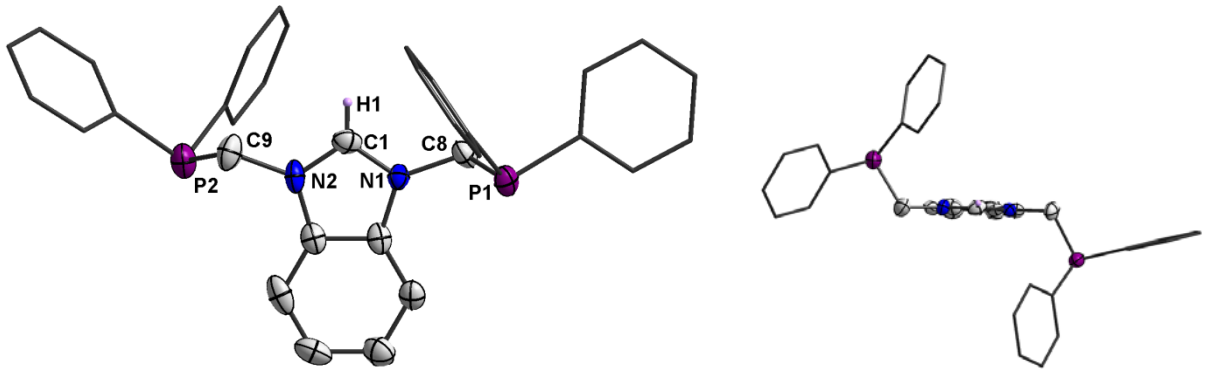

Figure 4.3 Orthogonal views of the solid-state structure of the cation in [H(4.2-Ph)][PF_6] with thermal ellipsoids at 50 % probability, with the exception of the phosphine substituents, which are modeled as "sticks". The PF_6 counter anion and all hydrogen atoms with the exception of the imidazolium proton have been omitted for clarity.

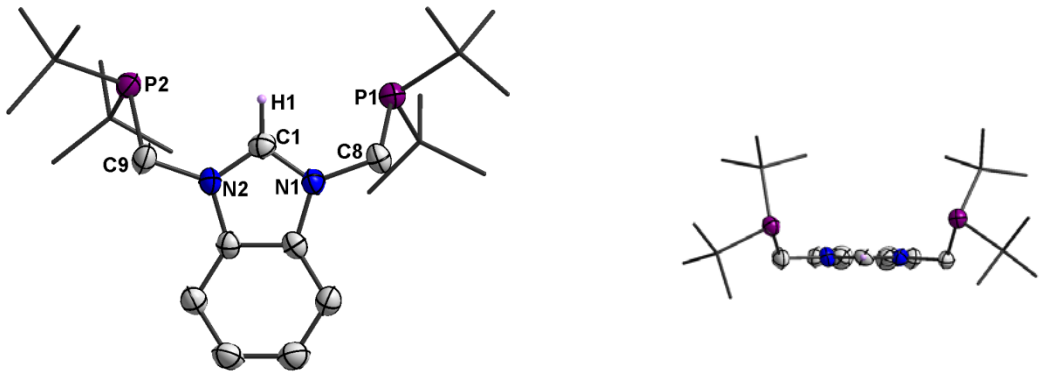

Figure 4.4 Orthogonal views of the solid-state structure of the cation in [H(4.2-*t*Bu)][PF_6] with thermal ellipsoids at 50 % probability, with the exception of the phosphine substituents, which are modeled as "sticks". The PF_6 counter anion and all hydrogen atoms with the exception of the imidazolium proton have been omitted for clarity.

Table 4.1 Selected bond lengths (Å) and angles (°) for PCP pincer ligand precursors [H(4.2-Ph)][PF_6] and [H(4.2-*t*Bu)][PF_6]

Parameter	[H(**4.2-Ph**)][PF_6]	[H(**4.2-*t*Bu**)][PF_6]
C1-N1	1.322(9)	1.329(4)
C1-N2	1.325(13)	1.338(5)
N1-C1-N2	111.4(7)	110.7(3)
H1-C1-N1	123.6(4)	125.6(2)
H1-C1-N2	124.1(5)	123.7(2)
P1-C8-C9-P2	153.5(5)	11.2(2)

The solid-state structures of the cations in [H(**4.2-Ph**)][PF_6] and [H(**4.2-*t*Bu**)][PF_6] revealed the expected trigonal planar geometry of the formamidinium moiety, with the sum of the three bond angles around the carbon centers being 359.1° and 360°, respectively. The C1-N1 and C1-N2 bond lengths for both complexes (1.322(9) Å and 1.325(13) Å for [H(**4.2-Ph**)][PF_6]; 1.329(4) Å and 1.338(5) Å for [H(**4.2-*t*Bu**)][PF_6]) correlate favourably to the average value of

1.324(14) Å found in reported crystal structures for imidazolium ions.[220,221] Furthermore, the bond lengths support the multiple-bond character anticipated in the 4-π-electron formamidinium N1-C1-N2 unit.

The phosphine pendant arms in compound [H(**4.2-Ph**)][PF_6] adopt an *anti* conformation (Figure 4.3) with respect to the plane of the imidazolium ring, while those present in compound [H(**4.2-*t*Bu)**][PF_6] adopt a *syn* conformation (Figure 4.4). The observed conformations are unusual on the grounds of steric repulsion, since the *tert*-butyl substituents in [H(**4.2-*t*Bu**)][PF_6] are expected to be more sterically demanding than the phenyl substituents in [H(**4.2-Ph**)][PF_6], so one could expected the conformation of [H(**4.2-*t*Bu**)][PF_6] to be *anti* as well. A closer look at the crystal structure of [H(**4.2-*t*Bu**)][PF_6] revealed that the conformation adopted by the phosphines is due to weak interactions between the *tert*-butyl phosphine substituents and the imidazolium proton with the hexafluorophosphate counter anion. In the case of compound [H(**4.2-*t*Bu**)][PF_6], both pendant arms interact with the counter anion, while in the case of [H(**4.2-Ph**)][PF_6] only one of them does.

4.3 Synthesis and Characterization of (PCP)Rh Complexes 4.3-*t*Bu and [4.4-*t*Bu][OTf]

The desired Rh complex **4.3-*t*Bu** was synthesized via the free carbene **4.2-*t*Bu**, which could be obtained through the deprotonation of compound [H(**4.2-*t*Bu**)][PF_6] with KHMDS in THF (Scheme 4.4). The free carbene **4.2-*t*Bu** was not isolated, but the success of the deprotonation was confirmed via the loss of the downfield signal at $\delta = 9.54$ ppm corresponding to the imidazolium proton in the ^{1}H NMR spectrum. The *in-situ* generated **4.2-*t*Bu** was then reacted with half an equivalent of $[Rh(cod)Cl]_2$ to generate complex **4.3-*t*Bu** (Scheme 4.4).

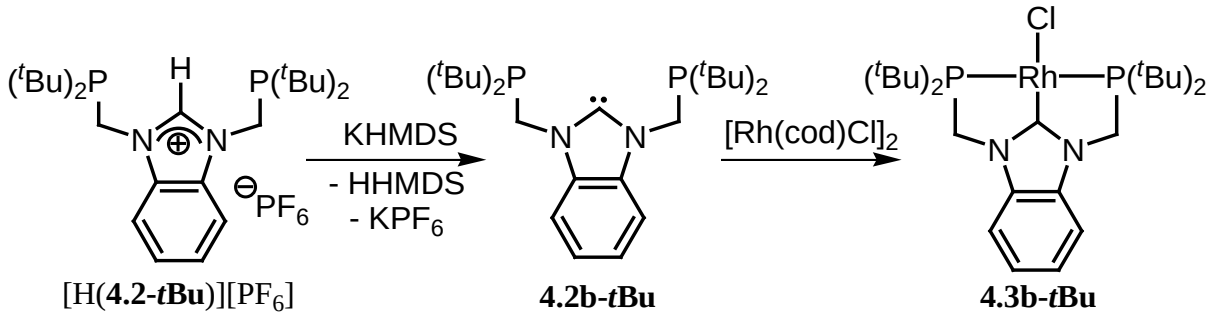

[H(**4.2-*t*Bu**)][PF_6] **4.2b-*t*Bu** **4.3b-*t*Bu**

Scheme 4.4 Synthesis of PCP pincer complex 4.3-*t*Bu via the free carbene 4.2-*t*Bu.

The success of the synthesis of complex **4.3-*t*Bu** was confirmed via multinuclear NMR spectroscopy. The ^{1}H NMR spectrum of the complex displayed two signals with a virtual triplet pattern (δ = 1.49 J_{PH} = 6.6, and 3.52 ppm J_{PH} = 1.8 Hz) that corresponded to the protons of the methyl groups in the *tert*-butyl substituents and to the methylene pendant arms. The virtual triplet coupling pattern observed for complex **4.3-*t*Bu** is commonly seen in symmetrical PCP pincer ligands and is attributed to virtual coupling of the protons to both phosphorus nuclei.[222-224] Hence, the observed virtual coupling confirms that the ligand is bound to the metal center via both phosphines, and that the phosphines are equivalent. The ^{31}P NMR spectrum of complex **4.3-*t*Bu** showed only one signal at 82.5 ppm, which is a doublet due to the coupling of the phosphorus to rhodium with a $^{1}J_{RhP}$ coupling constant of 154.2 Hz. The ^{13}C{^{1}H} NMR spectrum of complex **4.3-*t*Bu** revealed the presence of the downfield signal corresponding to the carbene carbon at 201.8 ppm, which displayed a doublet of triplets coupling pattern with a $^{1}J_{RhC}$ = 54 Hz and a $^{2}J_{PC}$ = 9.8 Hz. X-ray quality crystals of complex **4.3-*t*Bu** were obtained via slow evaporation of a concentrated solution in THF at room temperature, allowing for a solid-state structure determination (Figure 4.5). Selected bond length and angles for complex **4.3-*t*Bu** are summarized in Table 4.2. Metric parameters of related reported Rh complexes **3.J**,[182] **4.a,**[139] and **4.b**,[165] (Figure 4.6, and Figure 4.7) are also presented for comparison (Table 4.2).

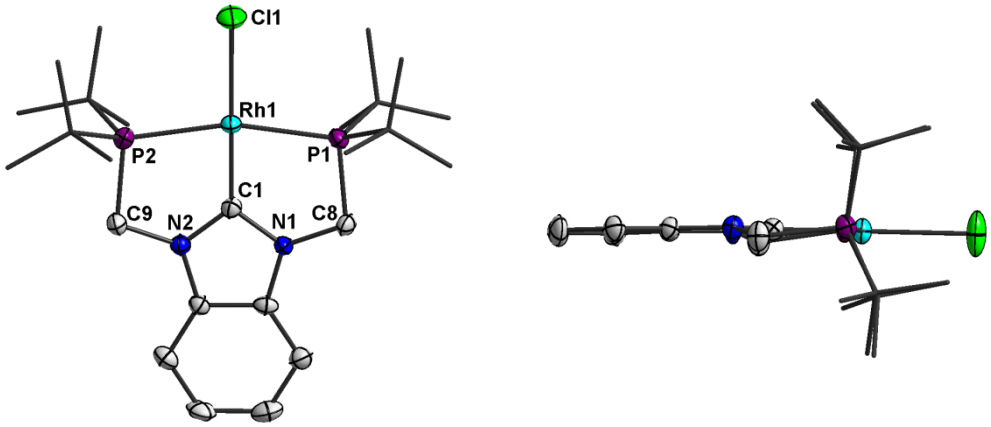

Figure 4.5 Solid-state molecular structure of complex 4.3-*t*Bu with thermal ellipsoids at 50 % probability, with the exception of the phosphine substituents, which are modeled as "sticks". All hydrogen atoms have been omitted for clarity.

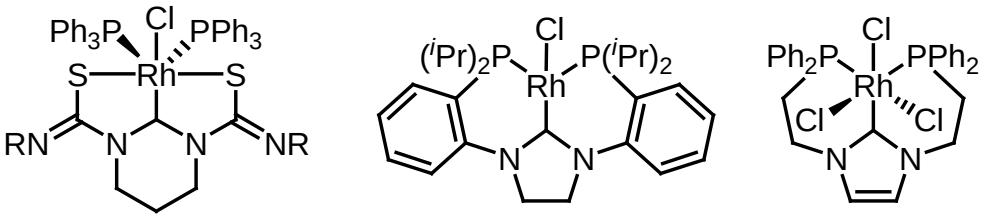

3.J
R = *p*-C_6H_4Cl

4.a

4.b

Figure 4.6 NHC based pincer complexes 3.J,[182] 4.a,[139] and 4.b[165] related to complex 4.3-*t*Bu.

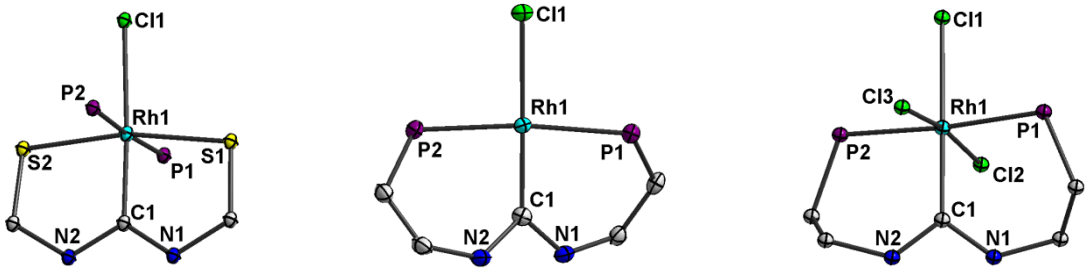

Figure 4.7 From left to right: Fragments from the solid-state molecular structure of complexes 3.J,[182] 4.a,[139] and 4.b[165] showing the rhodium coordination sphere and metallacycles with thermal ellipsoids at 50 % probability.

Table 4.2 Selected bond lengths (Å) and angles (°) for complexes 4.3-*t*Bu, 3.J,[182] 4.a,[139] and 4.b.[165]

Parameter	**4.3-*t*Bu**	**3.J**	**4.a**	**4.b**
C1-Rh1	1.888(4)	1.929(1)	1.928(6)	2.002(7)
Cl1-Rh1	2.413(1)	2.442(3)	2.410(2)	2.440(2)
P1-Rh1	2.288(1)	2.349(3)[a]	2.295(2)	2.371(2)
P2-Rh1	2.295(1)	2.335(5)[b]	2.300(2)	2.359(2)
C1-N1	1.377(4)	1.355(11)	1.379(6)	1.352(9)
C1-N2	1.372(6)	1.376(11)	1.374(6)	1.343(9)
C1-Rh1-Cl1	179.6(1)	177.0(3)	175.9(2)	176.1(2)
P1-Rh1-P2	162.5(4)	168.2(1)[c]	171.7(5)	175.4(7)
N1-C1-N2	104.7(3)	115.6(8)	105.(4)	106.1(6)
ϕ	4.0	5.2	42.0	27.3

(ϕ) = dihedral angle between the main planes defined by N1-C1-N2-Rh1 and C1-Rh1-P1-P2; a) S1-Rh1, b) S2-Rh1, c) S1-Rh1-S2.

The Rh1-C1 bond length in complex **4.3-*t*Bu** is considerably shorter than that in complexes **3.J**, **4.a** and **4.b**. Such a short Rh-C distance prompted us to further compare its value with other reported systems. A search through the Cambridge Crystallographic Data Center (CCDC) revealed that the Rh1-C1 bond in complex **4.3-*t*Bu** represents the shortest Rh-C bond observed in a PCP pincer complex, and more surprisingly the shortest Rh-C_{NHC} bond reported to date.[220,221] It appears that a series of factors contribute to optimize the carbene - metal interaction in complex **4.3-*t*Bu**. One of these factors is the small dihedral angle between the main planes defined by N1-C1-N2-Rh1 and C1-Rh1-P1-P2, which allows for better π-backbonding from the Rh metal center to the NHC. The P1-Rh1-P2 angle (162.5°) in complex **4.3-*t*Bu** is close to the average value found for classical PCP Rh complexes (160°) and narrower than the ones found in complexes **4.a** and **4.b** (175.4 and 171.7°).

In order to assess the electron donating properties of ligand **4.2-*t*Bu**, we decided to synthesize the carbonyl complex [**4.4-*t*Bu**][OTf] (Scheme 4.5). The electron donating abilities of additional ligands present in metal carbonyl complexes exert a significant influence on the degree of π-backbonding experienced by the carbonyl ligand, and therefore also influence the C≡O stretching IR absorptions.[68,199,225] Complex [**4.4-*t*Bu**][OTf] was synthesized by reacting a THF solution of complex **4.3-*t*Bu** with one equivalent of silver triflate, while bubbling in $CO_{(g)}$. The desired product was obtained as a yellow crystalline powder in quantitative yield after filtration of the silver chloride and removal of all volatiles under vacuum.

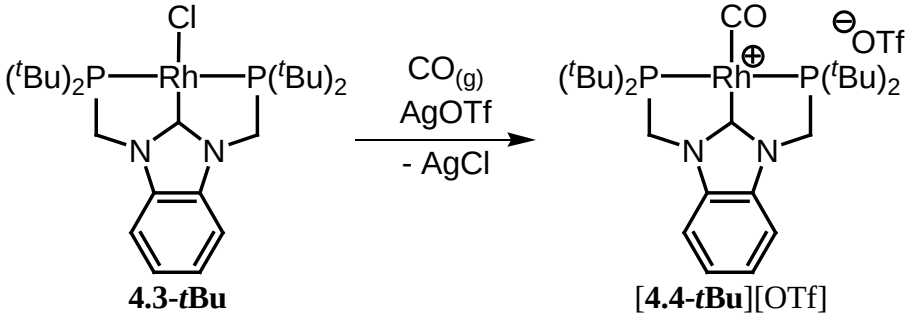

4.3-*t*Bu [**4.4-*t*Bu**][OTf]

Scheme 4.5 Synthesis of PCP-carbonyl complex [4.4-*t*Bu][OTf].

The $^{13}C\{^{1}H\}$ NMR spectrum of complex [**4.4-*t*Bu**][OTf] displayed a signal corresponding to the carbonyl carbon at 195.9 ppm, appearing as a doublet of triplets due to coupling to the Rh center as well as to both phosphorus nuclei ($^{1}J_{RhC}$ = 40.7 Hz and $^{2}J_{PC}$ = 10.8 Hz). The signal corresponding to the carbene carbon at 200.5 ppm also appeared as a doublet of triplets ($^{1}J_{RhC}$ = 58.8 Hz and $^{2}J_{PC}$ = 10.2 Hz). The ^{31}P NMR signal corresponding to the phosphines in complex [**4.4-*t*Bu**][OTf] (δ = 102.4 ppm, d, $^{1}J_{RhP}$ = 132.1 Hz) is downfield with respect to the signal observed for complex **4.3-*t*Bu** (δ = 82.5 ppm, d, $^{1}J_{RhP}$ = 154.2 Hz). The IR spectra of complex [**4.4-*t*Bu**][OTf] had an absorption band at 1982 cm^{-1}, which

corresponded to the C≡O stretching vibration. A comparison of this value with those of other similar rhodium pincer carbonyl complexes was presented in Chapter 3.

The solid-state structure of complex [**4.4-*t*Bu**][OTf] (Figure 4.8) was obtained from a crystal grown by slow evaporation of a concentrated solution of [**4.4-*t*Bu**][OTf] in THF at room temperature. The Rh1-C1 bond distance in [**4.4-*t*Bu**][OTf] (1.978(7) Å) is longer than that observed for complex **4.3-*t*Bu** (1.888(4) Å), which is in accordance with the stronger *trans*-influence of carbonyl versus chlorine. All other metric parameters obtained from the structure were within the ranges observed in similar systems, as discussed in Chapter 3.

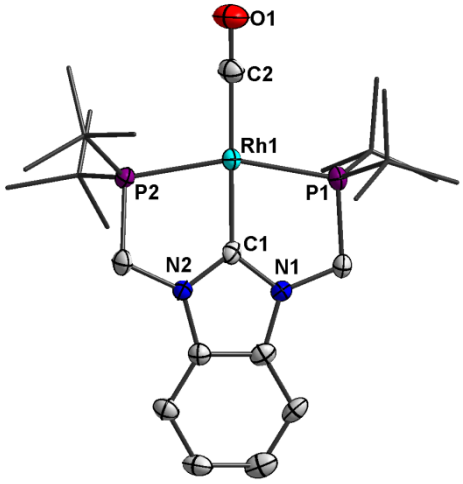

Figure 4.8 Solid-state structure of the cation in complex [4.4-*t*Bu][OTf] with thermal ellipsoids at 50 % probability, with the exception of the phosphine substituents, which are modeled as "sticks". All hydrogen atoms and the triflate counter anion have been omitted for clarity. Selected bond lengths and angles: Rh1-C1 1.978(7), Rh1-C2 1.869(9), Rh1-P1 2.302(2), Rh1-P2 2.300(2), C1-N1 1.343(9), C1-N2 1.349(8), C2-O1 1.150(9), C1-Rh1-C2 175.9(3), P1-Rh1-P2 160.41(7), N1-C1-N2 106.8(5). Dihedral angle between the main planes defined by N1-C1-N2-Rh1 and C1-Rh1-P1-P2 ϕ = 7.4°.

4.4 Synthesis and Characterization of (PCP)Pd and (PCP)Ni Complexes [4.8-*t*Bu][PF_6] and [4.9-*t*Bu][PF_6]

The synthesis of rhodium complexes **4.3-*t*Bu** and [**4.4-*t*Bu**][OTf] allowed for the investigation of the effect the size of the NHC ring has on the coordination properties of the pincer ligand. However, the main purpose for investigating ligand precursor [H(**4.2-*t*Bu**)][PF_6] was to explore its coordination properties with transition metals other than rhodium, overcoming the limitations of the six-membered carbene based ligand systems presented in Chapter 3. For this, we decided to investigate the synthesis of Ni and Pd complexes, inspired by complexes Ni(**[4.c]**[PF_6]), Pd(**[4.d]**[PF_6]) and Pt(**[4.e]**[PF_6]) of ligand precursor [H(**3.v**)][PF_6] (Scheme 4.6), reported by Fryzuk.[106]

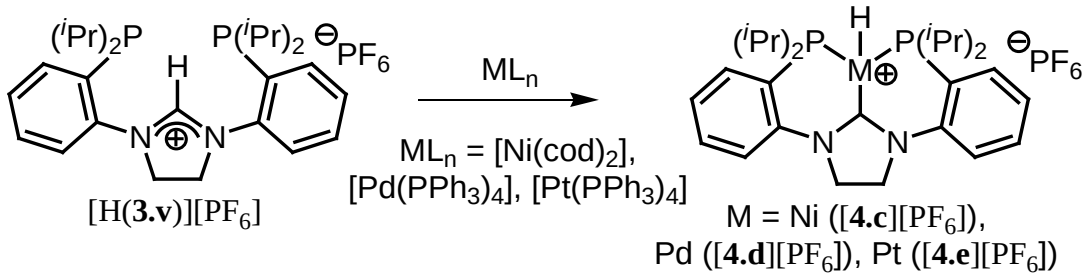

Scheme 4.6 Reported synthesis of transition metal complexes [4.c][PF_6], [4.d][PF_6], and [4.e][PF_6] with ligand precursor [H(3.v)][PF_6].[106]

The first attempt was aimed at the synthesis of Pd complex [**4.5-*t*Bu**][PF_6] (Scheme 4.7). The synthetic protocol employed was based on the reported procedure for the synthesis of complex [**4.d**][PF_6][106]: one equivalent of [$Pd(PPh_3)_4$] was reacted with one equivalent of the ligand precursor [H(**4.2-*t*Bu**)][PF_6] in THF at room temperature. The reaction progress was monitored via ^{31}P NMR spectroscopy.

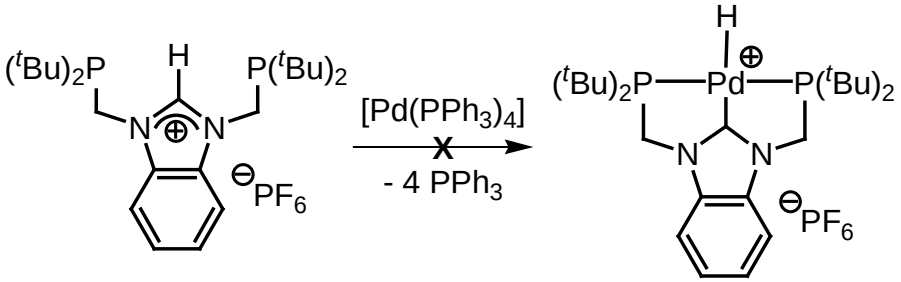

[H(**4.2-*t*Bu**)][PF_6] [**4.5-*t*Bu**][PF_6]

Scheme 4.7 Proposed synthesis of compound [4.5-*t*Bu][PF_6].

The ^{31}P NMR signal corresponding to the free ligand [H(**4.2-*t*Bu**)][PF_6] (δ = 25.8 ppm) was expected to disappear over time, along with the appearance of a downfield shifted signal corresponding to complex [**4.5-*t*Bu**][PF_6]. However, the ^{31}P NMR spectrum suggested that the expected reaction was not taking place. The reaction was allowed to proceed until no further change could be observed via NMR spectroscopy (10h). The $^{31}P\{^1H\}$ NMR spectrum of the reaction mixture displayed signals at 54.7 ppm (dd, J = 238 Hz, J = 29 Hz, 1P), 25.5 ppm (t, J = 29 Hz, 1P), 22.4 ppm (dd, J = 238Hz, J = 29Hz, 0.5P), 21.3 ppm (s, 1P), and 0.4 ppm (s, 2P) (Figure 4.9, top), as well as a signal corresponding to the PF_6^- counter anion (δ = -142.4 ppm, sept, $^1J_{PF}$ = 706 Hz, 1P). The signal for the free PPh_3 (δ = 0.4 ppm) integrated for two phosphorus nuclei, with respect to the PF_6^- signal, instead of four which would be expected if all the PPh_3 had been displaced from the metal center. In order to separate the free PPh_3 from the reaction mixture, all volatiles were removed under vacuum and the solids were washed thoroughly with hexanes. The $^{31}P\{^1H\}$ NMR spectrum of the hexane-washed product displayed no changes for the signals at 54.7 ppm, 25.5 ppm, 22.4 ppm, and -142.4 ppm, but the signal at 21.3 ppm also disappeared (Figure 4.9, bottom). The coupling constants and coupling patterns observed provided evidence of the relationship between the phosphorus signals. Fortunately, slow evaporation from a concentrated THF solution at -35 °C yielded X-ray quality

crystals allowing the unambiguous determination of the molecular structure of complex [**4.6-*t*Bu**][PF_6] (Figure 4.10). The signals on the NMR spectrum of clean [**4.6-*t*Bu**][PF_6] (Figure 4.9, bottom) have been assigned following the numbering scheme in the solid-state molecular structure presented in Figure 4.10.

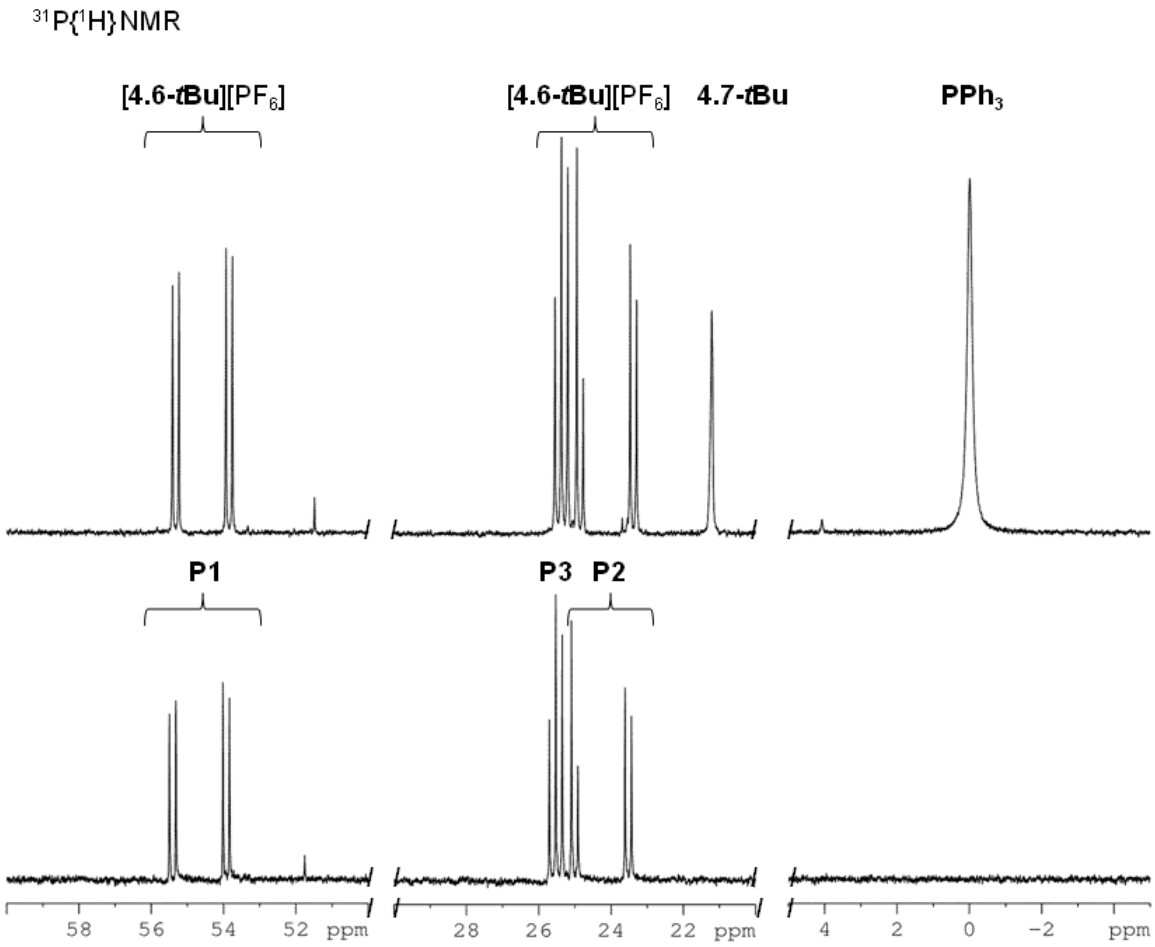

Figure 4.9 $^{31}P\{^1H\}$ NMR spectra of the reaction mixture obtained from the reaction of ligand precursor [H(4.2-*t*Bu)][PF_6] with [$Pd(PPh_3)_4$] before (top) and after (bottom) washings with hexane.

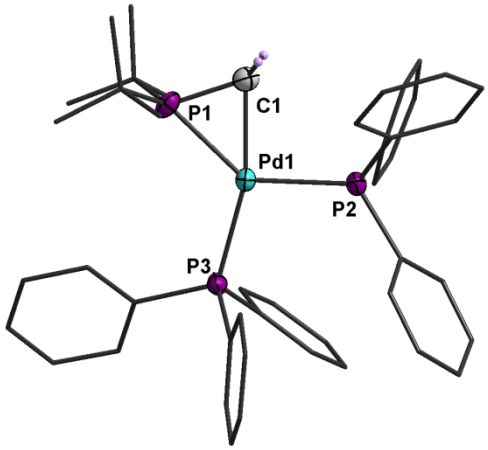

Figure 4.10 Solid-state structure of the cation in complex [4.6-*t*Bu][PF_6] with thermal ellipsoids at 50 % probability, with the exception of the phosphine substituents, which are modeled as "sticks". All hydrogen atoms, except the methylene protons, have been omitted for clarity.

From the structure of complex [**4.6-*t*Bu**][PF_6] it was concluded that the Pd metal center was activating a C-N bond from the side arm of the ligand, instead of the imidazolium C-H bond. The proposed reaction (Scheme 4.8) also accounts for the formation of only two free equivalents of PPh_3. The synthesis of compound [**4.6-*t*Bu**][PF_6] should be accompanied by the formation of the mono-substituted benzimidazole compound **4.7-*t*Bu**. However, attempts to isolate product **4.7-*t*Bu** were not carried out.

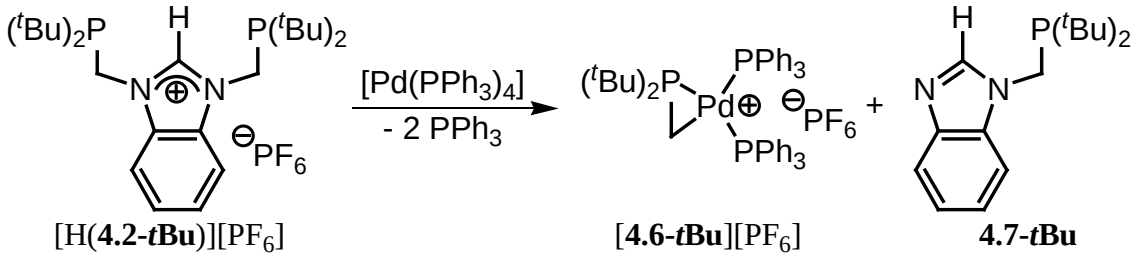

[H(**4.2-*t*Bu**)][PF_6] [**4.6-*t*Bu**][PF_6] **4.7-*t*Bu**

Scheme 4.8 Unexpected synthesis of complex [4.6-*t*Bu][PF_6] via a C-N bond activation.

Ligands of the type η^2-$CR_2PR'_2$ such as the one in complex [**4.6-*t*Bu**][PF_6], as well as their corresponding metal complexes are known. However, the solid-state molecular structure of

only three palladium complexes of this family have been reported (Figure 4.11).[226-228] Relevant fragments of the solid-state structures of complexes [**4.6-*t*Bu**][PF_6], [**4.f][BAr$^F_4$]**, **4.g** and **4.h** are presented in Figure 4.12, and selected bond lengths and angles are summarized in Table 4.3.

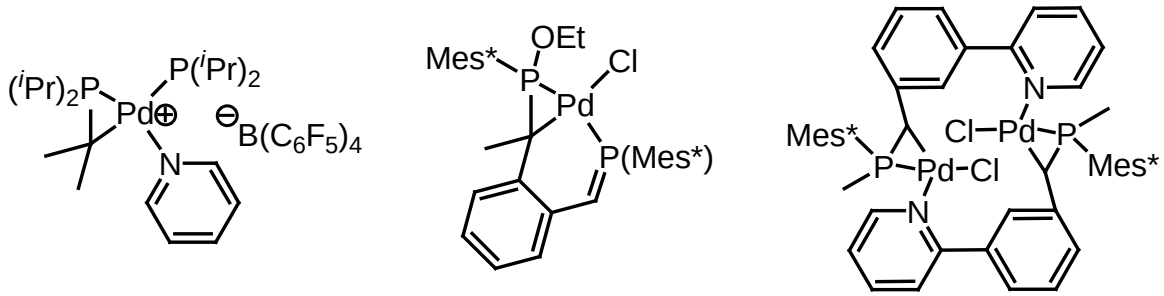

4.f **4.g** **4.h**

Mes* = 2,4,6-tri-*tert*-butylphenyl

Figure 4.11 Structurally characterized Pd complexes [4.f][BAr$^F_4$],[226] 4.g,[227] and 4.h.[228]

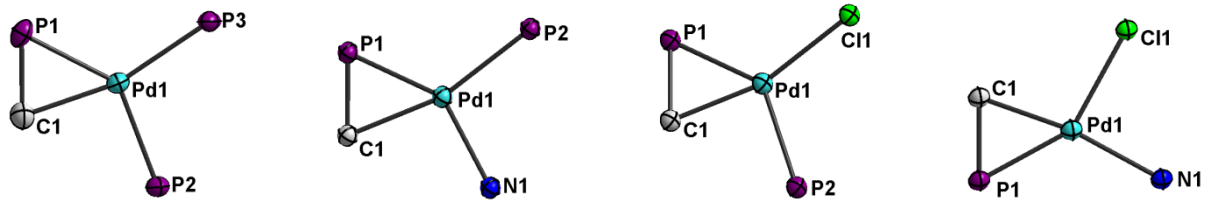

Figure 4.12 From left to right: Fragments of the solid-state molecular structure of complexes [4.6-*t*Bu][PF_6], [4.f][BAr$^F_4$],[226] 4.g,[227] and 4.h[228] showing the palladium coordination sphere with thermal ellipsoids at 50 % probability.

Table 4.3 Selected bond lengths (Å) and angles (°) for complex [4.6-*t*Bu][PF_6], and analogous reported complexes [4.f][$BAr^F{}_4$],[226] 4.g,[227] 4h.[228]

Parameter	[**4.6-*t*Bu**][PF_6]	[**4.f**][$BAr^F{}_4$]	**4.g**	**4.h**
C1-Pd1	2.133(8)	2.171(5)	2.101(5)	2.081(8)
P1-Pd1	2.283(2)	2.206(1)	2.232(1)	2.222(2)
C1-P1	1.738(9)	1.748(6)	1.752(4)	1.754(8)
Pd1-X1	2.336(2)[a]	2.168(4)[b]	2.325(1)[c]	2.411(2)[d]
Pd1-X2	2.332(2)[a]	2.376(1)[b]	2.385(1)[c]	2.168(6)[d]
Pd1-P1-C1	62.3(2)	65.4(2)	62.3(2)	61.8(2)
P1-C1-Pd1	71.5(3)	67.5(2)	70.1(2)	70.2(3)
C1-Pd1-P1	46.2(2)	47.1(2)	47.6(1)	48.0(2)
C1-Pd1-X1	92.0(2)[a]	95.5(2)[b]	86.9(1)[c]	99.2(2) [d]
P1-Pd1-X2	103.1(6)[a]	117.66(5)[b]	118.7(4)[c]	122.92(16)[d]
X1-Pd1-X2	118.2(6)[a]	99.9(1)[b]	107.8(4)[c]	89.73(16)[d]
$\sum\angle$ at Pd	359.56	360.16	361	359.85

a) X1 = P2, X2 = P3; b) X1 = N1, X2 = P2; c) X1 = P2, X2 = Cl1; d) X1 = Cl1, X2 = N1.

Complexes [**4.6-*t*Bu**][PF_6], [**4.f**][$BAr^F{}_4$], **4.g**, and **4.h** all display similar distorted square planar geometries around the palladium center with the sum of the angles around the metal center adding up to approximately 360°. The distance of the palladium centers from the plane generated by all the atoms in the metal coordination sphere are 0.0982(4)Å for [**4.6-*t*Bu**][PF_6], 0.0191(4)Å for [**4.f**][$BAr^F{}_4$], 0.0032(3)Å for **4.g**, and 0.0496(6)Å for **4.h**. The C1-P1 bond lengths of all four complexes are statistically identical. All the other parameters pertaining to the three-membered metalacycle are also quite similar, with all bond lengths within 0.1 Å and all angles within 3°. Complex [**4.6-*t*Bu**][PF_6] is the first example in which the carbon bound to palladium is unsubstituted, *i.e.* the parent methylene.

Formation of complex [**4.6-*t*Bu**][PF_6] could represent a contradiction to our working theory that pincer metal complexes of ligands that generate five membered metallacycles should be more stable than those of ligands that generate six membered ones. However, the reactivity observed could be taking place either before or after the formation of complex [**4.5-*t*Bu**][PF_6]. If the C-N bond activation required to generate complex [**4.6-*t*Bu**][PF_6] takes place prior to the C-H bond activation required for the synthesis of complex [**4.5-*t*Bu**][PF_6], then the reactivity leading to [**4.6-*t*Bu**][PF_6] may not be observed once full tridentate coordination of the ligand has occurred. In order to shed some light into the matter, the synthesis of Pd complex [**4.8-*t*Bu**][PF_6] via the free carbene **4.2-*t*Bu** (Scheme 4.9) was attempted. The free carbene **4.2-*t*Bu** was synthesized by reacting one equivalent of KHMDS with a solution of [H(**4.2-*t*Bu**)][PF_6] in THF. The reaction mixture was stirred at room temperature for 45 min. Compound **4.2-*t*Bu** was then reacted with a solution of [$Pd(CH_3CN)_2Cl_2$] in acetonitrile. The reaction mixture was refluxed for 4h, after which a precipitate formed. The precipitate was filtered, washed with fresh THF, and dried under vacuum yielding complex [**4.8-*t*Bu**][PF_6] as a yellow crystalline powder (70 % yield).

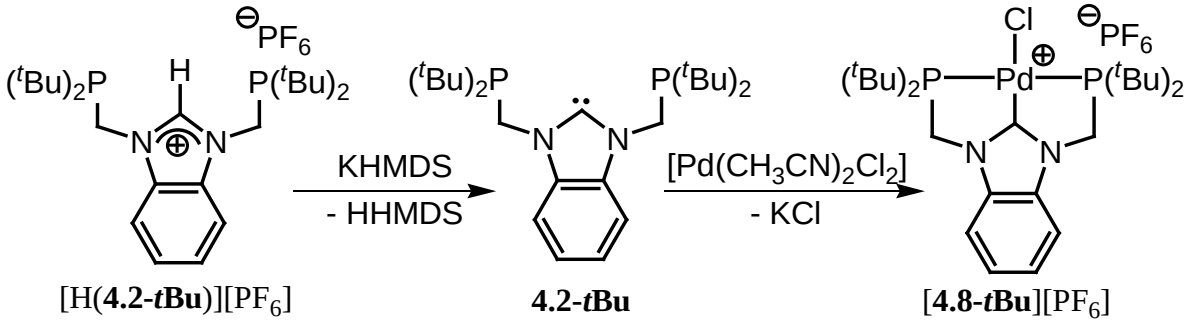

[H(**4.2-*t*Bu**)][PF_6] **4.2-*t*Bu** [**4.8-*t*Bu**][PF_6]

Scheme 4.9 Synthesis of PCP pincer complex [4.8-*t*Bu][PF_6] via the free carbene 4.2-*t*Bu

The successful synthesis of complex [**4.8-*t*Bu**][PF_6] was confirmed via multinuclear NMR spectroscopy. The ^{1}H NMR spectrum of [**4.8-*t*Bu**][PF_6] featured the corresponding signals for the *tert*-butyl protons and the methylene linkers at 1.53ppm (J_{PH} = 7.9 Hz) and 4.63 (J_{PH} = 2.2 Hz), respectively. These two signals displayed the expected virtual triplet pattern due to virtual coupling with both phosphorus centers, as observed in the case of the rhodium complex **4.3-*t*Bu**. The ^{31}P NMR spectrum of [**4.8-*t*Bu**][PF_6] has a signal at δ = 83.2 ppm, downfield shifted with respect to that of the ligand precursor [H(**4.2-*t*Bu**)][PF_6] (δ = 25.8 ppm), confirming the coordination of the phosphines to palladium. The signals in the ^{13}C{^{1}H} NMR spectrum of [**4.8-*t*Bu**][PF_6] corresponding to the *tert*-butyl substituents and to the methylene linkers displayed the same virtual coupling as that observed in the ^{1}H NMR spectrum. Most importantly, the ^{13}C{^{1}H} NMR spectrum displayed the downfield signal for the carbene carbon (t, δ = 177.5 ppm, $^2J_{PC}$ = 3 Hz).

X-ray quality single crystals of [**4.8-*t*Bu**][PF_6] were obtained via slow evaporation of a saturated dichloromethane solution at room temperature. The solid-state structure of the cation in complex [**4.8-*t*Bu**][PF_6] is presented in Figure 4.13. Selected bond lengths and angles of complex [**4.8-*t*Bu**][PF_6] and of related complexes [**4.d**][PF_6],[106] **4.i**,[174] [**4.j**][Cl],[137] and [**4.k**][BF_4]$_2$[166] (Figure 4.14) are summarized in Table 4.4. The structures of the palladium coordination spheres in complexes [**4.d**][PF_6],[106] **4.i**,[174] [**4.j**][Cl],[137] and [**4.k**][BF_4]$_2$[166] are presented in Figure 4.15.

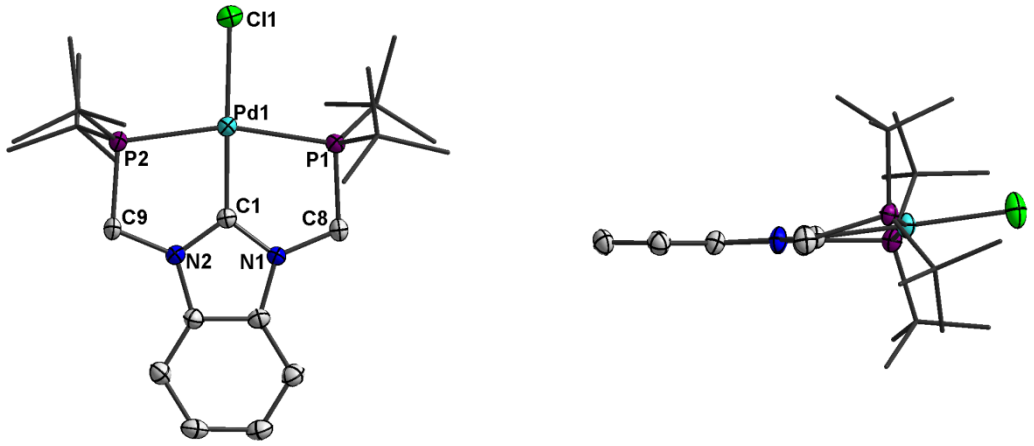

Figure 4.13 Solid-state structure of the cation in complex [4.8-*t*Bu][PF_6] with thermal ellipsoids at 50 % probability, with the exception of the phosphine substituents, which are modeled as "sticks". All hydrogen atoms and the PF_6^- counter anion have been omitted for clarity.

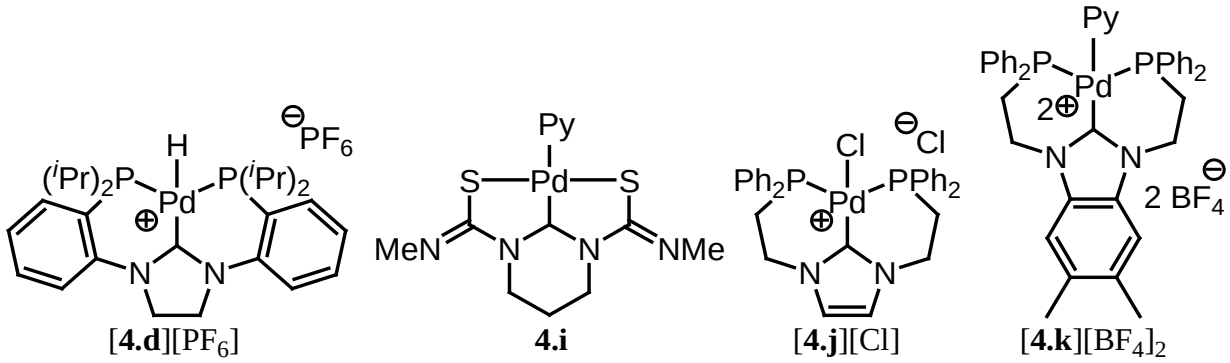

[**4.d**][PF_6] **4.i** [**4.j**][Cl] [**4.k**][BF_4]$_2$

Figure 4.14 Related palladium complexes of pincer ligands with an NHC in the central donor position [4.d][PF_6],[106] 4.i,[174] [4.j][Cl],[137] and [4.k][BF_4]$_2$[166]

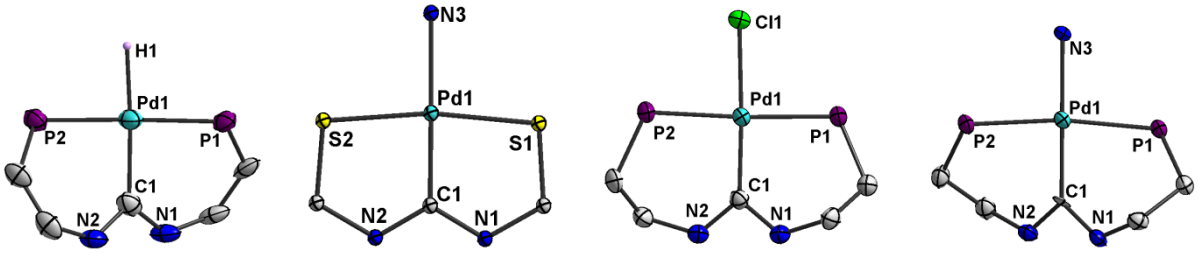

Figure 4.15 From left to right: Fragments from the solid-state structure of complexes [4.d][PF_6],[106] 4.i,[174] [4.j][Cl],[137] and [4.k][BF_4]$_2$[166] showing the palladium coordination sphere and the metallacycles, with thermal ellipsoids at 50 % probability.

Table 4.4 Selected bond lengths (Å) and angles (°) for complex [4.8-*t*Bu][PF_6], and analogous reported complexes [4.d][PF_6],[106] 4.i,[174] [4.j][Cl],[137] and [4.k][BF_4]$_2$.[166]

Parameter	[**4.8-*t*Bu**][PF_6]	[**4.d**][PF_6]	**4.i**	[**4.j**][Cl]	[**4.k**][BF_4]$_2$*
C1-Pd1	1.937(4)	2.037(8)	1.945(4)	1.983(7)	1.974(5), 1.980(6)
Pd1-P1	2.3188(11)	2.266(2)	2.287(1)[d]	2.325(2)	2.333(1), 2.326(2)
Pd1-P2	2.3312(11)	2.257(2)	2.280(1)[d]	2.297(2)	2.306(1), 2.318(1)
Pd1-X1	2.3250(12)[a]	1.77(7)[b]	2.109(3)[c]	2.333(2)[a]	2.076(4),[b] 2.079(5)[b]
N1-C1	1.333(5)	1.345(3)	1.352(6)	1.356(9)	1.347(6), 1.357(8)
C1-N2	1.347(5)	1.341(3)	1.339(5)	1.358(1)	1.371(6), 1.340(8)
N1-C1 -N2	107.9(4)	109.3(7)	118.9(4)	104.5(6)	106.4(4), 108.5(6)
C1-Pd1-X1	178.8(1)[a]	173.2(15)[b]	179.4(1)[c]	177.1(2)[a]	177.6(2),[b] 177.8(2)[b]
P1-Pd1-P2	163.2(4)	169.03(2)	170.5(4)[d]	176.22(7)	171.7(5), 171.2(6)
ϕ	7.9	35.5/41.5	3.6(2)[d]	27.1	43.8, 46.8

a) X1 = Cl1; b) X1 = H1; c) X1 = N3; d) P1 = S1, P2 = S2; (ϕ) = dihedral angle between the main plane s defined by N1-C1-N2-Pd1 and C1-Pd1-P1-P2. *There are two independent molecules in the asymmetric unit.

The Pd1-C1 bond distance in complex [**4.8-*t*Bu**][PF_6] (1.937(4) Å) is the shortest reported to date for a carbene in a palladium PCP pincer complex and falls in the low-end range of Pd-C_{NHC} bond distances (1.89-2.12 Å), and statistically the same as that in **4.j** (1.945(4) Å), a

palladium SCS complex.[220,221] An analysis of the dihedral angle formed between the main planes defined by C1-N1-C2-Pd1 and P1-Pd1-P2-C1 (ϕ, Table 4.4) reveals that complexes [**4.8-*t*Bu**][PF_6] and **4.j** have a small dihedral angle (7.9° and 3.6° respectively) in comparison to the other complexes (27.1-46.8°). Such a difference in the dihedral angle (ϕ) for complexes with five membered versus six membered metallacylces was also observed in the Rh analogs (*vide supra*), and is in accordance to what was theoretically calculated by Lee and coworkers.[137] They report that the energy barrier for the rotation of an imidazole-carbene has a rather small value (3.0 - 4.9 kcal/mol). Hence the imidazole can readily twist in order to minimize both the strain in the metallacycles, and the steric repulsion with the phosphine substituents. However, the authors also observed that, when substituting the ethylene linkers for methylene ones such as in complexes **4.3-*t*Bu** and [**4.8-*t*Bu**][PF_6], the dihedral angle becomes nearly 0°.

The stability of complex [**4.8-*t*Bu**][PF_6] towards thermal decomposition was evaluated by heating a toluene solution to 110 °C and monitoring the sample via multinuclear NMR spectroscopy. The sample showed no signs of decomposition even after 72 h of heating. In order to prove the stability of complex [**4.8-*t*Bu**][PF_6] in conditions similar to the ones that give rise to the formation of the C-N activated product [**4.6-*t*Bu**][PF_6], a THF solution of the complex with 3 equivalents of PPh_3 was maintained at 65 °C for 24 h. The reaction was monitored via multinuclear NMR spectroscopy and no signs of decomposition were observed. The stability displayed by complex [**4.8-*t*Bu**][PF_6] suggests that the C-N bond reactivity required for the formation of complex [**4.6-*t*Bu**][PF_6] takes place prior to full coordination of the pincer ligand. However, it is important to consider that complex [**4.8-*t*Bu**][PF_6] is a palladium chloride and not a palladium hydride. Hence the stability of complex [**4.8-*t*Bu**][PF_6] by its self is no

conclusive proof that the reactivity observed takes place prior to or subsequent to the formation of complex [**4.5-*t*Bu**][PF_6], and further experimental evidence is required.

Based on the success experienced during the synthesis of complex [**4.8-*t*Bu**][PF_6], it was decided to synthesize the nickel analog complex [**4.9-*t*Bu**][PF_6] via a similar synthetic route (Scheme 4.10). The ^{1}H NMR spectrum of complex [**4.9-*t*Bu**][PF_6] displayed the expected virtual triplet pattern for the signal corresponding to the *tert*-butyl substituents (δ = 1.58 ppm, J_{PH} = 7.5 Hz), and for the signal corresponding to the methylene linkers (δ = 4.45 ppm, J_{PH} = 2.2 Hz), which supports the symmetric nature of the complex.[222-224] The ^{31}P NMR spectrum had a signal at 81.5 ppm and a signal upfield at -143.4 ppm, with a relative integration ratio of 2:1 corresponding to the phosphine moieties and the hexafluorophosphate anion. The ^{13}C{^{1}H} NMR spectrum of complex [**4.9-*t*Bu**][PF_6] confirmed the presence of the carbene carbon with a downfield signal at 179.1 ppm, however, in this case the coupling to the phosphorus centers was not resolved.

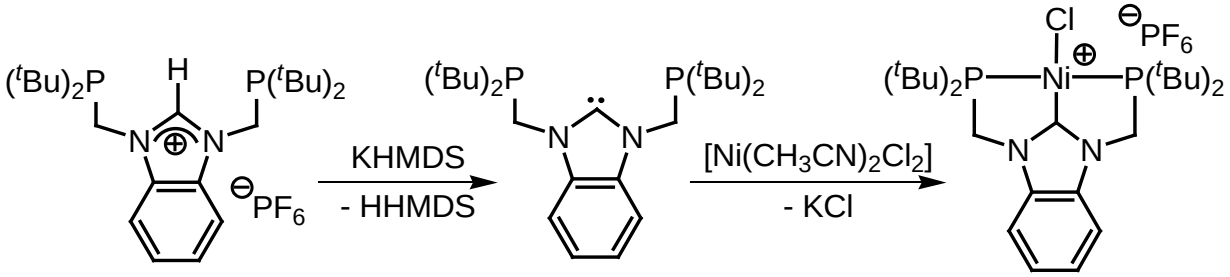

[H(**4.2-*t*Bu**)][PF_6] **4.2-*t*Bu** [**4.9-*t*Bu**][PF_6]

Scheme 4.10 Synthesis of complex PCP Ni complex [4.9-*t*Bu][PF_6].

X-ray quality crystals of complex [**4.9-*t*Bu**][PF_6] were obtained by slow evaporation of a concentrated solution in dichloromethane at room temperature. The solid-state structure of the cation in complex [**4.9-*t*Bu**][PF_6] (Figure 4.16) unambiguously confirmed the success of the

synthesis. Selected bond length and angles of complex [**4.9-*t*Bu**][PF_6] and of its analogs [**4.c**][PF_6],[106] **4.l**,[229] **4.m**,[144] and [**4.n**][PF_6][152] (Figure 4.17, Figure 4.18) are summarized in Table 4.5.

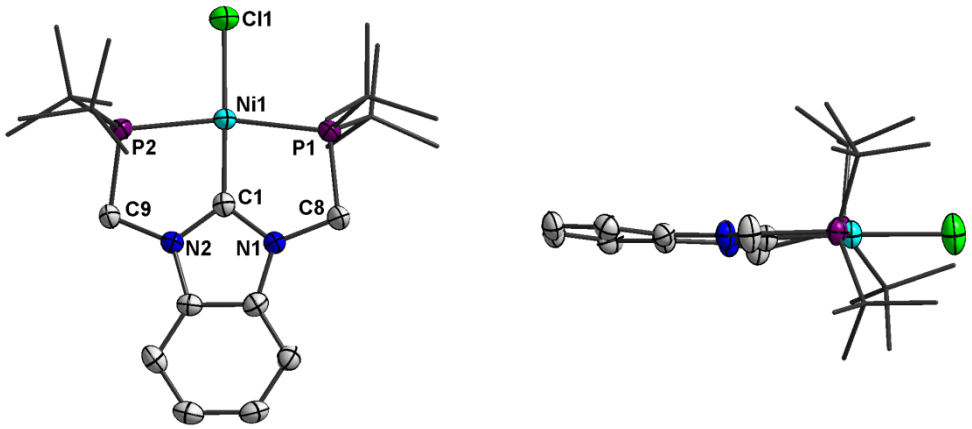

Figure 4.16 Solid-state structure of the cation in complex [4.9-*t*Bu][PF_6] with thermal ellipsoids at 50 % probability, with the exception of the phosphine substituents, which are modeled as "sticks". All hydrogen atoms and the PF_6^- counter anion have been omitted for clarity.

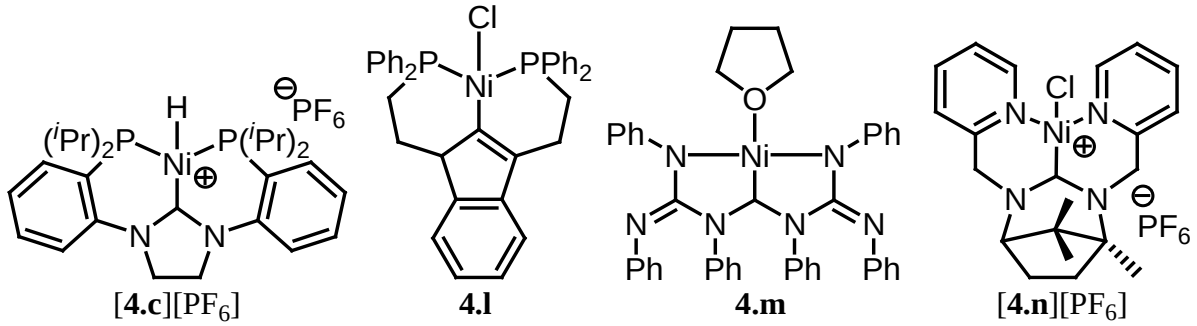

[**4.c**][PF_6] **4.l** **4.m** [**4.n**][PF_6]

Figure 4.17 Reported nickel complexes of pincer ligands with diamino carbene (DAC) moieties at the central donor position [4.c][PF_6],[106] 4.m[144] and [4.n][PF_6],[152] and of a pincer ligand with an indenyl moiety at the central donor position 4.l.[229]

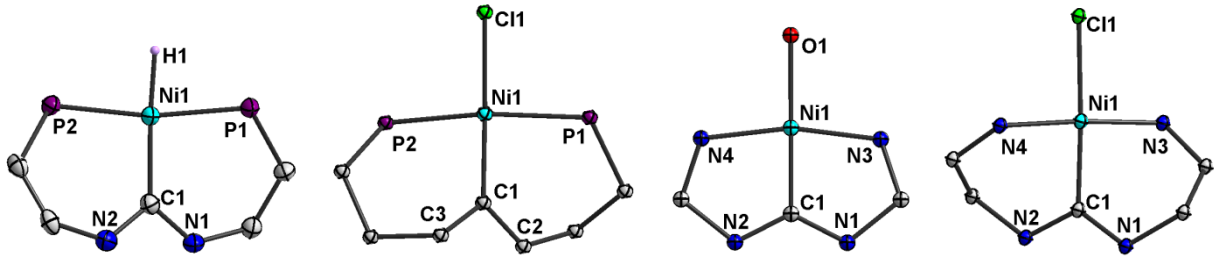

Figure 4.18 From left to right: Fragments from the solid-state structures of complexes [4.c][PF_6],[106] 4.l,[229] 4.m,[144] and [4.n][PF_6][152] showing the nickel coordination sphere and the metallacycles, with thermal ellipsoids at 50 % probability.

The Ni-C bond distance in complex [**4.9-*t*Bu**][PF_6] is amongst the shortest Ni-C_{NHC} bond distances reported to date, with complex **4.o**[230] (Figure 4.19) being the only one with a statistically shorter Ni-C bond distance (1.742(2) Å). The P1-Ni1-P1 angle in complex [**4.9-*t*Bu**][PF_6] is in the expected range for nickel PCP pincer complexes.

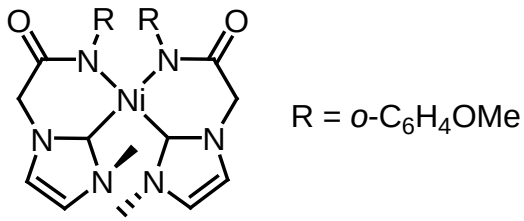

4.o

Figure 4.19 Nickel NHC complex 4.o.[230]

Table 4.5 Selected bond lengths (Å) and angles (°) for complex [4.9-*t*Bu][PF_6] and the reported analogs [4.c][PF_6],[106] 4.l,[229] 4.m,[144] and [4.n][PF_6].[152]

Parameter	**[4.9-*t*Bu][PF_6]**	[**4.c**][PF_6]	**4.l**	**4.m**	[**4.n**][PF_6]
C1-Ni1	1.815(5)	1.863(2)	1.888(3)	1.819(3)	1.873(8)
Ni1-P1	2.223(2)	2.1080(8)	2.215(1)	-	-
Ni1-P2	2.214(2)	2.1129(9)	2.177(1)	-	-
Ni1-N3	-	-	-	1.912(3)	1.911(7)
Ni1-N4	-	-	-	1.912(3)	1.899(6)
Ni-X1	2.158(2)[a]	1.387(4)[b]	2.209(1)[a]	1.964(3)[c]	2.219(2)[a]
C1-N1	1.352(8)	1.345(3)	1.360(3)	1.333(2)	1.321(1)
C1-N2	1.354(7)	1.341(3)	1.523(5)	1.333(2)	1.352(10)
C1-Ni1-X1	177.5(2)[a]	173.3(1)[b]	162.45(9)[a]	180.0[c]	176.9(3)[a]
P1-Ni1-P2	166.30(7)	169.0(3)	163.64(5)	-	-
N3-Ni1-N4	-	-	-	166.12(1)	176.1(3)
N1-C1-N2	106.3(5)	107.3(2)	109.3(2)	126.02(2)	118.8(7)
ϕ	6.9	33.5	50.4	0.1	48.2

a) X1 = Cl1; b) X1 = H1; c) X1 = O1. (ϕ) = dihedral angle between the main planes defined by N1-C1-N2-Rh1 and C1-Rh1-P1-P2 or C1-Rh1-N3-N4 (respectively).

In accordance to what was observed for the Rh and Pd complexes **4.3-*t*Bu** and [**4.8-*t*Bu**][PF_6] (*vide supra*), the value for the dihedral anglesϕ (Table 4.5) in the Ni complexes holds a relationship with the size of the metallacycles formed by the ligand upon coordination. With this in mind, a survey of available crystallographic data for Ni, Pd, and Rh complexes of pincer ligands with a diaminocarbene (DAC) backbone that would generate two six membered metallacycles or two five membered metallacycles upon coordination (Figure 4.20) was carried out. Figure 4.21 presents as a graph the M-C1 bond distance versus the dihedral angle ϕ between the main planes defined by N1-C1-N2-M and X2-M-X1-C1.

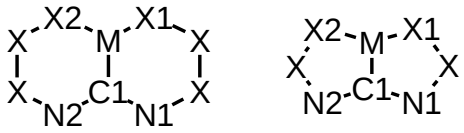

Figure 4.20 Molecular structure diagrams employed for the search in the CCDC. All bonds were defined as to include "any" type of bond.

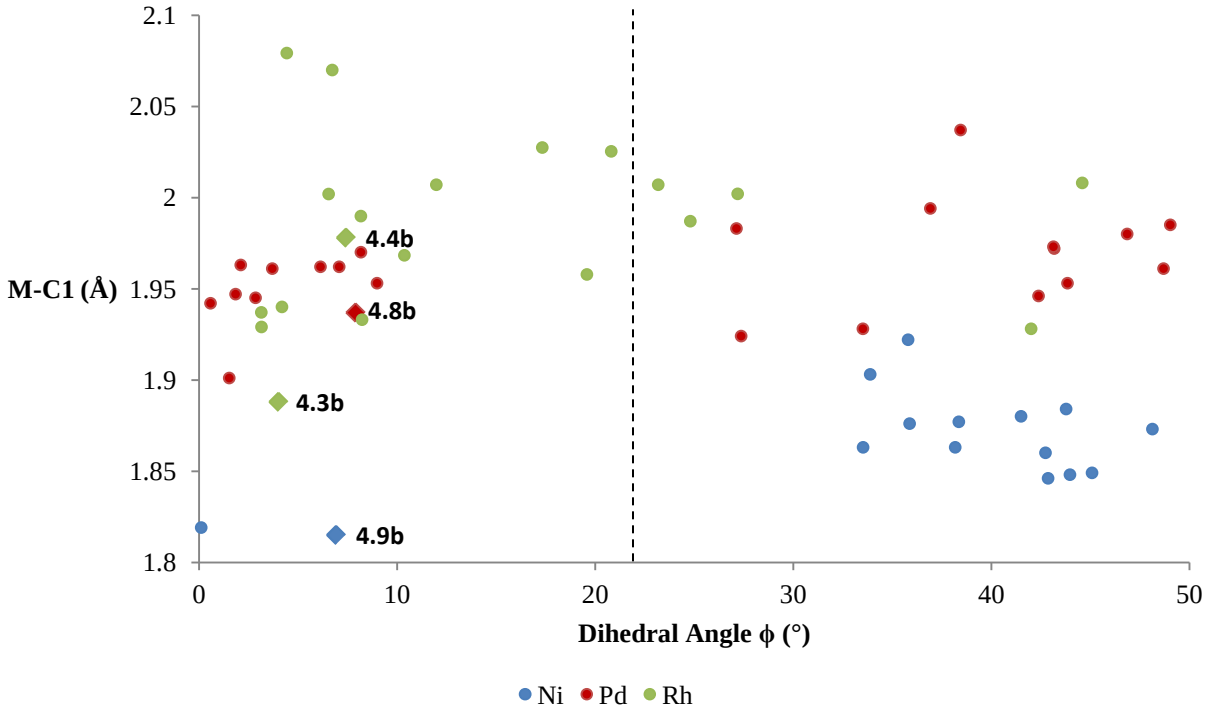

Figure 4.21 M-C1 (Å) vsϕ (°) for the reported complexes of Ni (•), Pd (•), and Rh (•) retrieved from the CCDC using the search query presented in Figure 4.20 and including the complexes reported in this Thesis.

All complexes with a dihedral angle ϕ < 22° are those of ligands that generate two five membered metallacycles, while all complexes with a dihedral angle ϕ > 22° are those of ligands that generate two six membered metallacycles. This confirms a relationship between the size of the metallacycles and the dihedral angle (ϕ). Furthermore, it appears that there is also a trend between the dihedral angle (ϕ) and the M-C1 bond length, where smaller dihedral angles tend to lead to shorter bonds and vice versa. However, it is clear that several other factors such as the nature of the ligand *trans* to C1, and the presence of other geometric constrains will have a stronger influence in the length of the M-C1 bond.[207] Nevertheless, a case can still be made for the role the dihedral angle (ϕ) plays on the length of the M-C1 bond.

The thermal stability of the nickel complex [**4.9-*t*Bu**][PF_6] was examined by heating its toluene solution to 110 °C and monitoring the reaction via multinuclear NMR spectroscopy. Similar to what was observed for the Pd complex [**4.8-*t*Bu**][PF_6], complex [**4.9-*t*Bu**][PF_6] did not show any signs of decomposition even after 72h of heating.

4.5 Synthesis and Characterization of (PCP)Mo Complex 4.10-*t*Bu

Only two pincer ligands with a carbon donor at the central position have been used to synthesize molybdenum pincer complexes (Figure 4.22): complex **4.p** reported in 2008 by Ganter,[173] and the series of complexes **4.q** which were just recently reported by Schrock.[231] Such a limited number of examples is surprising considering the number of reported Mo complexes of pincer ligands with nitrogen at the central donor position,[36,232,233] some of which date as far back as the 1980's.[234-237] With this in mind it was decided to attempt the synthesis of the molybdenum complex **4.10-*t*Bu** (Scheme 4.11).

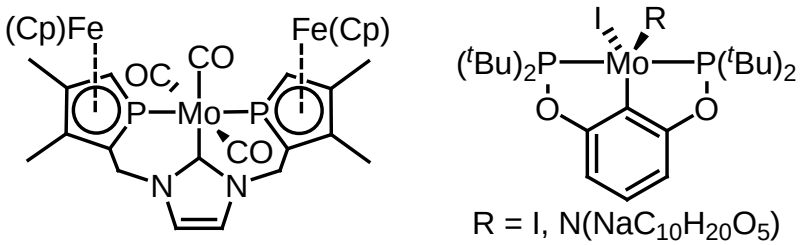

4.p **4.q**

Figure 4.22 Reported PCP pincer complexes of Mo 4.p and 4.q.

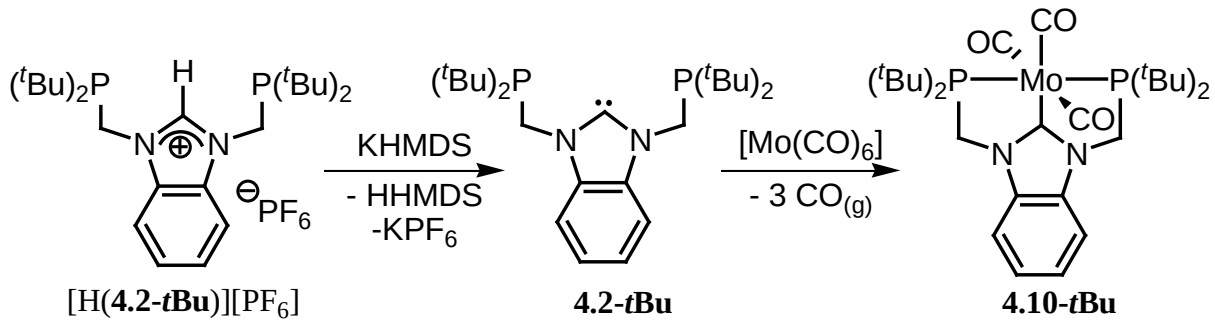

[H(**4.2-*t*Bu**)][PF$_6$] **4.2-*t*Bu** **4.10-*t*Bu**

Scheme 4.11 Synthesis of PCP Mo complex 4.10-*t*Bu

Compound [H(**4.2-*t*Bu**)][PF$_6$] was deprotonated with one equivalent of KHMDS in toluene. The resulting solution was filtered in order to remove the potassium hexafluorophosphate by-product, and added to a solution of one equivalent of [Mo(CO)$_6$] in toluene. The reaction mixture was stirred at room temperature for 2h and then analyzed via ^{31}P NMR spectroscopy. The ^{31}P NMR spectrum showed two signals one at 88.1 ppm and one at 16.6 ppm, with a relative integration ratio of 0.8:1. The spectrum seemed to represent what could be expected for a reaction that had not reached completion, since the observed downfield shift signal could be assigned to the desired product. The reaction was heated to 110 °C for 12h in order to promote completion. However, this effected no change in the ^{31}P NMR spectrum.

While the reaction mixture was slowly cooled down to room temperature, X-ray quality crystals started to grow. The solid-state molecular structure of the crystallized complex **4.11-*t*Bu** (Figure 4.23) helped explain the observed NMR spectra, since one phosphorus was bound to molybdenum (δ = 88.1 ppm) and the other one wasn't (δ = 16.6 ppm). Complex **4.11-*t*Bu** is an intermediate in the synthesis of complex **4.10-*t*Bu**. The reaction appears to require more energy in order for **4.11-*t*Bu** to eliminate the third equivalent of CO and allow for the tridentate coordination of the ligand **4.2-*t*Bu** (Scheme 4.12). Such reactivity with [$Mo(CO)_6$] had previously been observed by Ganter during the synthesis of complex **4.p** (Figure 4.22) with an analogous NHC based PCP pincer ligand.[173] The authors were able to structurally characterize the $Mo(CO)_4$ complex **4.r** (Figure 4.24) with a bidentate ligand related to the PCP ligand from complex **4.p**.[173] Selected bond lengths and angles for complexes **4.10-*t*Bu** and **4.r** are summarized in Table 4.6.

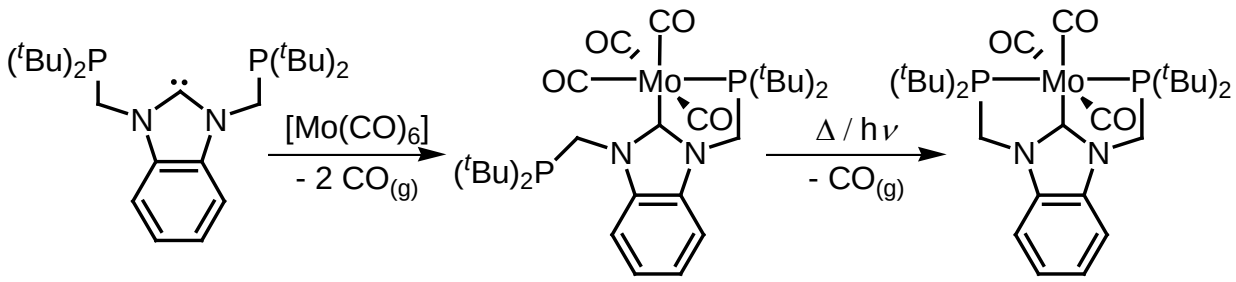

4.2-*t*Bu **4.11-*t*Bu** **4.10-*t*Bu**

Scheme 4.12 Synthesis of complex 4.10-*t*Bu through intermediate 4.11-*t*Bu

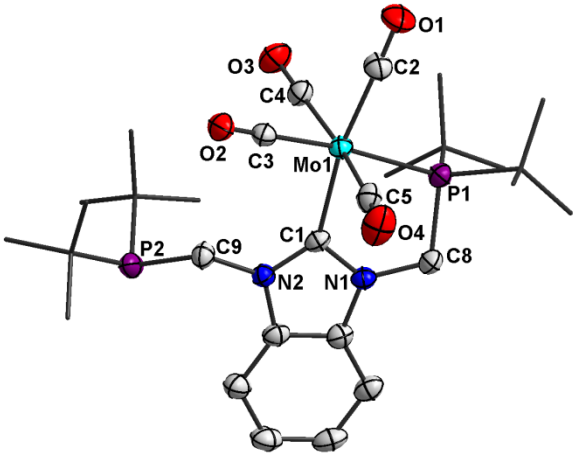

Figure 4.23 Solid-state molecular structure of complex 4.11-*t*Bu with thermal ellipsoids at 50 % probability, with the exception of the phosphine substituents, which are modeled as "sticks". All hydrogen atoms have been omitted for clarity.

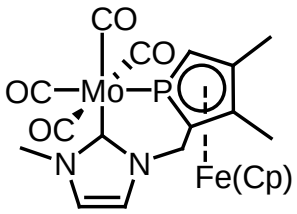

4.r

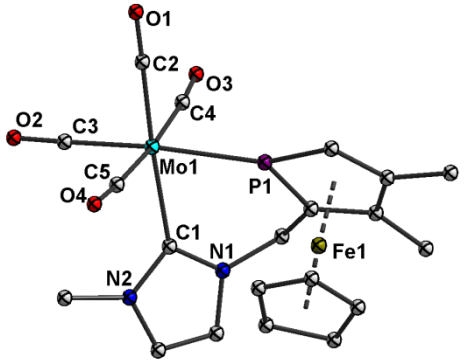

Figure 4.24 Complex 4.r[173] and its solid-state molecular structure with thermal ellipsoids at 50 % probability. All hydrogen atom have been omitted for clarity.

Table 4.6 Selected bond lengths (Å) and angles (°) for complexes 4.11-*t*Bu and 4.r[173]

Parameter	**4.11-*t*Bu**	**4.r**	Parameter	**4.11-*t*Bu**	**4.r**
C1-Mo1	2.238(4)	2.300(4)	C4-O3	1.148(6)	1.129(6)
C2-Mo1	1.984(4)	1.979(5)	C5-O4	1.142(6)	1.140(5)
C3-Mo1	1.964(3)	1.988(5)	C1-N1	1.367(5)	1.360(5)
C4-Mo1	2.034(4)	2.036(4)	C1-N2	1.357(5)	1.368(5)
C5-Mo1	2.034(4)	2.050(4)	C1-Mo1-C2	168.6(2)	176.1(1)
Mo1-P1	2.542(1)	2.486(1)	P1-Mo1-C3	174.3(1)	172.3(1)
C2-O1	1.149(6)	1.159(6)	C4-Mo1-C5	170.4(2)	175.1(2)
C3-O2	1.159(4)	1.143(6)	N1-C1-N2	104.8(3)	102.8(3)

The C1-Mo1 bond distance in complex **4.11-*t*Bu** (2.238(4)Å) is shorter than the one in complex **4.r**. The dihedral angle ϕ between the main plane s formed by N1-C1-N2-Mo1 and P1-Mo1-C1-C3 is 12.9° in complex **4.11-*t*Bu** and 38.8° in complex **4.r**. These values support once again the working theory that ligands that generate five membered metallacycles lead to smaller dihedral angles (ϕ) than those that generate six membered ones, even when there is only one metallacycle being formed such as in complexes **4.11-*t*Bu** and **4.r**.

Considering that heating the reaction mixture for 12 h at 110 °C did not promote the reaction to proceed (granted it was carried out in a close system) an attempt to promote the conversion of **4.11-*t*Bu** to **4.10-*t*Bu** via irradiation with UV-light was carried out. A toluene solution of **4.11-*t*Bu** was irradiated with UV-light (λ = 254 nm) in a mini-Rayonet photo reactor. The reaction progress was monitored via multinuclear NMR spectroscopy. The reaction took 96h of UV-irradiation to reach completion. However, it is important to point out that the irradiation experiment was also carried out in a sealed reaction vessel, which did not allow for the evacuation of the $CO_{(g)}$ formed, and in an aromatic solvent (toluene), which absorbs in the UV

range. Optimization of the reaction conditions required to synthesize complex **4.10-*t*Bu** was carried out. The successful synthesis of complex **4.10-*t*Bu** could be achieved by boiling a toluene solution of deprotonated ligand **4.2-*t*Bu** and one equivalent of [$Mo(CO)_6$] for 12 h under a stream of argon.

The $^{31}P\{^1H\}$ NMR spectrum of complex **4.10-*t*Bu** displayed only one downfield shifted signal at 118.7 ppm. The ^1H NMR spectrum of the complex displayed the expected signals for the protons from the *tert*-butyl substituents at 1.23 ppm and the methylene linkers at 3.82 ppm. However, the characteristic virtual triplet coupling pattern observed for these two signals in all the reported complexes of ligand **4.2-*t*Bu** so far, was only observed for the *tert*-butyl substituent signal (J_{PH} = 6 Hz) of complex **4.10-*t*Bu**. The signal corresponding to the methylene linkers was observed as a broad singlet. The $^{13}C\{^1H\}$ NMR spectrum of complex **4.10-*t*Bu** displayed the three expected downfield triplet resonances, one corresponding to the carbene center (δ = 233.1 ppm, $^2J_{PC}$ = 4.5 Hz) and two corresponding to the different carbonyl ligands (δ = 226.8 ppm, $^2J_{PC}$ = 8.5 Hz; δ = 223.2 ppm, $^2J_{PC}$ = 7.8 Hz).

The IR spectrum of complex **4.10-*t*Bu** showed two absorption bands at 1937 cm^{-1} and 1831 cm^{-1}. These values are comparable to those observed for the only other [$PCPMo(CO)_3$] complex, **4.p**, (1924 cm^{-1} and 1823 cm^{-1}),[173] and to those observed for [$(PPh_3)_3Mo(CO)_3$] (1934 cm^{-1} and 1835 cm^{-1}).[238]

The identity of complex **4.10-*t*Bu** was unambiguously determined via X-ray crystallography (Figure 4.25). Crystals of **4.10-*t*Bu** were obtained via slow evaporation of a concentrated toluene solution at room temperature. Selected bond lengths and angles of complexes **4.10-*t*Bu**, [**4.q-N**][$NaC_{10}H_{20}O_5$],[231] **4.s**,[239] and **4.t** [232] (Figure 4.26, and Figure 4.27) are summarized in Table 4.7.

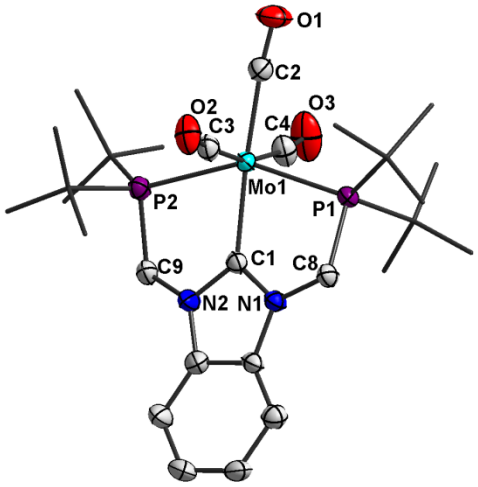

Figure 4.25 Solid-state molecular structure of complex 4.10-*t*Bu with thermal ellipsoids at 50 % probability, with the exception of the phosphine substituents, which are modeled as "sticks". All hydrogen atoms have been omitted for clarity.

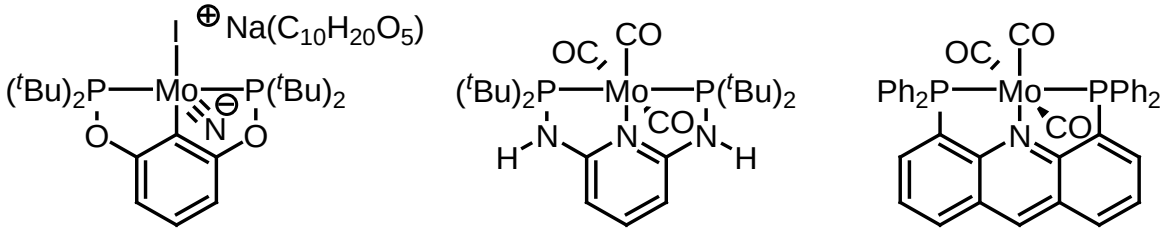

[**4.q-N**][$NaC_{10}H_{20}O_5$] **4.s** **4.t**

Figure 4.26 Related molybdenum complexes [4.q-N][$NaC_{10}H_{20}O_5$],[231] 4.s,[239] and 4.t.[232]

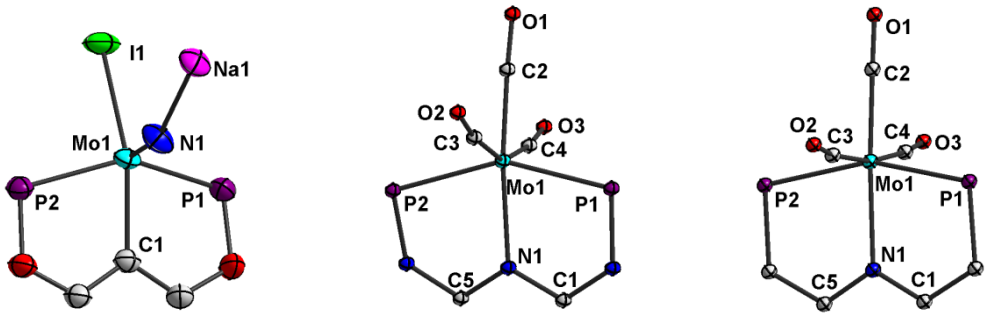

Figure 4.27 From left to right: Fragments from the solid-state structures of complexes [4.q-N][NaC$_{10}$H$_{20}$O$_5$],[231] 4.s,[239] and 4.t[232] showing the molybdenum coordination sphere and metallacycles with the thermal ellipsoids at the 50 % probability.

Table 4.7 Selected bond lengths (Å) and angles (°) for complexes 4.10-*t*Bu, [4.q-N][NaC$_{10}$H$_{20}$O$_5$],[231] 4.s,[239] and 4.t.[232]

Parameter	**4.10-*t*Bu**	[**4.q-N**][NaC$_{10}$H$_{20}$O$_5$]	**4.s**	**4.t**
C1-Mo1	2.151(3)	2.167(3)	2.2837(8)[b]	2.289(4)[b]
Mo1-P1	2.4682(10)	2.4314(8)	2.4638(3)	2.405(2)
Mo1-P2	2.5427(10)	2.4362(8)	2.4767(3)	2.426(2)
Mo1-C2	1.984(3)	2.8523(3)[a]	1.924(1)	1.948(6)
Mo1-C3	2.002(4)	-	2.011(2)	2.037(6)
Mo1-C4	2.011(4)	-	2.008(2)	2.002(6)
C2-O1	1.154(5)	-	1.178(2)	1.159(8)
C3-O2	1.157(5)	-	1.162(2)	1.130(8)
C4-O3	1.150(6)	-	1.159(1)	1.175(7)
C1-Mo1-C2	171.4(1)	149.55(7)[a]	168.79(4)[b]	176.9(2)[b]
P1-Mo1-P2	149.74(3)	146.20(3)	151.73(1)	156.80(6)
C3-Mo1-C4	164.9(2)	-	156.54(4)	170.5(2)

a) C2 = I1; b) C1 = N1.

The Mo-C1 bond in complex **4.10-*t*Bu** (2.151(3) Å) is only slightly shorter than that in complex [**4.q-N**][$NaC_{10}H_{20}O_5$] (2.167(3) Å), and shorter than those observed in the Mo-C_{NHC} complexes **4.11-*t*Bu** and **4.r** (2.238(4) and 2.300(4) Å, respectively). Such a shortening of the Mo1-C1 bond distance upon tridentate coordination of the pincer ligand is not surprising. The full coordination of the pincer ligand appears to generate strain in the molybdenum coordination sphere, as confirmed by the small angles around the metal center (C1-Mo1-C2, P1-Mo1-P2 and C3-Mo1-C4) for complexes **4.10-*t*Bu**, **4.s** and **4.t** in comparison to the ideal 180° angle expected for an octahedral geometry. Furthermore, a comparison of the angles around the Mo center in complex **4.10-*t*Bu** (171.4(1)°, 149.74(3)°, and 164.9(2)°) with those in complex **4.11-*t*Bu** (168.6(2)°, 174.3(1)°, and 170.4(2)°) shows the strain associated with the full coordination of the pincer ligand. Such an unfavorable geometry could explain why the transformation of complex **4.11-*t*Bu** to complex **4.10-*t*Bu** requires heating.

4.6 Conclusions and Outlook

Along with the ligands presented in Chapter 3, ligand **4.2-*t*Bu** is a member of a family of PCP pincer ligands with NHC backbones that generate five membered metallacycles upon coordination. The formation of two five membered metallacycles instead of larger rings appears to generate a better coordination geometry around the metal center and hence more robust complexes. This was indicated by the greater thermal stability displayed by the complexes of ligand **4.2-*t*Bu**. Furthermore, complexes of ligand **4.2-*t*Bu** have some on the shortest M-C bond distances (M = Pd, Ni, Rh, and Mo), pointing towards a strong interaction between the ligand and the metal center.

The accessibility of complexes with metals other than rhodium is a clear advantage of ligand **4.2-*t*Bu** over the other PCP pincer ligands reported in Chapter 3 (*vide supra*). However, the requirement to protect/deprotect the phosphines via oxidation with sulfur for the synthesis of compound [H(**4.2-*t*Bu**)][PF_6] has proven a major limitation. Large amounts of the ligands could not be synthesized in one batch and a more efficient synthetic protocol that involves either other protecting groups at the phosphines, or a better desulfurization technique is still required. In particular, the main limiting factor for the full desulfurization of the ligand precursor was the low solubility of the formamidinium salts [H(**4.1-Ph**)][PF_6], and [H(**4.1-*t*Bu**)][PF_6]. Improvements on the solubility properties of these type of ligand precursors should have a direct effect on the ability to fully reduce the phosphanethiones. Future work for this project should focus on the synthesis of ligand precursors [H(**4.12-*t*Bu**)][$BAr^F{}_4$] and [H(**4.13-*t*Bu**)][$BAr^F{}_4$], (Figure 4.28). Substitution of the phenylene backbone with either protons or methyl groups, and substitution of the PF_6^- counter anion with $BAr^F{}_4^-$ should both help increase the solubility of the resulting formamidinium salts.

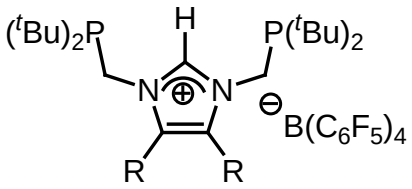

[H(**4.12-*t*Bu**)][$BAr^F{}_4$], R = H
[H(**4.13-*t*Bu**)]$BAr^F{}_4$], R = Me

Figure 4.28 Proposed pincer ligand precursor [H(4.12-*t*Bu)][$BAr^F{}_4$] and [H(4.13-*t*Bu)][$BAr^F{}_4$].

The synthesis of the Pd and Ni hydride complexes with ligand **4.2-*t*Bu** remains an avenue worth exploring, as they would allow for a better comparison between their stabilities and those

displayed by the analogous complexes reported by Fryzuk and coworkers.[138] The synthesis of the Pd complex should further allow the assessment of whether the C-N bond activation leading to the formation of complex **4.6-*t*Bu** can take place prior to or after the coordination of the ligand. In light of the observed C-N bond cleavage reactivity, the ability of the Pd complex [**4.8-tBu**][PF_6] to catalyze amination reactions should be investigated. Furthermore, ability of the Pd and Ni complexes [**4.8-tBu**][PF_6] and [**4.9-tBu**][PF_6] to catalyze cross-coupling reactions should also be investigated.

The synthesis of Mo complex **4.10-*t*Bu**, which is one of only three reported complexes of molybdenum with a PCP pincer ligand, further highlights the good ligand properties of **4.2-*t*Bu**. Taking into consideration the reported nitrogen activation reactivity observed for the molybdenum PNP pincer complex **1.n** (Figure 4.29),[36] the synthesis of an analogous nitrogen complex **4.14-*t*Bu** with ligand **4.2-*t*Bu**, and studies of its reactivity towards nitrogen reduction should be priorities. Ligand dissociation has been suggested as one of the reasons for why complex **1.n** was only able to generate 12 eq. of ammonia per molybdenum center.[231] The strong binding properties of ligand **4.2-*t*Bu** should make complex **4.14-*t*Bu** sturdier than complex **1N**, increasing the stability of the complex and hence avoiding catalyst decomposition.

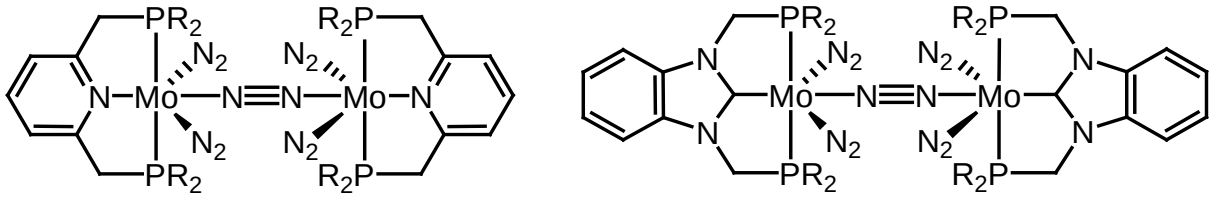

Figure 4.29 Reported complex 1.n, and proposed complex 4.14-*t*Bu.

Chapter Five: **Conclusions and Outlook**

5.1 Conclusions and Outlook

The goal of the research presented in this thesis was the synthesis of novel pincer ligands with strong σ-donors in the central position. Two approaches were taken in order to generate superior novel pincer ligands. The first one involved the incorporation of boryl ligands into pincer ligands; at the time this project was initiated boryl-based pincer ligands had not been reported. The second approach involved the synthesis of NHC-based pincer ligands with methylene-linked phosphines pendant donors, which better resembled the classical pincer ligand architecture in the formation of two five membered metallacylces upon coordination.

Pincer ligands with a central boryl donor were obtained using the PBP pincer ligand precursors **2.2-Ph** and **2.2-*t*Bu**, which formed palladium complexes via B-Cl bond activation. The incorporation of the boryl moiety into a multidentate ligand proved to be an efficient route to stabilize the reactive M-B bond. This was confirmed by the persistence of metal complex **2.3-Ph** under Heck cross-coupling reaction conditions. However, complex **2.3-Ph** was unsuccessful at catalyzing a simple cross-coupling reaction.

The pincer ligand precursors **2.2-Ph** and **2.2-*t*Bu** featured 1,3,2-diazaborole backbones. The five membered backbone ring along with the larger size of boron compared to carbon and nitrogen translated into pincer ligand complex **2.3-Ph** displaying a P-M-P bond angle (152.80(5)°) in the narrower range observed for pincer complexes. A narrower angle generates

undesired strain on the metallacycles and does not allow the ligand to fully donate its electron density to the metal center. With this in mind, two other novel pincer ligand precursors, **2.13-Ph** and **2.17-Me**, having a boron atom at the central donor position were synthesized. These ligand precursors feature an acyclic central donor moiety, which reduces geometric constrains from the ligand, allowing for more efficient coordination to the metal center.

Further investigations of the coordination properties of the acyclic boryl pincer ligands are still required. Additional reactivity studies pertaining to complexes **2.3** need to be conducted in order to assess the consequences the strong electron donating properties of the PBP ligands have on the palladium metal center.

Four NHC-based PCP pincer ligands that upon coordination generate five membered metallacycles were investigated. These ligands had varying backbones: phenylene (**4.2**), propylene (**3.1a**), and naphthylene (**3.1b**), as well as phenyl(**Ph**) and *tert*-butyl(***t*Bu**) substituents at phosphorus.

The NHC-based rhodium pincer complexes **3.5a-Ph**, **3.5a-*t*Bu**, and **3.5b-Ph** incorporating six-membered carbene backbone ligands **3.1a-Ph**, **3.1a-*t*Bu**, and **3.1b-Ph**, respectively**,** were synthesized via a double C-H bond activation. The working mechanism of the double C-H bond reaction was found to vary depending on the nature of the substituents at phosphorus, with the phenyl substituted ligands leading to hydrogen elimination, and the *tert*-butyl substituted ligands displaying a competitive reactivity between hydrogen elimination and hydrogenation of COD or CO (depending on the Rh starting material employed). The observed hydrogenation of COD and CO during the synthesis of the *tert*-butyl substituted Rh complex **3.5a-*t*Bu** cannot be explained based on steric grounds. However, it can be explained in terms of two important factors: i) The ligand with the more basic *tert*-butyl substituted

phosphines should be better at stabilizing the Rh(III) alkyl-hydride species generated after the first C-H bond activation, and ii) the phenyl substituted complexes **3.5a-Ph** and **3.5b-Ph** were found to crystallize out of solution as the reaction progressed, even at the boiling point of the solvent, while the *tert*-butyl substituted complex **3.5a-*t*Bu** was found to dissolve well. The increased stability of the Rh(III) alkyl-hydride with *tert*-butyl substituted phosphines increases the availability of these species for olefin coordination. Furthermore, the exchange of phenyls for *tert*-butyl substituents leads to a loss in the lattice energy, which could have an effect on the energetics of the hydrogen elimination step of the reaction.

Reactive organorhodium species could be successfully synthesized via the reaction of the soluble rhodium complex **3.5a-*t*Bu** with suitable organolithium reagents. The reactivity of these complexes towards small molecules with acidic protons revealed some promising results but further research into this reactivity is required.

Regarding the NHC-based pincer ligand with a five-membered backbone **4.2-*t*Bu**, the synthesis of rhodium, palladium, nickel and molybdenum complexes of the ligand displayed the widely applicable coordination properties of the ligand system. Strong interactions between this ligand and the metal center were confirmed by the prevalently short M-C_{NHC} bond distances found regardless of the metal center of choice. Namely, this ligand holds the record for the shortest Rh-C bond distance in a PCP pincer complex, the shortest Rh-C_{NHC} bond distance, the shortest Pd-C bond distance for an NHC in a PCP pincer complex and the shortest Mo-C_{NHC} bond distance in a pincer complex. Furthermore, the observed Ni-C bond distance is tied for the shortest Ni-C_{NHC} bond distances reported to date. A correlation between the M-C_{NHC} bond distance and the dihedral angle between the plane defined by the NHC ring and the main plane defined by the atoms bound to the metal center was found. Ligand **4.2-*t*Bu** appears to coordinate

in such a way that the dihedral angle is minimized, allowing for optimal orbital overlap between the NHC and the metal center. Due to time constrains, the reactivity properties of the complexes of ligand **4.2-*t*Bu** could not be investigated and hence further work on this project should heavily focus on this aspect.

Overall, the goals of this research project were met. A series of novel pincer ligands with strong electron donating moieties at the central donor position were successfully synthesized. Furthermore this research represents the first approach of the Roesler group to the field of ligands. A solid foundation has been laid and a large number of research avenues have been opened.

Chapter Six: **Experimental Details**

6.1 General Considerations

All procedures were carried out with the careful exclusion of air and moisture using standard Schlenk and glove box techniques. Starting materials were prepared according to literature procedures, or purchased from commercial suppliers.

6.1.1 Solvents

All solvents were dried and deoxygenated prior to use. Diethyl ether (Et_2O), pentane, toluene, tetrahydrofuran (THF), hexane, and benzene were dried by refluxing over benzophenone and sodium metal prior to distillation. They were then stored in 500 mL glass bombs over benzophenone and sodium metal. Dichloromethane (CH_2Cl_2) was dried by refluxing over calcium hydride prior to distillation, and stored in a 500 mL glass bomb. Deuterated solvents were purchased from Cambridge Isotope Laboratories, Inc. and Sigma-Aldrich, and dried prior to use. Tetrahydrofuran-d_8 (THF-d_8), and toluene-d_8 were dried by heating over potassium metal prior to vacuum transfer, and stored in 50 or 100 mL glass bombs. Benzene-d_6 (C_6D_6), was dried over sodium metal and benzophenone over prolonged periods of time prior to vacuum transfer, and stored in a 100 mL glass bomb. Dichloromethane-d_2 (CD_2Cl_2), and bromobenzene-d_5 ($C\text{-}_6D_5Br$) were dried by sonicating over calcium hydride prior to vacuum transfer, and stored in 50 or 100 ml glass bombs. Dimethylsulfoxide-d_6 (DMSO-d_6), and chloroform-d ($CDCl_3$) were stored over freshly activated *Grade 4Å* molecular sieves.

6.1.2 Reagents

The compounds: boron trichloride (1M in heptanes), trimethyl borate, borane dimethyl sulfide complex (2M in THF), elemental sulfur, potassium hexamethyldisilazane, silver(I) oxide, silver(I) triflate, mercury(II)acetate, triethylamine, ammonium hexafluorophosphate, trimethylorthoformate, triethylorthoformate, *o*-phenylenediamine, calcium hydride, lithium aluminum hydride, aniline, palladium(II) chloride, nickel(II) chloride, $Rh(CO)_2Cl]_2$, iron pentacarbonyl, molybdenum hexacarbonyl, phenyllithium (ca. 1.8M in di-*n*-butylether), methyllithium (ca. 1.6 M in diethylether), N-Boc-pyrrole, 2,2,6,6-tetramethylpiperidine, paraformaldehyde, formalin (37 w/v % formaldehyde in water), Raney®-Nickel (4200, slurry in H_2O, active catalyst), were commercial reagents purchased from Sigma-Aldrich, and used as received. Carbon monoxide was a commercial reagent purchased from Praxair Canada and used as received. Di-*tert*-butylphosphine, diphenylphosphine, and chlorodiphenylphosphine were commercial reagents purchased from Strem Chemicals Inc., and used as received. $[Rh(cod)Cl]_2$, and $[Pd(PPh_3)_4]$ were commercial reagents purchased from Pressure Chemical Co., and used as received. Di-*tert*-butylchlorophosphine,[240] di-*tert*-butylphosphine,[241] diphenylphosphinomethanol,[242] di-*tert*-butylphosphinomethanol,[242] hexahydropyrimidine,[243] 2,3-dihydro-1*H*-perimidine,[244] 2-(diphenylphosphino)-1*H*-pyrrole,[119] 2-lithio-*N*,*N*'-dimethylaniline,[245] *N*-lithio-2,2,6,6-tetramethyl piperidine,[119] and $[(\eta^3$-allyl)PdCp],[246] were prepared according to previously reported procedures. The compounds N^1,N^2-bis((diphenylphosphino)methyl)benzene-1,2-diamine **2.1-Ph**,[97] and N^1,N^2-bis((di-*tert*-butylphosphino)methyl)benzene-1,2-diamine **2.1-*t*Bu**,[83] were synthesized by slightly modified procedures from those reported:[94]

Synthesis of N^1,N^2-bis((diphenylphosphino)methyl)benzene-1,2-diamine, **2.1-Ph**.

A stirred suspension of paraformaldehyde (1.61 g, 53.7 mmol) on neat Ph_2PH (10g, 53.7 mmol) was heated to 125 °C for 6 h. The obtained Ph_2PCH_2OH was dissolved in CH_2Cl_2 (20 mL) and added to a solution of o-phenylenediamine (2.9 g, 26.9 mmol) in CH_2Cl_2 (25 mL). The resulting solution was stirred for 2 days at rt. The reaction mixture was dried with CaH_2 (2.5 g, 59.4 mmol) over a period of 30 min. The CaO formed and the excess CaH_2 were filtered off and the volatiles removed under vacuum. Recrystallization from CH_2Cl_2 at –45 ºC yielded colorless crystals of **2.1-*t*Bu** (11.5 g, 22.9 mmol, 85 %). ^{1}H NMR (400 MHz, C_6D_6): δ (ppm) = 3.27 (s, 2H, N*H*), 3.50 (d, $^2J_{PH}$ = 4.3 Hz, 4H, PCH_2N), 6.68 (AA'BB' system simplified as dd, J_{HH} = 3.4, 5.8 Hz, 2H, $C_6H_4N_2$), 6.92 (AA'BB' system simplified as dd, J_{HH} = 3.5, 5.5 Hz, 2H, $C_6H_4N_2$), 7.02-7.04 (m, 12H, *o*-C_6H_5 and *p*-C_6H_5), 7.33-7.39 (m, 8H, *m*-C6*H*5); ^{31}P{^{1}H} NMR (162 MHz, C_6D_6): δ (ppm) = -18.1 (s).

Synthesis of N^1,N^2-bis((di-*tert*-butylphosphino)methyl)benzene-1,2-diamine, **2.1-*t*Bu.**

A stirred suspension of paraformaldehyde (1.03 g, 34.2 mmol) on neat ^{t}Bu$_2$PH (5g, 34.1 mmol) was heated to 60 °C for 12 h. The obtained ^{t}Bu$_2$PCH$_2$OH was dissolved in CH_2Cl_2 (10 mL) and added to a solution of o-phenylenediamine (1.85 g, 17 mmol) in CH_2Cl_2 (25 mL). The resulting solution was then stirred for 2 days at rt. The reaction mixture was dried with CaH_2 (2 g, 47.5 mmol) over a period of 30 min. The CaO formed and the excess CaH_2 were filtered off and the volatiles removed under vacuum. Recrystallization from CH_2Cl_2 at –45 ºC yielded colorless crystals of **2.1-Ph** (5.92 g, 13.9 mmol, 82 %). ^{1}H NMR (400MHz, C_6D_6): δ (ppm) = 1.08 (d, $^3J_{PH}$ = 10.9 Hz, 36H, (CH_3)$_3$C), 3.18 (d, $^2J_{PH}$ = 5.5 Hz, 4H, PCH_2N), 3.55 (br-s, 2H, N*H*), 6.67 (AA'BB' system simplified as dd, J_{HH} = 3.7, 5.8 Hz, 2H, $C_6H_4N_2$), 6.73

(AA'BB' system simplified as dd, J_{HH} = 3.4, 5.6 Hz, 2H, $C_6H_4N_2$); $^{31}P\{^1H\}$ NMR (162 MHz, C_6D_6): δ (ppm) = 30.1 (s).

6.1.3 Analytical Instrumentation

The NMR spectra discussed herein were collected on Bruker Avance UGI-400, DRX-400, DRY-400, RDQ-400 and CFI-600 spectrometers. The chemical shifts are reported in : δ (ppm) = units (ppm) using the residual solvent peak as an internal reference for ^1H and $^{13}C\{^1H\}$ spectra: $CHDCl_2$ (t, 5.32 ppm, ^1H), CD_2Cl_2 (q, 53.5ppm, ^{13}C), DMSO-d_5 (q, 2.50 ppm, ^1H), DMSO-d_6 (sept, 39.70 ppm, ^{13}C), THF-d_7 (m, 3.58 ppm, ^1H), THF-d_8 (q, 67.57 ppm, ^{13}C), C_6HD_4Br (m, 6.94 ppm, ^1H), toluene-d_7 (q, 2.09 ppm, ^1H), toluene-d_8 (sept, 20.4, ^{13}C), C_6HD_5 (s, 7.16 ppm, ^1H), C_6D_6 (t, 128.39 ppm, ^{13}C), $CHCl_3$ (s, 7.24 ppm, ^1H), and $CDCl_3$ (t, 77.23 ppm, ^{13}C). 85 % H_3PO_4 was used as an external reference for ^{31}P and $^{31}P\{^1H\}$ spectra (0 ppm, ^{31}P), CF_3COOH was used as an external reference for ^{19}F spectra (-76.55 ppm, ^{19}F), and 15 % $BF_3.OEt_2$ in $CDCl_3$ was used as an external reference for ^{11}B and $^{11}B\{^1H\}$ spectra (0 ppm, ^{11}B).

Elemental analysis data was obtained with a Perkin-Elmer CHNS/O series II analyzer 2400. Low resolution ESI-mass spectra were collected with a Bruker Esquire 3000 ESI-Ion trap instrument and high resolution ESI-mass spectra were obtained with an Agilent 6520 MS-Quadrupole time of flight instrument. Low resolution EI-mass spectra were collected using a Finnigan MAT SSQ 7000 instrument.

6.1.4 X-Ray Crystallography

Solid-state molecular structures of compounds **2.1-Ph**, **2.1-*t*Bu**, **2.4-Ph**, **2.5**, **2.6**, **2.15-Me**, **2.16-Me**·LiOMe, H_2(**3.1b-Ph**), [H(**4.2-Ph**)][PF_6] and [H(**4.2-*t*Bu**)][PF_6], and of complexes **2.3-Ph**, **3.5a-Ph**, **3.5a-*t*Bu**, **3.5b-Ph**, **3.10b-Ph**, [**3.12b-Ph**][OTf], **3.14a-*t*Bu**, [**3.13a-Ph**][OTf], [**3.13a-*t*Bu**][OTf], **3.15a-*t*Bu**, **3.16a-*t*Bu**, **4.3-*t*Bu**, [**4.4-*t*Bu**][OTf], [**4.6_*t*Bu**][PF_6], [**4.8-*t*Bu**][PF_6], [**4.9-*t*Bu**][PF_6], **4.10-*t*Bu**, and **4.11-*t*Bu** were obtained. In all cases a single crystal was coated with Paratone 8277 oil (Exxon), and mounted on a glass fiber. All measurements were made on a Nonius KappaCCD diffractometer with graphite monochromated Mo-K_α radiation. Details of crystal data, data collection[247,248] and structure refinement are provided in appendix A. The data were corrected for Lorentz and polarization effects and for absorption using multi-scan methods.[247] The structures were solved by the direct methods[249,250] and expanded using Fourier techniques.[251,252] Crystal and structure refinement data is presented in Apendix A and full crystallographic data is available either in the attached CD at the end of this document, for printed versions, or in the attached file ucalgary_2013_borau-garcia_javier_fullcrystaldata, for internet access.

6.1.5 Computational Chemistry

All calculations were performed with the Gaussian 03[253] program package at the density functional level of theory using the PBE1PBE exchange-correlation functional.[254-257] Ahlrichs' triple-zeta valence basis sets augmented by two sets of polarization functions (def2-TZVPP) were used throughout the work.[258] The nature of stationary points found was confirmed by subsequent calculations of harmonic vibrational frequencies.

6.2 Experimental Details for Chapter Two

Synthesis of 2-chloro-1,3-bis((diphenylphosphino)methyl)-2,3-dihydro-1*H*-benzo[*d*][1,3,2] diazaborole **2.2-Ph**.

BCl_3 (3 mL, 1M solution in heptanes, 3 mmol) was added dropwise to a stirred solution of **2.1-Ph** (1.5 g, 2.97 mmol) in CH_2Cl_2 (35 mL). The reaction mixture was heated on a sealed container to 45 °C for 16 h after which it was allowed to cool down to rt. NEt_3 (0.88 mL, 6.3 mmol) was slowly added, and the reaction mixture was heated again to 45 °C for 36 h. The volatiles were removed under vacuum and the solids taken up on THF (35 mL). The ammonium chloride by-product was filtered off, the volatiles from the filtrate removed under vacuum and the obtained solid washed with pentanes (2 x 15 mL) and dried under vacuum yielding a white solid **2.2-Ph** (1.35 g, 2.47 mmol, 83 %). ^{1}H NMR (400 MHz, C_6D_6): δ (ppm) = 4.45 (d, $^{2}J_{PH}$ = 4.7 Hz, 4H, PC*H*$_2$N), 7.02 (AA'BB' system simplified as dd, J_{HH} = 3.2, 5.8 Hz, 2H, $C_6H_4N_2$), 7.19 (AA'BB' system simplified as dd, J_{HH} = 3.3, 5.5 Hz, 2H, $C_6H_4N_2$), 7.34-7.37 (m, 12H, *o*-C_6H_5 and *p*-C_6H_5), 7.41-7.45 (m, 8H, *m*-C_6H_5); ^{11}B{^{1}H} NMR (123.38 MHz, CD_2Cl_2): δ (ppm) = 25.9 (s); ^{13}C{^{1}H} NMR (101 MHz, CD_2Cl_2): δ (ppm) = 44.8 (d, $^{1}J_{PC}$ = 12.9 Hz, P*C*H$_2$N), 111.1 (d, $^{4}J_{PC}$ = 7.4 Hz, *3,6-C*$_6$H$_4$N$_2$), 120.1 (s, *4,5-C*$_6$H$_4$N$_2$), 129.1 (d, $^{2}J_{PC}$ = 6.8 Hz, *o-C*$_6$H$_5$), 129.6 (s, *1,2-C*$_6$H$_4$N$_2$), 133.8 (d, $^{3}J_{PC}$ = 18.9 Hz, *m-C*$_6$H$_5$), 136.5 (s, *p-C*$_6$H$_5$), 137.2 (d, $^{1}J_{PC}$ = 14.8 Hz, *ipso-C*$_6$H$_5$); ^{31}P{^{1}H} NMR (162 MHz, C_6D_6): δ (ppm) = -20.3 (s). Hi-res TOF MS EI+ (m/z (%)) $(M\text{-}Cl)^+$ Found: 513.18406, Calc.: 513.18513.

Synthesis of 2-chloro-1,3-bis((di-*tert*-butylphosphino)methyl)-2,3-dihydro-1*H*-benzo[*d*][1,3,2] diazaborole **2.2-*t*Bu**.

BCl_3 (2.4 mL, 1M solution in heptanes, 2.4 mmol) was added dropwise to a stirred solution of **2.1-*t*Bu** (1 g, 2.36 mmol) in CH_2Cl_2 (35 mL). The reaction mixture was heated on a sealed container to 45 °C for 16 h after which it was allowed to cool down to rt. NEt_3 (0.73 mL, 5.2 mmol) was slowly added, and the reaction mixture was heated again to 45 °C for 36 h. The volatiles were removed under vacuum and the solids taken up on THF (35 mL). The ammonium chloride by-product was filtered off and the volatiles from the filtrate removed under vacuum to yield an off-white solid **2.2-*t*Bu** (710 mg, 1.51 mmol, 64 %). ^{1}H NMR (400 MHz, CD_2Cl_2): δ (ppm) = 1.21 (d, $^3J_{PH}$ = 10.9 Hz, 36H, $(CH_3)_3C$), 4.11 (d, $^2J_{PH}$ = 2.6 Hz, 4H, PCH_2N), 6.99 (AA'BB' system simplified as dd, J_{HH} = 3.3, 5.9 Hz, 2H, $C_6H_4N_2$), 7.45 (AA'BB' system simplified as dd, J_{HH} = 3.3, 5.8 Hz, 2H, $C_6H_4N_2$); ^{11}B{^{1}H} NMR (128.38 MHz, CD_2Cl_2): δ (ppm) = 25.8 (s); ^{13}C{^{1}H} NMR (101 MHz, C_6D_6): δ (ppm) = 30.0 (d, $^2J_{PC}$ = 12.7 Hz, $PC(CH_3)_3$), 32.2 (d, $^1J_{PC}$ = 21.6 Hz, $PC(CH_3)_3$), 38.7 (d, $^1J_{PC}$ = 22.9 Hz, PCH_2N), 112.1 (d, $^4J_{PC}$ = 10.6 Hz, $C_6H_4N_2$), 119.4 (s, $C_6H_4N_2$), 136.9 (s, $C_6H_4N_2$); ^{31}P{^{1}H} NMR (162 MHz, C_6D_6): δ (ppm) = 16.1 (s). Hi-res TOF MS EI+ (m/z (%)) $(M+H)^+$ Found: 469.28201, Calc.: 469.28341.

Synthesis of [(*Ph-phenylene*-PBP)PdCl] **2.3-Ph**

$Pd(PPh_3)_4$ (421 mg, 0.37 mmol) was added to a stirred solution of **2.2-Ph** (200 mg, 0.37 mmol) in CH_2Cl_2 (20 mL). The reaction mixture was refluxed for 48 h, the solution went from a bright yellow to a deep red colour. The reaction was allowed to cool down to rt. Hexanes (80 mL) were added to the reaction mixture precipitating a red solid which was isolated

by filtration and further washed with hexanes (30 mL) affording **2.3-Ph** as a light red solid (215 mg, 0.33 mmol, 88 %). X-ray quality crystals of **2.3-Ph** were obtained by slow evaporation from a concentrated solution in CH_2Cl_2 at -35 °C. ^{1}H NMR (400 MHz, C_6D_6): δ (ppm) = 4.62 (vt, J_{PH} = 2.9 Hz, 4H, PC*H*$_2$N), 6.98-7.06 (m, 4H, $C_6H_4N_2$), 7.43-7.52 (m, 12H, *o*-C_6H_5 and *p*-C_6H_5), 7.92-8.01 (m, 8H, *m*-C_6H_5); ^{11}B{^{1}H} NMR (123.38 MHz, CD_2Cl_2): δ (ppm) = 38.9 (s); ^{13}C{^{1}H} NMR (101 MHz, CD_2Cl_2): δ (ppm) = 49.1 (vt, J_{PC} = 20.5 Hz, P*C*H$_2$N), 110.1 (s, *3,6*-$C_6H_4N_2$), 119.1 (s, *4,5*-$C_6H_4N_2$), 129.6 (vt, J_{PC} = 5.2 Hz, *m*-C_6H_5), 131.5 (s, *p*-C_6H_5), 132.9 (vt, J_{PC} = 19.6 Hz, *1,2*-$C_6H_4N_2$), 133.9 (vt, J_{PC} = 7.4 Hz, *o*-C_6H_5), 138.7 (d, $^1J_{PC}$ = 10.6 Hz, *ipso*-C_6H_5); ^{31}P{^{1}H} NMR (162 MHz, C_6D_6): δ (ppm) = 43.0 (s). Hi-res TOF MS EI+ (m/z (%)) $(M-Cl)^+$ Found: 619.08423, Calc.: 619.08556

Synthesis of [(*^{t}Bu-phenylene*-PBP)PdCl] **2.3-*t*Bu**

$Pd(PPh_3)_4$ (308 mg, 27 mmol) was added to a stirred solution of **2.2-*t*Bu** (125 mg, 27 mmol) in toluene (25 mL). The reaction mixture was heated to 100 °C for 36 h, the solution changed colour from a bright yellow to a light red. The reaction was allowed to cool down to rt and all the volatiles were removed under vacuum. The solids were washed three times with hexanes (3 x 10 mL) and dried under vacuum yielding **2.3-*t*Bu** (115 mg, 20 mmol, 74 %). ^{1}H NMR (400 MHz, CD_2Cl_2): δ (ppm) = 1.45 (vt, J_{PH} = 6.1 Hz, 36H, PC(C*H*$_3$)$_3$), 3.87 (d, $^2J_{PH}$ = 5.8 Hz, 4H, PC*H*$_2$N), 6.96 (AA'BB' system simplified as dd, J_{HH} = 4.2, 7.4 Hz, 2H, $C_6H_4N_2$), 7.28 (AA'BB' system simplified as dd, J_{HH} = 4.2, 7.4 Hz, 2H, $C_6H_4N_2$) ; ^{11}B{^{1}H} NMR (128.38 MHz, CD_2Cl_2): δ (ppm) = 38.6 (s); ^{13}C{^{1}H} NMR (101 MHz, CD_2Cl_2): δ (ppm) = 30.0 (vt, J_{PC} = 3.5 Hz, PC(*C*H$_3$)$_3$), 36.1 (vt, J_{PC} = 6.5 Hz, P*C*(CH$_3$)$_3$), 40.0

(d, $^{1}J_{PC}$ = 15.1 Hz, P*C*H_2N), 109.4 (s, *3,6*-$C_6H_4N_2$), 119.1 (s, *4,5*-$C_6H_4N_2$), 134.2 (s, *1,2*-$C_6H_4N_2$) ; $^{31}P\{^{1}H\}$ NMR (162MHz, CD_2Cl_2): δ (ppm) = 88.3.

Synthesis of N^1,N^2-bis((diphenylphosphorothioyl)methyl)benzene-1,2-diamine **2.4**.

Elemental sulfur (0.196 g, 0.76 mmol) was added to a solution of **2.1-Ph** (1.55 g, 3.07 mmol) in CH_2Cl_2 (50 mL). The reaction mixture was stirred for 3 h after which all the volatiles were removed under vacuum yielding a light yellow crystalline powder. Recrystallization from a concentrated solution in CH_2Cl_2 at -35 °C afforded an analytically pure sample of **2.4** (1.24g, 2.52 mmol, 82 %). ^{1}H NMR (400 MHz, CD_2Cl_2): δ (ppm) = 3.95 (d, $^{2}J_{PH}$ = 7.6 Hz, 4H, PC*H*$_2$N), 4.25 (s, 2H, N*H*), 6.71 (AA'BB' system simplified as dd, J_{HH} = 3.5, 5.6 Hz, 2H, $C_6H_4N_2$), 7.04 (AA'BB' system simplified as dd, J_{HH} = 3.4, 5.7 Hz, 2H, $C_6H_4N_2$), 7.43-7.49 (m, 8H, *o*-C_6H_5), 7.50-7.56 (m, 4H, *p*-C_6H_5), 7.84-7.91 (m, 8H, *m*-C_6H_5); $^{13}C\{^{1}H\}$ NMR (101 MHz, CD_2Cl_2): δ (ppm) = 47.3 (d, $^{1}J_{PC}$ = 63.4 Hz, P*C*H_2N), 113.8 (s, $C_6H_4N_2$), 120.9 (s, $C_6H_4N_2$), 129.3 (d, $^{2}J_{PC}$ = 12.1 Hz, *o*-C_6H_5), 131.6 (s, $C_6H_4N_2$), 132.0 (d $^{3}J_{PC}$ = 10.1 Hz, *m*-C_6H_5), 132.4 (s, *p*-C_6H_5), 137.7 (d, $^{1}J_{PC}$ = 12.1 Hz, *ipso*-C_6H_5); $^{31}P\{^{1}H\}$ NMR (162 MHz, CD_2Cl_2): δ (ppm) = 41.7 (s). Hi-res MS ESI+ (m/z (%)) $(M+H)^+$ Found: 569.13844, Calc.: 569.13984.

Synthesis of 2-chloro-1,3-bis((diphenylphosphorothioyl)methyl)-2,3-dihydro-1*H*-benzo[*d*][1,3,2]diazaborole **2.5**.

BCl_3 (0.88 mL, 1M solution in heptanes, 0.88 mmol) was added dropwise to a stirred solution of **2.4** (500 mg, 0.88 mmol) in CH_2Cl_2 (25 mL). The reaction mixture was heated on a sealed container to 45 °C for 16 h and then cooled down to rt. The volatiles were removed under

vacuum, the solid obtained was washed with pentanes (2 x 15 mL), and dried under vacuum yielding **2.5** as an off white solid (382 mg, 0.62 mmol, 70 %). X-ray quality crystals of **2.5** were obtained by slow evaporation of a concentrated solution in benzene at rt. ^{1}H NMR (400 MHz, CD_2Cl_2): δ (ppm) = 4.79 (d, $^{2}J_{PH}$ = 3.0 Hz, 4H, PC*H*$_2$N), 6.55 (AA'BB' system simplified as dd, J_{HH} = 3.5, 5.9 Hz, 2H, $C_6H_4N_2$), 6.62 (AA'BB' system simplified as dd, J_{HH} = 3.5, 5.9 Hz, 2H, $C_6H_4N_2$), 7.43-7.50 (m, 8H, *o*-C_6H_5), 7.51-7.58 (m, 4H, *p*-C_6H_5), 7.81-7.90 (m, 8H, *m*-C_6H_5); ^{11}B{^{1}H} NMR (123.38 MHz, CD_2Cl_2): δ (ppm) = 27.2 (s); ^{13}C{^{1}H} NMR (101 MHz, CD_2Cl_2): δ (ppm) = 49.1 (d, $^{1}J_{PC}$ = 58.6 Hz, P*C*H$_2$N), 111.2 (s, *3,6*-$C_6H_4N_2$), 120.2 (s, *4,5*-$C_6H_4N_2$), 129.1 (d, $^{2}J_{PC}$ = 12.0 Hz, *o*-C_6H_5), 131.6 (s, *1,2*-$C_6H_4N_2$), 132.4 (d, $^{1}J_{PC}$ = 9.8 Hz, *ipso*-C_6H_5), 132.5 (d, $^{3}J_{PC}$ = 10.0 Hz, *m*-C_6H_5), 135.8 (s, *p*-C_6H_5); ^{31}P{^{1}H} NMR (162 MHz, C_6D_6): δ (ppm) = 39.3 (s).

Synthesis of 1,3-bis((diphenylphosphorothioyl)methyl)-2,3-dihydro-1*H*-benzo[*d*][1,3,2] diazaborole **2.6**.

$LiAlH_4$ (20 mg, 0.52 mmol) was slowly added to a solution of **2.5** (300 mg, 0.49 mmol) in THF (20 mL) and the reaction mixture was stirred for 1 h. The solid by-products of the reduction along with the excess $LiAlH_4$ were removed by filtration. The volatiles were removed under vacuum and the obtained solid was washed twice with benzene (2 x 15 mL) yielding PhSBSH as a white solid (260 mg, 0.45 mmol, 92 %). X-ray quality crystals of **2.6** were obtained by slow evaporation from a concentrated solution in THF at -35 °C. {^{11}B}^{1}H NMR (400 MHz, THF-d_8): δ (ppm) = 4.29 (s, 1H, NB(*H*)N), 4.88 (d, $^{2}J_{PH}$ = 4.1 Hz, 4H, PC*H*$_2$N), 6.47 (AA'BB' system simplified as dd, J_{HH} = 3.2, 5.9 Hz, 2H, $C_6H_4N_2$), 6.60 (AA'BB' system simplified as dd, J_{HH} = 3.2, 5.9 Hz, 2H, $C_6H_4N_2$), 7.33-7.42 (m, 8H, *o*-C_6H_5), 7.42-7.50 (m, 4H,

p-C_6H_5), 7.85-7.96 (m, 8H, *m*-C_6H_5); $^{11}B\{^1H\}$ NMR (123.38 MHz, THF-d_8): δ (ppm) = 23.7 (s); $^{13}C\{^1H\}$ NMR (101 MHz, THF-d_8): δ (ppm) = 31.0 (s, P*C*H_2N), 108.9 (s, *3,6*-$C_6H_4N_2$), 119.6 (s, *4,5*-$C_6H_4N_2$), 127.4 (s, *1,2*-$C_6H_4N_2$), 127.9 (d, $^2J_{PC}$ = 5.4 Hz, *o*-C_6H_5), 129.4 (d, $^1J_{PC}$ = 12.4 Hz, *ipso*-C_6H_5), 132.9 (d, $^3J_{PC}$ = 20.9 Hz, *m*-C_6H_5), 139.5 (s, *p*-C_6H_5); $^{31}P\{^1H\}$ NMR (162 MHz, THF-d_8): δ (ppm) = 39.1 (s). Hi-res TOF MS EI+ (m/z (%)) $(M+H)^+$ Found: 578.1338, Calc.: 578.1340.

Synthesis of bis((diphenylphosphino)methyl)borochloridate **2.13-Ph**

BCl_3 (1.16 mL, 1M solution in heptanes, 1.16 mmol) was added dropwise to a stirred solution of diphenylphosphinomethanol (500 mg, 2.31 mmol), and triethylamine (234 mg, 0.32 mL, 2.31 mmol) in benzene (25 mL). The reaction mixture was heated on a sealed container to 80 °C for 16 h and then cooled down to rt. The triethylaminehydrochloride by product was filtered off and all the volatiles from the filtrate were removed under vacuum. Compound **2.13-Ph** was obtained as a thick colorless oil (490 mg, 1.03 mmol, 89 %) which contained residual solvent. ^1H NMR (400 MHz, C_6D_6): δ (ppm) = 4.38 (bs, 4H, PCH_2N), 7.06 (m, 12H, *o*-C_6H_5, and *p*-C_6H_5), 7.51 (bs, 8H, *m*-C_6H_5); $^{11}B\{^1H\}$ NMR (123.38 MHz, C_6D_6): δ (ppm) = 18.3 (s); $^{31}P\{^1H\}$ NMR (162 MHz, C_6D_6): δ (ppm) = -11.2 (s).

Attempted synthesis of bis(2-dimethylaminophenyl)-borinic acid methyl ester **2.14-Me** with isolation of **2.15-Me** and **2.16-Me•**LiOMe.

2-lithio-*N,N'*-dimethylaniline (1 g, 7.9 mmol) was dissolved in toluene (20 mL). This solution was added dropwise to a chilled solution (-78 °C) of trimethylborate (408 mg, 0.44 mL, 3.9 mmol) in hexanes (5 mL). The reaction mixture was stirred and allowed to warn up to rt.

overnight. The LiOMe by-product was removed by filtration and all the volatiles from the filtrate were removed under vacuum yielding a yellow oil (1.1g). X-ray quality crystals of **2.15-Me** were obtained by slow evaporation from a concentrated solution in hexanes at -30 °C, and X-ray quality crystals of **2.16-Me•**LiOMe were obtained by slow evaporation from a concentrated solution in benzene at room temperature. The $^{11}B\{^{1}H\}$ NMR (123.38 MHz, THF-d_8) of the yellow oil: δ (ppm) = 3.3 (s), 5.1 (bs).

Synthesis of bis(2-dimethylaminophenyl)borinicacid **2.17-Me**

2-lithio-*N*,*N'*-dimethylaniline (3 g, 23.6 mmol) was dissolved in toluene (50 mL). This solution was added dropwise to a chilled solution (-78 °C) of trimethylborate (1.22 g, 1.32 mL, 11.8 mmol) in hexanes (10 mL). The reaction mixture was stirred and allowed to warn up to rt. overnight. Water (20 mL) was added to the reaction mixture. All volatiles were removed under vacuum. The solid obtained was extracted with toluene (2 x 30 mL), the fractions were combined and all the volatiles removed under vacuum yielding compound **2.17-Me** as a white crystalline solid (2.855 g, 10.6 mmol, 90 % yield). ^{1}H NMR (400 MHz, D_2O): δ (ppm) = 2.73 (bs, 12H, $N(CH_3)_2$), 7.23 (t, 2H, $^{3}J_{HH}$ = 7.1 Hz, C_6H_4BN), 7.32 (t, 2H, $^{3}J_{HH}$ = 7.7 Hz, C_6H_4BN), 7.41 (d, 2H, $^{3}J_{HH}$ = 7.7 Hz, C_6H_4BN), 7.62 (d, 2H, $^{3}J_{HH}$ = 7.1 Hz, C_6H_4BN); $^{11}B\{^{1}H\}$ NMR (123.38 MHz, D_2O): δ (ppm) = 3.9 (s).

6.3 Experimental Details for Chapter Three

Synthesis of 1,3-bis((diphenylphosphino)methyl)-hexahydropyrimidine H_2(**3.1a-Ph**).

Ph_2PCH_2OH (2.69 g, 12 mmol) was added to a solution of hexahydropyrimidine (0.54 g, 6 mmol) in CH_2Cl_2 (20 mL) and stirred at 55 °C for 20 h. The reaction mixture was dried with excess CaH_2. The CaO and CaH_2 were filtered off and the volatiles were removed under vacuum yielding a thick colorless oil H_2(**3.1a-Ph**) (2.48 g, 5.1 mmol, 82.7 %), pure by NMR. After several days, the product solidified into a colorless wax. ^{1}H NMR (400 MHz, CD_2Cl_2): δ (ppm) = 1.69 (q, $^3J_{HH}$ = 5.12 Hz, 2H, $CH_2CH_2CH_2$), 2.83 (br-t, 4H, NCH_2CH_2), 3.26 (d, $^2J_{PH}$ = 4.6 Hz, 4H, PCH_2N_2), 3.67 (s, 2H, NCH_2N), 7.31-7.35 (m, 12H, *o*-C_6H_5, *p*-C_6H_5), 7.42-7.48 (m, 8H, *m*-C_6H_5). $^{13}C\{^1H\}$ NMR (101 MHz, CD_2Cl_2): δ (ppm) = 21.8 (s, $CH_2CH_2CH_2$), 53.7 (br-d, PCH_2N), 56.9 (s, NCH_2CH_2), 76.5 (t, $^3J_{PC}$ = 9.1 Hz, NCH_2N), 128.3 (d, $^3J_{PC}$ = 6.6 Hz, *m*-C_6H_5), 128.5 (s, *p*-C_6H_5), 132.8 (d, $^2J_{PC}$ = 18.1 Hz, *o*-C_6H_5), 138.6 (d, $^1J_{PC}$ = 13.6 Hz, *ipso*-C_6H_5); ^{31}P NMR (162 MHz, CD_2Cl_2): δ (ppm) = = -25.9 (s). TOF MS EI+ (m/z (%)): 481.18 (1) [M^+], 297.06 (99) [M-P(C_6H_5)$_2^+$]. Anal. Calc for $C_{30}H_{32}N_2P_2$ (%): C, 74.67; H, 6.68; N, 5.81. Found: C, 74.24; H, 6.27; N, 5.73.

Synthesis of 1,3-bis((di-*tert*-butylphosphino)methyl)-hexahydropyrimidine H_2(**3.1a-*t*Bu**)

(*t*-Bu)$_2PCH_2OH$ (2.50 g, 14.2 mmol) was added to a solution of hexahydropyrimidine (611 mg, 7.1 mmol) in CH_2Cl_2 (30 mL) and stirred at rt for 72 h. The reaction mixture was dried with excess CaH_2. The CaO and excess CaH_2 were filtered off and the volatiles were removed under vacuum yielding a thick colorless oil H_2(**3.1a-*t*Bu**) (2.49 g, 6.2 mmol, 87 %), pure by NMR. After several days, the product solidified into a colorless wax. ^{1}H NMR (400 MHz,

C_6D_6): δ (ppm) = 1.17 (d, $^3J_{PH}$ = 10.5 Hz, 36H, PC(CH_3)$_3$), 1.52 (br-s, 2H, $CH_2CH_2CH_2$), 2.67 (d, $^2J_{PH}$ = 3.0 Hz, 4H, PCH_2N_2), 2.69 (br-s, 2H, NCH_2CH_2), 3.54 (br-s, 2H, NCH_2N); $^{13}C\{^1H\}$ NMR (101 MHz, CD_2Cl_2): δ (ppm) = 22.9 (s, $CH_2CH_2CH_2$), 30.4 (d, $^2J_{PC}$ = 13.1 Hz, PC(CH_3)$_3$), 31.3 (d, $^1J_{PC}$ = 22.7 Hz, PC(CH_3)$_3$), 51.0 (d, $^1J_{PC}$ = 11.7 Hz, PCH_2N), 56.9 (d, $^3J_{PC}$ = 8.1 Hz, NCH_2CH_2), 78.8 (t, $^3J_{PC}$ = 8.8 Hz, NCH_2N); $^{31}P\{^1H\}$ NMR (162 MHz, CD_2Cl_2): δ (ppm) = 11.6 (s). Hi-res MS ESI+ (m/z (%)) $(M+H)^+$ Found: 403.33614, Calc.: 403.33655.

Synthesis of 1,3-bis((diphenylphosphino)methyl)-2,3-dihydro-1*H*-perimidine H_2(**3.1b-Ph**)

Ph_2PCH_2OH (2.37 g, 11 mmol) was added to a solution of 2,3-dihydro-1*H*-perimidine (0.93 g, 5.5 mmol) in CH_2Cl_2 (20 mL) and stirred at 55 °C for 20 h. The reaction mixture was dried with excess CaH_2. The CaO and excess CaH_2 were filtered off and the volatiles removed under vacuum. The solid obtained was washed with pentanes (2 x 15mL) and recrystallized from a concentrated solution in CH_2Cl_2 at -35 °C to afford colourless X-ray quality crystals of H_2(**3.1b-Ph**) (780 mg, 1.4 mmol, 25.2 %). ^1H NMR (400 MHz, CD_2Cl_2): δ (ppm) = 4.00 (d, $^2J_{PH}$ = 4.5 Hz, 4H, PCH_2N), 4.18 (s, 2H, NCH_2N), 6.62 (d, $^3J_{HH}$ = 7.4 Hz, 2H, 2,7-$C_{10}H_6$), 7.20 (dd, $^3J_{HH}$ = 8.2 Hz, $^4J_{HH}$ = 0.9 Hz, 2H, 4,5-$C_{10}H_6$), 7.27 (dd, $^3J_{HH}$ = 8.2 Hz, 2H, $^3J_{HH}$ = 7.5 Hz, 3,6-$C_{10}H_6$), 7.34-7.38 (m, 12H, *o*-C_6H_5, *p*-C_6H_5), 7.44-7.50 (m, 8H, *m*-C_6H_5); $^{13}C\{^1H\}$ NMR (101 MHz, CD_2Cl_2): δ (ppm) = 53.3 (d, $^1J_{PC}$ = 10.1 Hz, PCH_2N), 68.0 (t, $^3J_{PC}$ = 7.1 Hz, NCH_2N), 106.0 (d, $^4J_{PC}$ = 4.3 Hz, *2,7*-$C_{10}H_6$), 116.7 (s, *9*-$C_{10}H_6$), 118.4 (s, *4,5*-$C_{10}H_6$), 127.1 (s, *3,6*-$C_{10}H_6$), 129.2 (d, $^3J_{PC}$ = 7.02 Hz, *m*-C_6H_5), 129.5 (s, *p*-C_6H_5), 133.6 (d, $^2J_{PC}$ = 18.8 Hz, *o*-C_6H_5), 135.6 (s, *10*-$C_{10}H_6$), 138.2 (d, $^1J_{PC}$ = 14.6 Hz, *ipso*-C_6H_5), 143.8 (s, *1,8*-$C_{10}H_6$); $^{31}P\{^1H\}$ NMR (162 MHz, CD_2Cl_2): δ (ppm) = -25.5 (s). TOF MS EI+

(m/z (%)): 566.18 (2) [M^+], 381.13 (99) [M-P(C_6H_5)$_2^+$]. Anal. Calc for $C_{37}H_{32}N_2P_2$ (%): C, 78.43; H, 5.64; N, 4.94. Found: C, 78.60; H, 5.71; N, 4.89.

Synthesis of [(*Ph-Propylene*-PCP)RhCl] **3.5a-Ph**

[Rh(cod)Cl]$_2$ (60 mg, 0.12 mmol) was added to a solution of H_2(**3.1a-Ph**) (116 mg, 0.24 mmol) in THF (5 mL). The solution was heated to 65 °C for 3h to afford a yellow crystalline solid. The solution was decanted and the solid washed with pentane (10 mL) and dried under vacuum affording X-ray quality yellow crystals of **3.5a-Ph** (136 mg, 0.22 mmol, 92 %). ^{1}H NMR (400 MHz, CD_2Cl_2): δ (ppm) = 2.03 (p, $^3J_{HH}$ = 6.0 Hz, 2H, $CH_2CH_2CH_2$), 3.23 (t, $^3J_{HH}$ = 6.0 Hz, 4H, NCH_2CH_2), 4.26 (vt, J_{PH} = 2.4 Hz, 4H, PCH_2N), 7.40-7.44 (m, 12H, *o*-C_6H_5, *p*-C_6H_5), 7.88-8.00 (m, 8H, *m*-C_6H_5); ^{1}H{^{13}C} NMR (101 MHz, DMSO-d_6): δ (ppm) = 19.8 (s, $CH_2CH_2CH_2$), 44.1 (s, NCH_2CH_2), 61.0 (br-s, PCH_2N), 128.5 (s, *m*-C_6H_5), 130 (s, *p*-C_6H_5), 132.9 (vt, J_{PC} = 6.4 Hz, *o*-C_6H_5), 134.0 (br-s, *ipso*-C_6H_5), 204.6 (br-s, N*C*(Rh)N); ^{31}P{^{1}H} NMR (162 MHz, CD_2Cl_2): δ (ppm) = 25.8 (d, $^1J_{RhP}$ = 153.9 Hz). TOF MS EI+ (m/z (%)): 618.09 (99) [M^+]. Anal. Calc. for $C_{30}H_{30}N_2P_2RhCl\cdot0.5THF$ (%): C, 57.98; H, 5.17; N, 4.23. Found: C, 57.47; H, 5.34; N, 3.84.

Synthesis of [(*tBu-Propylene*-PCP)RhCl] **3.5a-*t*Bu**

[Rh(cod)Cl]$_2$ (60 mg, 0.12 mmol) was added to a solution of H_2(**3.1a-*t*Bu**) (97 mg, 0.24 mmol) in C_6H_6 (10 mL). The solution was heated to 80 °C for 2 days to afford a yellow precipitate. The precipitate was filtered, washed with pentane (10 mL) and dried under vacuum affording a light yellow powder **3.5a-*t*Bu** (102 mg, 0.19 mmol, 80 %). X-ray quality crystals of **3.5a-*t*Bu** were obtained by slow evaporation of a concentrated solution in THF at -35 °C. ^{1}H

NMR (400 MHz, THF-d_8): δ (ppm) = 1.39 (vt, J_{PH} = 6.3 Hz, 36H, PC(CH_3)$_3$), 1.89 (q, $^3J_{HH}$ = 6.0 Hz, 2H, $CH_2CH_2CH_2$), 3.08 (t, $^3J_{HH}$ = 6.0 Hz, 4H, NCH_2CH_2), 3.49 (br-vt, 4H, PCH_2N); $^{13}C\{^1H\}$ NMR (101 MHz, THF-d_8): δ (ppm) = 22.2 (s, $CH_2CH_2CH_2$), 30.1 (vt, J_{PC} = 3.7 Hz, PC(CH_3)$_3$), 35.3 (dvt, J_{PC} = 6 Hz, $^2J_{RhC}$ = 1 Hz, P(C(CH_3)$_3$) 45.3 (vt, J_{PC} = 5 Hz, NCH_2CH_2), 55.1 (dvt, J_{PC} = 8.9 Hz, $^2J_{RhC}$ = 1.6 Hz, PCH_2N), 208.9 (dt, $^1J_{RhC}$ = 58.6 Hz, $^2J_{PC}$ = 8.2 Hz, NC(Rh)N); $^{31}P\{^1H\}$ NMR (162 MHz, THF-d_8): δ (ppm) = 62.0 (d, $^1J_{RhP}$ = 157.3 Hz). Hi-res MS ESI+ (m/z (%)) $(M - Cl)^+$ Found: 503.21807, Calc.: 503.21858. Anal. Calc. for $C_{22}H_{46}ClN_2P_2Rh$ (%): C, 49.03; H, 8.60; N, 5.20. Found: C, 49.40; H, 8.75; N, 5.09.

Synthesis of [(*Ph-Naphthylene*-PCP)RhCl] **3.5b-Ph**

$[Rh(cod)Cl]_2$ (60 mg, 0.12 mmol) was added to a solution of H_2(**3.1b-Ph**) (136 mg, 0.24 mmol) in THF (5 mL). The solution was heated to 65 °C for 2h to afford an orange crystalline solid. The solution was decanted and the crystals washed with pentane (10 mL) and dried under vacuum affording X-ray quality orange crystals of **3.5b-Ph** (162 mg, 0.23 mmol, 96 %). ^1H NMR (400 MHz, CD_2Cl_2): δ (ppm) = 4.67 (vt, J_{PH} = 2.4 Hz, 4H, PCH_2N), 6.77 (dd, $^3J_{HH}$ = 6.60 Hz, $^4J_{HH}$ = 1.80 Hz, 2H, *2,7*-$C_{10}H_6$), 7.34-7.39 (m, 4H, *3,4,5,6*-$C_{10}H_6$), 7.43-7.50 (m, 12H, *o*-C_6H_5, *p*-C_6H_5), 7.91-8.02 (m, 8H, *m*-C_6H_5). $^{13}C\{^1H\}$ NMR (100 MHz, CD_2Cl_2): δ (ppm) = 58.23 (vt, J_{PC} = 15 Hz, PCH_2N), 106.2 (s, *2,7*-$C_{10}H_6$), 117.5 (s, *9*-$C_{10}H_6$), 120.1 (s, *4,5*-$C_{10}H_6$), 128.1 (s, *3,6*-$C_{10}H_6$), 128.7 (vt, J_{PC} = 5.0 Hz, *m*-C_6H_5), 130.20 (s, *p*-C_6H_5), 130.92 (s, *1,8*-$C_{10}H_6$), 131.7 (s, 10-$C_{10}H_6$), 133.8 (vt, J_{PC} = 7.0 Hz, *o*-C_6H_5), 134.1 (vt, J_{PC} = 20.2 Hz, *ipso*-C_6H_5), 207.0 (dt, $^1J_{RhC}$ = 62.0 Hz, $^2J_{PC}$ = 9.0 Hz, NC(Rh)N); $^{31}P\{^1H\}$ NMR (162 MHz, CD_2Cl_2): δ (ppm) = 24.3 (d, $^1J_{RhP}$ = 152.3 Hz). TOF MS EI+ (m/z (%)): 702.08 (2)

[M^+]. Anal. Calcd. for $C_{37}H_{30}N_2P_2RhCl\cdot THF$ (%): C, 63.62; H, 4.82; N, 3.62. Found: C, 63.69; H, 4.96; N, 3.38.

Synthesis of [(*Ph-Propylene*-PCP)$RhCl_2(CD_2Cl_2)$] **3.10a-Ph**

3.5a-Ph (50 mg, 0.08 mmol) was dissolved in CD_2Cl_2 (0.5 mL) and allowed to react at rt for 2 h. All volatiles were removed under vacuum yielding a yellow powder **3.10a-Ph** (49 mg, 0.07 mmol, 88 %). ^{1}H NMR (400 MHz, CD_2Cl_2): δ (ppm) = 2.20 (p, $^3J_{HH}$ = 5.8 Hz, 2H, $CH_2CH_2CH_2$), 3.55 (t, $^3J_{HH}$ = 6.0 Hz, 4H, NCH_2CH_2), 4.74 (dvt, $^2J_{HH}$ = 13.4 Hz, J_{PH} = 3.0 Hz, 2H, PCH_aH_bN), 4.80 (dvt, $^2J_{HH}$ = 13.4 Hz, J_{PH} = 3.0 Hz, 2H, PCH_aH_bN), 7.41-7.47 (m, 12H, *o*-C_6H_5, *p*-C_6H_5), 7.75-7.79 (m, 4H, *m*-C_6H_5), 8.00-8.03 (m, 4H, *m*-C_6H_5). $^{13}C\{^1H\}$ NMR (100 MHz, CD_2Cl_2): δ (ppm) = 20.9 (s, $CH_2CH_2CH_2$), 46.6 (vt, J_{PC} = 16.1 Hz, PCH_2N), 60.1 (vt, J_{PC} = 5.2 Hz, NCH_2CH_2), 128.6 (vt, J_{PC} = 5.1 Hz, *m*-C_6H_5), 129.2 (vt, J_{PC} = 4.8 Hz, *m*-C_6H_5), 130.6 (vt, J_{PC} = 26.3 Hz, *i*-C_6H_5), 130.8 (vt, J_{PC} = 23.2 Hz, *i*-C_6H_5), 131.1 (s, *p*-C_6H_5), 131.3 (s, *p*-C_6H_5), 132.4 (vt, J_{PC} = 5.4 Hz, *o*-C_6H_5), 134.8 (vt, J_{PC} = 6.0 Hz, *o*-C_6H_5), 201.2 (dt, $^1J_{RhC}$ = 45.3 Hz, $^2J_{PC}$ = 5.2 Hz, N*C*(Rh)N). $^{31}P\{^1H\}$ NMR (162 MHz, CD_2Cl_2): δ (ppm) = 28.4 (d, $^1J_{RhP}$ = 108.6 Hz). Hi-res MS ESI+ (m/z (%)) $(M - Cl)^+$ Found: 667.04501, Calc.: 667.04673.

Synthesis of [(*Ph-Naphthylene*-PCP)$RhCl_2(CD_2Cl)$] **3.10b-Ph**

3.5b-Ph (50 mg, 0.07 mmol) was dissolved in CD_2Cl_2 (0.5 mL) and allowed to react at rt for 24 h affording a light yellow precipitate. The solution was decanted and the solid dissolved in DMSO-d_6 (0.5 mL). X-ray quality crystals of **3.10b-Ph** (47 mg, 0.06 mmol, 86 %) were obtained by slow diffusion of Et_2O into a saturated solution in DMSO-d_6. ^{1}H NMR (400 MHz,

DMSO-d_6): δ (ppm) = 5.27 (dvt, $^2J_{HH}$ =14.8 Hz, J_{PH} = 2.5 Hz, 2H, PCH_aH$_b$N), 5.58 (dvt, $^2J_{HH}$ = 14.8 Hz, J_{PH} = 2.5 Hz, 2H, PCH$_a$$H_b$N), 7.41-7.45 (m, 2H, *2,7*-C$_{10}H_6$), 7.46-7.60 (m, 12H, *o*-C$_6H_5$, *p*-C$_6H_5$), 7.61-7.68 (m, 4H, *3,4,5,6*-C$_{10}H_6$), 7.84-7.94 (m, 4H, *m*-C$_6H_5$), 8.20-8.31 (m, 4H, *m*-C$_6H_5$); ^{13}C{^{1}H} NMR (100 MHz, DMSO-d_6): δ (ppm) = 41.0 (br-s, Rh*C*D$_2$Cl), 56.0 (vt, J_{PC} =17.3 Hz, P*C*H$_2$N), 109.0 (s, *2,7*-*C*$_{10}$H$_6$), 118.3 (s, *9*-*C*$_{10}$H$_6$), 122.4 (s, *4,5*-*C*$_{10}$H$_6$), 128.3 (vt, J_{PC} = 5.4 Hz, *m*-*C*$_6$H$_5$), 128.5 (s, *p*-*C*$_6$H$_5$), 128.7 (vt, J_{PC} = 4.4 Hz, *m*-*C*$_6$H$_5$), 129.8 (s, 10-*C*$_{10}$H$_6$), 129.9 (vt, J_{PC} = 27.1 Hz, *i*-*C*$_6$H$_5$), 130.8 (s, *3,6*-*C*$_{10}$H$_6$), 131.6 (vt, J_{PC} = 5.0 Hz, *o*-*C*$_6$H$_5$), 133.4 (vt, J_{PC} = 5.1 Hz, *1,8*-*C*$_{10}$H$_6$), 134.3 (vt, J_{PC} = 6.0 Hz *o*-*C*$_6$H$_5$), 203.9 (dt, $^1J_{CRh}$ = 49.1 Hz, $^2J_{PC}$ = 5.2 Hz, N*C*(Rh)N). ^{31}P{^{1}H} NMR (162 MHz, DMSO-d_6): δ (ppm) = = 25.2 (d, $^1J_{RhP}$ = 105.3 Hz). TOF MS EI+ (m/z (%)): 702.03 (99) (M - CD_2Cl_2)$^+$.

Synthesis of [(*Ph-Propylene*-PCP)RhPPh$_3$]OTf [**3.12a-Ph**][OTf]

Triphenylphosphine (10 mg, 0.04 mmol) and silver triflate (10 mg, 0.04 mmol) were added to a solution of **3.5a-Ph** (22 mg, 0.04 mmol) in C$_6$D$_5$Br (0.5 mL). The reaction was observed to be quantitative by multinuclear NMR. ^{1}H NMR (400 MHz, C$_6$D$_5$Br): δ (ppm) = 1.57 (p, $^3J_{HH}$ = 5.6 Hz, 2H, CH$_2$C*H*$_2$CH$_2$), 2.96 (t, $^3J_{HH}$ = 5.88 Hz, 4H, NC*H*$_2$CH$_2$), 4.31 (br-s, 4H, PC*H*$_2$N), 7.18-7.25 (m, 21H, *o*-C$_6H_5$, *p*-C$_6H_5$, P(*o*-C$_6H_5$)$_3$, P(*p*-C$_6H_5$)$_3$), 7.45-7.56 (m, 14H, *m*-C$_6H_5$); ^{19}F NMR (376 MHz, C$_6$D$_5$Br): δ (ppm) = -76.1 (s, SO$_3$C*F*$_3$); ^{31}P{^{1}H} NMR (162 MHz, C$_6$D$_5$Br): δ (ppm) = 35.5 (dt, $^1J_{RhP}$ = 122.0 Hz, $^2J_{PP}$ = 34.4 Hz, 1P, Rh*P*Ph$_3$), 40.7 (dd, $^1J_{RhP}$ = 148.6 Hz, $^2J_{PP}$ = 34.4 Hz, 2P, *P*C*P*Rh).

Synthesis of [(*Ph-Naphthylene*-PCP)RhPPh$_3$]OTf [**3.12b-Ph**][OTf]

Triphenylphosphine (10 mg, 0.04 mmol) and silver triflate (10 mg, 0.04 mmol) were added to a solution of **3.5b-Ph** (26 mg, 0.04 mmol) in C_6D_5Br (0.5 mL). Slow evaporation of the solvent at rt yielded orange X-ray quality crystals of [**3.12b-Ph**][OTf] (35 mg, 0.034 mmol, 85 %). ^{1}H NMR (400 MHz, C_6D_5Br): δ (ppm) = 4.81 (s, 4H, PC*H*$_2$N), 6.50 (d, $^3J_{HH}$ = 7.76 Hz, 2H, *2,7*-$C_{10}H_6$), 7.0-7.2 (m, $^3J_{HH}$= 8.32 Hz, 4H, *3,4,5,6*-$C_{10}H_6$), 7.25-7.40 (m, 21H, *o*-C_6H_5, *p*-C_6H_5, P(*o*-C_6H_5)$_3$, P(*p*-C_6H_5)$_3$), 7.35-7.45 (m, 6H, P(*m*-C_6H_5)$_3$), 7.61-7.72 (m, 8H, *m*-C_6H_5); ^{19}F NMR (376 MHz, C_6D_5Br): δ (ppm) = -77.2 (s, SO_3CF_3); ^{31}P{^{1}H} NMR (162 MHz, C_6D_5Br): δ (ppm) = 32.6 (dt, $^1J_{RhP}$ = 119.5 Hz, $^2J_{PP}$= 34.9 Hz, 1P, Rh*P*Ph$_3$), 38.1 (dd, $^1J_{RhP}$= 144.9 Hz, $^2J_{PP}$= 34.9 Hz, 2P, (*P*C*P*)Rh). TOF MS EI+ (m/z (%)): 816.00(74) [M-P(C_6H_5)$_3$]$^+$.

Synthesis of [(*Ph-Propylene*-PCP)RhCO]OTf **[3.13a-Ph][OTf]**

Complex **3.5a-Ph** (150 mg, 0.24 mmol) and AgOTf (62 mg, 0.24 mmol) were mixed in a round bottom flask and placed under a flow of carbon monoxide. THF (20 mL) was bubbled with carbon monoxide for 15 min and then injected into the reaction mixture. The reaction was stirred and bubbled with carbon monoxide for 15 min after which the silver chloride by-product was removed by filtration. The volatiles from the filtrate were removed under vacuum yielding [**3.13a-Ph**][OTf] as a yellow solid (175 mg, 0.23 mmol, 96 %). X-ray quality crystals of [**3.13a-Ph**][OTf] were obtained by slow evaporation of a concentrated solution in THF at -35 °C. ^{1}H NMR (400 MHz, THF-d_8): δ (ppm) = 1.99 (p, $^3J_{HH}$ = 5.8 Hz, 2H, $CH_2CH_2CH_2$), 3.51 (t, $^3J_{HH}$ = 5.8 Hz, 4H, NC*H*$_2$$CH_2$), 4.85 (vt, J_{PH} = 2.4 Hz, 4H, PC*H*$_2$N), 7.46-7.52 (m, 12H, *o*-, *p*-C_6H_5), 7.75-7.83 (m, 8H, *m*-C_6H_5). ^{13}C{^{1}H} NMR (100 MHz, THF-d_8): δ (ppm) = 20.6 (s, $CH_2CH_2CH_2$), 44.5 (vt, J_{PC} = 4.9 Hz, NCH_2CH_2), 64.3 (vt, J_{PC} = 16.8 Hz), 122.6

(quart, $^{1}J_{FC}$ = 320.1 Hz, SO_3CF_3), 130.1 (vt, J_{PC} = 5.4 Hz, *m*-C_6H_5), 132.1 (s, *p*-C_6H_5), 132.4 (dvt, $^{2}J_{RhC}$ = 1.2 Hz, J_{PC} = 23.7 Hz, *i*-C_6H_5), 134.0 (dvt, $^{3}J_{RhC}$ = 0.6 Hz, J_{PC} = 7.3 Hz, *o*-C_6H_5), 197.1 (br-s, Rh*C*O), 205.4 (dt, $^{1}J_{RhC}$ = 42.02 Hz, $^{2}J_{PC}$ = 9.6 Hz, N*C*(Rh)N); ^{19}F NMR (376 MHz, THF-d_8): δ (ppm) = -78.8 (s, SO_3CF_3); ^{31}P{^{1}H} NMR (162 MHz, THF-d_8): δ (ppm) = 43.2 (d, $^{1}J_{RhP}$ = 135.6 Hz). Hi-res MS ESI+ (m/z (%)) $(M+)^+$ Found: 611.08895, Calc.: 611.08829. Anal. Calc. for $C_{32}H_{30}F_3N_2O_4P_2RhS$ (%): C, 50.54; H, 3.98; N, 3.68. Found: C, 50.49; H, 3.94; N, 3.57. IR (KBr pellet): ν 1979.98 cm^{-1}, vs, C≡O.

Synthesis of [(*tBu-Propylene*-PCP)RhCO]OTf **[3.13a-tBu][OTf]**

Dicarbonyl rhodium(I) chloride dimer (60 mg, 0.15 mmol) was added to a solution of **3.5a-*t*Bu** (124 mg, 0.31 mmol) in THF (10 mL). The solution was heated to 65 °C for 24 h to afford a yellow solution. The volatiles were removed under vacuum yielding a yellow powder **3.13b-Cl** (164 mg , 0.29 mmol, 94 %) the fact that the Cl is not coordinated to the Rh center was confirmed by NMR. **3.13b-Cl** (164 mg, 0.29 mmol) was dissolved in THF (10 mL) and reacted with AgOTf (75 mg, 0.29 mmol). The silver chloride by-product was filtered off and the volatiles from the filtrate removed under vacuum affording [**3.13a-*t*Bu**][OTf] (191 mg, 0.28 mmol, 97 %) as a yellow solid. X-ray quality crystals of [**3.13a-*t*Bu**][OTf] were obtained by slow evaporation of a concentrated solution in THF at -35 °C. ^{1}H NMR (400 MHz, DMSO-d_6): δ (ppm) = 1.31 (vt, J_{PH} = 7.2 Hz, 36H, PC(CH_3)$_3$), 1.87 (q, $^{3}J_{HH}$ = 5.6 Hz, 2H, $CH_2CH_2CH_2$), 3.36 (t, $^{3}J_{HH}$ = 5.6 Hz, 4H, NC$H_2$$CH_2$), 4.22 (br-vt, 4H, PC$H_2$N); ^{13}C{^{1}H} NMR (101 MHz, DMSO-d_6): δ (ppm) = 19.3 (s, $CH_2CH_2CH_2$), 28.6 (vt, J_{PC} = 2.9 Hz, PC(*C*H_3)$_3$), 35.3 (dvt, J_{PC} = 9.1 Hz, $^{2}J_{RhC}$ = 1.2 Hz, P(*C*(CH$_3$)$_3$) 42.7 (vt, J_{PC} = 4.2 Hz, N*C*$H_2$$CH_2$), 55.6 (vt, J_{PC} = 11.8 Hz, P*C*H_2N), 122.6 (quart, $^{1}J_{FC}$ = 320.1 Hz, SO_3CF_3), 199.6 (dt, $^{1}J_{RhC}$ = 58.6 Hz,

$^{2}J_{PC}$ = 11.8 Hz, Rh*C*O), 203.5 (dt, $^{1}J_{RhC}$ = 42.1 Hz, $^{2}J_{PC}$ = 8.3 Hz, N*C*(Rh)N); ^{19}F NMR (376 MHz, DMSO-d_6): δ (ppm) = -78.8 (s, SO_3CF_3); $^{31}P\{^{1}H\}$ NMR (162 MHz, DMSO-d_6): δ (ppm) = 82.8 (d, $^{1}J_{RhP}$ = 129.8 Hz). Hi-res MS ESI+ (m/z (%)) $(M+)^+$ Found: 531.21283, Calc.: 531.21349. IR (KBr pellet): ν 1974.29 cm^{-1}, vs, C≡O.

Synthesis of [(*Ph-Naphthylene*-PCP)RhCO]OTf **[3.13b-Ph][OTf]**

Complex **3.5b-Ph** (150 mg, 0.21 mmol) and AgOTf (55 mg, 0.21 mmol) were mixed in a round bottom flask and placed under a flow of carbon monoxide. THF (20 mL) was bubbled with carbon monoxide for 15 min and then injected into the reaction mixture. The reaction was stirred and bubbled with carbon monoxide for 15 min after which the silver chloride by-product was removed by filtration. The volatiles from the filtrate were removed under vacuum yielding [**3.13b-Ph**][OTf] as an orange solid (170 mg, 0.20 mmol, 96 %). ^{1}H NMR (400 MHz, THF-d_8): δ (ppm) = 5.25 (vt, J_{PH} = 2.6 Hz, 4H, PCH_2N), 7.06-7.16 (m, 4H, *2,4,5,7*-$C_{10}H_6$), 7.22-7.28 (m, 2H, *3,6*-$C_{10}H_6$), 7.49-7.59 (m, 12H, *o*-C_6H_5, *p*-C_6H_5), 7.95-8.05 (m, 8H, *m*-C_6H_5). $^{13}C\{^{1}H\}$ NMR (100 MHz, THF-d_8): δ (ppm) = 56.1 (vt, J_{PC} = 18.0 Hz, P*C*H_2N), 106.7 (s, *3,6*-$C_{10}H_6$), 117.1 (s, *10*-$C_{10}H_6$), 119.8 (s, *4,5*-$C_{10}H_6$), 122.6 (quart, $^{1}J_{FC}$ = 320.1 Hz, SO_3CF_3), 126.0 (s, *2,7*-$C_{10}H_6$), 127.0 (vt, J_{PC} = 5.8 Hz, *m*-C_6H_5), 128.5 (vt, J_{PC} = 26.0 Hz, *i*-C_6H_5), 130.5 (vt, J_{PC} = 5.5 Hz, *p*-C_6H_5), 131.1 (vt, J_{PC} = 7.7 Hz, *o*-C_6H_5), 132.7 (s, *9*-$C_{10}H_6$), 135.13 (vt, J_{PC} = 7.5 Hz, *1,8*-$C_{10}H_6$), 195.2 (br-s, Rh*C*O), 208.5 (dt, $^{1}J_{RhC}$ = 48.0 Hz, $^{2}J_{PC}$ = 10.0 Hz, N*C*(Rh)N); ^{19}F NMR (376 MHz, THF-d_8): δ (ppm) = -78.8 (s, SO_3CF_3); $^{31}P\{^{1}H\}$ NMR (162 MHz, THF-d_8): δ (ppm) = 38.8 (d, $^{1}J_{RhP}$ = 131.2 Hz). Hi-res MS ESI+ (m/z (%)) $(M+)^+$ Found: 695.08698, Calc.: 695.08829. IR (KBr pellet): ν 2010.66 cm^{-1}, vs, C≡O.

Synthesis of [(*tBu-Propylene*-PC(H_2)P)Rh(CO)Cl]$_3$ **3.14a-*t*Bu**

Dicarbonyl rhodium(I) chloride dimer (40 mg, 0.10 mmol) was added to a solution of **3.5a-*t*Bu** (81 mg, 0.20 mmol) in C_6H_6 (10 mL). The solution was heated to 80 °C for 2 hours affording, X-ray quality, yellow crystals of **3.14a-*t*Bu** (85 mg, 0.05 mmol, 75 %) which could be isolated by filtration. ^{1}H NMR (400 MHz, DMSO-d_6): δ (ppm) = 1.34 (vt, J_{PH} = 7.3 Hz, 36H, PC(CH_3)$_3$), 1.82 (q, $^3J_{HH}$ = 5.6 Hz, 2H, $CH_2CH_2CH_2$), 3.28 (t, $^3J_{HH}$ = 5.6 Hz, 4H, NC$H_2$$CH_2$), 4.12 (br-vt, 4H, PC$H_2$N); ^{13}C{^{1}H} NMR (101 MHz, DMSO-d_6): δ (ppm) = 19.6 (s, $CH_2CH_2CH_2$), 28.5 (br-vt, PC(CH_3)$_3$), 34.3 (vt, J_{PC} = 10.2 Hz, P(C(CH_3)$_3$), 43.6 (vt, J_{PC} = 3.8 Hz, NCH_2CH_2), 55.2 (vt, J_{PC} = 13.3 Hz, PCH_2N), 194.6 (dt, $^1J_{RhC}$ = 46.5 Hz, $^2J_{PC}$ = 10.7 Hz, RhCO); ^{31}P{^{1}H} NMR (162 MHz, DMSO-d_6): δ (ppm) = 96.3 (d, $^1J_{RhP}$ = 90.6 Hz). Anal. Calc. for $C_{69}H_{144}Cl_3N_6O_3P_6Rh_3$•$C_6H_6$ (%): C, 50.47; H, 8.47; N, 4.71. Found: C, 51.01; H, 8.21; N, 4.59.

Synthesis of [(*tBu-Propylene*-PCP)RhPh] **3.15a-*t*Bu**

Complex **3.5a-*t*Bu** (90 mg, 0.17 mmol) was dissolved in THF (10 mL) and reacted with a slight excess of PhLi (0.11 mL, 1.8M in di-*n*-butylether, 0.20 mmol). The reaction mixture was heated to 65 °C for 30 min affording a dark orange solution. The volatiles were removed under vacuum affording an orange solid **3.15a-*t*Bu** (87 mg, 0.15 mmol, 88 %). X-ray quality crystals of **3.15a-*t*Bu** were obtained by slow evaporation of a concentrated solution in THF at - 35 °C. ^{1}H NMR (400 MHz, C_6D_6): δ (ppm) = 1.29 (vt, J_{PH} = 6.2 Hz, 36H, PC(CH_3)$_3$), 1.41 (q, $^3J_{HH}$ = 6.0 Hz, 2H, $CH_2CH_2CH_2$), 2.45 (t, $^3J_{HH}$ = 6.0 Hz, 4H, NC$H_2$$CH_2$), 3.34 (br-vt, 4H, PC$H_2$N), 7.03 (br-vt, J_{HH} = 7.2 Hz, 1H, *p*-C_6H_5Rh), 7.32 (br-vt, J_{HH} = 7.4 Hz, 2H, *o*-C_6H_5Rh), 8.14 (br-d, J_{HH} = 7.3 Hz, 2H, *m*-C_6H_5Rh); ^{13}C{^{1}H} NMR (101 MHz, C_6D_6): δ (ppm) = 21.7

(s, $CH_2CH_2CH_2$), 30.4 (vt, J_{PC} = 3.7 Hz, $PC(CH_3)_3$), 36.0 (dvt, $^2J_{RhC}$ = 2.5 Hz, J_{PC} = 5.4 Hz, $P(C(CH_3)_3)$, 43.3 (vt, J_{PC} = 4.2 Hz, NCH_2CH_2), 58.3 (vt, J_{PC} = 8.7 Hz, PCH_2N), 119.4 (s, *p*-C_6H_5Rh), 125.1 (d, $^3J_{RhC}$ = 1.1 Hz, *p*-C_6H_5Rh), 128.9 (s, *i*-C_6H_5Rh), 143.7 (t, $^3J_{PC}$ = 1.86 Hz, *o*-C_6H_5Rh), 178.9 (dt, $^1J_{RhC}$ = 27.3 Hz, $^2J_{PC}$ = 13.9 Hz, N*C*(Rh)N); $^{31}P\{^1H\}$ NMR (162 MHz, C_6D_6): δ (ppm) = 65.1 (d, $^1J_{RhP}$ = 167.9 Hz).

Synthesis of [(*tBu-Propylene*-PCP)RhMe] **3.16a-*t*Bu**

Complex **3.5a-*t*Bu** (115 mg, 0.21 mmol) was dissolved in toluene (10 mL) and reacted with a slight excess of MeLi (5 mg, 0.23 mmol). The reaction mixture was sonicated for 30 min affording a dark orange solution. The by-product LiCl and excess MeLi were filtered off and the volatiles from the filtrate removed under vacuum affording an orange solid **3.16a-*t*Bu** (102 mg, 0.20 mmol, 93 %) pure by NMR. X-ray quality crystals of **3.16a-*t*Bu** were obtained by slow evaporation of a concentrated solution in toluene at - 35 °C. ^1H NMR (400 MHz, toluene-d_8): δ (ppm) = 0.29 (dt, $^2J_{RhH}$ = 1.64 Hz, $^3J_{PH}$ = 5.5 Hz, 3H, RhCH_3), 1.36 (vt, J_{PH} = 6.0 Hz, 36H, $PC(CH_3)_3$), 1.42 (q, $^3J_{HH}$ = 5.9 Hz, 2H, $CH_2CH_2CH_2$), 2.52 (t, $^3J_{HH}$ = 5.9 Hz, 4H, NCH_2CH_2), 3.33 (br-vt, 4H, PCH_2N); $^{13}C\{^1H\}$ NMR (101 MHz, toluene-d_8): δ (ppm) = -15.5 (dt, $^1J_{RhC}$ = 20.0 Hz, $^2J_{PC}$ = 12.5 Hz, RhCH_3), 21.6 (s, $CH_2CH_2CH_2$), 30.0 (vt, J_{PC} = 3.8 Hz, $PC(CH_3)_3$), 34.8 (dvt, $^2J_{RhC}$ = 2.2 Hz, J_{PC} = 4.8 Hz, $P(C(CH_3)_3)$, 43.0 (vt, J_{PC} = 4.5 Hz, NCH_2CH_2), 57.8 (vt, J_{PC} = 8.6 Hz, PCH_2N), 217.7 (dt, $^1J_{RhC}$ = 40.3 Hz, $^2J_{PC}$ = 8.5 Hz, N*C*(Rh)N); $^{31}P\{^1H\}$ NMR (162 MHz, toluene-d_8): δ (ppm) = 68.0 (d, $^1J_{RhP}$ = 167.3 Hz). Anal. Calc. for $C_{23}H_{49}N_2P_2Rh$ (%): C, 53.28; H, 9.53; N, 5.40. Found: C, 53.40; H, 9.25; N, 4.99.

6.4 Experimental Details for Chapter Four

Synthesis of 1,3-bis((diphenylphosphorothioyl)methyl)-2,3-dihydro-1*H*-benzo[d]imidazolium hexafluorophosphate [H(**4.1-Ph**)][PF_6]

An intimate mixture of **2.4** (1.55 g, 2.73 mmol), NH_4PF_6 (0.444 g, 2.73 mmol), and triethyl orthoformate (30 mL) in a round bottom flask was adapted to a distillation bridge and heated to 100 °C for 5 h with stirring. The ethanol by-product was distilled off as the reaction proceeded. Excess triethyl orthoformate was removed under vacuum and the crude product obtained was suspended in hexanes (20 mL), filtered, and washed twice with pentane (2 x 15 mL) yielding a pure sample of [H(**4.1-Ph**)][PF_6] as a white crystalline solid (1.52g, 2.09 mmol, 76.5 %).^{1}H NMR (400 MHz, DMSO-d_6): δ (ppm) = (ppm) = 6.16 (d, $^3J_{PH}$ = 4.8 Hz, 4H, PCH_2N), 7.16 (br-s, 2H, $C_6H_4N_2$), 7.24 (br-s, 2H, $C_6H_4N_2$), 7.48-7.69 (m, 12H, *o*-C_6H_5, *p*-C_6H_5), 7.91-8.05 (m, 8H, *m*-C_6H_5) 9.69 (s, 1H, NC(*H*)N); ^{13}C{^{1}H} NMR (101 MHz, DMSO-d_6): δ (ppm) = (ppm) = 48.7 (d, $^1J_{PC}$ = 53.4 Hz, P*C*H_2N), 113.3 (s, *3,6*-$C_6H_4N_2$), 125.8 (s, *4,5*-$C_6H_4N_2$), 128.8 (d, $^2J_{PC}$ = 12.8 Hz, *o*-C_6H_5), 129.4 (s, *1,2*-$C_6H_4N_2$), 130.4 (s, *p*-C_6H_5), 131.5 (d, $^3J_{PC}$ = 11.2 Hz, *m*-C_6H_5), 132.6 (s, *ipso*-C_6H_5), 142.8 (s, N*C*(H)N); ^{19}F NMR (376 MHz, DMSO-d_6): δ (ppm) = (ppm) = -72.2 (d, $^1J_{PF}$ = 711 Hz, PF_6); ^{31}P{^{1}H} NMR (162 MHz, DMSO-d_6): δ (ppm) = (ppm) = -143.1 (sept, 1P, $^1J_{PF}$ = 711 Hz, *P*F_6), 40.9 (s, 2P, $CH_2P(C_6H_5)_2$). Hi-res MS ESI+ (m/z (%)) $(M)^+$ Found: 579.12591, Calc.: 579.12419.

Synthesis of N^1,N^2-bis((di-tert-butylphosphorothioyl)methyl)benzene-1,2-diamine **2.4-*t*Bu**

Elemental sulfur (0.418 g, 1.63 mmol) was added to a solution of **2.1-*t*Bu** (2.77 g, 6.55 mmol) in CH_2Cl_2 (50 mL). The reaction mixture was stirred at room temperature for 3 h after which all the volatiles were removed under vacuum yielding a white crystalline powder. Recrystallization from a concentrated solution in CH_2Cl_2 at -35 °C afforded an analytically pure sample of **2.4-*t*Bu** (2.75g, 5.63 mmol, 86 %). ^{1}H NMR (400 MHz, C_6D_6): δ (ppm) = 1.12 (d, $^3J_{PH}$ = 14.8 Hz, 36H, (CH_3)$_3$C), 3.18 (dd, $^2J_{PH}$ = 7.0 Hz, $^3J_{HH}$ = 5.2 Hz, 4H, PCH_2N), 5.07 (dt, $^3J_{PH}$ = 9.5 Hz, $^3J_{HH}$ = 5.2 Hz, 2H, N*H*), 6.76 (AA'BB' system simplified as dd, J_{HH} = 3.5, 5.6 Hz, 2H, $C_6H_4N_2$), 7.06 (AA'BB' system simplified as dd, J_{HH} = 3.4, 5.7 Hz, 2H, $C_6H_4N_2$); ^{13}C{^{1}H} NMR (101 MHz, C_6D_6): δ (ppm) = (ppm) = 27.6 (s, PC(*C*H$_3$)$_3$), 36.1 (d, $^1J_{PC}$ = 47.5 Hz, P*C*(CH$_3$)$_3$), 37.6 (d, $^1J_{PC}$ = 41.4 Hz, P*C*H$_2$N), 112.2 (s, *C*$_6$H$_4$N$_2$), 120.0 (s, *C*$_6$H$_4$N$_2$), 138.7 (d, $^3J_{PC}$ = 10.7 Hz, *C*$_6$H$_4$N$_2$); ^{31}P{^{1}H} NMR (162 MHz, C_6D_6): δ (ppm) = (ppm) = 79.6 (s). Hi-res TOF MS EI+ (m/z (%)) $(M+H)^+$ Found: 488.2601, Calc.: 488.2578.

Synthesis of 1,3-bis((di-*tert*-butylphosphorothioyl)methyl)-2,3-dihydro-1*H*-benzo[d]imidazolium hexafluorophosphate [H(**4.1-*t*Bu**)][PF_6]

An intimate mixture of **2.4-*t*Bu** (1.25 g, 2.55 mmol), NH_4PF_6 (0.417 g, 2.55 mmol), and trimethyl orthoformate (15 mL) in a round bottom flask was adapted to a distillation bridge and heated to 100 °C for 12 h with stirring. The methanol by-product was distilled off as the reaction proceeded. Excess trimethyl orthoformate was removed under vacuum and the crude product was suspended in hexanes (20 mL), filtered and washed twice with pentane (2 x 15 mL) yielding a white solid. The product was recrystallized from a concentrated solution in CH_2Cl_2 by addition of pentane affording an analytically pure sample of [H(**4.1-*t*Bu**)][PF_6] (1.36g, 2.11 mmol, 82.8 %). ^{1}H NMR (400 MHz, CD_2Cl_2): δ (ppm) = (ppm) = 1.40 (d, $^3J_{PH}$ = 15.9 Hz, 36H,

PC(CH_3)$_3$), 4.93 (d, $^2J_{PH}$ = 2.9 Hz, 4H, PCH_2N), 7.73 (AA'BB' system simplified as dd, J_{HH} = 3.2, 6.3 Hz, 2H, $C_6H_4N_2$), 7.92 (AA'BB' system simplified as dd, J_{HH} = 3.2, 6.3 Hz, 2H, $C_6H_4N_2$), 10.07 (s, 1H, NC(*H*)N); $^{13}C\{^1H\}$ NMR (101 MHz, CD_2Cl_2): δ (ppm) = 27.8 (s, PC(CH_3)$_3$), 39.4 (d, $^1J_{PC}$ = 39.2 Hz, P*C*(CH_3)$_3$), 40.3 (d, $^1J_{PC}$ = 31.2 Hz, P*C*H_2N), 114.1 (s, *3,6*-$C_6H_4N_2$), 128.2 (s, *4,5*-$C_6H_4N_2$), 131.7 (s, *1,2*-$C_6H_4N_2$), 143.1 (s, N*C*(H)N); ^{19}F NMR (376 MHz, CD_2Cl_2): δ (ppm) = (ppm) = -72.3 (d, $^1J_{PF}$ = 711 Hz, PF_6); $^{31}P\{^1H\}$ NMR (162 MHz, CD_2Cl_2): δ (ppm) = (ppm) = -143.5 (sept. $^1J_{PF}$ = 711 Hz, 1P, *P*F_6) 80.6 (s, 2P, CH_2P[C(CH_3)$_3$]$_2$). Hi-res MS ESI+ (m/z (%)) Found: 499.249197, Calc.: 499.24939. Anal. Calc. for $C_{25}H_{45}F_6N_2P_3S_2$ (%): C, 46.58; H, 7.04; N, 4.35. Found: C, 46.86; H, 7.08; N, 4.53.

Synthesis of 1,3-bis((diphenylphosphino)methyl)-2,3-dihydro-1*H*-benzo[d]imidazolium hexafluorophosphate [H(**4.2-Ph**)][PF_6]

Desulfurization of [H(**4.1-Ph**)][PF_6] was carried out following a literature procedure.[219] A mixture of freshly dried Raney®-Nickel (10g), [H(**4.1-Ph**)][PF_6] (0.45 g, 0.62 mmol), and MeOH (50 mL) was vigorously stirred for 7 days. The reaction mixture was filtered and the crude product was extracted from the filter with CH_2Cl_2 (2 x 20 mL). The fractions were combined and the volatiles removed under vacuum to afford a white crystalline powder (0.18 g, 0.27 mmol, 43.5 %). X-ray quality crystals of [H(**4.2-Ph**)][PF_6] were obtained by slow evaporation of a saturated solution in CH_2Cl_2 at -35 °C. Due to the low solubility of both PhSCSPF6 and PhbenzylPCPPF6, attempts to scale up the desulfurization process were met without success. ^1H NMR (400 MHz, DMSO-d_6): δ (ppm) = (ppm) = 5.49 (d, $^2J_{PH}$ = 4Hz, 4H, PCH_2N), 7.30-7.36 (m, 12H, *o*-C_6H_5, *p*-C_6H_5), 7.40-7.48 (m, 8H, *m*-C_6H_5) 7.58 (br-s, 2H,

$C_6H_4N_2$), 7.80 (br-s, 2H, $C_6H_4N_2$), 9.63 (s, 1H, NC(*H*)N); ^{19}F NMR (376 MHz, DMSO-d_6): δ (ppm) = (ppm) = -72.2 (d, $^1J_{PF}$ = 711 Hz, PF_6); ^{31}P{^{1}H} NMR (162 MHz, DMSO-d_6) -143.8 (sept, $^1J_{PF}$ = 711 Hz, 1P, *P*F_6), -13.7 (s, 2P, $CH_2P(C_6H_5)_2$).

Synthesis of 1,3-bis((di-*tert*-butylphosphino)methyl)-2,3-dihydro-1*H*-benzo[d]imidazolium hexafluorophosphate [H(**4.2-*t*Bu**)][PF_6]

Desulfurization of [H(**4.1-*t*Bu**)][PF_6] was carried out following a literature procedure.[219] A mixture of freshly dried Raney®-Nickel (10g), [H(**4.1-*t*Bu**)][PF_6] (0.90 g, 1.4 mmol), and MeOH (30 mL) was vigorously stirred. The reaction progress was monitored via ^{31}P NMR spectroscopy. Once complete desulfurization was achieved, the reaction mixture was filtered, the volatiles removed under vacuum and the crude product washed twice with pentane (2 x 15 mL) and dried yielding an analytically pure sample of [H(**4.2-*t*Bu**)][PF_6] (0.64 g ,1.09mmol, 78.2 %). X-ray quality crystals were obtained from a saturated solution of [H(**4.2-*t*Bu**)][PF_6] in CH_2Cl_2 at -35 °C. ^{1}H NMR (400 MHz, CD_2Cl_2): δ (ppm) = (ppm) = 1.22 (d, $^3J_{PH}$ = 11.9 Hz, 36H, PC(C*H*$_3$)$_3$), 4.60 (s, 4H, PC*H*$_2$N), 7.73 (AA'BB' system simplified as dd, *J* = 3.2, 6.3 Hz, 2H, $C_6H_4N_2$), 7.99 (AA'BB' system simplified as dd, *J* = 3.2, 6.3 Hz, 2H, $C_6H_4N_2$), 9.54 (s, 1H, NC(*H*)N). ^{13}C{^{1}H} NMR (101 MHz, CD_2Cl_2) 29.6 (d, $^2J_{PC}$ = 13.4 Hz, PC(*C*H$_3$)$_3$), 32.7 (d, $^1J_{PC}$ = 19.8 Hz, P*C*(CH$_3$)$_3$), 43.2 (d, $^1J_{PC}$ = 30.5 Hz, P*C*H$_2$N), 114.7 (d, $^4J_{PC}$ = 4.5 Hz, *3,6*-*C*$_6$H$_4$N$_2$), 128.0 (s, *4,5*-*C*$_6$H$_4$N$_2$), 132.8 (s, *1,2*-*C*$_6$H$_4$N$_2$), 142.0 (t, $^3J_{PC}$ = 14 Hz, N*C*(H)N); ^{19}F NMR (376 MHz, CD_2Cl_2): δ (ppm) = -72.3 (d, $^1J_{PF}$ = 711 Hz, PF_6); ^{31}P{^{1}H} NMR (162 MHz, CD_2Cl_2): δ (ppm) = -143.4 (sept, $^1J_{PF}$ = 711 Hz, 1P, *P*F_6), 25.8 (s, 2P, $CH_2P[C(CH_3)_3]_2$). Hi-res MS ESI+ (m/z (%)) Found: 435.304922, Calc.: 435.305249.

Synthesis of [(^{t}*Bu-phenylene*-PCP)RhCl] **4.3-*t*Bu**

Compound [H(**4.2-*t*Bu**)][PF_6] (150 mg, 0.26 mmol) was dissolved in THF (10 mL), cooled to -78°C reacted with KHMDS (50 mg, 0.26 mmol) and allowed to warm up to rt over 1/2 h. [Rh(cod)Cl]$_2$ (61.5 mg, 0.13 mmol) was added and the reaction mixture was stirred for 4 h. The volatiles were removed under vacuum and the obtained solid was recrystallized out of fresh THF (5 mL) at -35 °C yielding **4.3-*t*Bu** as orange, X-ray quality, single crystals (115 mg, 0.20 mmol, 78 %). ^{1}H NMR (400 MHz, CD_2Cl_2): δ (ppm) = 1.49 (vt, J_{PH} = 6.6 Hz, 36H, PC(C*H*$_3$)$_3$), 3.52 (vt, J_{PH} = 1.83 Hz, 4H, PC*H*$_2$N), 6.68 (AA'BB' system simplified as dd, *J* = 3.1, 5.8 Hz, 2H, $C_6H_4N_2$), 6.99 (AA'BB' system simplified as dd, *J* = 3.1, 5.7 Hz, 2H, $C_6H_4N_2$); ^{13}C{^{1}H} NMR (101 MHz, CD_2Cl_2): δ (ppm) = 30.2 (vt, J_{PC} = 3.5Hz, PC(*C*H$_3$)$_3$), 36.0 (vt, J_{PC} = 5.06 Hz, P*C*(CH$_3$)$_3$), 41.8 (vt, J_{PC} = 7.3 Hz, P*C*H$_2$N), 109.4 (s, *3,6*-*C*$_6$H$_4$N$_2$), 122.2 (s, *4,5*-*C*$_6$H$_4$N$_2$), 135.4 (s, *1,2*-*C*$_6$H$_4$N$_2$), 201.8 (dt, $^{1}J_{RhC}$ = 54 Hz, $^{2}J_{PC}$ = 9.8 Hz, N*C*(Rh)N); ^{31}P{^{1}H} NMR (162 MHz, CD_2Cl_2): δ (ppm) = 82.5 (d, $^{1}J_{RhP}$ = 154.2 Hz). Hi-res MS ESI+ (m/z (%)) $(M+H)^+$ Found: 573.179568, Calc.: 573.179606 Anal. Calc. for $C_{25}H_{44}ClN_2P_2Rh$ (%): C, 52.41; H, 7.74; N, 4.89. Found: C, 52.79; H, 7.89; N, 4.89.

Synthesis of [(^{t}*Bu-phenylene*-PCP)RhCO]OTf [**4.4-*t*Bu**][OTf]

Complex **4.3-*t*Bu** (100 mg, 0.17 mmol) and AgOTf (45 mg, 0.17 mmol) were mixed in a round bottom flask and placed under a flow of carbon monoxide. THF (10 mL) was bubbled with carbon monoxide for about 10 min and then injected into the reaction mixture. The reaction was stirred and bubbled with carbon monoxide for 15 min after which the silver chloride by-product was removed by filtration. The volatiles from the filtrate were removed under

vacuum yielding [**4.4-*t*Bu**][OTf] as a light orange solid (105 mg, 0.15 mmol, 86 %). X-ray quality crystals of [**4.4-*t*Bu**][OTf] were obtained from slow evaporation of a concentrated solution in THF at rt. ^{1}H NMR (400 MHz, DMSO-d_6): δ (ppm) = 1.37 (vt, J_{PH} = 7.4 Hz, 36H, PC(CH_3)$_3$), 5.02 (br-s, 4H, PCH_2N), 7.53 (AA'BB' system simplified as dd, J = 3.0, 6.0 Hz, 2H, $C_6H_4N_2$), 7.85 (AA'BB' system simplified as dd, J = 3.1, 6.0 Hz, 2H, $C_6H_4N_2$); ^{13}C{^{1}H} NMR (101 MHz, DMSO-d_6): δ (ppm) = 28.7 (vt, J_{PC} = 3.1 Hz, PC(CH$_3$)$_3$), 36.0 (vt, J_{PC} = 8.0 Hz, PC(CH$_3$)$_3$), 44.4 (vt, J_{PC} = 12.3 Hz, PCH$_2$N), 113.3 (s, *3,6*-$C_6H_4N_2$), 122.1 (quart, $^{1}J_{CF}$ = 321.9 Hz, O$_3$SCF$_3$), 124.4 (s, *4,5*-$C_6H_4N_2$), 133.2 (vt, J_{PC} = 3.9 Hz, *1,2*-$C_6H_4N_2$), 195.9 (dt, $^{1}J_{RhC}$ = 40.7 Hz, $^{2}J_{PC}$ = 10.8 Hz, RhCO), 200.5 (dt, $^{1}J_{RhC}$ = 58.8 Hz, $^{2}J_{PC}$ = 10.2 Hz, NC(Rh)N); ^{19}F (376 MHz, DMSO-d_6): δ (ppm) = -79.3 (s, O$_3$SCF_3^-); ^{31}P{^{1}H} NMR (162 MHz, DMSO-d_6): δ (ppm) = 102.4 (d, $^{1}J_{RhP}$ = 132.1 Hz). Hi-res MS ESI+ (m/z (%)) $(M)^+$ Found: 565.19675, Calc.: 565.19784. IR (KBr pellet): ν 1982 cm^{-1}, vs, C≡O.

Synthesis of [(η^2-CP-CH$_2$P(^{t}Bu)$_2$)Pd(PPh$_3$)$_2$]PF$_6$ [**4.6-*t*Bu**][PF$_6$]

[Pd(PPh$_3$)$_4$] (199 mg, 0.17 mmol) was added to a solution of [H(**4.2-*t*Bu**)][PF$_6$] (100 mg, 0.17 mmol) in THF (30 mL). The reaction mixture was stirred for 12 h. All the volatiles were removed under vacuum and the obtained solid was washed thrice with hexanes (15 ml x 3) and dried under vacuum yielding compound [**4.6-*t*Bu**][PF$_6$] as an off white crystalline solid (102 mg, 0.13 mmol, 76 % yield). X-ray quality crystals of complex [**4.6-*t*Bu**][PF$_6$] were obtained by slow evaporation of a THF solution at -35 °C. ^{1}H NMR (400 MHz, THF-d_8): δ (ppm) = 1.22 (d, $^{2}J_{PH}$ = 17.1 Hz, 18H, P(C(CH_3)$_3$)$_2$), 1.58 (m, 2H, PCH_2Pd), 7.17 (m, 6H, *o*-C$_6H_5$P), 7.3 (m, 12H, *o*-C$_6H_5$P, *p*-C$_6H_5$P), 7.42 (m, 12H, m-C$_6H_5$P); ^{19}F (376 MHz, THF-d_8): δ (ppm) = -74.4 (d, $^{1}J_{PF}$ = 711 Hz, PF_6); ^{31}P{^{1}H} NMR (162 MHz, THF-d_8):

δ (ppm) = -142.8 (sept, $^1J_{PF}$ = 711 Hz, 1P, *P*F_6), 24.3 (dd, $^2J_{PP}$ = 240.0 Hz, $^2J_{PP}$ = 28.2 Hz, 1P, *P*Ph_3 *trans* to P(^{t}Bu)$_2$), 25.5 (t, $^2J_{PP}$ = 28.2 Hz, 1P, *P*Ph_3 cis to P(^{t}Bu)$_2$), 54.7 (dd, $^2J_{PP}$ = 240.0 Hz, $^2J_{PP}$ = 28.2 Hz, 1P, CH_2*P*(^{t}Bu)$_2$).

Synthesis of [(^{t}*Bu-phenylene*-PCP)PdCl]PF_6 **4.8-PF$_6$**

$PdCl_2$ (76 mg, 0.43 mmol) and acetonitrile (25 mL) were placed in a two-neck round bottom flask adapted with a reflux condenser and refluxed for 2 h time in which all the $PdCl_2$ dissolved. The freshly made acetonitrile solution of $PdCl_2(CH_3CN)_2$ was allowed to cool down to rt. **H-4.2-PF$_6$** (250 mg, 0.43 mmol) was dissolved in THF (3 mL), reacted with KHMDS (86 mg, 0.43 mmol) and allowed to sit for 15 min. The freshly deprotonated **4.2-*t*Bu** was slowly added to the $PdCl_2(CH_3CN)_2$ solution. The reaction mixture was refluxed for 8 h affording a light yellow precipitate. The precipitate was filtered, washed with THF (5 mL) and dried under vacuum to yield [**4.8-*t*Bu**][PF_6] (224 mg, 0.31 mmol, 71 %). X-ray quality crystals of [**4.8-*t*Bu**][PF_6] were obtained from slow evaporation of a concentrated solution in CH_2Cl_2 at rt. ^{1}H NMR (400 MHz, CD_2Cl_2): δ (ppm) = 1.53 (vt, J_{PH} = 7.9 Hz, 36H, PC(C*H*$_3$)$_3$), 4.63 (vt, J_{PH} = 2.2 Hz, 4H, PC*H*$_2$N), 7.61 (AA'BB' system simplified as dd, *J* = 3.1, 6.1 Hz, 2H, $C_6H_4N_2$), 7.79 (AA'BB' system simplified as dd, *J* = 3.1, 6.1 Hz, 2H, $C_6H_4N_2$); ^{13}C{^{1}H} NMR (101 MHz, CD_2Cl_2): δ (ppm) = 29.3 (vt, J_{PC} = 2.8 Hz, PC(*C*H$_3$)$_3$), 37.8 (vt, J_{PC} = 7.2Hz, P*C*(CH$_3$)$_3$), 43.7 (vt, J_{PC} = 11.0 Hz, P*C*H$_2$N), 113.6 (s, *3,6*-*C*$_6$H$_4$N$_2$), 126.8 (s, *4,5*-*C*$_6$H$_4$N$_2$), 133.6 (vt, J_{PC} = 4.7 Hz, *1,2*-*C*$_6$H$_4$N$_2$), 177.5 (t, $^2J_{PC}$ = 3 Hz, N*C*(Pd)N); ^{19}F NMR (376 MHz, CD_2Cl_2): δ (ppm) = -74.6 (d, $^1J_{PF}$ = 711 Hz, P*F*$_6$); ^{31}P{^{1}H} NMR (162 MHz, CD_2Cl_2): δ (ppm) = -142.8 (sept, $^1J_{PF}$ = 711 Hz, 1P, *P*F_6), 83.2 (s, 2P, CH_2*P*[C(CH$_3$)$_3$)$_2$]). Hi-res MS

ESI+ (m/z (%)) $(M)^+$ Found: 571.1716, Calc.: 571.17188 Anal. Calc. for $C_{25}H_{44}ClF_6N_2P_3Pd$ (%): C, 41.62; H, 6.15; N, 3.88. Found: C, 41.55; H, 5.76; N, 3.89.

Synthesis of [(*^{t}Bu-phenylene*-PCP)NiCl]PF_6 [**4.9-*t*Bu**][PF_6]

$NiCl_2$ (22 mg, 0.17 mmol) and acetonitrile (25 mL) were placed in a two-neck round bottom flask adapted with a reflux condenser and refluxed for 4 h time in which all the $NiCl_2$ dissolved. The freshly made acetonitrile solution of $NiCl_2(CH_3CN)_2$ was allowed to cool down to rt. [H(**4.2-*t*Bu**)][PF_6] (100 mg, 0.17 mmol) was dissolved in THF (3 mL), reacted with KHMDS (35 mg, 0.17 mmol) and allowed to sit for 15 min. The freshly deprotonated **4.2-*t*Bu** was slowly added to the $NiCl_2(CH_3CN)_2$ solution. The reaction mixture was refluxed for 8 h affording a light orange precipitate. The precipitate was filtered, washed with THF (5 mL) and dried under vacuum to yield [**4.9-*t*Bu**][PF_6] (85 mg, 0.13 mmol, 76 %). X-ray quality crystals of [**4.9-*t*Bu**][PF_6] were obtained from slow evaporation of a concentrated solution in CH_2Cl_2 at rt. ^{1}H NMR (400 MHz, CD_2Cl_2): δ (ppm) = 1.58 (vt, J_{PH} = 7.5 Hz, 36H, PC(C*H*$_3$)$_3$), 4.45 (vt, J_{PH} = 2.2 Hz, 4H, PC*H*$_2$N), 7.56 (AA'BB' system simplified as dd, *J* = 3.2, 6.2 Hz, 2H, $C_6H_4N_2$), 7.67 (AA'BB' system simplified as dd, *J* = 3.2, 6.2 Hz, 2H, $C_6H_4N_2$); ^{13}C{^{1}H} NMR (101 MHz, CD_2Cl_2): δ (ppm) = 29.5 (s, PC(*C*H$_3$)$_3$), 37.7 (s, P*C*(CH$_3$)$_3$), 42.6 (s, P*C*H$_2$N), 113.0 (s, *3,6*-*C*$_6$H$_4$N$_2$), 126.6 (s, *4,5*-*C*$_6$H$_4$N$_2$), 134.5 (s, *1,2*-*C*$_6$H$_4$N$_2$), 179.1 (br-s, N*C*(Ni)N); ^{19}F NMR (376 MHz, CD_2Cl_2): δ (ppm) = -74.6 (d, $^1J_{PF}$ = 711 Hz, P*F*$_6$); ^{31}P{^{1}H} NMR (162 MHz, CD_2Cl_2): δ (ppm) = -143.4 (sept, $^1J_{PF}$ = 711 Hz, 1P, *P*F$_6$), 81.5 (s, 2P, CH$_2$*P*[C(CH$_3$)$_3$)$_2$]). Hi-res MS ESI+ (m/z (%)) $(M)^+$ Found: 527.20223, Calc.: 527.20162 Anal. Calc. for $C_{25}H_{44}ClF_6N_2P_3Ni$ (%): C, 44.57; H, 6.58; N, 4.16. Found: C, 44.46; H, 6.19; N, 4.11.

Synthesis of [(*^{t}Bu-phenylene*-PCP)Mo(CO)$_3$] **4.10-*t*Bu**

Compound [H(**4.2-*t*Bu**)][PF_6] (100 mg, 0.17 mmol) was dissolved in toluene (10 mL), reacted with KHMDS (35 mg, 0.17 mmol) and allowed to stir for 30 min. The solution of freshly deprotonated **4.2-*t*Bu** was filtered, and slowly added to a solution of $Mo(CO)_6$ (45 mg, 0.17 mmol) in toluene (10 mL). The reaction mixture was refluxed for 12 h under a constant flow of argon. The resulting solution was concentrated under vacuum (ca. 5 mL) and cool down obtaining a fine crystalline green precipitate. The precipitate was filtered, washed with cold toluene (5 mL) and dried under vacuum to yield **4.10-*t*Bu** as a light yellow crystalline solid (80 mg, 0.13 mmol, 77 %). X-ray quality crystals of **4.10-*t*Bu** were obtained from slow evaporation of a concentrated solution in toluene at rt. ^{1}H NMR (400 MHz, toluene-d_8): δ (ppm) = 1.23 (vt, J_{PH} = 5.9 Hz, 36H, PC(CH_3)$_3$), 3.8 (bs, 4H, PCH_2N), 6.78 (AA'BB' system simplified as dd, J = 3.1, 5.8 Hz, 2H, $C_6H_4N_2$), 7.00 (AA'BB' system simplified as dd, J = 3.1, 5.8 Hz, 2H, $C_6H_4N_2$); ^{13}C{^{1}H} NMR (101 MHz, toluene-d_8): δ (ppm) = 30.5 (vt, J_{CP} = 3.1 Hz, PC(CH$_3$)$_3$), 37.8 (vt, J_{CP} = 3.2 Hz, PC(CH$_3$)$_3$), 45.8 (vt, J_{PC} = 6.8 Hz, PCH$_2$N), 109.9 (s, *3,6*-$C_6H_4N_2$), 122.3 (s, *4,5*-$C_6H_4N_2$), 135.3 (s, *1,2*-$C_6H_4N_2$), 223.2 (t, $^2J_{PC}$ = 7.8 Hz, MoCO *trans* to NCN), 226.8 (t, $^2J_{PC}$ = 8.5 Hz, Mo(CO)$_2$ *cis* to NCN), 233.1 (t, $^2J_{PC}$ = 4.5 Hz, NC(Mo)N); ^{31}P{^{1}H} NMR (162 MHz, toluene-d_8): δ (ppm) = 118.7 (s). Hi-res MS ESI+ (m/z (%)) (M^+) Found: 617.19505, Calc.: 617.19603.

Synthesis of [(η^2-CP-^{t}*Bu-phenylene*-PCP)Mo(CO)$_4$] **4.11-*t*Bu**

Compound [H(**4.2-*t*Bu**)][PF_6] (40 mg, 0.07 mmol) was dissolved in toluene (3 mL), reacted with KHMDS (14 mg, 0.07 mmol) and allowed to stir for 30 min. The solution of freshly deprotonated **4.2-*t*Bu** was filtered, and slowly added to a solution of $Mo(CO)_6$ (18 mg, 0.07 mmol) in toluene (2 mL). The reaction mixture was heated to 110 °C for 12 h in a sealed

vessel. The resulting solution was allowed to cool down slowly allowing for the formation of X-ray quality colorless crystals of **4.11-*t*Bu** (35 mg, 0.055 mmol, 79 %). ^{1}H NMR (400 MHz, toluene-d_8): δ (ppm) = 1.08 (d, $^{3}J_{PH}$ = 12.7 Hz, 18H, P(C(CH_3)$_3$)$_2$), 1.14 (d, $^{3}J_{PH}$ = 11.3 Hz, 18H, MoP(C(CH_3)$_3$)$_2$), 3.72 (d, $^{2}J_{PH}$ = 2.6 Hz, 2H, MoPCH_2N), 5.00 (d, $^{2}J_{PH}$ = 2.7 Hz, 2H, PCH_2N), 6.85 (m, 1H, $C_6H_4N_2$), 7.02 (m, 2H, $C_6H_4N_2$), 8.25 (m, 1H, $C_6H_4N_2$); ^{31}P{^{1}H} NMR (162 MHz, toluene-d_8): δ (ppm) = 16.7, (s, 1P, CH_2P(C(CH_3)$_3$)$_2$), 88.1 (s, 1P, CH_2(Mo)P(C(CH_3)$_3$)$_2$).

References

(1) Moulton, C. J.; Shaw, B. L. *J. Chem. Soc., Dalton Trans.* **1976**, 1020.

(2) Al-Salem, N. A.; Empsall, H. D.; Markham, R.; Shaw, B. L.; Weeks, B. *J. Chem. Soc., Dalton Trans.* **1979**, 1972.

(3) Crocker, C.; Empsall, H. D.; Errington, R. J.; Hyde, E. M.; Mcdonald, W. S.; Markham, R.; Norton, M. C.; Shaw, B. L.; Weeks, B. *J. Chem. Soc., Dalton Trans.* **1982**, 1217.

(4) Crocker, C.; Errington, R. J.; McDonald, W. S.; Odell, K. J.; Shaw, B. L.; Goodfellow, R. J. *J. Chem. Soc., Chem. Comm.* **1979**, 498.

(5) Al-Salem, N. A.; Mcdonald, W. S.; Markham, R.; Norton, M. C.; Shaw, B. L. *J. Chem. Soc., Dalton Trans.* **1980**, 59.

(6) Crocker, C.; Errington, R. J.; Markham, R.; Moulton, C. J.; Odell, K. J.; Shaw, B. L. *J. Am. Chem. Soc.* **1980**, *102*, 4373.

(7) Briggs, J. R.; Constable, A. G.; Mcdonald, W. S.; Shaw, B. L. *J. Chem. Soc., Dalton Trans.* **1982**, 1225.

(8) Crocker, C.; Errington, R. J.; Markham, R.; Moulton, C. J.; Shaw, B. L. *J. Chem. Soc., Dalton Trans.* **1982**, 387.

(9) Errington, R. J.; Mcdonald, W. S.; Shaw, B. L. *J. Chem. Soc., Dalton Trans.* **1982**, 1829.

(10) Errington, R. J.; Shaw, B. L. *J. Organomet. Chem.* **1982**, *238*, 319.

(11) van Koten, G.; Jastrzebski, J. T. B. H.; Noltes, J. G.; Spek, A. L.; Schoone, J. C. *J. Organomet. Chem.* **1978**, *148*, 233.

(12) van Koten, G.; Timmer, K.; Noltes, J. G.; Spek, A. L. *J. Chem. Soc., Chem. Comm.* **1978**, 250.

(13) van Koten, G. *Pure Appl. Chem.* **1989**, *61*, 1681.

(14) Albrecht, M.; van Koten, G. *Angew. Chem. Int. Ed.* **2001**, *40*, 3750.

(15) Szabo, K. J. *Top. Organomet. Chem.* **2013**, *40*, 203.

(16) Hawk, J. L.; Craig, S. L. *Top. Organomet. Chem.* **2013**, *40*, 319.

(17) Morales-Morales, D.; Jensen, C. M. *The Chemistry of Pincer Compounds*; 1st ed.; Elsevier: Amsterdam ; Boston, 2007.

(18) Albrecht, M.; Gossage, R. A.; Lutz, M.; Spek, A. L.; van Koten, G. *Chem. Eur. J.* **2000**, *6*, 1431.

(19) Albrecht, M.; Schlupp, M.; Bargon, J.; van Koten, G. *Chem. Comm.* **2001**, 1874.

(20) Schlupp, M.; Weil, T.; Berresheim, A. J.; Wiesler, U. M.; Bargon, J.; Müllen, K. *Angew. Chem. Int. Ed.* **2001**, *40*, 4011.

(21) Lagunas, M. C.; Gossage, R. A.; Spek, A. L.; van Koten, G. *Organometallics* **1998**, *17*, 731.

(22) Sutter, J. P.; Beley, M.; Collin, J. P.; Veldman, N.; Spek, A. L.; Sauvage, J. P.; van Koten, G. *Mol. Cryst. Liq. Cryst. Sci. Technol., Sect. A* **1994**, *252*, 507.

(23) Steenwinkel, P.; Grove, D. M.; Veldman, N.; Spek, A. L.; van Koten, G. *Organometallics* **1998**, *17*, 5647.

(24) James, S. L.; Veldman, N.; Spek, A. L.; vanKoten, G. *Chem. Comm.* **1996**, 253.

(25) Freeman, G. R.; Williams, J. A. G. *Top. Organomet. Chem.* **2013**, *40*, 89.

(26) Pregosin, P. S. *Coord. Chem. Rev.* **1982**, *44*, 247.

(27) Albrecht, M.; Rodriguez, G.; Schoenmaker, J.; van Koten, G. *Org. Lett.* **2000**, *2*, 3461.

(28) Gunanathan, C.; Ben-David, Y.; Milstein, D. *Science* **2007**, *317*, 790.

(29) Small, B. L.; Brookhart, M. *J. Am. Chem. Soc.* **1998**, *120*, 7143.

(30) Chirik, P. J.; Wieghardt, K. *Science* **2010**, *327*, 794.

(31) Ahuja, R.; Punji, B.; Findlater, M.; Supplee, C.; Schinski, W.; Brookhart, M.; Goldman, A. S. *Nat. Chem.* **2011**, *3*, 167.

(32) Kohl, S. W.; Weiner, L.; Schwartsburd, L.; Konstantinovski, L.; Shimon, L. J. W.; Ben-David, Y.; Iron, M. A.; Milstein, D. *Science* **2009**, *324*, 74.

(33) Eisenberg, R. *Science* **2009**, *324*, 44.

(34) Zhao, J.; Goldman, A. S.; Hartwig, J. F. *Science* **2005**, *307*, 1080.

(35) Askevold, B.; Nieto, J. T.; Tussupbayev, S.; Diefenbach, M.; Herdtweck, E.; Holthausen, M. C.; Schneider, S. *Nature Chemistry* **2011**, *3*, 532.

(36) Arashiba, K.; Miyake, Y.; Nishibayashi, Y. *Nat. Chem.* **2011**, *3*, 120.

(37) Yandulov, D. V.; Schrock, R. R. *Science* **2003**, *301*, 76.

(38) Choi, J.; Wang, D. Y.; Kundu, S.; Choliy, Y.; Emge, T. J.; Krogh-Jespersen, K.; Goldman, A. S. *Science* **2011**, *332*, 1545.

(39) Sakaki, S.; Kikuno, T. *Inorg. Chem.* **1997**, *36*, 226.

(40) Braunschweig, H.; Kollann, C.; Rais, D. *Angew. Chem. Int. Ed.* **2006**, *45*, 5254.

(41) Braunschweig, H.; Colling, M. *Coord. Chem. Rev.* **2001**, *223*, 1.

(42) Mannig, D.; Noth, H. *Angew. Chem. Int. Ed.* **1985**, *24*, 878.

(43) Burgess, K.; Ohlmeyer, M. J. *Chem. Rev.* **1991**, *91*, 1179.

(44) Wadepohl, H. *Angew. Chem. Int. Ed.* **1997**, *36*, 2441.

(45) Beletskaya, I.; Pelter, A. *Tetrahedron* **1997**, *53*, 4957.

(46) Marder, T. B.; Norman, N. C. *Top. Catal.* **1998**, *5*, 63.

(47) Crudden, C. M.; Edwards, D. *Eur. J. Org. Chem.* **2003**, 4695.

(48) Chen, H. Y.; Schlecht, S.; Semple, T. C.; Hartwig, J. F. *Science* **2000**, *287*, 1995.

(49) Cho, J. Y.; Tse, M. K.; Holmes, D.; Maleczka, R. E.; Smith, M. R. *Science* **2002**, *295*, 305.

(50) Ishiyama, T.; Miyaura, N. *J. Organomet. Chem.* **2003**, *680*, 3.

(51) Ishiyama, T.; Nobuta, Y.; Hartwig, J. F.; Miyaura, N. *Chem. Comm.* **2003**, 2924.

(52) Hartwig, J. F.; Cook, K. S.; Hapke, M.; Incarvito, C. D.; Fan, Y. B.; Webster, C. E.; Hall, M. B. *J. Am. Chem. Soc.* **2005**, *127*, 2538.

(53) Coventry, D. N.; Batsanov, A. S.; Goeta, A. E.; Howard, J. A. K.; Marder, T. B.; Perutz, R. N. *Chem. Comm.* **2005**, 2172.

(54) Chotana, G. A.; Rak, M. A.; Smith, M. R. *J. Am. Chem. Soc.* **2005**, *127*, 10539.

(55) Mkhalid, I. A. I.; Coventry, D. N.; Albesa-Jove, D.; Batsanov, A. S.; Howard, J. A. K.; Perutz, R. N.; Marder, T. B. *Angew. Chem. Int. Ed.* **2006**, *45*, 489.

(56) Entwistle, C. D.; Marder, T. B. *Angew. Chem. Int. Ed.* **2002**, *41*, 2927.

(57) Entwistle, C. D.; Marder, T. B. *Chem. Mater.* **2004**, *16*, 4574.

(58) Braunschweig, H.; Rais, D. *Angew. Chem. Int. Ed.* **2005**, *44*, 7826.

(59) Ehlers, A. W.; Baerends, E. J.; Bickelhaupt, F. M.; Radius, U. *Chem. Eur. J.* **1998**, *4*, 210.

(60) Boehme, C.; Uddin, J.; Frenking, G. *Coord. Chem. Rev.* **2000**, *197*, 249.

(61) Uddin, J.; Boehme, C.; Frenking, G. *Organometallics* **2000**, *19*, 571.

(62) Kays, D. L.; Aldridge, S. *Struct. Bonding* **2008**, *130*, 29.

(63) Melaimi, M.; Soleilhavoup, M.; Bertrand, G. *Angew. Chem. Int. Ed.* **2010**, *49*, 8810.

(64) Irikura, K. K.; Goddard, W. A.; Beauchamp, J. L. *J. Am. Chem. Soc.* **1992**, *114*, 48.

(65) Wanzlick, H. W.; Schonher, H.-J. *Angew. Chem. Int. Ed.* **1968**, *7*, 141.

(66) Öfele, K. *Angew. Chem. Int. Ed.* **1968**, *7*, 950.

(67) Arduengo, A. J.; Harlow, R. L.; Kline, M. *J. Am. Chem. Soc.* **1991**, *113*, 361.

(68) Kelly III, R. A.; Clavier, H.; Giudice, S.; Scott, N. M.; Stevens, E. D.; Bordner, J.; Samardjiev, I.; Hoff, C. D.; Cavallo, L.; Nolan, S. P. *Organometallics* **2007**, *27*, 202.

(69) Huang, J. K.; Schanz, H. J.; Stevens, E. D.; Nolan, S. P. *Organometallics* **1999**, *18*, 2370.

(70) Cazin, C. S. J. *N-heterocyclic carbenes in transition metal catalysis and organocatalysis*; Springer: New York, 2010.

(71) Green, J. C.; Scurr, R. G.; Arnold, P. L.; Cloke, F. G. N. *Chem. Comm.* **1997**, 1963.

(72) Boehme, C.; Frenking, G. *Organometallics* **1998**, *17*, 5801.

(73) Lee, M. T.; Hu, C. H. *Organometallics* **2004**, *23*, 976.

(74) Garrison, J. C.; Simons, R. S.; Kofron, W. G.; Tessier, C. A.; Youngs, W. J. *Chem. Comm.* **2001**, 1780.

(75) Tulloch, A. A. D.; Danopoulos, A. A.; Kleinhenz, S.; Light, M. E.; Hursthouse, M. B.; Eastham, G. *Organometallics* **2001**, *20*, 2027.

(76) Irvine, G. J.; Lesley, M. J. G.; Marder, T. B.; Norman, N. C.; Rice, C. R.; Robins, E. G.; Roper, W. R.; Whittell, G. R.; Wright, L. J. *Chem. Rev.* **1998**, *98*, 2685.

(77) Onozawa, S.-y.; Hatanaka, Y.; Sakakura, T.; Shimada, S.; Tanaka, M. *Organometallics* **1996**, *15*, 5450.

(78) Rickard, C. E. F.; Roper, W. R.; Williamson, A.; Wright, L. J. *Organometallics* **1998**, *17*, 4869.

(79) Irvine, G. J.; Rickard, C. E. F.; Roper, W. R.; Williamson, A.; Wright, L. J. *Angew. Chem. Int. Ed.* **2000**, *39*, 948.

(80) Sivignon, G.; Fleurat-Lessard, P.; Onno, J. M.; Volatron, F. *Inorg. Chem.* **2002**, *41*, 6656.

(81) Zhu, J.; Lin, Z. Y.; Marder, T. B. *Inorg. Chem.* **2005**, *44*, 9384.

(82) Braunschweig, H.; Brenner, P.; Muller, A.; Radacki, K.; Rais, D.; Uttinger, K. *Chem. Eur. J.* **2007**, *13*, 7171.

(83) Segawa, Y.; Yamashita, M.; Nozaki, K. *J. Am. Chem. Soc.* **2009**, *131*, 9201.

(84) Spokoyny, A. M.; Reuter, M. G.; Stern, C. L.; Ratner, M. A.; Seideman, T.; Mirkin, C. A. *J. Am. Chem. Soc.* **2009**, *131*, 9482.

(85) van der Boom, M. E.; Milstein, D. *Chem. Rev.* **2003**, *103*, 1759.

(86) Fryzuk, M. D. *Can. J. Chem.* **1992**, *70*, 2839.

(87) Fan, L.; Foxman, B. M.; Ozerov, O. V. *Organometallics* **2004**, *23*, 326.

(88) Liang, L. C. *Coord. Chem. Rev.* **2006**, *250*, 1152.

(89) Sangtrirutnugul, P.; Tilley, T. D. *Organometallics* **2007**, *26*, 5557.

(90) MacInnis, M. C.; MacLean, D. F.; Lundgren, R. J.; McDonald, R.; Turculet, L. *Organometallics* **2007**, *26*, 6522.

(91) Korshin, E. E.; Leitus, G.; Shimon, L. J. W.; Konstantinovski, L.; Milstein, D. *Inorg. Chem.* **2008**, *47*, 7177.

(92) Mankad, N. P.; Rivard, E.; Harkins, S. B.; Peters, J. C. *J. Am. Chem. Soc.* **2005**, *127*, 16032.

(93) Clark, G. R.; Irvine, G. J.; Roper, W. R.; Wright, L. J. *J. Organomet. Chem.* **2003**, *680*, 81.

(94) Zhang, Q. Z.; Ly, T.; Slawin, A. M. Z.; Woollins, J. D. *Rev. Roum. Chim.* **2002**, *47*, 1015.

(95) *Strem Chemical Co. Pricing: diphenylphosphine (50g, US$ 192.00); di-tert-butylphosphine (5g, US$ 115.00).*

(96) Onozawa, S.-y.; Tanaka, M. *Organometallics* **2001**, *20*, 2956.

(97) Segawa, Y.; Yamashita, M.; Nozaki, K. *Organometallics* **2009**, *28*, 6234.

(98) Hill, A. F.; Lee, S. B.; Park, J.; Shang, R.; Willis, A. C. *Organometallics* **2010**, *29*, 5661.

(99) El-Zaria, M. E.; Arii, H.; Nakamura, H. *Inorg. Chem.* **2011**, *50*, 4149.

(100) Hasegawa, M.; Segawa, Y.; Yamashita, M.; Nozaki, K. *Angew. Chem. Int. Ed.* **2012**, *51*, 6956.

(101) Enzmann, A.; Eckert, M.; Ponikwar, W.; Polborn, K.; Schneiderbauer, S.; Beller, M.; Beck, W. *Eur. J. Inorg. Chem.* **2004**, 1330.

(102) Miyazaki, F.; Yamaguchi, K.; Shibasaki, M. *Tetrahedron Lett.* **1999**, *40*, 7379.

(103) Ohff, M.; Ohff, A.; van der Boom, M. E.; Milstein, D. *J. Am. Chem. Soc.* **1997**, *119*, 11687.

(104) Eberhard, M. R. *Org. Lett.* **2004**, *6*, 2125.

(105) Cook, J. B.; Nicholson, B. K.; Smith, D. W. *J. Organomet. Chem.* **2004**, *689*, 860.

(106) Steinke, T.; Shaw, B. K.; Jong, H.; Patrick, B. O.; Fryzuk, M. D. *Organometallics* **2009**, *28*, 2830.

(107) Krenske, E. H. *J. Org. Chem.* **2011**, *77*, 1.

(108) Rajendran, K. V.; Gilheany, D. G. *Chem. Comm.* **2012**, *48*, 817.

(109) Rowland, R. S.; Taylor, R. *J. Phys. Chem.* **1996**, *100*, 7384.

(110) Noth, H.; Vahrenka.H *Chem. Ber.* **1966**, *99*.

(111) Gates, P. N.; McLauchlan, E. J.; Mooney, E. F. *Spectrochim. Acta* **1965**, *21*, 1445.

(112) Brown, H. C.; Ravindra.N *J. Organomet. Chem.* **1973**, *61*, C5.

(113) Young, D. E.; Mcachran, G. E.; Shore, S. G. *J. Am. Chem. Soc.* **1966**, *88*, 4390.

(114) Kanzelberger, M.; Singh, B.; Czerw, M.; Krogh-Jespersen, K.; Goldman, A. S. *J. Am. Chem. Soc.* **2000**, *122*, 11017.

(115) Gusev, D. G.; Fontaine, F. G.; Lough, A. J.; Zargarian, D. *Angew. Chem. Int. Ed.* **2003**, *42*, 216.

(116) Castonguay, A.; Spasyuk, D. M.; Madern, N.; Beauchamp, A. L.; Zargarian, D. *Organometallics* **2009**, *28*, 2134.

(117) Castonguay, A.; Beauchamp, A. L.; Zargarian, D. *Inorg. Chem.* **2009**, *48*, 3177.

(118) Payet, E.; Auffrant, A.; Le Goff, X. F.; Floch, P. L. *J. Organomet. Chem.* **2010**, *695*, 1499.

(119) Semmelhack, M. F.; Chlenov, A.; Ho, D. M. *J. Am. Chem. Soc.* **2005**, *127*, 7759.

(120) Good, C. D.; Ritter, D. M. *J. Am. Chem. Soc.* **1962**, *84*, 1162.

(121) Hofmeister, H. K.; Vanwazer, J. R. *J. Inorg. Nucl. Chem.* **1964**, *26*, 1209.

(122) Roesler, R.; Piers, W. E.; Parvez, M. *J. Organomet. Chem.* **2003**, *680*, 218.

(123) Cullen, W. R.; Rettig, S. J.; Trotter, J.; Wickenheiser, E. B. *Can. J. Chem.* **1988**, *66*, 2007.

(124) Bourissou, D.; Guerret, O.; Gabbaï, F. P.; Bertrand, G. *Chem. Rev.* **2000**, *100*, 39.

(125) Jacobsen, H.; Correa, A.; Poater, A.; Costabile, C.; Cavallo, L. *Coord. Chem. Rev.* **2009**, *253*, 687.

(126) Hobbs, M. G.; Knapp, C. J.; Welsh, P. T.; Borau-Garcia, J.; Ziegler, T.; Roesler, R. *Chem. Eur. J.* **2010**, *16*, 14520.

(127) Díez-González, S.; Nolan, S. P. *Coord. Chem. Rev.* **2007**, *251*, 874.

(128) Danopoulos, A. A.; Tsoureas, N.; Green, J. C.; Hursthouse, M. B. *Chem. Comm.* **2003**, 756.

(129) Becker, E.; Stingl, V.; Dazinger, G.; Mereiter, K.; Kirchner, K. *Organometallics* **2007**, *26*, 1531.

(130) Fantasia, S.; Jacobsen, H.; Cavallo, L.; Nolan, S. P. *Organometallics* **2007**, *26*, 3286.

(131) Nielsen, D. J.; Magill, A. M.; Yates, B. F.; Cavell, K. J.; Skelton, B. W.; White, A. H. *Chem. Comm.* **2002**, 2500.

(132) Crabtree, R. H. *J. Organomet. Chem.* **2005**, *690*, 5451.

(133) Yang, X.; Hall, M. B. *J. Am. Chem. Soc.* **2008**, *130*, 1798.

(134) Gründemann, S.; Albrecht, M.; Loch, J. A.; Faller, J. W.; Crabtree, R. H. *Organometallics* **2001**, *20*, 5485.

(135) Loch, J. A.; Albrecht, M.; Peris, E.; Mata, J.; Faller, J. W.; Crabtree, R. H. *Organometallics* **2002**, *21*, 700.

(136) Peris, E.; Loch, J. A.; Mata, J.; Crabtree, R. H. *Chem. Comm.* **2001**, 201.

(137) Lee, H. M.; Zeng, J. Y.; Hu, C.-H.; Lee, M.-T. *Inorg. Chem.* **2004**, *43*, 6822.

(138) Steinke, T.; Shaw, B. K.; Jong, H.; Patrick, B. O.; Fryzuk, M. D.; Green, J. C. *J. Am. Chem. Soc.* **2009**, *131*, 10461.

(139) Shaw, B. K.; Patrick, B. O.; Fryzuk, M. D. *Organometallics* **2012**, *31*, 783.

(140) Stylianides, N.; Danopoulos, A. A.; Pugh, D.; Hancock, F.; Zanotti-Gerosa, A. *Organometallics* **2007**, *26*, 5627.

(141) Navarro, J.; Torres, O.; Martín, M.; Sola, E. *J. Am. Chem. Soc.* **2011**, *133*, 9738.

(142) Zanardi, A.; Peris, E.; Mata, J. A. *New J. Chem.* **2008**, *32*, 120.

(143) Hahn, F. E.; Holtgrewe, C.; Pape, T.; Martin, M.; Sola, E.; Oro, L. A. *Organometallics* **2005**, *24*, 2203.

(144) Hoberg, H.; Burkhart, G.; Krüger, C.; Tsay, Y. H. *J. Organomet. Chem.* **1981**, *222*, 343.

(145) Spencer, L. P.; Winston, S.; Fryzuk, M. D. *Organometallics* **2004**, *23*, 3372.

(146) Spencer, L. P.; Beddie, C.; Hall, M. B.; Fryzuk, M. D. *J. Am. Chem. Soc.* **2006**, *128*, 12531.

(147) Magill, A. M.; McGuinness, D. S.; Cavell, K. J.; Britovsek, G. J. P.; Gibson, V. C.; White, A. J. P.; Williams, D. J.; White, A. H.; Skelton, B. W. *J. Organomet. Chem.* **2001**, *617–618*, 546.

(148) Haider, J.; Kunz, K.; Scholz, U. *Adv. Synth. Catal.* **2004**, *346*, 717.

(149) Friese, V.; Nag, S.; Wang, J.; Santoni, M.-P.; Rodrigue-Witchel, A.; Hanan, G. S.; Schaper, F. *Eur. J. Inorg. Chem.* **2011**, 39.

(150) Liu, B.; Liu, X.; Chen, C.; Chen, C.; Chen, W. *Organometallics* **2011**, *31*, 282.

(151) Krüger, A.; Kluser, E.; Müller-Bunz, H.; Neels, A.; Albrecht, M. *Eur. J. Inorg. Chem.* **2012**, 1394.

(152) Newman, P. D.; Cavell, K. J.; Kariuki, B. M. *Organometallics* **2010**, *29*, 2724.

(153) Newman, P. D.; Cavell, K. J.; Hallett, A. J.; Kariuki, B. M. *Dalton Trans.* **2011**, *40*, 8807.

(154) Das Adhikary, S.; Samanta, T.; Roymahapatra, G.; Loiseau, F.; Jouvenot, D.; Giri, S.; Chattaraj, P. K.; Dinda, J. *New J. Chem.* **2010**, *34*, 1974.

(155) Liu, Q.-X.; Li, H.-L.; Zhao, X.-J.; Ge, S.-S.; Shi, M.-C.; Shen, G.; Zang, Y.; Wang, X.-G. *Inorg. Chim. Acta.* **2011**, *376*, 437.

(156) Michon, C.; Ellern, A.; Angelici, R. J. *Inorg. Chim. Acta.* **2006**, *359*, 4549.

(157) Hongfa, C.; Su, H.-L.; Bazzi, H. S.; Bergbreiter, D. E. *Org. Lett.* **2009**, *11*, 665.

(158) Liao, C.-Y.; Chan, K.-T.; Zeng, J.-Y.; Hu, C.-H.; Tu, C.-Y.; Lee, H. M. *Organometallics* **2007**, *26*, 1692.

(159) Yagyu, T.; Oya, S.; Maeda, M.; Jitsukawa, K. *Chem. Lett.* **2006**, *35*, 154.

(160) Romain, C.; Miqueu, K.; Sotiropoulos, J.-M.; Bellemin-Laponnaz, S.; Dagorne, S. *Angew. Chem. Int. Ed.* **2010**, *49*, 2198.

(161) Zhang, D.; Aihara, H.; Watanabe, T.; Matsuo, T.; Kawaguchi, H. *J. Organomet. Chem.* **2007**, *692*, 234.

(162) Zhang, D.; Liu, N. *Organometallics* **2008**, *28*, 499.

(163) Zhang, D.; GengShi, G.; Wang, J.; Yue, Q.; Zheng, W.; Weng, L. *Inorg. Chem. Commun.* **2010**, *13*, 433.

(164) Chiu, P. L.; Lee, H. M. *Organometallics* **2005**, *24*, 1692.

(165) Zeng, J. Y.; Hsieh, M.-H.; Lee, H. M. *J. Organomet. Chem.* **2005**, *690*, 5662.

(166) Hahn, F. E.; Jahnke, M. C.; Pape, T. *Organometallics* **2006**, *25*, 5927.

(167) Kaufhold, O.; Stasch, A.; Edwards, P. G.; Hahn, F. E. *Chem. Comm.* **2007**, 1822.

(168) Kaufhold, O.; Stasch, A.; Pape, T.; Hepp, A.; Edwards, P. G.; Newman, P. D.; Hahn, F. E. *J. Am. Chem. Soc.* **2008**, *131*, 306.

(169) Flores-Figueroa, A.; Kaufhold, O.; Hepp, A.; Fröhlich, R.; Hahn, F. E. *Organometallics* **2009**, *28*, 6362.

(170) Flores-Figueroa, A.; Pape, T.; Weigand, J. J.; Hahn, F. E. *Eur. J. Inorg. Chem.* **2010**, 2907.

(171) Gischig, S.; Togni, A. *Organometallics* **2004**, *23*, 2479.

(172) Gischig, S.; Togni, A. *Eur. J. Inorg. Chem.* **2005**, 4745.

(173) Willms, H.; Frank, W.; Ganter, C. *Chem. Eur. J.* **2008**, *14*, 2719.

(174) Matsumura, N.; Kawano, J.-i.; Fukunishi, N.; Inoue, H.; Yasui, M.; Iwasaki, F. *J. Am. Chem. Soc.* **1995**, *117*, 3623.

(175) Yasui, M.; Yoshida, S.; Kakuma, S.; Shimamoto, S.; Matsumura, N.; Iwasaki, F. *B. Chem. Soc. Jpn.* **1996**, *69*, 2739.

(176) Manabe, N.; Yasui, M.; Nishiyama, H.; Shimamoto, S.; Matsumura, N.; Iwasaki, F. *B. Chem. Soc. Jpn.* **1996**, *69*, 2771.

(177) Iwasaki, F.; Manabe, N.; Yasui, M.; Matsumura, N.; Kamiya, N.; Iwasaki, H. *B. Chem. Soc. Jpn.* **1996**, *69*, 2749.

(178) Iwasaki, F.; Yasui, M.; Yoshida, S.; Nishiyama, H.; Shimamoto, S.; Matsumura, N. *B. Chem. Soc. Jpn.* **1996**, *69*, 2759.

(179) Sellmann, D.; Allmann, C.; Heinemann, F.; Knoch, F.; Sutter, J. *J. Organomet. Chem.* **1997**, *541*, 291.

(180) Iglesias-Siguenza, J.; Ros, A.; Diez, E.; Magriz, A.; Vazquez, A.; Alvarez, E.; Fernandez, R.; Lassaletta, J. M. *Dalton Trans.* **2009**, 8485.

(181) Fliedel, C.; Sabbatini, A.; Braunstein, P. *Dalton Trans.* **2010**, *39*, 8820.

(182) Iwasaki, F.; Nishiyama, H.; Yasui, M.; Kusamiya, M.; Matsumura, N. *B. Chem. Soc. Jpn.* **1997**, *70*, 1277.

(183) Özdemir, I.; Demir, S.; Çetinkaya, B.; Toupet, L.; Castarlenas, R.; Fischmeister, C.; Dixneuf, P. H. *Eur. J. Inorg. Chem.* **2007**, 2862.

(184) Lee, J. H.; Yoo, K. S.; Park, C. P.; Olsen, J. M.; Sakaguchi, S.; Prakash, G. K. S.; Mathew, T.; Jung, K. W. *Adv. Synth. Catal.* **2009**, *351*, 563.

(185) Öfele, K.; Herrmann, W. A.; Mihalios, D.; Elison, M.; Herdtweck, E.; Scherer, W.; Mink, J. *J. Organomet. Chem.* **1993**, *459*, 177.

(186) Werner, H. *Angew. Chem. Int. Ed.* **2010**, *49*, 4714.

(187) Kloek, S. M.; Heinekey, D. M.; Goldberg, K. I. *Angew. Chem. Int. Ed.* **2007**, *46*, 4736.

(188) Feller, M.; Ben-Ari, E.; Gupta, T.; Shimon, L. J. W.; Leitus, G.; Diskin-Posner, Y.; Weiner, L.; Milstein, D. *Inorg. Chem.* **2007**, *46*, 10479.

(189) Hahn, C.; Spiegler, M.; Herdtweck, E.; Taube, R. *Eur. J. Inorg. Chem.* **1998**, 1425.

(190) Clot, E.; Chen, J.; Lee, D.-H.; Sung, S. Y.; Appelhans, L. N.; Faller, J. W.; Crabtree, R. H.; Eisenstein, O. *J. Am. Chem. Soc.* **2004**, *126*, 8795.

(191) Burford, R. J.; Piers, W. E.; Parvez, M. *Organometallics* **2012**, *31*, 2949.

(192) Kuznetsov, V. F.; Lough, A. J.; Gusev, D. G. *Inorg. Chim. Acta.* **2006**, *359*, 2806.

(193) Preetz, A.; Drexler, H.-J.; Fischer, C.; Dai, Z.; Börner, A.; Baumann, W.; Spannenberg, A.; Thede, R.; Heller, D. *Chem. Eur. J.* **2008**, *14*, 1445.

(194) Fulmer, G. R.; Miller, A. J. M.; Sherden, N. H.; Gottlieb, H. E.; Nudelman, A.; Stoltz, B. M.; Bercaw, J. E.; Goldberg, K. I. *Organometallics* **2010**, *29*, 2176.

(195) Nonnenmacher, M.; Kunz, D.; Rominger, F. *Organometallics* **2008**, *27*, 1561.

(196) Lappert, M. F.; Maskell, R. K. *J. Organomet. Chem.* **1984**, *264*, 217.

(197) Gade, L. H.; César, V.; Bellemin-Laponnaz, S. *Angew. Chem. Int. Ed.* **2004**, *43*, 1014.

(198) César, V.; Bellemin-Laponnaz, S.; Wadepohl, H.; Gade, L. H. *Chem. Eur. J.* **2005**, *11*, 2862.

(199) Chianese, A. R.; Li, X.; Janzen, M. C.; Faller, J. W.; Crabtree, R. H. *Organometallics* **2003**, *22*, 1663.

(200) Huang, K.-W.; Grills, D. C.; Han, J. H.; Szalda, D. J.; Fujita, E. *Inorg. Chim. Acta.* **2008**, *361*, 3327.

(201) Kossoy, E.; Rybtchinski, B.; Diskin-Posner, Y.; Shimon, L. J. W.; Leitus, G.; Milstein, D. *Organometallics* **2009**, *28*, 523.

(202) Montag, M.; Efremenko, I.; Cohen, R.; Shimon, L. J. W.; Leitus, G.; Diskin-Posner, Y.; Ben-David, Y.; Salem, H.; Martin, J. M. L.; Milstein, D. *Chem. Eur. J.* **2010**, *16*, 328.

(203) Fryzuk, M. D.; Macneil, P. A.; Rettig, S. J. *Organometallics* **1986**, *5*, 2469.

(204) Huang, J. K.; Haar, C. M.; Nolan, S. P.; Marshall, W. J.; Moloy, K. G. *J. Am. Chem. Soc.* **1998**, *120*, 7806.

(205) Doyle, M. J.; Lappert, M. F.; Pye, P. L.; Terreros, P. *J. Chem. Soc., Dalton Trans.* **1984**, 2355.

(206) Wolf, S.; Plenio, H. *J. Organomet. Chem.* **2009**, *694*, 1487.

(207) Anderson, K. M.; Orpen, A. G. *Chem. Comm.* **2001**, 2682.

(208) Schwartsburd, L.; Iron, M. A.; Konstantinovski, L.; Ben-Ari, E.; Milstein, D. *Organometallics* **2011**, *30*, 2721.

(209) Hanson, S. K.; Heinekey, D. M.; Goldberg, K. I. *Organometallics* **2008**, *27*, 1454.

(210) Bernskoetter, W. H.; Schauer, C. K.; Goldberg, K. I.; Brookhart, M. *Science* **2009**, *326*, 553.

(211) Walter, M. D.; White, P. S.; Schauer, C. K.; Brookhart, M. *New J. Chem.* **2011**, *35*, 2884.

(212) Bagno, A.; Saielli, G. *Phys. Chem. Chem. Phys.* **2011**, *13*, 4285.

(213) Appleton, T. G.; Bennett, M. A. *Inorg. Chem.* **1978**, *17*, 738.

(214) Schönberg, H.; Boulmaâz, S.; Wörle, M.; Liesum, L.; Schweiger, A.; Grützmacher, H. *Angew. Chem. Int. Ed.* **1998**, *37*, 1423.

(215) Longato, B.; Coppo, R.; Pilloni, G.; Corvaja, C.; Toffoletti, A.; Bandoli, G. *J. Organomet. Chem.* **2001**, *637*, 710.

(216) Ho, V. M.; Watson, L. A.; Huffman, J. C.; Caulton, K. G. *New J. Chem.* **2003**, *27*, 1446.

(217) Nolan, S. P. *N-Heterocyclic Carbenes in Synthesis*; Wiley-VCH ; John Wiley distributor: Weinheim Chichester, 2006.

(218) Kühl, O. *Functionalised N-Heterocyclic Carbene Complexes*; Wiley: Hoboken, NJ, USA, 2010.

(219) Gilbertson, S. R.; Wang, X. F. *J. Org. Chem.* **1996**, *61*, 434.

(220) Allen, F. H. *Acta Crystallogr. Sect. B* **2002**, *58*, 380.

(221) Bruno, I. J.; Cole, J. C.; Edgington, P. R.; Kessler, M.; Macrae, C. F.; McCabe, P.; Pearson, J.; Taylor, R. *Acta Crystallogr. Sect. B* **2002**, *58*, 389.

(222) Chase, P. A.; Gagliardo, M.; Lutz, M.; Spek, A. L.; van Klink, G. P. M.; van Koten, G. *Organometallics* **2005**, *24*, 2016.

(223) Gorla, F.; Venanzi, L. M.; Albinati, A. *Organometallics* **1994**, *13*, 43.

(224) Rimml, H.; Venanzi, L. M. *J. Organomet. Chem.* **1983**, *259*, C6.

(225) Herrmann, W. A.; Schütz, J.; Frey, G. D.; Herdtweck, E. *Organometallics* **2006**, *25*, 2437.

(226) Thirupathi, N.; Amoroso, D.; Bell, A.; Protasiewicz, J. D. *Organometallics* **2005**, *24*, 4099.

(227) Jouaiti, A.; Geoffroy, M.; Bernardinelli, G. *Chem. Comm.* **1996**, 437.

(228) van der Sluis, M.; Beverwijk, V.; Termaten, A.; Bickelhaupt, F.; Kooijman, H.; Spek, A. L. *Organometallics* **1999**, *18*, 1402.

(229) Groux, L. F.; Bélanger-Gariépy, F.; Zargarian, D. *Can. J. Chem.* **2005**, *83*, 634.

(230) Ray, S.; Shaikh, M. M.; Ghosh, P. *Eur. J. Inorg. Chem.* **2009**, *2009*, 1932.

(231) Hebden, T. J.; Schrock, R. R.; Takase, M. K.; Muller, P. *Chem. Comm.* **2012**, *48*, 1851.

(232) Hillebrand, S.; Bartkowska, B.; Bruckmann, J.; Krüger, C.; Haenel, M. W. *Tetrahedron Lett.* **1998**, *39*, 813.

(233) Lang, H.-F.; Fanwick, P. E.; Walton, R. A. *Inorg. Chim. Acta.* **2002**, *329*, 1.

(234) Berg, J. M.; Holm, R. H. *Inorg. Chem.* **1983**, *22*, 1768.

(235) Edwards, A. J.; Slim, D. R.; Guerchais, J. E.; Kergoat, R. *J. Chem. Soc., Dalton Trans.* **1980**, 289.

(236) Wieghardt, K.; Holzbach, W.; Weiss, J. *Z. Naturforsch. B* **1982**, *37*, 680.

(237) Schirmer, W.; Flörke, U.; Haupt, H. J. *Z. Anorg. Allg. Chem.* **1987**, *545*, 83.

(238) Abel, E. W.; Bennett, M. A.; Wilkinson, G. *J. Chem. Soc.* **1959**, 2323.

(239) Benito-Garagorri, D.; Becker, E.; Wiedermann, J.; Lackner, W.; Pollak, M.; Mereiter, K.; Kisala, J.; Kirchner, K. *Organometallics* **2006**, *25*, 1900.

(240) Eisenträger, F.; Göthlich, A.; Gruber, I.; Heiss, H.; Kiener, C. A.; Krüger, C.; Ulrich Notheis, J.; Rominger, F.; Scherhag, G.; Schultz, M.; Straub, B. F.; Volland, M. A. O.; Hofmann, P. *New J. Chem.* **2003**, *27*, 540.

(241) Meiners, J.; Friedrich, A.; Herdtweck, E.; Schneider, S. *Organometallics* **2009**, *28*, 6331.

(242) Hellmann, H.; Birkner, H.; Bader, J.; Schumacher, O. *Liebigs. Ann. Chem.* **1962**, *659*, 49.

(243) Locke, J. M.; Crumbie, R. L.; Griffith, R.; Bailey, T. D.; Boyd, S.; Roberts, J. D. *J. Org. Chem.* **2007**, *72*, 4156.

(244) Pozharskii, A. F.; Starshikov, N. M. *Khim. Geterotsikl. Soedin.* **1978**, 1418.

(245) Chernichenko, K.; Nieger, M.; Leskela, M.; Repo, T. *Dalton Trans.* **2012**, *41*, 9029.

(246) Shaw, B. L. *Proc. Chem. Soc. (London)* **1960**, 247.

(247) Otwinowski, Z.; Minor, W. *Macromolecular Crystallography, Part A* **1997**, *276*, 307.

(248) Hooft, R. *COLLECT: Users Manual, Nonius B.V.*; Delft.: The Netherlands, 1998.

(249) Beurskens, P. T.; Admiraal, G.; Beurskens, G.; Bosman, W. P.; de Gelder, R.; Israel, R.; Smits, J. M. M. *The DIRDIF-94 program system, Technical Report of the Crystallography Laboratory* University of Nijmegen, The Netherlands, 1994.

(250) Smykalla, C.; Beurskens, P. T.; Bosman, W. P.; Garciagranda, S. *J. Appl. Crystallogr.* **1994**, *27*, 661.

(251) Altomare, A.; Cascarano, G.; Giacovazzo, C.; Guagliardi, A. *J. Appl. Crystallogr.* **1993**, *26*, 343.

(252) Sheldrick, G. M. *Acta Crystallogr. Sect. A* **2008**, *64*, 112.

(253) Frisch, M. J.; Trucks, G. W.; Schlegel, H. B.; Scuseria, G. E.; Robb, M. A.; Cheeseman, J. R.; Scalmani, G.; Barone, V.; Mennucci, B.; Petersson, G. A.; Nakatsuji, H.; Caricato, M.; Li, X.; Hratchian, H. P.; Izmaylov, A. F.; Bloino, J.; Zheng, G.; Sonnenberg, J. L.; Hada, M.; Ehara, M.; Toyota, K.; Fukuda, R.; Hasegawa, J.; Ishida, M.; Nakajima, T.; Honda, Y.; Kitao, O.; Nakai, H.; Vreven, T.; Montgomery, J., J. A.; Peralta, J. E.; Ogliaro, F.; Bearpark, M.; Heyd, J. J.; Brothers, E.; Kudin, K. N.; Staroverov, V. N.; Kobayashi, R.; Normand, J.; Raghavachari, K.; Rendell, A.; Burant, J. C.; Iyengar, S. S.; Tomasi, J. C., M.; Rega, N.; Millam, N. J.; Klene, M.; Knox, J. E.; Cross, J. B.; Bakken, V.; Adamo, C.; Jaramillo, J.; Gomperts, R.; Stratmann, R. E.; Yazyev, O.; Austin, A. J.; Cammi, R.; Pomelli, C.; Ochterski, J. W.; Martin, R. L.; Morokuma, K.; Zakrzewski, V. G.; Voth, G. A.; Salvador, P.; Dannenberg, J. J.; Dapprich, S.; Daniels, A. D.; Farkas, Ö.; Foresman, J. B.; Ortiz, J. V.; Cioslowski, J.; Fox, D. J. *Gaussian 09, Revision A.1* Wallingford, Connecticut, 2009.

(254) Perdew, J. P.; Burke, K.; Ernzerhof, M. *Phys. Rev. Lett.* **1996**, *77*, 3865.

(255) Perdew, J. P.; Emzerhof, M.; Burke, K. *J. Chem. Phys.* **1996**, *105*, 9982.

(256) Perdew, J. P.; Burke, K.; Ernzerhof, M. *Phys. Rev. Lett.* **1997**, *78*, 1396.

(257) Adamo, C.; Barone, V. *Chem. Phys. Lett.* **1999**, *314*, 152.

(258) Weigend, F.; Ahlrichs, R. *Phys. Chem. Chem. Phys.* **2005**, *7*, 3297.

Appendix A

Crystal and Structure Refinement Data

Table A.1 Crystal and Structure Refinement Details for 2.1-Ph, 2.1-*t*Bu, and 2.3-Ph.

	2.1-Ph	**2.1-*t*Bu**	**2.3-Ph**
Empirical formula	$C_{32}H_{30}N_2P_2$	$C_{24}H_{46}N_2P_2$	$C_{32}H_{28}BClN_2P_2Pd$
Formula weight	504.52	424.57	655.16
Crystal system	Orthorhombic	Monoclinic	Tetragonal
Space group	P b c n	C 2/c	P 41 21 2
a (Å)	17.3852(4)	19.2922(4)	15.1761(5)
b (Å)	10.1655(6)	13.2076(5)	15.1761(5)
c (Å)	15.3051(4)	13.8532(5)	13.9103(6)
α (°)	90	90	90
β (°)	90	132.103(2)	90
γ (°)	90	90	90
V (Å^3)	2704.86(19)	2618.93(15)	3203.1(2)
Z	4	4	4
d_{calc} (g cm^{-3})	1.239	1.077	1.358
Absorption coef. (mm^{-1})	0.184	0.178	0.785
F(000)	1064	936	1328
θ range (°)	2.34 to 25.99	2.10 to 25.00	3.06 to 27.46
Reflections collected	4965	8413	7160
Independent reflections	2660	2310	3656
Completeness to θ	99.8 %	99.9 %	99.6 %
Data/Restraints/Parameters	2660/0/167	2310/0/131	3656/0/175
Goodness-of-Fit on F^2	1.000	1.076	1.053
$R_1(F)$ [$I>2\sigma(I)$]	0.0571	0.0438	0.0537
$wR_2(F^2)$ [all data]	0.1469	0.1037	0.1310
Largest diff. peak and hole e.Å^{-3}	0.469 / -0.361	0.330 / -0.276	1.152 / -0.813

Table A.2 Crystal and Structure Refinement details for 2.4, 2.5, and 2.6.

	2.4	**2.5**	**2.6**
Empirical formula	$C_{33}H_{32}Cl_2N_2P_2S_2$	$C_{32}H_{28}BClN_2P_2S_2$	$C_{32}H_{29}BN_2P_2S_2$
Formula weight	653.57	612.88	578.44
Crystal system	Triclinic	Monoclinic	Monoclinic
Space group	P -1	P 21/c	P 21/c
a (Å)	10.6535(3)	9.0410(4)	12.5702(3)
b (Å)	10.6892(3)	19.7680(11)	8.6181(4)
c (Å)	15.7183(4)	16.9820(7)	27.2765(11)
α (°)	106.6830(10)	90	90
β (°)	99.321(2)	96.753(3)	101.165(2)
γ (°)	103.6400(10)	90	90
V ($Å^3$)	1614.75(8)	3014.0(2)	2898.97(19)
Z	2	4	4
d_{calc} (g cm^{-3})	1.344	1.351	1.325
Absorption coef. (mm^{-1})	0.456	0.397	0.320
F(000)	680	1272	1208
θ range (°)	2.70 to 26.00	2.39 to 24.99	2.02 to 25.00
Reflections collected	11423	14869	7379
Independent reflections	6271	5266	5051
Completeness to θ	98.7 %	99.4 %	99.0 %
Data/Restraints/Parameters	6271/0/378	5266/0/361	5051/0/356
Goodness-of-Fit on F^2	1.013	1.005	1.073
$R_1(F)$ [$I>2\sigma(I)$]	0.0439	0.0854	0.0995
$wR_2(F^2)$ [all data]	0.1216	0.1929	0.2143
Largest diff. peak and hole e.$Å^{-3}$	0.551 / -0.543	0.452 / -0.451	0.521 / -0.530

Table A.3 Crystal and Structure Refinement details for 2.15-Me, 2.16-Me·LiOMe, and H_2(3.1b-Ph).

	2.15-Me	**2.16-Me**·LiOMe	H_2(**3.1b-Ph**)
Empirical formula	$C_{16}H_{20}BLiN_2O$	$C_{17}H_{22}BLiN_2O$	$C_{37}H_{32}N_2P_2$
Formula weight	274.09	288.12	566.59
Crystal system	Trigonal	Monoclinic	Monoclinic
Space group	P -3	P 21/c	P 21/c
a (Å)	15.1035(9)	18.0342(8)	10.2100(2)
b (Å)	15.1035(7)	12.8991(6)	17.7320(5)
c (Å)	12.1752(5)	14.8573(7)	19.026(5)
α (°)	90	90	90
β (°)	90	114.308(3)	12.108(2)
γ (°)	120	90	90
V ($Å^3$)	2405.3(2)	3149.893)	2917.69(13)
Z	6	8	4
d_{calc} (g cm^{-3})	1.135	1.215	1.290
Absorption coef. (mm^{-1})	0.069	0.074	0.179
F(000)	876	1232	1192
θ range (°)	2.70 to 24.98	2.74 to 25.00	2.30 to 27.46
Reflections collected	4370	8920	23861
Independent reflections	2775	5386	6641
Completeness to θ	98.3 %	96.9 %	99.5 %
Data/Restraints/Parameters	2775/0/190	5386/0/397	6641/0/370
Goodness-of-Fit on F^2	1.042	1.080	1.175
$R_1(F)$ [$I>2\sigma(I)$]	0.0726	0.0786	0.0618
$wR_2(F^2)$ [all data]	0.1681	0.1668	0.1394
Largest diff. peak and hole e.$Å^{-3}$	0.326 / -0.277	0.304 / -0.281	0.564 / -0.293

Table A.4 Crystal and Structure Refinement Details for 3.5a-Ph, 3.5a-*t*Bu, 3.5b-Ph.

	3.5a-Ph	**3.5a-*t*Bu**	**3.5b-Ph**
Empirical formula	$C_{34}H_{38}ClN_2OP_2Rh$	$C_{22}H_{46}ClN_2P_2Rh$	$C_{37}H_{30}ClN_2P_2Rh$
Formula weight	690.96	538.91	702.93
Crystal system	Orthorhombic	Monoclinic	Tetragonal
Space group	P 21 21 21	P 21/c	P 43 21 2
a (Å)	13.8230(6)	12.1912(5)	15.1380(4)
b (Å)	14.9610(5)	15.4234(3)	15.1380(4)
c (Å)	15.0150(7)	15.0696(4)	15.2320(3)
α (°)	90	90	90
β (°)	90	109.628(1)	90
γ (°)	90	90	90
V (Å^3)	3105.2(2)	2668.89(14)	3490.55(15)
Z	4	4	4
d_{calc} (g cm^{-3})	1.478	1.341	1.338
Absorption coef. (mm^{-1})	0.770	0.871	0.684
F(000)	1424	1136	1432
θ range (°)	1.92 to 27.48	2.64 to 26.00	2.33 to 27.47
Reflections collected	6894	18813	7162
Independent reflections	6894	5239	3984
Completeness to θ	98.7 %	99.9 %	99.4 %
Data/Restraints/Parameters	6894/0/327	5239/0/253	3984/0/197
Goodness-of-Fit on F^2	1.110	1.028	1.062
$R_1(F)$ [I>2σ(I)]	0.0631	0.0372	0.0424
$wR_2(F^2)$ [all data]	0.1724	0.0818	0.1073
Largest diff. peak and hole e.Å^{-3}	0.899 / -0.777	0.474 / -0.389	0.321 / -0.543

Table A.5 Crystal and Structure Refinement Details for 3.10b-Ph, [3.12b-Ph][OTf], [3.13a-Ph][OTf]

	3.10b-Ph	[**3.12b-Ph**][OTf]	[**3.13a-Ph**][OTf]
Empirical formula	$C_{39}H_{34}Cl_5N_2P_2Rh$	$C_{62}H_{50}BrF_3N_2O_3P_3RhS$	$C_{32}H_{30}F_3N_2O_4P_2RhS$
Formula weight	872.78	1235.83	760.49
Crystal system	Triclinic	Monoclinic	Triclinic
Space group	P -1	P 21/c	P -1
a (Å)	12.0120(6)	13.9460(2)	9.3233(2)
b (Å)	12.1420(6)	20.3730(5)	12.0781(4)
c (Å)	14.9930(9)	25.1030(5)	15.4314(5)
α (°)	69.640(3)	90	81.840(1)
β (°)	75.982(3)	123.1270(10)	72.622(4)
γ (°)	61.488(3)	90	74.593(2)
V ($Å^3$)	1793.75(17)	5973.0(2)	1595.08(8)
Z	2	4	2
d_{calc} (g cm^{-3})	1.616	1.374	1.583
Absorption coef. (mm^{-1})	0.971	1.124	0.759
F(000)	884	2512	772
θ range (°)	2.12 to 25.00	1.39 to 27.45	3.04 to 25.00
Reflections collected	11584	23281	10468
Independent reflections	6242	13508	5554
Completeness to θ	98.8 %	99.0 %	98.9 %
Data/Restraints/Parameters	6242/0/441	13508/0/685	5554/0/406
Goodness-of-Fit on F^2	1.079	1.084	1.080
$R_1(F)$ [I>2σ(I)]	0.0768	0.0623	0.0396
$wR_2(F^2)$ [all data]	0.1583	0.1691	0.1024
Largest diff. peak and hole e.$Å^{-3}$	1.200 / -1.449	0.747 / -0.763	0.784 / -0.712

Table A.6 Crystal and Structure Refinement Details for [3.13a-tBu][OTf], 3.14a-*t*Bu, 3.15a-*t*Bu

	[**3.13a-tBu**][OTf]	**3.14a-*t*Bu**	**3.15a-*t*Bu**
Empirical formula	$C_{24}H_{46}F_3N_2O_4P_2RhS$	$C_{78}H_{153}Cl_3N_6O_3P_6Rh_3$	$C_{28}H_{51}N_2P_2Rh$
Formula weight	680.54	1823.96	580.56
Crystal system	Monoclinic	Triclinic	Monoclinic
Space group	P 21/c	P -1	P 21/c
a (Å)	8.5672(3)	15.5592(4)	10.7822(3)
b (Å)	16.0551(4)	17.9983(6)	13.5381(4)
c (Å)	23.3125(6)	18.8765(6)	20.3015(6)
α (°)	90	108.906(3)	90
β (°)	106.675(1)	108.068(3)	103.152(2)
γ (°)	90	96.510(2)	90
V ($Å^3$)	3071.13(15)	4618.0(2)	2895.69(14)
Z	4	2	4
d_{calc} (g cm^{-3})	1.472	1.312	1.336
Absorption coef. (mm^{-1})	0.777	0.765	0.721
F(000)	1416	1926	1232
θ range (°)	1.56 to 25.00	2.09 to 25.00	1.82 to 25.00
Reflections collected	9828	23363	18091
Independent reflections	5327	15806	5066
Completeness to θ	98.5 %	97.1 %	99.7 %
Data/Restraints/Parameters	5327/0/347	15806/18/902	5066/0/298
Goodness-of-Fit on F^2	1.059	1.158	1.098
$R_1(F)$ [$I>2\sigma(I)$]	0.0552	0.0851	0.0634
$wR_2(F^2)$ [all data]	0.1647	0.1818	0.1223
Largest diff. peak and hole e.$Å^{-3}$	0.741 / -1.260	0.847 / -0.708	0.648 / -0.510

Table A.7 Crystal and Structure Refinement Details for 3.16a-*t*Bu, [H(4.2-Ph)][PF_6], [H(4.2-*t*Bu)][PF_6]

	3.16a-*t*Bu	[H(**4.2-Ph**)][PF_6]	[H(**4.2-*t*Bu**)][PF_6]
Empirical formula	$C_{23}H_{49}N_2P_2Rh$	$C_{33}H_{29}F_6N_2P_3$	$C_{25}H_{45}F_6N_2P_3$
Formula weight	518.49	660.49	580.54
Crystal system	Monoclinic	Triclinic	Monoclinic
Space group	P 21/c	P -1	P 21/c
a (Å)	10.0073(4)	13.2005(3)	16.1142(4)
b (Å)	25.5372(3)	13.3824(2)	12.4553(5)
c (Å)	14.2595(10)	18.7991(6)	17.4061(4)
α (°)	90	75.382(2)	90
β (°)	125.974(1)	72.940(1)	120.623(2)
γ (°)	90	82.428(3)	90
V ($Å^3$)	2949.1(2)	30066.06(13)	3409.09(18)
Z	4	4	4
d_{calc} (g cm^{-3})	1.168	1.431	1.131
Absorption coef. (mm^{-1})	0.698	0.258	0.222
F(000)	1104	1360	1232
θ range (°)	3.00 to 25.00	1.16 to 25.00	2.90 to 25.00
Reflections collected	16558	20547	21970
Independent reflections	5114	10735	5986
Completeness to θ	98.6 %	99.4 %	99.8 %
Data/Restraints/Parameters	5114/0/253	10735/0/681	5986/0/329
Goodness-of-Fit on F^2	1.044	1.093	1.061
$R_1(F)$ [I>2σ(I)]	0.0539	0.1200	0.0762
$wR_2(F^2)$ [all data]	0.1390	0.2481	0.1894
Largest diff. peak and hole e.$Å^{-3}$	1.805 / -0.737	0.992 / -0.483	1.186 / -0.240

Table A.8 Crystal and Structure Refinement Details for 4.3-*t*Bu, [4.4-*t*Bu][OTf], [4.6-*t*Bu][PF_6].

	4.3-*t*Bu	[**4.4-*t*Bu**][OTf]	[**4.6-*t*Bu**][PF_6]
Empirical formula	$C_{31}H_{50}ClN_2P_2Rh$	$C_{27}H_{44}F_3N_2O_4P_2RhS$	$C_{45}H_{50}F_6P_4Pd$
Formula weight	651.03	714.55	935.13
Crystal system	Monoclinic	Triclinic	Triclinic
Space group	P 21/c	P -1	P -1
a (Å)	11.5742(3)	12.4984(4)	13.2944(3)
b (Å)	23.3165(7)	16.9432(4)	18.7191(2)
c (Å)	15.4041(3)	16.9903(5)	20.1165(4)
α (°)	90	111.668(2)	64.326(2)
β (°)	129.035(1)	90.792(2)	87.974(5)
γ (°)	90	107.310(1)	88.826(1)
V ($Å^3$)	3229.07(14)	3161.07(16)	4509.04(16)
Z	4	4	4
d_{calc} (g cm^{-3})	1.339	1.501	1.378
Absorption coef. (mm^{-1})	0.733	0.760	0.608
F(000)	1368	1480	1920
θ range (°)	2.27 to 27.54	1.30 to 26.00	1.53 to 25.00
Reflections collected	13730	22586	30155
Independent reflections	7321	12209	15808
Completeness to θ	98.4 %	98.3 %	99.5 %
Data/Restraints/Parameters	7321/0/334	12209/0/721	15808/0/1032
Goodness-of-Fit on F^2	1.005	1.033	1.096
$R_1(F)$ [$I>2\sigma(I)$]	0.0422	0.0665	0.0679
$wR_2(F^2)$ [all data]	0.1315	0.1560	0.2004
Largest diff. peak and hole e.$Å^{-3}$	0.566 / -0.564	1.004 / -0.631	0.876 / -1.098

Table A.9 Crystal and Structure Refinement Details for [4.8-*t*Bu][PF_6], [4.9-*t*Bu][PF_6], and 4.10-*t*Bu.

	[**4.8-*t*Bu**][PF_6]	[**4.9-*t*Bu**][PF_6]	**4.10-*t*Bu**
Empirical formula	$C_{25}H_{44}ClF_6N_2P_3Pd$	$C_{25}H_{44}ClF_6N_2NiP_3$	$C_{28}H_{44}MoN_2O_3P_2$
Formula weight	721.38	673.69	614.53
Crystal system	Monoclinic	Triclinic	Monoclinic
Space group	P 21/c	P -1	C c
a (Å)	8.2290(3)	8.4132(3)	8.9232(3)
b (Å)	12.7810(4)	12.6705(4)	31.2655(4)
c (Å)	29.6540(1)	15.2681(4)	10.9612(4)
α (°)	90	108.873(2)	90
β (°)	96.310(1)	98.892(2)	105.552(2)
γ (°)	90	89.816(2)	90
V ($Å^3$)	3099.96(18)	1519.65(8)	2946.08
Z	4	2	4
d_{calc} (g cm^{-3})	1.546	1.472	1.386
Absorption coef. (mm^{-1})	0.894	0.940	0.585
F(000)	1480	704	1288
θ range (°)	1.38 to25.00	1.70 to 25.00	2.33 to 27.61
Reflections collected	15627	10079	12110
Independent reflections	5389	5276	6729
Completeness to θ	98.9 %	99.1 %	98.8 %
Data/Restraints/Parameters	5389/0/343	5276/0/343	6729/0/353
Goodness-of-Fit on F^2	1.024	1.057	1.080
$R_1(F)$ [I>2σ(I)]	0.0423	0.0701	0.0342
$wR_2(F^2)$ [all data]	0.1342	0.1719	0.0785
Largest diff. peak and hole e.$Å^{-3}$	0.949 / -0.697	0.831 / -0.473	0.417 / -0.433

Table A.10 Crystal and Structure Refinement Details for 4.11-*t*Bu.

	4.11-*t*Bu
Empirical formula	$C_{29}H_{44}MoN_2O_4P_2$
Formula weight	642.54
Crystal system	Monoclinic
Space group	C c
a (Å)	8.4403(3)
b (Å)	23.5212(9)
c (Å)	16.5925(5)
α (°)	90
β (°)	104.425(2)
γ (°)	90
V ($Å^3$)	3190.20(19)
Z	4
d_{calc} (g cm^{-3})	1.338
Absorption coef. (mm^{-1})	0.545
F(000)	1344
θ range (°)	2.15 to 27.70
Reflections collected	6598
Independent reflections	6591
Completeness to θ	98.1 %
Data/Restraints/Parameters	6591/2/344
Goodness-of-Fit on F^2	1.191
$R_1(F)$ [$I>2\sigma(I)$]	0.0351
$wR_2(F^2)$ [all data]	0.0966
Largest diff. peak and hole e.$Å^{-3}$	0.378 / -0.336